# SKI-JUMP ENERGY DISSIPATION

## DESIGN OF A SKI-JUMP TO MAXIMISE ENERGY DISSIPATION AND AERATION

by

Cameron Neal Fraser

*Thesis presented at the University of Stellenbosch*

*in fulfilment of the requirements for the degree of*

*Master of Engineering*

*(MEng)*

*Faculty of Civil Engineering*
*University of Stellenbosch*
*Private Bag X1, 7602 Matieland, South Africa*

Supervisor: Prof. G.R. Basson

March 2016

# DECLARATION

By submitting this thesis electronically, I declare that the entirety of the work contained therein is my own, original work, that I am the authorship owner thereof (unless to the extent explicitly otherwise stated) and that I have not previously in its entirety or in part submitted it for obtaining any qualification.

Date: March 2016

# ABSTRACT (ENGLISH)

One of the most effective and economical methods for the dissipation of hydraulic energy from flood waters is to project the flows into a free trajectory jet form to a location where the impact creates a plunge pool in the downstream river bed. This type of energy dissipation can be created by a ski-jump energy dissipator which has become an increasingly popular form of hydraulic energy dissipation for large dams in recent years due to its ability to safely convey high velocity flow in excess of 30m/s to the downstream river, however very limited definitive and comprehensive guidelines have been created. There is not only insufficient documentation for the conceptual and detailed design of ski-jump energy dissipators, there is also insufficient documentation for the dimensioning of the downstream plunge pools. Both are necessary to guarantee that the passage of major floods do not threaten the structural integrity of the permanent works.

The origins of ski-jumps can be dated back as far as the mid-1930s where they were successfully introduced on the Dordogne hydraulic scheme in France. This revolutionary scheme designed a circular arc spillway over the power plant with the intention of conveying high velocity flow in the form of a trajectory jet over power plant and plunge down onto the riverbed at a substantially far distance away from any dam apparatuses as to mitigate potential structural damage. Due to the success of this design, it became very popular in France, Spain and Portugal. During the period 1930-1940 the first spillways of its kind were constructed under its new name, “Saut de ski”.

This research includes hydraulic testing of different ski-jump buckets for a general design. The objective of this is to obtain a design that would maximise energy dissipation and enhance air entrainment as well as establishing a comprehensive guideline to the design of ski-jumps. Energy dissipation by a ski-jump may be assessed by evaluating a number of identified contributing parameters by means of a physical hydraulic model. The parameters of importance include; 1) the geometric profile of the water jet trajectory such as the trajectory distance, trajectory height, horizontal and transverse impact width; 2) dynamic impact pressure distribution; 3) maximum dynamic impact pressure head; 4) impact velocity head; and 5) air entrainment. These results demonstrate the significant effect of the Froude number, bucket angle and bucket shape. The results for the different ski-jump buckets of all mentioned parameters are presented, descripted and discussed, and concluding with the design that best dissipates energy for the ski-jump buckets tested. This design was able to improve the pressure distribution area significantly as well as decrease the maximum dynamic pressure head by up to 20m when compared to a standard 40$^{o}$ circular shaped flip bucket design. An increase in the aeration by up to 20% at the centreline was achieved when compared to a standard design.

# OPSOMMING (AFRIKAANS)

Een van die mees effektiefste en ekonomieste metodes om van hidrouliese energie van vloedwater wat oor ‘n dam-oorloop vloei te demp, is om die vloei te projekteer in die vorm van ‘n vrye straal na ‘n plonspoel stoomaf van die damwal. Hierdie tipe energie demping kan gedoen word met behulp van ‘n energie dempende ski-sprong. Oor die afgelope jare word die ski-sprong toenemend gebruik vir die oorlope van groot damme. Die rede hiervoor is dat dit die vermoë het om die water wat oor ‘n dam vloei veilig na ‘n plonspoel stroom-af van ‘n damwal te verplaas. Daar bestaan egter beperkte riglyne vir die ontwerp van ski-sprong oorloop strukture. Daar is nie net onvoldoende riglyne vir die ontwerp van ski-sprong oorlope nie, maar ook onvoldoende riglyne vir die afmetings van die gepaardgaande plonspoel stroom-af van die damwal. Albei komponente van ‘n ski-sprong oorloop is uiters noodsaaklik om te verseker dat groot vloede nie die strukturele integriteit van ‘n damwal bedreig nie.

Die oorsprong van die ski-sprong kan terug gedateer word so ver as die middel 1930’s waar dit in die Dordogne hidrouliese skema in Frankryk suksesvol toegepas is. Hierdie revolusionêre skema het ‘n sirkerlvormige boog oorloop met ‘n krag stasie aan die stroom-af kant daarvan. Die oorloop is ontwerp om die hoë snelheid vloei van die dam-oorloop in die vorm van 'n geprojekteerde straal oor die kragstasie te verplaas na ‘n plons-poel in die rivierbedding. As gevolg van die sukses van hierdie ontwerp, was dit baie gewild in Frankryk, Spanje en Portugal. Gedurende die tydperk 1930-1940 is die eerstes van hierdie tipe oorloop gebou onder die nuwe naam, "Saut de ski" of ski-sprong.

Hierdie navorsing sluit hidrouliese toetse van verskillende ski-sprong vorms in met die doel om ‘n vorm vir die ski-sprong te ontwikkel wat energie demping maksimeer en belugting van die geprojekteerde straal te, verbeter asook om meer omvattende ontwerp riglyne te definieer.

In hierdie ondersoek word energie demping van verskillende ski-sprong vorms ge-evalueer deur middel van die meting van die belangrikste parameters in ‘n fisiese hidrouliese model.

Die parameters van belang wat ondersoek is sluit in; 1) die geometriese profiel van die water straal se trajek soos, die trajek afstand, trajek hoogte en horisontale en dwars impak breedte; 2) dinamiese impak druk verspreiding op die vlak van die plonspoel; 3) die maksimum dinamiese impak druk hoogte; 4) impak snelheidshoogte; en 5) belugting van die geprojekteerde straal.

Die resultate van hierdie ondersoek toon dat die Froude nommer asook die projekteringshoek en vorm van die ski-sprong ‘n beduidende invloed het. Die resultate van die ondersoek van die verskillende ski-sprong vorms in terme van bogenoemde parameters word aangebied, beskryf en bespreek. Op basis van die resultate word die ski-sprong vorm met die beste energie dempingseienskappe aangedui. Die beste ontwerp was in staat om die druk verspreiding in die plonspoel aansienlik te verbeter, sowel as die maksimum dinamiese druk hoogte met tot 20m te verlaag in vergelyking met 'n standaard 40$^{o}$ sirkel

vormige ski-sprong ontwerp. Die beste ontwerp het ook 'n toename in die belugting van die geprojekteerde straal met tot 20% op die middellyn getoon in vergelyking met 'n standaard ontwerp.

# ACKNOWLEDGEMENTS

Without the help, support and guidance from the employees and departments of Stellenbosch University as well as my parents, the completion of this Thesis would not have been possible.

A special thanks is extended to the study leader, Prof GR Basson, for his continual guidance, support and valuable assistance throughout the entirety of this Thesis. Finally to the Stellenbosch University Civil Engineering Department for the financial and administrative support for the duration of this Thesis as well as the duration of my Degree.

# DISCLAIMER

The contents of this report reflect the view of the author, who is responsible for the facts and accuracy of the data presented herein. The contents do not necessarily reflect the official views or policies of Stellenbosch University.

# TABLE OF CONTENTS

# LIST OF FIGURES

# LIST OF TABLES

# LIST OF ABBREVIATIONS

| | |
|---|---|
| $\alpha_o$ | *Spillway angle with the horizontal* |
| $\alpha_j$ | *Angle of deflection of the water jet* |
| $\beta_b$ | *Angle of the ski-jump bucket from the spillway to lip* |
| $\beta_j$ | *Transverse jet expansion angle* |
| $\beta_s$ | *Convergence ratio of sidewalls of slit type flip bucket* |
| $C$ | *Variable discharge coefficient* |
| $C_c$ | *Contraction coefficient relative to $y_g$ (0.61 for vertical sluice gate under free discharge)* |
| $C_o$ | *Discharge coefficient for the design head* |
| $C_r$ | *Radius coefficient in the range 0.6 to 0.8* |
| $d_1$ | *Depth of flow entering ski-jump bucket* |
| $d_s$ | *Depth of scour* |
| $E$ | *Young's modulus* |
| $F_r$ | *Froude number* |
| $F_1$ | *Froude number at bucket invert* |
| $\gamma$ | *Specific weight of water* |
| $g$ | *Gravitational acceleration, 9.81 $m/s^2$* |
| $H_e$ | *Actual head being considered on the spillway crest* |
| $h_b$ | *Height of ski-jump bucket* |
| $h_f$ | *Frictional head losses* |
| $h_l$ | *Local head losses* |
| $h_{min}$ | *Minimum height of ski-jump bucket* |
| $h_{m(l)}$ | *Height of the maximum point along a ski-jump trajectory for the lower nappe* |
| $h_{m(u)}$ | *Height of the maximum point along a ski-jump trajectory for the upper nappe* |
| $h_1$ | *Flow depth on the ski-jump bucket,* |

| | |
|---|---|
| $H_o$ | *Design Head above dam spillway crest* |
| $H_s$ | *Head above the ski-jump bucket invert* |
| $h_P$ | *Pressure head* |
| $H_T$ | *Total energy head at the upstream section* |
| $H_{vj}$ | *Velocity head at the point of impact of a ski-jump jet* |
| $k$ | *Coefficient of air resistance* |
| $K_a$ | *Abutment contraction coefficient* |
| $K_p$ | *Pier contraction coefficient* |
| $L$ | *Effective length of spillway crest* |
| $L'$ | *Net length of spillway crest* |
| $\lambda$ | *Scale factor* |
| $L_k$ | *Cavitation cloud length* |
| $L_s$ | *Spillway length at the crest* |
| $N$ | *Number of piers* |
| $\phi$ | *Impact angle of ski-jump jet* |
| $P$ | *Pressure or bucket pressure* |
| $P_{dM}$ | *Maximum dynamic pressure head* |
| $P_T$ | *Theoretical unit load on the bucket invert* |
| $\rho$ | *Fluid density* |
| $Q$ | *Characteristic discharge* |
| $Q_o$ | *Design discharge* |
| $q$ | *Unit discharge relative to the spillway length* |
| $\bar{q}$ | *Unit discharge relative to the flow depth* |
| $r$ or $R$ | *Radius of bucket curvature, in m; and* |
| $R_{min}$ | *Minimum bucket radius* |
| $R_e$ | *Reynolds number* |
| $\sigma$ | *Flow cavitation index or surface tensions* |
| $\sigma_s$ | *Cavitation index when damage begins* |

| | |
|---|---|
| $\mu$ | *Dynamic viscosity* |
| $V$ | *Characteristic flow velocity* |
| $v_o$ | *Initial velocity in the upstream dam section* |
| $v_1$ | *Flow velocity entering the ski-jump bucket* |
| $v_2$ | *Impact velocity of the ski-jump jet* |
| $W_j$ | *Longitudinal impact width of a ski-jump jet* |
| $X_{H(u)}$ | *Horizontal trajectory distance of the upper nappe of a ski-jump jet* |
| $X_{H(l)}$ | *Horizontal trajectory distance of the lower nappe of a ski-jump jet* |
| $x_{m(u)}$ | *Horizontal distance to the maximum height of the trajectory of a ski-jump jet (upper nappe)* |
| $x_{m(l)}$ | *Horizontal distance to the maximum height of the trajectory of a ski-jump jet (lower nappe)* |
| $x$ | *Horizontal coordinate of the jet trajectory with the bucket lip as the origin* |
| $y$ | *Vertical coordinate of the jet trajectory with the bucket lip as the origin* |
| $Y$ | *Elevation difference between the ski-jump bucket invert and the tailwater level* |
| $y_G$ | *Sluice Gate opening* |

# CHAPTER 1: INTRODUCTION

*In this chapter a background knowledge is provided of the course with which hydraulic structures has taken from first introduction to the present situation. Next a description of the project will be given where the purpose will be highlighted including the goals and limitations. Further on, an overall method of approach will be presented. This chapter concludes with the general thesis layout and chapter-by-chapter overview.*

## 1.1 BACKGROUND ON HYDRAULIC STRUCTURES

Hydraulic structures may be defined according to Hager & Boes (2014) as engineering components, which allow the improvement and/or modification of flow features in water engineering thus yielding better desired flow conditions when compared to natural water flow. This improvement is usually focussed on the conveyance efficiency through the reduction of resistance while modification is necessary when water bodies are required to be deflected, expanded or reduced. These structures require design flexibility as well as high strength due to imposed forces generated from high velocities, large discharges as well as large hydrostatic pressures, therefore are constructed mainly of concrete.

### 1.1.1 HYDRAULIC STRUCTURES FROM THE NINETEENTH TO THE TWENTY-FIRST CENTURY

Hydraulics research before the end of the Second World War was largely focussed on questions concerning hydraulic structures. There was a realisation in the nineteenth century that the storage of water in dams and reservoirs played an essential role in society in relation to topics such as water supply, flood protection as well as energy production.

Dams were built taller and wider with the advancement of dam engineering technologies and therefore discharges became larger and flow velocities became increasingly higher. Succeeding the Second World War the global development of large dams in excess of 100m in height is remarkably illustrated by the dramatic increase in the total number of dams from 30 in 1945 to 500 by 1990 (Hager & Boes, 2014). Along with the advancements in technology and construction techniques, new problems such as cavitation damage, scour and abrasion to the hydraulic structures arose. These hydraulic problems were studied only by the countries directly involved with innovative dam undertakings at the time, with the USA national authorities (US Bureau of Reclamation and US Army Corps of Engineers) in the forefront and the Soviet Union not so far behind.

Further difficulties in hydraulic engineering arose during the 1960s and 1970s including density currents, water abstraction and large reservoir stratification. These difficulties took the focus off the development of dam structures as it was assumed that the problems associated with them at the time were solved.

The introduction of numerical computations became a core focus of hydraulic engineering in the late 1970s and 1980s which resulted in further neglect of dam structures to a point where there was a

perception amongst engineers that suggested it was old fashioned to conduct further research on dam structures.

During recent years, dam structures have experienced a revival. This resurrection of interest came about due to various factors including advancement in hydraulic instrumentation, the worldwide search for clean renewable energy, the need for experimental data for computational fluid dynamics (CFD) modelling and the incrementally increasing demand for the access to water.

### 1.1.2 SKI-JUMP ENERGY DISSIPATING HYDRAULIC STRUCTURE

One of the most effective and economical methods for the dissipation of hydraulic energy of water overflowing dam walls from flood waters is to project the flows into a free trajectory jet form to a location where the impact creates a plunge pool in the downstream river bed. This type of energy dissipation has become an increasingly popular form of hydraulic energy dissipation for large dams in recent years, however very limited definitive and comprehensive guidelines have been created. There is not only insufficient documentation for the conceptual and detailed design of flip buckets, there is also insufficient documentation for the dimensioning of the downstream plunge pools. Both are extremely necessary to guarantee that the passage of major floods do not threaten the structural integrity of the permanent works (Mason, 1993).

In dam engineering, ski-jumps are a common hydraulic structures with the function of deflecting high velocity discharge from large dam spillways and chutes to produce a free jet trajectory. This type of hydraulic structure utilised the effects of air resistance and air entrainment in combination with impact diffusion to dissipate the energy and alleviate risk of downstream erosion.

The main component of a ski-jump energy dissipator is the ski-jump bucket or flip bucket which is not an energy dissipator in itself but plays an integral part of the energy dissipation process. In general flip buckets are designed and constructed with horizontal cross sections. The primary purpose of the flip bucket is to deflect high velocity flow up and into the air in the form of a jet trajectory where the location of impact fall at a sufficient distance from the dam toe as to mitigate any risk of structural damage.

## 1.2 PROJECT DESCRIPTION

### 1.2.1 PURPOSE

The purpose of this thesis is to maximise the energy dissipation and aeration of a ski-jump dissipating structure through the design of different ski-jumps by evaluating the aeration characteristics of the trajectory jet before and after the bucket location as well as the impact pressures of the falling jet on the surface below.

#### 1.2.1.1 GOAL

The aim of the thesis is to perform experiments on a hydraulic model of a typical ski-jump dissipating structure with different flip bucket designs in the hydraulics laboratory at the Department of Civil Engineering at Stellenbosch University in order to determine the most appropriate bucket design in terms of the highest aeration concentration of the trajectory jet and lowest pressure distribution at the point of impact.

#### 1.2.1.2 LIMITATIONS

This thesis does not take the effect of pre-aerated approach flow by flow splitters, chute aerators or bucket splitter teeth into consideration. The reason for not including bucket splitter teeth in the hydraulic model is due to the fact that large dams are being considered where the flow velocities present at the bucket are excessively high and would result in considerable cavitation damage to the ski-jump spillway in prototype scale. The objective of this thesis was to design a ski-jump that would enhance the energy dissipation and aeration. Buckets were designed based on a theoretical approach and tests were conducted which specifically assessed the energy dissipation potential, whether or not these same designs are acceptable in terms of bucket pressures and cavitational damage was not included in this research.

### 1.2.2 METHOD

A hydraulic assessment of different ski-jump flip buckets were conducted on an experimental model at the Department of Civil Engineering at the University of Stellenbosch. Eight different flip buckets with seven flow conditions each were tested in order to choose the best design of ski-jump flip bucket to maximise energy dissipation and aeration.

The experiments that were conducted included the measurement of trajectory geometric characteristics of the water jet, the dynamic impact pressure head on the plunge pool and the impact velocity head. High velocity flow would be discharged from the ski-jump model with the flip bucket deflecting the flow into the air following a parabolic trajectory before falling into the plunge pool below. Dynamic pressure head occurs at the point of impact, which were recorded with pressure transducers. The extracted data was tabulated, processed and displayed in graphical format where it could then be used to evaluate the energy loss within the system when compared to the initial energy head. The impact velocities could be used in a similar manner. The air entrainment at a point directly after jet take-off was measured and compared between flip buckets to highlight which flip bucket introduces the greatest concentration of air into the core of the water jet.

On the basis of the analysed data the ski-jump bucket design which dissipated the maximum energy was identified.

## 1.3 THESIS LAYOUT AND CHAPTER OVERVIEW

A chapter by chapter summary is presented below to give a better understanding of what this dissertation entails.

**Chapter 2: Literature Review**

The **Literature Review** begins with an introduction into what a ski-jump spillway is and a brief insight into its origin. An introduction to energy dissipation is then covered with a detailed explanation on the types of energy dissipation and mechanisms involved as well as the associated energy dissipating structures. In the next section, the selection of the type of energy dissipating structure for specific conditions is covered. This is followed by an in depth literature review of ski-jump energy dissipating structures which is the main focal point of this dissertation. In this section the ski-jump energy dissipating system is broken up into smaller systems which are comprehensively described individually. This chapter ends with a section on one of the major concerns relating to high velocity flow, namely cavitation damage.

**Chapter 3: Hydraulic Design Criteria of Ski-Jump/ Flip Bucket Type**

There is a research gap in the design of ski-jump energy dissipators thus the addition of this chapter sought to compile existing guidelines into a single document that clearly defines calculations and considerations that must be present when designing a ski-jump energy dissipator.

**Chapter 4: Physical Hydraulic Model and Test Procedure**

In this chapter, the empirical portion of this dissertation begins. Firstly a general description of the physical model is covered. The next part of this chapter deals with theoretical information regarding the scale effects associated with hydraulic modelling. A detailed description of the design and construction phase of the physical model is then addressed. This chapter concludes with the testing and procedures that were employed in the testing phase including data acquisition and handling methods.

**Chapter 5: Experimental Results**

In this chapter the results of the ski-jump hydraulic model are presented and briefly discussed. The results include the geometric data obtained from photograph scaling, the dynamic impact pressure data obtained from the pressure transducers the aeration data captured with the air probe and the impact velocity data acquired from the GoPro action camera and tracker software.

**Chapter 6: Analysis**

In this section of this thesis the analysis of the results is presented, compared with the relevant theory and discussed in detail. The last section of this chapter quantifies the energy dissipation and presents it as a percentage of the total initial energy.

**Chapter 7: Conclusion and Recommendations**

The chapter summarises the results where final conclusions are discussed and whether or not the objectives of the dissertation have been met. The dissertation ends with a critique of the chosen methods employed and recommendations as how the research could possibly be improved in view of future research in this field.

# CHAPTER 2: LITERATURE REVIEW

## 2.1 DAM ENGINEERING

One of the most essential civil engineering activities throughout all history is said to be Dam Engineering. In ancient times access to vast amounts of water for daily consumption and irrigation was limited to locations of large rivers. It is believed that the early stages in development of all great civilisations encompassed the construction of dams applicable to their needs. Dams, in their early existence, were constructed with the primary function of a storage reservoir so that access to water was possible throughout the year including the dryer seasons. Moreover, dams were envisioned to fulfil the arising need for irrigation at the time of organised agricultural development. A trend emerged where the proficiency within water engineering and the ability to retain and control the use of water within a civilisation created a close link to the most successful and economically powerful civilisations (Novak, et al., 2007).

In present day, modern civil engineers still regard the engineering and utilisation of water structures and resources among the most essential contributions made to a society. Within all nations, the construction of dams embodies a major investment in basic infrastructure. Nowadays the foremost function of dams is to offer a safe detainment and storage of water which requires correct applications of dam engineering design while satisfying the necessities of every site's local, technical and economic conditions (Novak, et al., 2007).

## 2.2 DAMS AND DAM FAILURE

The classification of dams may fall under a number of different categories, of which three broad classifications exist. These tree main categories of dam classification are classification by their use, classification by their hydraulic design and classification by their construction materials (USBR, 1987).

### 2.2.1 CLASSIFICATION ACCORDING TO USE.

The classification of dams may be based upon the certain function they serve. Three relevant examples of these functions are for storage, diversion or detention.

Storage dams have the function of impounding water for water supply, recreational activities, fish and wildlife, hydroelectric power generation and irrigation during periods of excess supply for periods of scarce supply (USBR, 1987).

Diversion dams are generally constructed to create a water level necessary for conveyance systems such as canals and ditches. Often these types of dams are used for irrigation purposes and off-channel-location municipal and industrial storage reservoirs (USBR, 1987).

Detention dams are constructed with the intention of retarding flood runoff and diminishing the consequence of flash floods. Detention dams are also referred to as attenuation dams. The purpose of these dams are to contain the flood capacity of a large flood while simultaneously releasing a flood of lesser magnitude. Therefore the detention dam temporarily retains the flood for only the duration of the flood.

### 2.2.2 CLASSIFICATION BY HYDRAULIC DESIGN

In terms of hydraulic design dams may be classified as either overflow or non-overflow dams. Overflow dams are designed to convey flow over the crest via an open channel spillway and non-overflow dams are those designed so that overtopping does not exist. Overflow dams are generally constructed of concrete, or at least the spillway is, whereas non-overflow dams have the option to be constructed from earthfill and rockfill.

More commonly than not, these two types of dams are incorporated into one structure where characteristics of both are present (USBR, 1987). An example of such a dam would be an earthfill dam with a concrete overflow spillway.

### 2.2.3 CLASSIFICATION BY MATERIALS

Design speaking, the most common form of dam classification is by materials used for its construction. The following dams are considered to be the more common types of dams constructed nowadays (USBR, 1987). **Figure 2.1** shows a visual representation of these dam types.

#### *2.2.3.1 Earthfill dams*

This type of dam is classified under the broader group, embankment dams. It is considered to be the most preferred dam type due to the fact that the material used in its construction is predominantly the same as that excavated from the site and is generally locally available which makes it an economical option.

#### *2.2.3.2 Rockfill dams*

Rockfill dams, also classified under the broader group of embankment dams, use different rock grading sizes to create the necessary stability. In order to provide the essential ‘watertighness’, an impervious membrane is incorporated into the dam which may be constructed of a concrete slab, steel plates, impervious soil core asphaltic-concrete paving or any combination thereof.

#### *2.2.3.3 Concrete gravity dams*

As the name suggests the dam is constructed from concrete. These types of dams generally have steep slopes that require strong rock foundations to be constructed upon. This type of dam may be incorporated into earthfill or rockfill dams as an overflow spillway. The construction of gravity dams nowadays generally use the method of roller compacted concrete (RCC).

#### 2.2.3.4 Concrete Arch Dams

Concrete arch dams are generally constructed in narrow gorges where sound rock exist capable of counterattacking arch thrust. Typically two types of arch dams are commonly implemented, namely the single arch dams which is limited to a span crest length to height ratio of 10:1 and the multiple ach dam which may comprise of numerous single arch spans reinforced by enormous supporting buttresses.

#### 2.2.3.5 Concrete Buttress Dams

This type of dam is constructed as multiple ach structures with a flat deck. It is said to use 60% less concrete than that of solid gravity dams. However, additional reinforced steel and formwork is necessary which generally compensates for concrete savings.

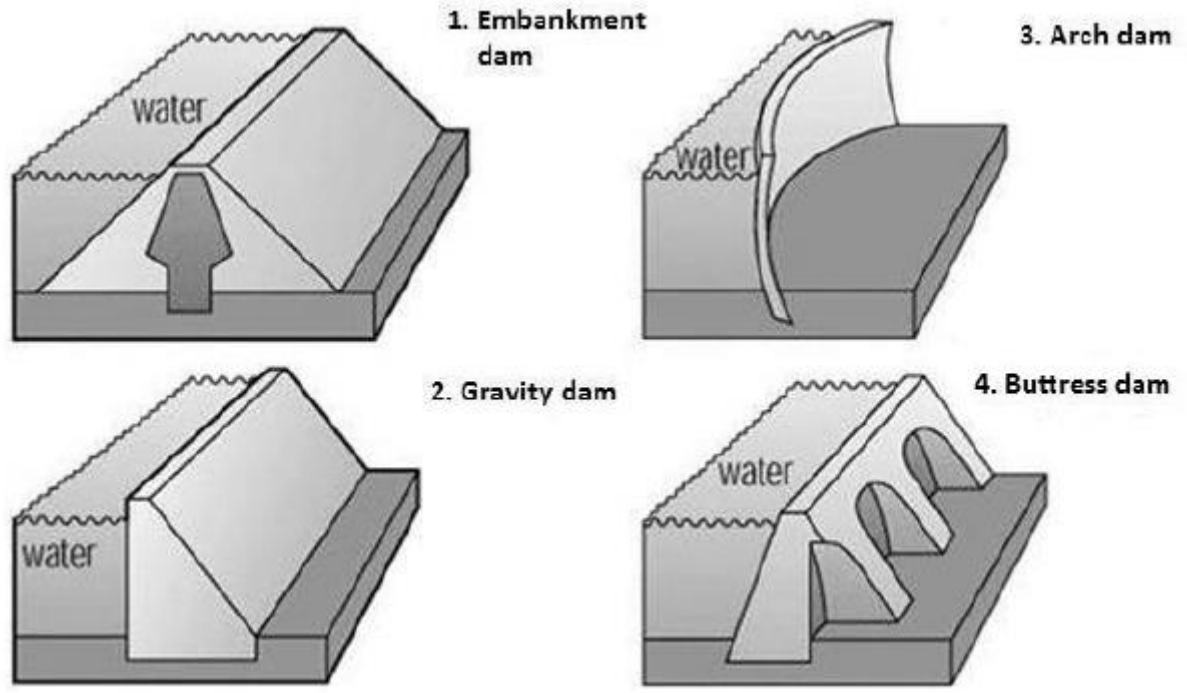


*FIGURE 2.1 : FOUR DIFFERENT DAM PROFILES (GARDO & LINDHOLM, 2013).*

### 2.2.4 SPILLWAYS, OUTLETS AND ANCILLARY WORKS

All dams require auxiliary structures and facilities to provide the ability to carry out its intended purpose safely and efficiently. The safe passage of extreme floods is an important operational function which is required by all dams. This includes controlled and uncontrolled discharge from the dam. Therefore spillways and outlet works are crucial for safe operation (Novak, et al., 2007).

## 2.3 ORIGIN OF SKI-JUMP ENERGY DISSIPATING STRUCTURES AND PROGRESSION THEREOF

At large dams, ski-jumps in combination with plunge pools are commonly used as an effective and economic form of energy dissipation. **Figure 2.2** below depicts a typical ski-jump spillway one can

expect at an arch dam. Ski-jump energy dissipating structures may be divided into various hydraulic sections, which perform different functions within the energy dissipation system as a whole. These sections include a control structure, approach chute, deflector (flip bucket) and impact basin (Heller, 2009). Each hydraulic section and their contributions to the ski-jump energy dissipator will be elaborated upon in detail in **Section 2.8** of this document.

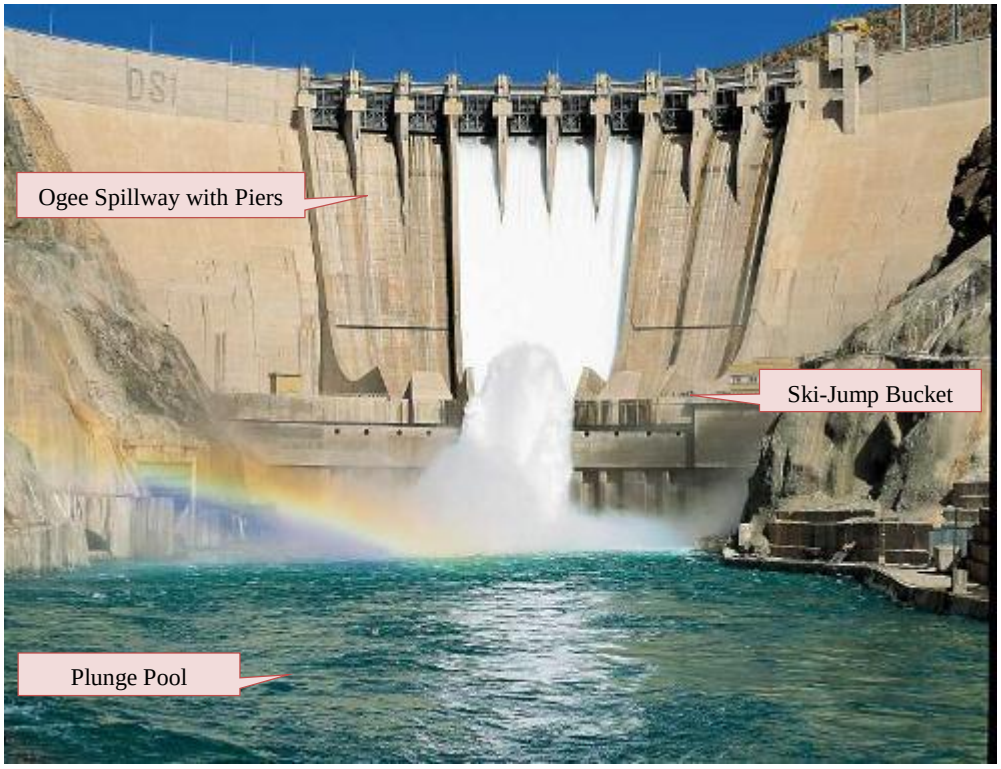


*FIGURE 2.2: SKI JUMP OF KARAKAYA DAM, TURKEY, IN OPERATION WITH PLUNGE POOL IN FOREGROUND (HELLER, 2009).*

The origins of ski-jumps can be dated back as far as the mid-1930s where they were successfully introduced on the Dordogne hydraulic scheme in France where jet flow observations were documented in detail. This scheme was revolutionary as the roof of the power plant was designed to form the lower section of the spillway as a circular arc. This design was the first of its kind where the intention was to send the high velocity flow in the form of a trajectory jet over power plant and plunge down onto the riverbed at a substantially far distance away from any dam structures. The discharge of water at dam structures has always been an issue due to scour formation at the point of impingement. As a result of this type of spillway design the formation of scour could be relocated to a safe distance from the dam foundations thereby alleviating any risk of structural damage. Due to the success of this design, it became very popular in France, Spain and Portugal. During the period 1930-1940, the first spillways of its kind were constructed under its new name, “Saut de ski” (Gardo & Lindholm, 2013). In 1959, Rhone and Peterka expanded on the research conducted by the U.S. Bureau of Reclamation whereby improving the design of flip buckets (Omidvarinia & Musavi Jahromi, 2013). According to Mason (1993), free

trajectory jets used for hydraulic energy dissipation at dams was established with the completion of the twin ski-jump spillway chutes positioned above the L'Aigle Dam power station (**Figure 2.3**).

The first observed and computed model pressures where conducted in 1961 for a ski-jump bucket. It was identified by Balloffet (1961) that the difference in the average maximum pressure head between the model and theoretical is 4% provided that the ratio of the depth of flow in the bucket to the bucket radius of curvature is reasonably small.

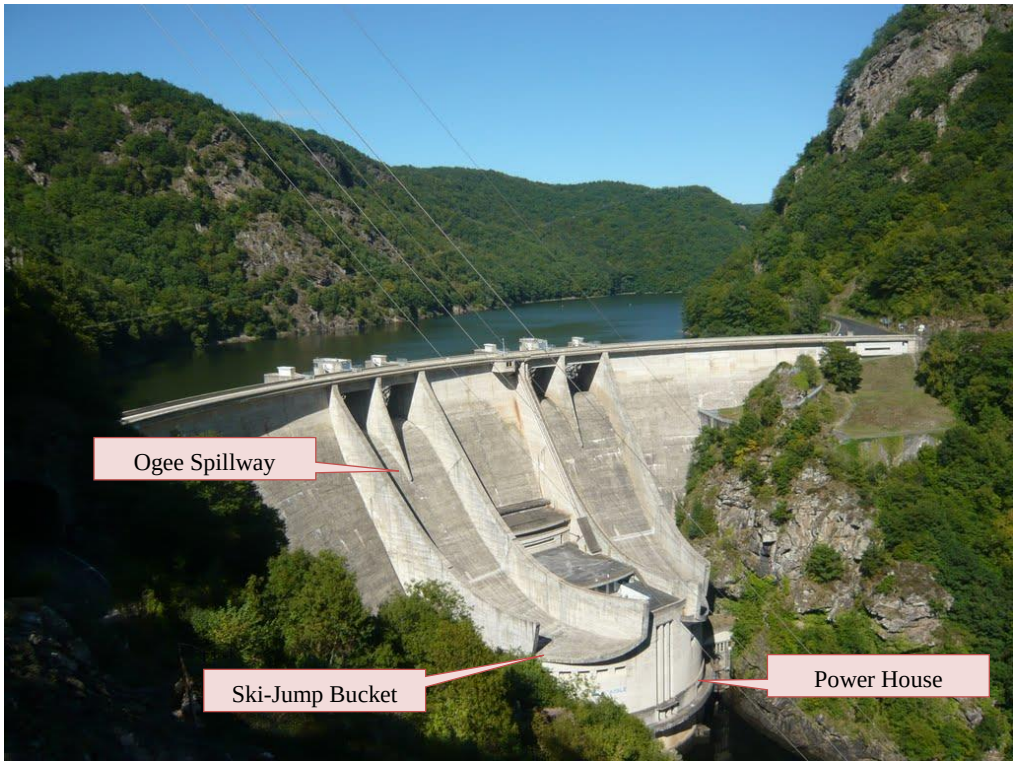


*FIGURE 2.3: L'AIGLE DAM TWIN SKI-JUMP SPILLWAY CHUTES ON THE DORDOGNE RIVER, FRANCE*

The studies of Balloffet (1961) were further validated by Chen & Yu (1965) where the pressure distribution along a cylindrical bucket was determined for an angle of deflection, $\alpha_b$ between 75° and 95° (from spillway chute to bucket lip) using the potential flow equations. The result of this study yielded similar trends to that of Balloffet's approach (Omidvarinia & Musavi Jahromi, 2013).

Viscosity in bucket flow was first researched by Chen & Yu (1965) and improved upon by Lenau & Cassidy (1969). They were able to determine the insignificance of the effect of viscosity in the bucket as well as the relationship between the relative bucket curvature, $h_1/r$, Froude number, $Fr$, and the maximum hydraulic pressure present on the bucket.

Ski-jump flow prototype findings were summarised in the studies of Rajan and Shivashankara Rao (1980) cited by Juon, et al. (2000) where a general design standard was achieved and is described as follows:

- cylindrical bucket shape

- bucket deflection angle in the range 20$^{o}$ to 40$^{o}$
- ratio of the bucket height to the bucket radius in the order of 0.1
- bucket radius represented as a function of the specific discharge and approach velocity
- cavitation consideration in the design of the bucket lip
- bucket lip well above tailwater elevation.

Mason (1993) took the findings of Rajan and Shivashankara Rao (1980) and expanded on them through additional studies where the following additions to the guidelines were recommended:

- minimum bucket radius three to five times the approach flow depth
- free board of side walls by accounting for the air-water flow bulkage
- lip angle or deflection angle between 20$^{o}$ and 35$^{o}$
- spread angle of jet in air about 5$^{o}$ to 10$^{o}$
- splitter teeth are not recommended due to cavitation risks

## 2.4 ENERGY DISSIPATION

One of the most important concepts in any hydraulic structure is its ability to dissipate energy. Energy dissipation efficiency is the one fundamental reason for all research into hydraulic structures. The question of how to convey water from a large dam to the downstream river without causing grievous harm to the environment, river or dam structure itself is one which has been on the mind of hydraulic engineers for decades. As dams become larger so does the amount of hydraulic energy.

## 2.5 ESSENCE OF HYDRAULIC ENERGY DISSIPATION

The inflow to every energy dissipating structure is said to have the characteristics of turbulent jets where the momentum is partly or totally defeated in a mixing process and therefore the jet form may define the dissipator's characteristics (Vischer & Hager, 1995).

The types of jets that may be seen in dissipating structures include:

- free jets,
- submerged jets,
- wall jets,
- surface jets,
- radial jets,
- oscillating jets,
- split jets,
- counter-current jets, and
- rotating jets.

### 2.5.1 ENERGY DISSIPATION BY EXPANSION AND DEFLECTION

A sudden expansion in the cross-sectional area of flow introduces an energy loss known as the Borda-Carnot loss. It can be described as a loss due to impact where a fast flowing current impacts with a slower current, which in turn promotes flow separation and a zone of large velocity gradients. Many energy dissipation structures are based on this principal for the reason that the tailwater velocity would be much smaller than the inflow velocity (Vischer & Hager, 1995).

In the case of a ski-jump, a free jet impacting on a pool of water is said to exhibit similar impact properties as that of a typical expansion and therefore can be classified as such. The impact of the high velocity free jet into a pool induces a rapid deceleration of the jet flow. However, efficient energy dissipation can only be warranted if the condition of an adequate cushion of water is satisfied.

### 2.5.2 ENERGY DISSIPATION BY AIR ENTRAINMENT

#### *2.5.2.1 Air Entrainment*

In open channel flow the presence of air increases the flows cross-sectional area which must be accounted for in the design of spillway and chute sidewalls. In addition the shear stress is reduced by the presence of air within the boundary layer therefore there must be a consideration for the increase of momentum especially in the design of a ski-jump spillway. Furthermore a mitigation of cavitation may occur in high-velocity flows when air is present (Falvey, 1990).

There are two ways in which air may be entrained into a flow. One of these ways is through self-aeration and the other is though impact with a surface.

#### *2.5.2.2 Self-Aerated Flow*

Surface air entrainment is a phenomenon that occurs in rapidly flowing water where air on the surface is mixed with the surface. This type of flow occurs naturally in rivers and is referred to by Falvey (1990) as white water. Hydraulic engineers refer to the entrapment of air by natural causes as self-aerated flow. Self-aerated flow is of particular interest to engineers as it influences velocity, depth of flow, energy dissipation and turbulence, as well as other flow characteristics. Their degree of influence is yet to be fully understood, (Thandaveswara, 2011). For self-aerated flow to occur there are two conditions that need to be satisfied (Vischer & Hager, 1998):

1. Fully turbulent flow must be present where the flow depth is equal to the boundary layer, and
2. The surface eddies must have a greater kinetic energy than that of the surface tension energy.

*Self-aeration on chutes*

Chanson (1993) conducted a study on self-aerated flows on chutes and spillways where the two conditions mentioned above are described in more detail. There are several explanations that exist in literature that describe the mechanisms behind self-aeration. According to Chanson (1993), Keulegan and Patterson (1940) were involved in the analysis of wave instability in open channel flow and their

findings suggested that if the Froude number, Fr, is greater than 1.5, then small breaking waves at the free surface entraps air into it by water droplets falling back into the water flow. Hino (1961) and Ervine and Falvey (1987) believed that the entrapment of air is the result of turbulent velocity fluctuations on the free surface. Chanson (1993) came to the conclusion that air entrapment occurs when both surface tension and gravity effects have been overcome due to a large enough level of turbulence.

### *Self-aeration on spillway*

Velocities entering a spillway chute are low and the characteristics of the flow exhibit a smooth transparent glass like surface. As the flow accelerates over the spillway the surface water becomes rougher and the transparency progressively diminishes until atmospheric air is completely infused and dispersed within the flow. The layer between the transparent glass like flow and the rougher flow is referred to as the boundary layer. Turbulence occurs and the boundary layer grows until it reaches the surface where the bubbles are distributed throughout the entire flow depth. This point is called the point of inception (Chanson, 1993). **Figure 2.4** shows the growth of the boundary layer until the point of inception. Prior research assumed that the point of inception occurred at a critical velocity and distance from the spillway chute entrance. Up to the inception point the pressure gradient, spillway curvature and approach velocity influence the velocity distribution. The flow depth, channel slope and roughness of the surface yield additional complications in the air entrainment process (Thandaveswara, 2011).

Directly downstream of the inception point, both air and water mix forming a layer that spreads progressively through the fluid. The growth rate of this layer is small and the distribution of air concentration gradually varies with distance from the point of inception. Eventually the growth rate becomes insignificant and flow becomes uniform. This region is referred to as the uniform equilibrium flow region (Chanson, 1993).

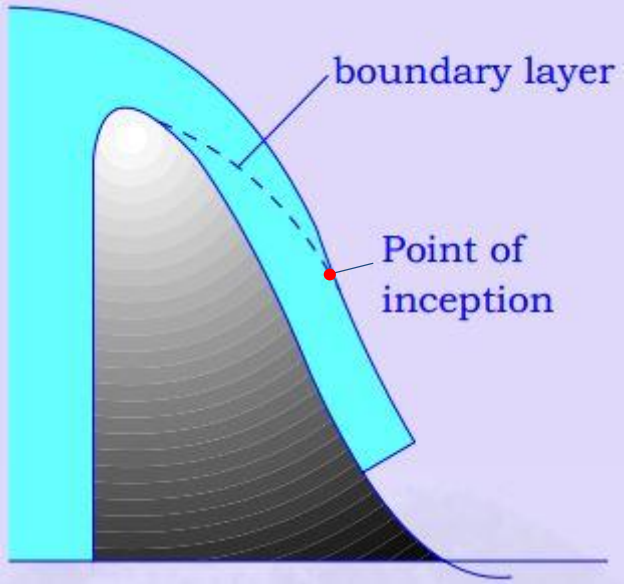


FIGURE 2.4 : GROWTH OF THE BOUNDARY LAYER *(THANDAVESWARA, 2011)*

#### *2.5.2.3 Aeration by Impact*

*Aerators*

Spillways and chutes releasing floods are a typical element of large dams. It is a protection measure for the dam against overtopping in the event of a flood where the dam water level would exceed the design elevation. With these high heads certain complications arise that do not need to be accounted for with smaller dams. One of the main problems with high-head spillways is cavitational damages to the spillway or chute. An important aspect of any large dam spillway design is to avoid cavitation to preserve the life of the spillway and dam. Chute aerators are a common design feature on most large dams. The aerators separate the high velocity flow from the spillway by means of a step in the spillway chute. This encourages air entrainment to occur from the lower surface of the water jet creating a better air water mixture and alleviating the onset of cavitation.

As mentioned above energy dissipation is in essence a process of mixing. The kinetic energy of a flow may be dispersed by a process in which a fast flowing current is introduced into a slow flowing one and vice-versa. This is the fundamental basis on which numerous energy dissipating structures are designed upon. Unfortunately high levels of kinetic energy dispersion are impossible to be achieved when mixing a fast flowing current with ambient air. Although every mixing process consumes energy, there is very little energy lost though the entrainment of air into a high velocity flow. The reason behind this is that impact between water and air is the underlying process where the densities of the two substances are approximately 999 kg/m$^3$ and 1.225 kg/m$^3$ respectively at a sea level with a temperature of 15$^o$C. Therefore depending on the temperature and pressure the density of water is 800 to 900 times that of air. As a result the losses due to impact are negligible, even with relatively high air concentrations (Vischer & Hager, 1995). Nowadays bottom aerators are used to combat and avoid cavitation on

spillway chutes and were once thought to also be an effective means of energy dissipation, which is no longer the case as stated by Vischer & Hager (1995).

### 2.5.3 ENERGY DISSIPATION BY JET DIFFUSION

According to Vischer & Hager (1998), the disintegration of a water jet traveling through the air may be enhanced by the following:

- approach turbulence,
- approach swirl,
- approach geometry,
- counter-current wind, and
- fluid properties.

Current studies on the disintegration of water jets are mostly carried out under a controlled laboratory environment where space and water supply limitations exist. Normally the diameters of the studies water jets are small in diameter and therefore significant surface tension and viscosity effects are present. There are a very few general results actually available for the disintegration of water jets in air due to the large number of influencing factors. From the study of their previously published information, Vischer & Hager (1995) were able to confirm that the enhancement of the disintegration process may be achieved by incorporation the following aspects into a water jet:

- a non-circular cross-sectional jet to counter the compactness,
- increase the turbulence level by ‘roughening’ the jet (consideration to cavitation),
- rapid bucket to air transition, and
- introducing air into the jet to create an air-water mixture at the take-off zone.

As mentioned in the previous section, air entrainment does not yield significant energy dissipation. This statement is only valid for energy dissipation in spillways and chutes where air entrainment is limited to the confines of the structure. If the degree of air entrainment is large enough the current may be transformed into a spray where the energy dissipation can be relatively substantial. Through the transformation from a water jet with air bubbles to a cloud of droplets in air the capacity of energy dissipation dramatically improves. The water droplets, now moving individually as opposed to a unit, are less resistant to the forces of air the smaller they are. Therefore these droplets would be greatly affected by a wind current.

With dam spillways in consideration the ski-jump and flip bucket type structures may generate considerable spray but they are limited in terms of energy dissipation. The reason they can only be classified as partial energy dissipators is due to the fact that their nappes are generally too thick to be dispersed completely over the course of their trajectory. For increased diffusion designers have been

known to add flaring gate piers and splitters either on the spillway crest or bucket (Vischer & Hager, 1995).

## 2.6 TYPES OF ENERGY DISSIPATING STRUCTURES

There are numerous energy dissipating structures that exist today, which can be grouped under three distinct types; stilling basins, bucket type energy dissipators and two stage stilling basins. Depending on the required project specifications, degree of energy dissipation and erosion control one or more of these energy dissipators highlighted in **Section 2.6.1** to **2.6.3** can be used alone or in combination (Bureau of Indian Standards, 2012).

### 2.6.1 STILLING BASINS

Stilling basins are the most common energy dissipating structures used in current time. The stilling basin type energy dissipators use the formation of a hydraulic jump and jet diffusion to alleviate the energy. There are several variations of the stilling basin type energy dissipators including (Bureau of Indian Standards, 2012):

a) Hydraulic jump type stilling basins:
   i. horizontal apron type, and
   ii. sloping apron type.
b) Jet diffusion stilling basins:
   i. jet diffusion stilling basin,
   ii. interacting jet dissipators,
   iii. free jet stilling basin,
   iv. hump stilling basin, and
   v. impact stilling basin.

### 2.6.2 BUCKET TYPE ENERGY DISSIPATORS

Three types of bucket energy dissipaters are listed below. These are the main three types of bucket type energy dissipators where option c) is the focus of this thesis and will be dealt with in detail throughout the remainder of this document:

a) Solid roller bucket,
b) Slotted roller bucket, and
c) Ski-jump (or flip or trajectory) bucket.

### 2.6.3 TWO STAGE ENERGY DISSIPATOR

Two-stage energy dissipators divide the energy dissipation system into two where the first stage, generally a stilling basin type dissipator, dissipates a major portion of the energy while the second stage dissipates the remaining. This is an effective alternative in a situation where excessive excavation is needed for an ordinary energy dissipator or when the river is situated in a deep gorge where the flow is

not aligned with the energy dissipator and therefore splitting the dissipator into two sections enables realignment. **Figure 2.5** shows three examples of two stage energy dissipators.

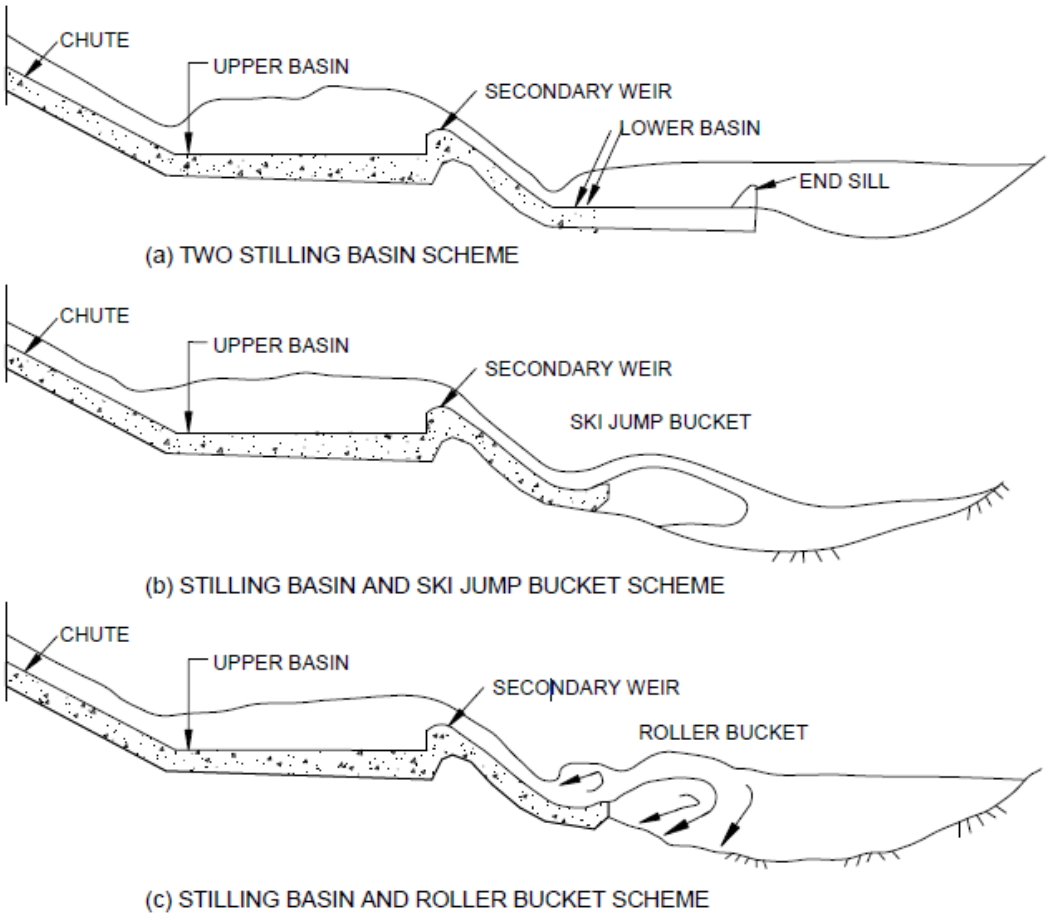


*FIGURE 2.5: TYPES OF TWO STAGE ENERGY DISSIPATORS (BUREAU OF INDIAN STANDARDS, 2012)*

## 2.7 SELECTION OF TYPE OF ENERGY DISSIPATORS

The decision an engineer is required to make of selecting a type of energy dissipator for a specific set of requirement is not an easy task even for the most experienced and competent hydraulic engineers. There is no fast way to approach the subject nor fixed criterion for the decision. The Bureau of Indian Standards (2012) suggests that the following points should be given adequate attention before giving a final selection of the type of energy dissipator to be utilised:

A. frequency and intensity of flood flows,
B. the degree of protection to be provided for very high floods,
C. type of dam and its spillway,
D. proximity of power house, tailrace and other structures,
E. nature of foundations,
F. velocity and nature of flow,
G. elevations of tailwater at various discharges,

H. type and amount of bed material rolling over the spillway,
I. safety of existing structures downstream, and
J. any other special consideration, such as the formation of deep plunge pools in close proximity to the dam or spillway.

The recommendations in the selection of energy dissipators highlighted by the Bureau of Indian Standards (2012) above can only be viewed as broad guidelines. The final selection can be made once model studies have been conducted where the concluding results are acceptable. **Sections 2.7.1** to **2.7.8** below expands on these recommendations.

### 2.7.1 TYPE OF DAM AND ITS SPILLWAY

Certain dam types have recommended energy dissipation types due to the ergonomics of the dam, as well as the material from which it is constructed. Usually earth dams are accompanied by a chute spillway where a hydraulic jump type energy dissipator is recommended including baffle blocks and endsills if necessary. Arch dams generally use free fall or drop spillways and require stilling deep pools for the energy dissipation of its plunging jets. Jet diffusion is the best type of energy dissipation for high velocity flows from bottom outlet works or high dams and therefore ski-jumps/ flip bucket or roller buckets may be implemented. However energy dissipation selection for a specific dam type may be subject to change in the presence of certain topographical features (Bureau of Indian Standards, 2012).

### 2.7.2 NATURE OF FOUNDATIONS

The nature of the foundations upon which the energy dissipating structure will be constructed may govern the type of structure. In the case that the river bed consists of solid rock, the most suitable energy dissipating structure could possibly be a bucket type one where at most short stilling basin is required. According to the Bureau of Indian Standards (2012), a hydraulic jump type stilling basin with a long apron including baffle blocks and end sill may be more suitable in a situation where the river bed is made up of softer material such as alluvial deposits or jointed and fractured rock.

### 2.7.3 VELOCITY OF FLOW

If high flow velocities are expected for the energy dissipator, in excess of 30 m/s, it is important to remember that the higher the velocity the more susceptible the structure is to cavitational damage in the event of negative surface pressures. It is therefore not recommended to implement flow velocity retarders such as baffling blocks within stilling basing or flow splitters/teeth on bucket type energy dissipators (Bureau of Indian Standards, 2012).

### 2.7.4 ELEVATION OF TAILWATER AT VARIOUS DISCHARGES

In order to produce an effective design the tailwater data and its accuracy is of utmost importance (Bureau of Indian Standards, 2012). Tailwater data should be retrieved and compiled into a tailwater rating curve where the downstream water depth/elevations are plotted against the discharge. This curve,

along with a hydraulic jump curve, is a prerequisite for the most efficient and economic hydraulic structures.

### 2.7.5 JUMP HEIGHT IS ALWAYS ABOVE THE TAILWATER DEPTH

The effect of the hydraulic jump being larger than the tailwater level is that the tailwater depth is insufficient to keep the hydraulic jump at the toe of the structure. The jump will attempt to move away from the structure and across the stilling basin at high velocity which may cause damage to the downstream riverbed. To alleviate this problem and achieve sufficient energy dissipation the Bureau of Indian Standards (2012) recommends the following in no particular order:

a) making the jump depth equal to that of the tailwater depth for all discharges by lowering the floor elevation downstream of the dam. This may lead to three alternatives,
   i. a horizontal floor but depressed below the river bed level,
   ii. a depressed floor but rising towards the downstream end, and
   iii. a depressed floor but sloping away from the toe of the dam.
b) stilling basin with baffles or stills at river bed level,
c) stilling basin with a low subsidiary dam downstream, and
d) ski-jump bucket.

### 2.7.6 JUMP HEIGHT IS LESS THAN THE TAILWATER DEPTH

When the tailwater depth is sufficiently higher than the hydraulic jump it is the inclination of the tailwater to submerge the jump resulting in high velocity flows traveling long distances along the riverbed underneath the tailwater. In order to correct this imperfect hydraulic jump Bureau of Indian Standards (2012) suggests the following modifications to improve energy dissipation:

a. sloping apron; and
b. roller bucket type of energy dissipators.

### 2.7.7 JUMP HEIGHT MORE THAN TAILWATER DEPTH AT LOW DISCHARGES AND LESS AT HIGHER DISCHARGES

In such a case where the hydraulic jump depth is greater than the tailwater at low discharges and lower at higher discharges it is recommended to artificially create sufficient water depth to ensure the hydraulic jump forms on the apron at lower discharges. The Bureau of Indian Standards (2012) recommends the alternatives below:

a) stilling basin with a low secondary dam; and

b) stilling basin with baffle piers or some form of dentate sill.

### 2.7.8 JUMP HEIGHT BELOW THE TAILWATER DEPTH AT LOW DISCHARGES AND ABOVE AT HIGHER DISCHARGES

For a condition such as this a few alternatives for its correction exists. The first option is to ensure sufficient tailwater depth in order to form a hydraulic jump during high flows by the construction of a secondary dam or to implement a sloping apron. The second option can be considered in the case where the downstream riverbed comprises of sound rock and therefore a bucket type energy dissipator may be implemented where for high discharges it acts as a ski-jump and for lower discharges as a roller bucker, (Bureau of Indian Standards, 2012).

## 2.8 SKI-JUMP ENERGY DISSIPATING STRUCTURES

A typical ski-jump energy dissipating structure as show in **Figure 2.6** consists of five main hydraulic sections:

1. control structure and approach chute,
2. deflection and take-off,
3. dispersion and trajectory of the water jet,
4. impact and scour of jet, and
5. downstream tailwater.

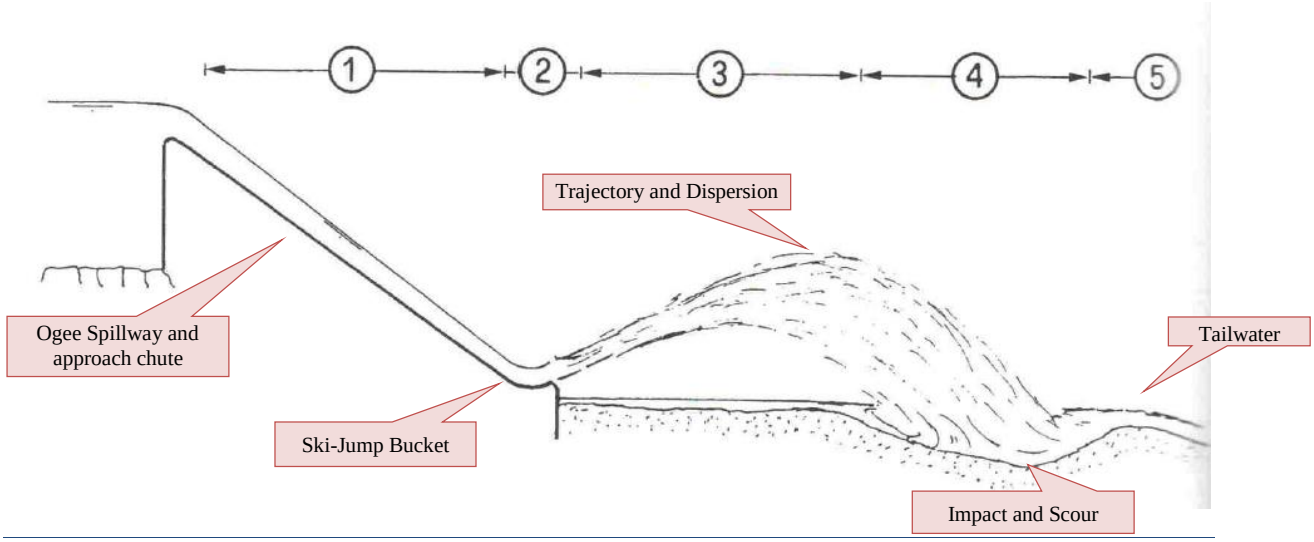


*FIGURE 2.6: SKI-JUMP REACH SECTIONS. (VISCHER & HAGER, 1998)*

### 2.8.1 RELEASE CONTROL STRUCTURE AND APPROACH CHUTE

The control structure of a ski-jump energy dissipating structure is considered to be one of the most important aspects along with the flip bucket. Usually on most dissipating structures the control structure is an ogee spillway. It is vital for this structure to be designed properly with the specific regional hydrologic records under consideration as it will govern the required capacity the spillway needs to convey.

The hydraulics of an ogee spillway can be determined based on the USBR (1987) guidelines. These guidelines state that the discharge over an ogee crest is given by the equation,

$$Q = CLH_e^{\frac{3}{2}} \qquad \textit{EQUATION 2.1}$$

Where: Q = discharge

C = variable discharge coefficient

L = Effective length of crest

$H_e$ = actual head being considered on the crest, including velocity of approach head, $h_e$.

The variable discharge coefficient, C, is dependent on the four variables given in the equation below:

$$C = C_0 \frac{C_e}{C_o} \frac{C_{inclined}}{C_{vertical}} \frac{C_s}{C_o} \qquad \textit{EQUATION 2.2}$$

Where

$C_o$ is the discharge coefficient for the design head and depends on the ratio of the approach depth, P to the design head, $H_o$, i.e. $P/H_o$. The factor $C_e/C_o$ is the ratio of coefficients and is dependent on the ratio of the actual head, $H_e$ to the design head, $H_o$ i.e. $H_e/H_o$. The inclination factor $C_{inclined}/C_{vertical}$ depends on the slope of the upstream face as well as the $P/H_o$ ratio. The factor $C_s/C_o$ is the discharge coefficient due to the apron effects and depends on the vertical position of the downstream apron.

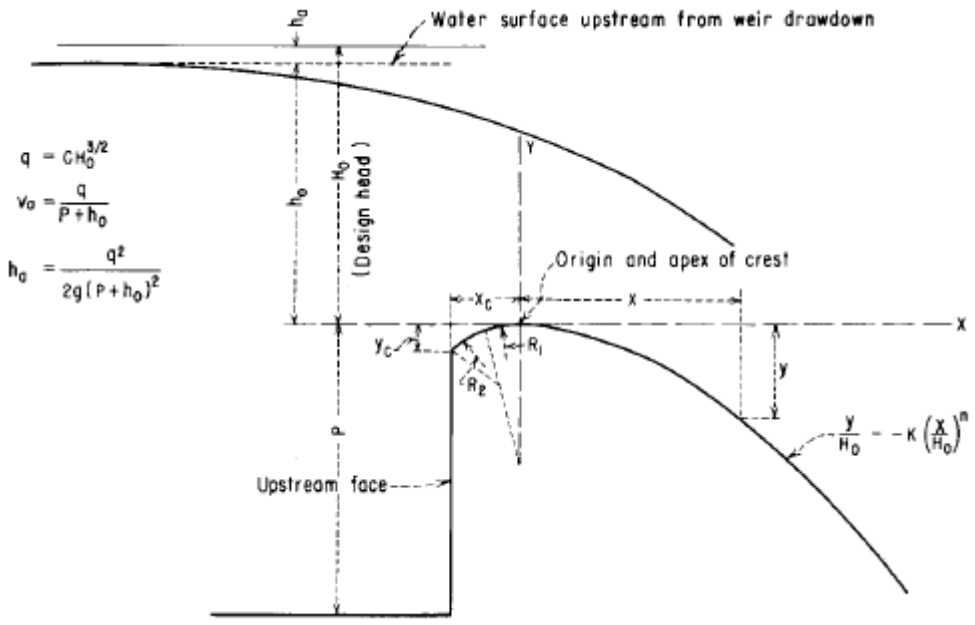


*FIGURE 2.7: ELEMENTS OF NAPPE-SHAPED CREST PROFILE (USBR, 1987)*

#### 2.8.1.1 Process for the Hydraulic Design of an Ogee Spillway

This section indicates the process one can follow for the hydraulic design of an ogee spillway. This process is valid provided the following parameters are known:

- design discharge,
- dam height, and
- spillway length.

*Flow depth*

With a known flow the actual head, $H_e$ can be found by rearranging **Equation 2.1** with an initial assumed variable discharge coefficient, C. The crest height of the spillway, P is generally a given design parameter. Typically the design head acts at 75% of a certain flood peak discharge. With this information the $P/H_o$ or $P/(0.75H_e)$ ratio can be obtained. The design head discharge coefficient can then be read off **Figure A- 3** in Appendix III. The ratio $C/C_o$ is read off **Figure A- 4** in the Appendix III with the aid of the $H_e/H_o$ ratio (1.333 for 75% Design Head). The other discharge coefficients are also read off **Figure A- 5** and **Figure A- 6** in the Appendix III.

Once all the discharge coefficients have been found the effective spillway length may be determined with **Equation 2.3** below where the net length of the spillway crest is given a value based on design specifications for the required flow rate per metre length ($m^3/s$ /m):

$$L = L' - 2(NK_p + K_a)H_e \qquad \text{EQUATION 2.3}$$

Where:

L = Effective length of crest,

L' = net length of crest,

N = number of piers,

$K_p$ = pier contraction coefficient,

$K_a$ = abutment contraction coefficient, and

$H_e$ = actual head on crest

The pier contraction coefficient, $K_p$, is affected by the shape and location of the pier nose, the thickness of the pier, the design head and the approach velocity. Pier contraction coefficients may be assumed as follows for conditions of design head (USBR, 1987):

- for square nosed piers with corners rounded on a radius equal to about 0.1 of the pier thickness: $K_p = 0.02$,
- for round-nosed piers: $K_p = 0.01$, and
- for pointed-nose piers: $K_p = 0.0$

The abutment contraction coefficient is affected by the shape of the abutment, the angle between the upstream approach wall and the direction of flow, the head in relation to the design head and the approach velocity. For design head conditions the following abutment contraction coefficients may be assumed (USBR, 1987):

- for square abutments with headwall at 90° to the flow direction, when $0.5H_o \leq r \leq 0.15H_o$: $K_a$=0.10, and
- for rounded abutments where $r > 0.5H_o$ and headwall is placed not more than 45° to the direction of flow: $K_a = 0.0$

where r is the abutment rounding.

By combining the discharge coefficients a new variable discharge coefficient is achieved through **Equation 2.2**. This process is iterated over until a constant value of C is achieved. Thus, resulting in a constant actual head ($H_e$) and design head ($H_o$) which will be used in the further calculations.

In order to separate the design head, $H_o$, into the velocity head, $h_a$, and the design water depth, $h_o$, **Equations 2.4** to **2.6** are simultaneously solved,

$$v_a = \frac{q}{P + h_o} \qquad \textit{EQUATION 2.4}$$

$$h_a = \frac{{v_a}^2}{2g} \qquad \textit{EQUATION 2.5}$$

$$H_o = h_o + h_a \qquad \textit{EQUATION 2.6}$$

Once $h_o$ and $h_a$ have been obtained the ogee profile can be determined.

According to the Minestry of Science and Technology (2013) the USBR conducted extensive experiments to obtain the profile of the overflow spillways with the upstream face either vertical or inclined at various angles. Standard shapes of crests were developed by the U.S Army Corps of Engineers (USACE) based on the USBR data.

*Downstream Profile*

The profile downstream of the apex of an ogee is plotted with **Equation 2.7** below,

$$\frac{y}{H_o} = -K\left(\frac{x}{H_o}\right)^n \qquad \textit{EQUATION 2.7}$$

Where K and n can be determined from **Figure A- 7**, which was taken from the USBR (1978) using the ratio $h_a/H_o$. Refer to **Figure 2.7** to identify the parameters of the ogee profile. Note that the origin is the ogee crest and has coordinates (0, FSL).

*Upstream Profile*

As can be seen from **Figure 2.7** there are two radii at different positions that define the upstream shape. The position and lengths of these radii are as follows:

- radius 1, $R_1 = 0.5H_o$ and is located directly below the ogee crest apex and spans a horizontal distance of $0.175H_o$ in the negative x-direction from the crest.
- radius 2, $R_2 = 0.2H_o$ and is located along the path of $R_1$ further most point. The arc of this radius ends at the upstream face which is located a distance of $0.282H_o$ ($x_c$) from the crest.

### 2.8.2 DEFLECTION AND TAKE-OFF OF SKI JUMPS

#### *2.8.2.1 Ski jump Spillway Bucket*

The deflection of the flow from its original direction is an integral element of a ski-jump energy dissipating structure. The bucket of a ski-jump is the component that deflects this flow and throws it into the air. The primary purpose of the flip bucket is to deflect flows of high velocity as far away from the dam and other operational features as possible. This is to protect the dam and spillway from scour and prevent dam failure. The secondary purpose of the flip bucket is to dissipate the required energy to prevent scour and erosion of the downstream river bed and valley banks.

Although, the ski-jump bucket itself is not considered to be an energy dissipator, it is an integral part of the energy dissipation system (Omidvarinia & Musavi Jahromi, 2013). Through friction the bucket is able to dissipate only a small amount of energy which is only a slight fraction of the total energy dissipated by the entire ski-jump system. A moderate amount of the energy dissipation occurs during the trajectory of the jet to the impact location where the jet spreads and frays. Along the trajectory path large volumes of air is entrained into the jet due to extreme turbulence. Significant spray occurs as a result of the portion of energy dissipated by the water and air interaction and its effects should be considered for adjacent structures, specifically in colder regions where sub-zero temperatures exist. The majority of energy dissipated by the ski-jump system is accounted for at the point impact of the jet with the tailwater and riverbed. This impact will have sufficient forces to change the topography of the riverbed, even if the bed material comprises of hard rock. It is therefore important that the use of ski-jumps should only be recommended in the case where bed scour caused by the impacting jet would not adversely affect the dam and other operational structures including the ski-jump flip bucket or be unacceptably destructive towards the environment. One major benefit in cases where the flip bucket may be implemented is that it is more economically viable than traditional stilling basins or roller buckets, however additional planning and design input is recommended due to the presence of more uncertainties with regard to appropriateness (U.S. Army Corps of Engineers, 1990).

In the design of a flip bucket, the parameters of primary significance are the bucket geometry (including the radius, length and lip height), the bucket boundary pressures and the jet trajectory characteristics. These parameters may be manipulated in a way so that desired specifications for a specific project is

met, such as trajectory length, spray, impact location as well as impact angle of the jet. In most cases the design of flip buckets is based upon observations derived from model studies. It is for this reason that any deviation from existing design guidelines should be accompanied by hydraulic model studies to validate operation (U.S. Army Corps of Engineers, 1990).

According to Vischer & Hager (1995), a poor design of the ski-jump bucket may cause the following problems:

- energy dissipation by dispersion may be insufficient if the bucket trajectory angle is too small.
- impact of the water jet may fall in an improper location, such as impacting the valley side instead of the river bed causing excessive erosion.
- if the bucket radius is too small, structural failure of the bucket may occur due to high pressure loads.

### *Plain Flip Bucket*

When it comes to ski-jump energy dissipators sometimes a simplistic flip bucket design is the most suited for the spillway in question. This is purely due to economic reasons. There is also very limited research available on alternative flip bucket designs. Most research, although also limited, has been conducted on the conventional flip buckets including the triangular-shaped flip bucket and the circular-shaped flip bucket.

#### *Circular-Shaped Flip Bucket*

The circular-shaped flip bucket (**Figure 2.8**) is the traditional flip bucket used for ski-jump energy dissipators. This bucket is utilised the most because of its simplistic design including a uniform radius and deflection angle. Extensive research has been conducted on this type of ski-jump bucket by countries such as America, China and India, each with their own guidelines.

Steiner, et al. (2008) investigated the ski-jump hydraulics of the circular-shaped flip bucket in a physical model that resulted in a generic design criteria for the flip bucket geometry angle and radius, as well as jet trajectories and bucket pressures.

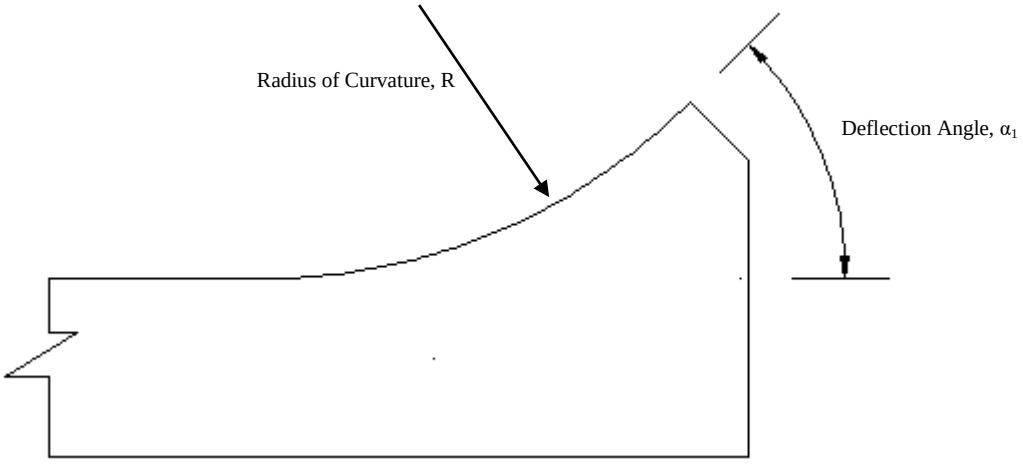


*FIGURE 2.8: CIRCULAR-SHAPED FLIP BUCKET*

The plain circular-shaped flip bucket may be accompanied by diverging sidewall. This slightly enhances the dispersion of the jet trajectory. The following equation governs the maximum angle with which the sidewalls may be diverted (USBR, 1987):

$$tan\,\alpha = \frac{1}{3F_o} \qquad \textit{EQUATION 2.8}$$

Where: $F_o$ is the Froude number at the begining of the contraction $= v_o/(gh_o)^{1/2}$

$\alpha$ = angular variation of side walls with respect to channel centreline

v = velocity at the beginning of the contraction

h = depth at the beginning of the contraction

*Triangular-Shaped Flip Bucket*

An attractive alternative to the regularly implemented circular-shaped ski-jump bucket is the triangular flip bucket, also known as triangular wedge-shaped flip bucket that best describes its form. This substitute is said to be attractive for specifically two reasons namely, it is easy to construct in comparison to the traditional circular buckets and is the basis for three-dimensional flip bucket design (Steiner, et al., 2008). However, it was unknown whether the hydraulic performance equalled that of the circular-shaped flip bucket. **Figure 2.9** shows a simple sketch of a triangular-shaped flip bucket.

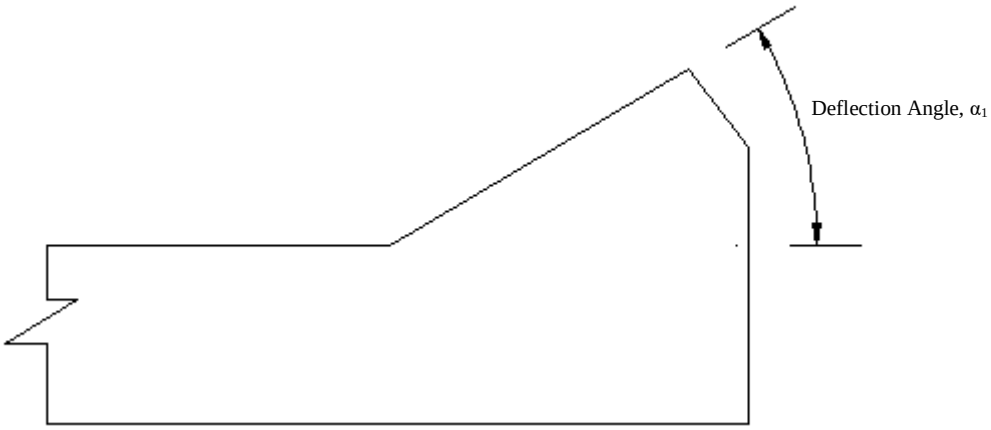


*FIGURE 2.9: TRIANGULAR-SHAPED FLIP BUCKET*

For the purpose of comparing the triangular-shaped flip bucket to the conventional circular-shaped flip bucket research was undertaken by the Laboratory of Hydraulics, Hydrology and Glaciology in Zurich. This facility conducted experiments where a triangular wedge-shaped bucket was slotted into a flume previously used to conduct experiments on a circular-shaped bucket. The outcome of this experiment was to answer three specific questions (Steiner, et al., 2008):

- What hydraulic performance differences exist between the circular and triangular shaped buckets?
- What is the extent of energy dissipation across a ski-jump?
- What choking flow characteristics are present in triangular-shaped buckets?

This systematic investigation concluded that from visual observations no apparent disadvantages were perceived in the geometry when compared to the conventional ski-jump bucket, although hydraulically speaking there were definite differences. It was determined that the peak dynamic pressure was substantially greater in magnitude for the triangular-shaped bucket than that of the circular-shaped bucket, however the total dynamic pressure force was smaller in comparison, due to the long extension of the pressure load of the circular-shaped bucket. It was also concluded that the triangular-shaped flip bucket may be both cheaper and less complicated to construct (Steiner, et al., 2008). **Figure 2.10** shows three photographs taken during the investigation of Steiner, et al. (2008).

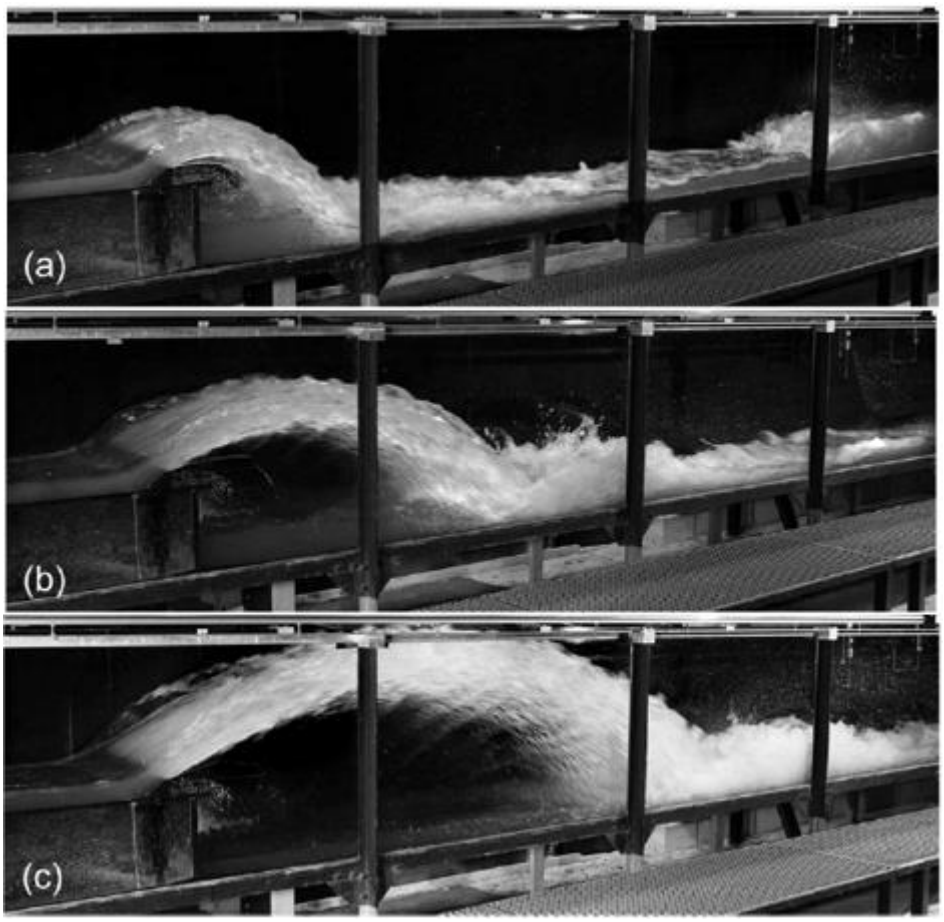


*FIGURE 2.10 : PHOTO SERIES OF TRIANGULAR WEDGE-SHAPED SKI-JUMP (A) $F_O$ = 3, (B) $F_O$ = 5, (C) $F_O$ = 7 (STEINER, ET AL., 2008)*

### *Deflector Bucket*

In terms of the research that has been conducted on deflector buckets, one could say that little attention has been received, even though these structures exist in numerous locations.

One of these studies includes an experimental setup piloted by Omidvarinia & Musavi Jahromi (2013) in the hydraulics laboratory of Shahid Chammran University in Iran where various deflector designs were tested on an ogee spillway with a deflector bucket for numerous flows and tailwater depths. The purpose of this hydraulic experiment was to determine the amount of energy dissipation in comparison to an ogee spillway without a deflector. All tests were conducted in a 15m long, 0.3m wide and 0.5m high flume with flows of up to 25 litres per second.

### *Conversion/ Slit-Type Flip Bucket*

In the last 20 years, China has taken a keen interest in large-scale hydropower projects at high dams and have undergone rapid development in this field. Due to the large unit discharges and deep valley topography associated with these large dams many new challenges have been faced concerning energy

dissipation and scour control. With this in mind, the slit-type flip bucket proved to be highly efficient due to their geometric characteristics (Wu, et al., 2012).

The contracted slit deforms the approach flow by a transverse contraction and longitudinal extension of the jet at the lip of the flip bucket. In simple terms the jet is changed into a higher and narrower one. This deformation is said to increase the flow dispersion by promoting air entrainment and the turbulence of flow thereby greatly increasing energy dissipation (Wu, et al., 2012). On a traditional flip bucket the trajectory angles of the upper and lower boundaries of the jet are roughly equal, however on the slit type flip bucket the trajectory angles of the upper and lower boundaries can vary from -10° to +45° (Vischer & Hager, 1995).

The jet from a slit-type bucket can achieve acceptable aeration and diffusion, including motion and turbulent diffusion, due to the different motion directions existing in the jet particles and therefore differing from traditional buckets (Wu, et al., 2006). **Figure 2.11** shows the difference in impact scour profile of a slit type flip bucket.

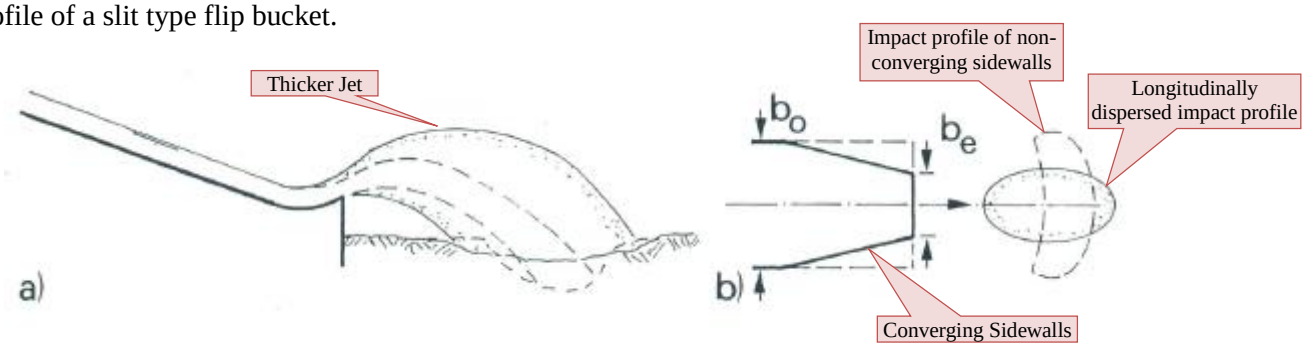


*FIGURE 2.11: SLIT-TYPE FLIP BUCKET TRAJECTORY AND IMPACT PROFILE (VISCHER & HAGER, 1995, P. 118)*

In the case of a contracted terminal overfall, various types of flow may occur depending three main parameters, the contraction angle θ, the convergence ratio $\beta_s = b_e/b_o \leq 1$ (refer to **Figure 2.11 (b)**), and the approach Froude number $F_o = V_o/(gh_o)^{1/2}$. The flow types below are depicted in **Figure 2.12** (Vischer & Hager, 1995):

a) hydraulic jump due to chocking,
b) low degree of jet flow spreading,
c) sufficient degree of jet flow spreading, and
d) overforced flow with large shock formation.

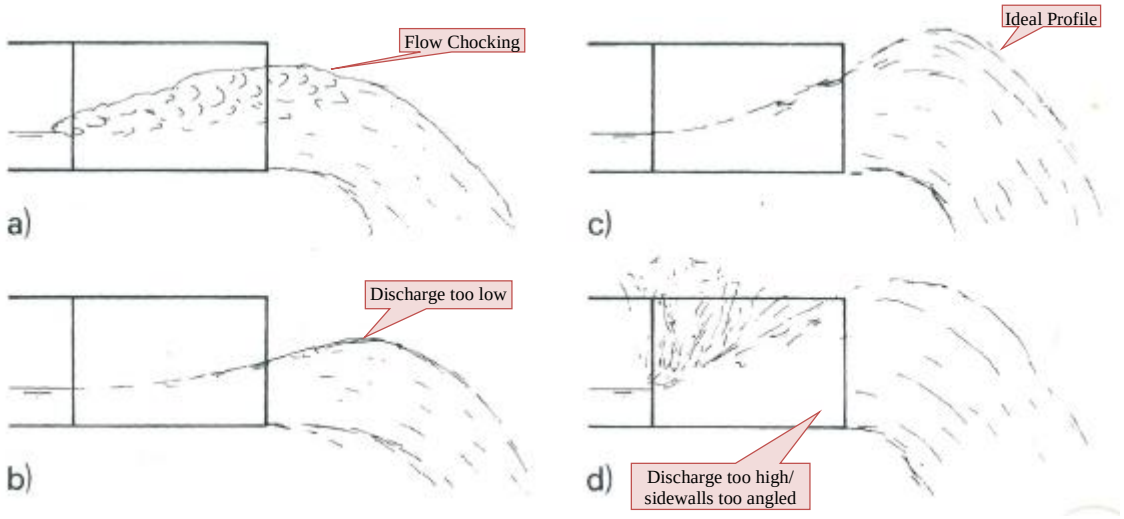


*FIGURE 2.12: FLOW TYPES AT TERMINAL CONTRACTED OVERFALL (VISCHER & HAGER, 1995, P. 118)*

With reference to **Figure 2.12** flow type c) is desired for optimal performance of the slit-type terminal overfall. According to Vischer & Hager (1995), for a Froude number of $4< F_o<10$, the convergence ratio $\beta_s$ should range from 1/4 to 1/6. For the slit-type flip bucket, the flow types are similar to that of the contracted terminal overfall. It is also strictly recommended that the convergence angle, $\beta_s$ of the sidewalls is no greater than 1:4 (length: width) which is relatively $14^o$. It is believed that angles greater than $14^o$ for Froude numbers in excess of 10 create forces on the sidewalls which tend to project water vertically instead of channelling it.

Two successful examples of the slit-type flip bucket ski-jump are the 157m high Dong Jiang hydropower project located on the Lishui River southwest of Zixing City in the Hunan Province (**Figure 2.13**) and the 200.5m high Guangzhao Dam located on the Beipan River near Guangzhao in the Guizhou Province (**Figure 2.14**).

*FIGURE 2.13: SLIT-TYPE FLIP BUCKET OF DONG JIANG DAM SPILLWAY (GUOCHEN, 2013)*


*FIGURE 2.14: SLIT-TYPE FLIP BUCKET OF GUANGZHAO DAM SPILLWAY (THOMAS, 2013)*

### 2.8.3 TRAJECTORY

#### *2.8.3.1 Transverse Jet Expansion*

According to Vischer & Hager (1998) the reanalysis of a previous Russian based study of the transverse jet expansion of a rectangular jet showed that it is mainly dependant on the bucket flow depth relative to the fall height, $H_S$, and the unit discharge relative to the spillway length, $\bar{q} = q/\left(gL_s{}^3\right)^{1/2}$. From experimental data the following empirical formula (**Equation 2.9**) for the approximation of the transverse jet expansion angle $\beta_j$ was determined:

$$tan\,\beta_j = \frac{1.05(h_1/H_s)^{1/2}}{tanh(6\bar{q}^{1/3})} \qquad \textit{EQUATION 2.9}$$

Where $h_1$ is the flow depth on the ski-jump bucket,

$H_s$ is the head above the ski-jump bucket invert, and

$\bar{q}$ is the unit discharge relative to the spillway length.

This estimation of $\beta_j$ is very important in the determination of the impact zone of a ski-jump jet and typically ranges between 5° to 10° (Vischer & Hager, 1998). With all theoretical equations there are parameters and conditions which are impossible to account for, therefore prototype values may differ considerably. It is important to note that the transverse jet expansion and impact widths for design purposes should not be based solely on the theoretical values but also on physical model studies. **Figure 2.15** show a definition sketch for the transverse jet expansion angle.

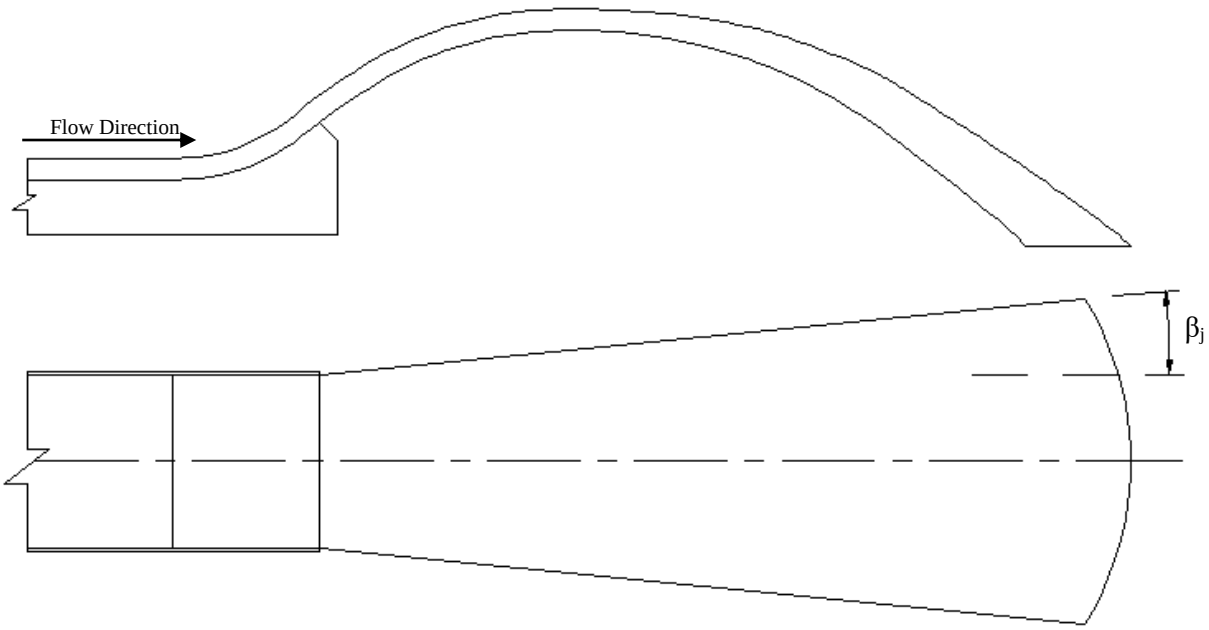


FIGURE 2.15: TRANSVERSE JET EXPANSION

### 2.8.3.2 Jet Trajectory Geometry

Free jet computations are conducted with the use or parabolic trajectory that can be described as "the curve of a mass point of constant density under the influence of gravity" (Wahl, et al., 2009). The trajectory the jet adopts is dependent on the available flow energy at the lip, as well as the angle at which the jet exits the ski-jump bucket. Other factors affecting the jet trajectory that cannot be quantified accurately include jet disintegration and aerodynamic interactions. Therefore, only a simplified theoretical approach can be undertaken in the computation of jet trajectory where a general air resistance factor accounts for the energy losses. It is important to note that the theoretical jet trajectories may differ considerably from observed trajectories.

The trajectory profile of a water jet may be determined with **Equation 2.10** (USBR, 1987, p. 387), with the origin of the coordinates situated at the end of the flip bucket lip. This equation plots the theoretical path the water jet would follow as it leaves the flip bucket.

$$y = x\,tan\alpha_j - \frac{1}{4kH_j cos^2\alpha_j}x^2 \qquad \text{EQUATION 2.10}$$

Where $H_j = {v_j}^2/2g$ is the take-off velocity head with take-off velocity, $v_j$,

y is the vertical coordinate of the jet trajectory with the bucket lip as the origin,

x is the horizontal coordinate of the jet trajectory with the bucket lip as the origin,

$\alpha_j$ is the angle of deflection of the water jet, and

k is the coefficient of air resistance.

*Derivation of the trajectory profile equation*

The following theoretical kinematic equations of motion were used for the derivation of **Equation 2.10** where parameters x, $v_j$, $v_i$, g and t represent the kinematic quantities displacement, initial velocity, final velocity, acceleration and time.

$$x = v_j t \qquad \text{EQUATION 2.11}$$

$$v_i^2 = v_j^2 + 2gx \qquad \text{EQUATION 2.12}$$

$$v_i = v_j + gx \qquad \text{EQUATION 2.13}$$

$$x = v_i t + \frac{1}{2} g t^2 \qquad \text{EQUATION 2.14}$$

Where **Equation 2.11** uses the horizontal component of velocity and **Equation 2.12**, **Equation 2.13** and **Equation 2.14** use the vertical component of velocity.

For projectile motion the maximum trajectory elevation is where the slope is equal to zero, therefore the vertical component of velocity is equal to zero at this point. With the use of **Equation 2.12** and taking the initial vertical component of the velocity as $v_j sin\alpha_j$. The maximum jet height above the bucket lip $h_m$ can be derived as follows:

$$(0)^2 = (v_j sin\alpha_j)^2 + 2(-g)h_m$$

$$\therefore \quad h_m = \frac{v_j^2 sin^2\alpha_j}{2g}$$

Now velocity head, $H_j = v_j^2/2g$

$$\therefore \quad h_m = H_j sin^2\alpha_j$$

USBR (1987) states that in order to obtain a better estimate for the trajectory profile of a water jet a coefficient, k is needed which compensates for energy loss, air resistance causing a velocity reduction, internal turbulence and jet disintegration. Theoretical computations use a value of 0.9 to account for these losses.

**Equation 2.13** represents the maximum trajectory elevation after applying the air resistance coefficient.

$$h_m = kH_j sin^2\alpha_j \qquad \text{EQUATION 2.15}$$

Using the horizontal component of the velocity, $v_j cos\alpha_j$ the horizontal distance from the bucket lip to the maximum jet elevation, $x_m$ is derived using **Equation 2.11**:

$$x_m = (v_j cos\alpha_j)t$$

The time it takes the trajectory to reach it peak can be determined from **Equation 2.13** whereas before the initial velocity is the vertical component and the final velocity is zero:

$$0 = v_j sin\alpha_j + (-g)t$$

$$\therefore \quad t = \frac{v_j sin\alpha_j}{g}$$

Now substituting in time yields:

$$x_m = (v_j cos\alpha_j)\frac{v_j sin\alpha_j}{g}$$

Simplifying with $H_j = {v_j}^2/2g$ and applying the coefficient for air resistance gives **Equation 2.16** below.

$$x_m = 2kH_j sin\alpha_j cos\alpha_j \qquad \textit{EQUATION 2.16}$$

Once the position ($x_m$, $h_m$) for the maximum trajectory elevation has been found it is possible to determine the trajectory profile equation. **Equation 2.17** is the general equation for all parabolic curves which is the same profile as can be expected from trajectory motion.

$$y = ax^2 + bx + c \qquad \textit{EQUATION 2.17}$$

By substituting in three coordinates along the trajectory path the general ski-jump trajectory profile can be determined. The first coordinate is determined by assuming that the origin of the trajectory is at the ski-jump bucket lip, thus by substituting (0,0) into **Equation 2.17** parameter c can be found to be 0.

$$0 = a(0)^2 + b(0) + c$$

$$\therefore \quad c = 0$$

The second coordinate is the maximum elevation position of the trajectory ($x_m$, $h_m$) which has been previously determined as **Equation 2.15** and **Equation 2.16**. The mathematical steps for substituting this position into **Equation 2.17** are shown below taking into account that c = 0 and $b = -4akH_j sin\alpha_j cos\alpha_j$.

$$kH_j sin^2\alpha_j = a(2kH_j sin\alpha_j cos\alpha_j)^2 + b\left(2kH_j sin\alpha_j cos\alpha_j\right) + 0$$

$$\therefore \quad b = \frac{kH_j sin^2\alpha_j - 4a(kH_j sin\alpha_j cos\alpha_j)^2}{\left(2kH_j sin\alpha_j cos\alpha_j\right)}$$

$$\therefore \quad b = \frac{tan\alpha_j}{2} - 2akH_j sin\alpha_j cos\alpha_j$$

The second unknown, b, can be determined by assuming that at the maximum elevation position of the trajectory ($x_m$, $h_m$) the gradient is zero i.e. the derivative of **Equation 2.17** is equal to zero.

$$\frac{dy}{dx} = 2ax + b = 0$$

$$\therefore \quad 2a(2kH_j sin\alpha_j cos\alpha_j) + \frac{tan\alpha_j}{2} - 2akH_j sin\alpha_j cos\alpha_j = 0$$

$$\therefore \quad a = -\frac{tan\alpha_j}{4kH_j sin\alpha_j cos\alpha_j}$$

$$\therefore \quad a = -\frac{1}{4kH_j cos^2\alpha_j}$$

Now substituting a back into b;

$$b = \frac{tan\alpha_j}{2} - 2(-\frac{tan\alpha_j}{4kH_j sin\alpha_j cos\alpha_j})kH_j sin\alpha_j cos\alpha_j$$

$$\therefore \quad b = tan\alpha_j$$

Finally substituting parameters a, b and c into **Equation 2.17** gives

$$y = -\frac{1}{4kH_j cos^2\alpha_j}x^2 + tan\alpha_j x$$

Air resistance is an important factor to consider when designing for a ski-jump especially in large dams where high heads are used. Although for flow velocities less than 20m/s air resistance does not make much of an impact, however, the higher the flow velocity the larger the air resistance. It is reported that for flow velocities of 40m/s air resistance may affect the horizontal throw distances of a ski jump jet trajectory by as much as 30% from the theoretical value (FEMA, 2010).

#### *2.8.3.3 Spray*

Air entrainment into the trajectory jet of a ski-jump is an important aspect of the energy dissipation system as a whole. This interaction of air and water creates the white water which can be seen on any ski-jump energy dissipator. The air present around the water particles promotes further separation of the water jet to a point where some of it becomes spray. There are specifically four types of spray that may occur within a water jet namely, (1) splash drop, (2) rainstorm, (3) atomisation by rain and (4) atomisation by wind (refer to **Figure 2.16**).

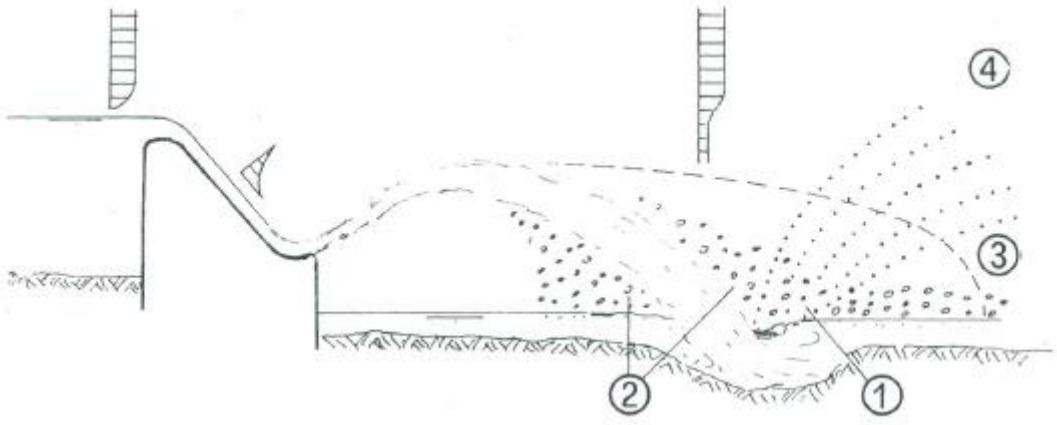


*FIGURE 2.16: CLASSIFICATION OF SPRAY FLOW INDUCES BY SKI-JUMP (VISCHER & HAGER, 1995)*

The spray produced by a ski-jump jet is a positive sign of good energy dissipation as there is a lot of air entrainment into the system. However, there are negative effects of the spray, one of these is that there is generally a high moisture content created by the spray which may damage equipment within structures surrounding the dam. In dams with high siltation levels there is a concern with corrosion of

metals. Another negative effect is that in colder climates where freezing conditions exist the spray settles on structures as an ice layer which continuously builds itself creating large ice blocks to form which may sometimes impede the correct operation of the ski-jump (FEMA, 2010). **Figure 2.17** shows an example of a ski-jump where large areas of solid ice have formed due to the spray.

*FIGURE* 2.17*: OPERATION OF THE FLIP BUCKET CAUSED SIGNIFICANT ICING DUE TO WATER VAPOUR* (FEMA, 2010)

### 2.8.4 IMPACT AND SCOUR OF JET

The following part of this section will describe the scour phenomenon downstream of the spillway. Scour is a process that occurs in both stilling basin and plunge pool type energy dissipators, but due to the main focus of this thesis being on the topic of ski-jump energy dissipators that utilise the assistance of plunge pools in their process of energy dissipation, scour formation in stilling basins will not be discussed while plunge pool scour will be explained in detail.

One of the major engineering concerns that has been a recurring topic for a long time is the spilling of excess flood waters from dams. One of the main contributing factors to this concern is the different kinds of erosion, specifically local erosion, which may be referred to as scour. Scouring may be defined as “a dynamic process ruled by the interaction between air, water and rock” (Gardo & Lindholm, 2013). Certain hydraulic structures are able to convey the excess flood waters to the downstream river but not without numerous risks that need consideration. The discharge from such structures may potentially cause scour to their foundations, as well as the river bed in the case where the strength of the river bed is exceeded by the impact force of spilled water.

In the process of an impacting jet upon the tailwater and river bed downstream of a ski-jump energy dissipator, air is entrained into the jet causing a reduction in energy and ultimately a reduction in the scour potential of the impacting jet on the river bed. The scour of side embankments to a river and structure toe may occur as a result of a poorly designed ski-jump where the topographical and geological parameters are not adequately taken into consideration. A design such as this has the potential to jeopardise the integrity of the valley slopes or the structure itself causing erosion, landslides and even structural failure. An example of an inappropriately ski-jump design is the Nacimiento Dam ski-jump in California, where after experiencing a flood in 1969 a scour basin of tens of meters was witnessed (Heller, 2009).

According to Heng, et al. (2009), there are three major effects of the scouring process including:

- the endangerment of structural stability through structural failure or increased seepage,
- downstream riverbed and valley side slope endangerment, and
- the deposition of eroded material far downstream of the structure resulting in elevated tailwater levels at the structure.

It is therefore highly imperative that a prediction for the scour impacts be determined for a time-varying scenario, as well as with reference to structural design.

For the safety evaluation of hydraulic structures relating to scour, two physical processes are of the utmost importance, namely hydrodynamic uplift and hydrodynamic jacking. Hydrodynamic jacking is a process in which the rock mass is broken up through the propagation of impact dynamic pressures into the joints and fractures of the underlying rock mass, while hydrodynamic uplift is the process which ejects the broken up rock mass from the river bed. These two processes are considered to be somewhat complex and include phenomena of transient pressure waves including oscillations and resonance within the rock mass faults (Bollaert & Schleiss, 2003).

#### *2.8.4.1 Estimation of Scour*

The study of scour of a dam structure and its downstream river reach is generally conducted under the controlled conditions of reduced scale physical models. According to De Almeida Manso (2006), scour is a function of the following:

- jet type and trajectory length,
- discharge time series,
- tailwater pool depth, and
- impact resistance of the riverbed including rock characteristics and is mechanical condition.

Numerous uncertainties exist within each of these above mentioned properties and therefore an estimate for the scour depth and profile which is likely to be achieved over the dam lifetime is the priority in

most practical cases. In the process of this estimate it is possible to identify and consider additional protection measures.

There are several methods that exist for the prediction of ultimate scour, which is defined as "the scour depth that corresponds to an equilibrium situation" (De Almeida Manso, 2006). These methods can be divided into four groups; namely hydrodynamic methods, empirical methods derived from observations of models and prototypes, semi empirical methods and physical based methods.

### *2.8.4.2 Scour in plunging pool*

The formation of scour in a plunge pool usually takes place at the location of the impingement of the free falling jet from a ski-jump spillway on the tailwater surface. For many years scour from a free falling jet has become a major concern for the stability of the downstream channel as well as the hydraulic structure itself. **Figure 2.18** shows a definition sketch for the parameters involved in the scour of a ski-jump plunge pool. The parameters in **Figure 2.18** are defined as follows:

- H is the energy head at the ski-jump bucket,
- $H_1$ is the energy head in the downstream tailwater,
- R is the radius of curvature of the ski-jump bucket,
- θ is the deflection angle of the ski-jump bucket,
- GL is the original ground level of the river bed,
- dw is the depth of water at the downstream tailwater,
- TWL is the tailwater level,
- q is the unit discharge relative to the ski-jump width, and
- t is the depth of scour relative to the TWL.

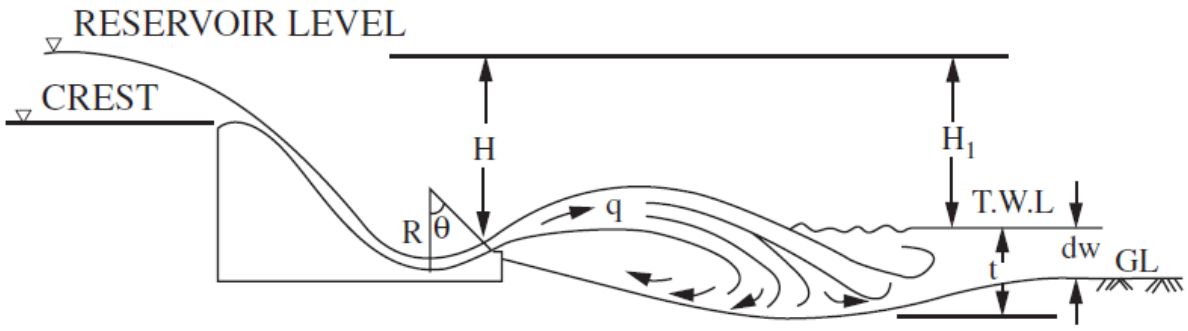


*FIGURE 2.18: SCOUR IN PLUNGING POOL DEFINITION SKETCH (AZMATHULLAH, ET AL., 2006)*

This process of scour formation can be divided into six successive physical-mechanical processes. **Figure 2.19** highlights these processes and their locations.

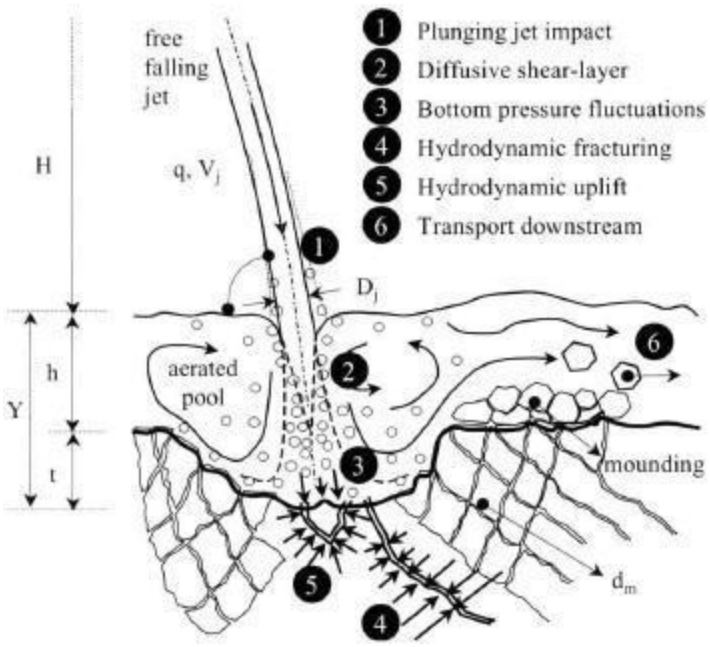


*FIGURE 2.19: PHYSICAL-MECHANICAL PROCESSES ASSOCIATED WITH PLUNGE POOL SCOUR (BOLLAERT & SCHLEISS, 2003)*

The first process is the plunging jet impact which is the initial impingement of the jet into the tailwater surface. This is followed by a diffusive shear-layer which created turbulence within the surrounding water. The third process occurs when the jet comes into contact with the bed rock where fluctuating pressures may be observed. Hydrodynamic fracturing or jacking then occurs which may be intensified by air locking, followed by hydrodynamic uplift which were both previously described. The separation and uplift of single block mass initiates the final process of transportation which includes the conveyance of the broken-up rock mass to a downstream location where velocities and turbulence are small enough to allow settling and deposition also referred to as mounding (Bollaert & Schleiss, 2003).

### 2.8.5 ENERGY DISSIPATION OF SKI-JUMP TYPE ENERGY DISSIPATING STRUCTURE

In modern spillway designs it is common to see free falling jets used as the preferred method for increased energy dissipation which may be achieved from a ski-jump type energy dissipator with a flip bucket. The ski-jump type energy dissipator was initially used in the early 1950's where proceeding that date was further developed with the assistance of scaled models. The ski-jump energy dissipator is regarded to be an economic alternative to the stilling basin type energy dissipators in situations where favourable geological conditions exist.

As previously mentioned there are specifically five main hydraulic sections within a ski-jump energy dissipating structure namely, the control structure and approach chute, deflection and take-off, dispersion and trajectory, impact and scour, and the downstream tailwater. Individually these hydraulic sections do not dissipate a substantial amount of energy but as a system, energy dissipation may be seen as large.

At large dams with large spillway discharges the magnitude of energy that must be dissipated to prevent erosion of the downstream river is massive. It is therefore necessary to incorporate energy dissipating systems into all aspects of a spillway design.

The conveyance of water from the dam to the downstream channel involves several hydraulic phenomena and is therefore best to consider the energy dissipation process upon a spillway in five different stages as depicted in **Figure 2.20** (Novak, et al., 2007):

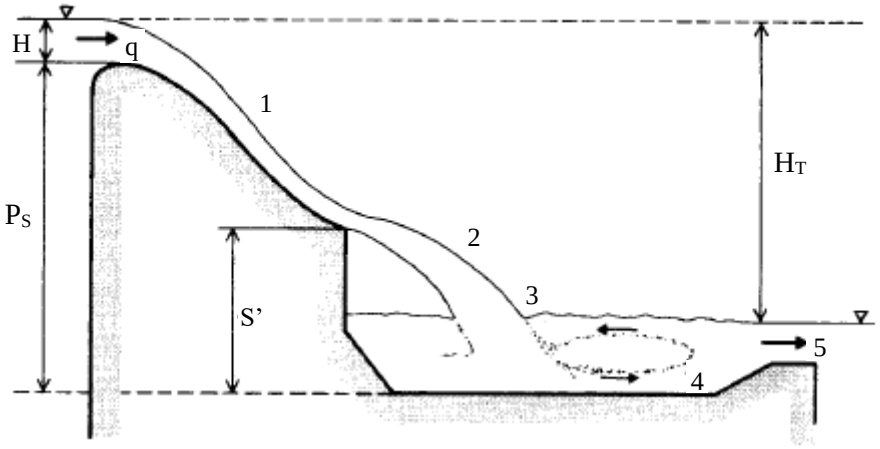


*FIGURE 2.20: DEFINITION SKETCH FOR THE FIVE PHASES OF ENERGY DISSIPATION (NOVAK, ET AL., 2007).*

1. On the spillway surface,
2. In a free-falling jet,
3. At impact into the downstream pool,
4. In the stilling basin, and
5. At the outflow into the river

The energy dissipation perceived in the trajectory jet is not very significant whether the jet is solid black water with no air entrainment or more commonly disintegrated white water. There is only about 12% of the total energy that is dissipated by the ski-jump jet alone. Energy dissipation on a ski-jump spillway may be considerably enlarged by separation of the overfall jet into multiple streams that introduces additional air entrainment or through orientating two ski-jump spillways in such a way that their jets collide over the river.

When referring to the phases of energy dissipation of spillways (**Figure 2.20**), the third phase is considered to yield substantial energy dissipation benefits. This phase includes the impact of the jet trajectory into the downstream plunge pool. Most of the energy losses in the first three phases are due to the impact of water with either the spillway surface or air and the compression of air bubbles. In addition to these the third phase induces the impact of a high velocity jet with a relative low velocity water body.

## 2.9 CAVITATION

Damage to hydraulic structures is the result of several mechanisms, where cavitational damage is seen as the greatest contributor. Cavitation of hydraulic structures may be caused by a variety of conditions. Surface irregularities is an example of one of these conditions, where cavitational damage is caused by the downstream end of collapsing bubbles. With time the concrete surface will be stripped exposing the aggregate and leaving an elongated hole in its place. This rough surfaced hole will in turn create larger collapsing bubbles and as time progresses, the cavitation hole will get exponentially larger with high velocity flow impacting on the downstream end of the hole (Falvey, 1990).

**Figure 2.21** shows an example of cavitation on a ski-jump bucket. Due to the high velocity flow, once the onset of cavitation occurs it escalates relatively rapidly. According to FEMA (2010) the damage that occurred to the ski-jump flip bucket shown in **Figure 2.21** was due to incorrect design. This specific flip bucket required regular maintenance after each large flood release.

*FIGURE 2.21: DISCHARGE FROM THE UPSTREAM SLIDE GATE RESULTED IN SIGNIFICANT CAVITATION DAMAGE TO THE INVERT OF THE FLIP BUCKET (FEMA, 2010)*

### 2.9.1 FACTORS AFFECTING SURFACE CAVITATION DAMAGE

Factors concerning the potential for cavitational damage of a surface, according to Falvey (1990) include:

- cause of the cavitation,
- location of the damage,
- magnitude of the flow velocity,
- air concentration of the water,
- surface resistance to damage, and
- length of time of surface exposure.

#### *2.9.1.1 Cause of Cavitation*

As previously mentioned, the occurrence of cavitation will happen when the local pressure within flowing water falls below vapour pressure. An example of this is when the piezometric pressure in a pipe falls below atmospheric pressure during the down surge of a water hammer wave. Although in hydraulic structures the more common causes of cavitation are flow surface irregularities (Falvey, 1990).

Cavitation is also the result of shear flows which may be the result of two conditions; the intersection of high velocity flow and relatively quiescent flow, and flow adjacent to the flow direction. Both these conditions have the possibility of occurrence on the flip bucket section of a ski-jump spillway especially during initial stages of flood releases from controlled ogee spillways. If there is insufficient drainage on the flip bucket water will pool in it and when the flood water flow down the spillway there will be an initial existence of shear flow causing negative pressures and cavitation.

#### *2.9.1.2 Damage Location*

Cavitation damage according to Falvey (1990) primarily occurs downstream from the cavitation source. It was determined that for a cylindrical structure when the length of the cavitation cloud is equal to the diameter of the structure damage will occur. The following equation represents the length of the cavitation cloud, $L_k$:

$$\frac{L_k}{H} = 2\left(\frac{\sigma_s}{\sigma}\right)^{2.63} \qquad \textit{EQUATION 2.18}$$

Where:

H = characteristic dimension such as pipe radius, offset height etc.

$L_k$ = cavitation cloud length,

σ = flow cavitation index, and

$\sigma_s$ = cavitation index when damage begins, corresponds to cavitation index when $L_k/H = 1$.

The prediction of the distance to the maximum damage location can be estimated with **Equation 2.18**. Analysis of studies conducted on the Glen Canyon Dam tunnel spillways has shown that as the discharge and height of the surface irregularity increase so does the distance to the damage location.

#### *2.9.1.3 Velocity Effect*

There is an assumption that exists with credible merit where when the flow velocity exceeds some critical value a potential for cavitation damage is present. This critical value is dependant on several factors, but for geometric changing structures where flow direction is abruptly changed a flow velocity exceeding 10m/s has cavitation potential (Falvey, 1990).

#### *2.9.1.4 Surface Resistance to Cavitation Damage*

There are several factors that affect the resistance of the surface to damage including the materials ultimate strength, ductility and homogeneity. It is still unclear what the most significant strength characteristics of a material are when concerned with surface resistance. On metal surfaces collapsing bubbles impact the surface causing deformation which in turn results in tensile forces within the material. With concrete the significant factor is also the tensile forces. Therefore the most important parameter with regard to surface resistance is the tensile strength of the material. According to Falvey (1990), the properties of strength and durability can be classified under a single parameter, resilience which can be defined as the integral of the stress-strain curve of a material.

Unfortunately there have been no relationships developed to date that accurately quantify the damage amount of a specific material for a specified amount of cavitation. However, a correlation has been made for the residence of different materials for a specified cavitation. At an international conference on the wear of materials some data for a study conducted in 1990 on the cavitation of materials under controlled conditions was presented. Some findings of this study is displayed in **Table 2.1**. Each material was tested in a venturi device with a flow velocity of 30 m/s. The time recorded reflected the time it took for cavitation to create a hole 13mm deep.

*TABLE 2.1: TIME TAKEN FOR 13MM CAVITATION FOR DIFFERENT MATERIALS, V= 30M/S (FALVEY, 1990)*

| Material | Hours |
|---|---|
| **Concrete** | 3 |
| **Polymer Concrete** | 125 |
| **Copper** | 240 |
| **Carbon Steel** | 860 |
| **Stainless Steel** | 6000 |

The relative damage development for conventionally used materials in hydraulic structures is depicted in **Figure 2.22**.

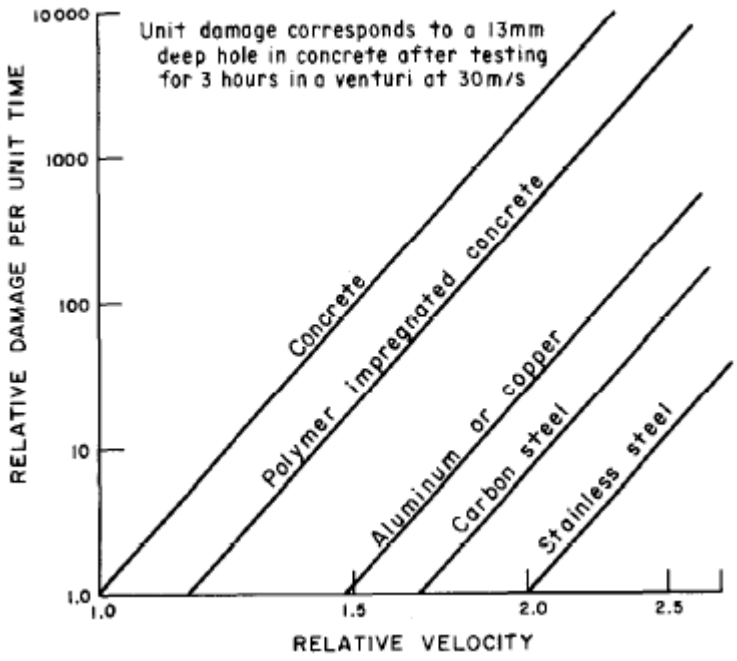


*FIGURE 2.22: COMPARATIVE CAVITATION RESISTANCE OF VARIOUS MATERIALS, (FALVEY, 1990)*

### *2.9.1.5 Air Content Effect*

In a venturi-type testing facility, tests were performed with low and high air concentrations in a controlled environment where a correlation between the air concentration and cavitational damage of a surface was determined. At low air concentrations, an inverse relationship was found to exist between the air concentration and damage. At high concentrations of air (in the order of 0.07 moles of air per mole water), over a testing period of 2 hours, the cavitation damage was found to have been almost entirely eliminated (Falvey, 1990).

There were two assumptions in 1945 with regard to the presence of air in high-velocity flow. One of these assumptions was along the lines that air introduced beneath a prism of water would create a cushion between the high-velocity flow and the surface. The other was that subatmospheric pressures are relieved in the presence of air. It was later discovered that neither of these assumptions were true (Falvey, 1990).

Today, two theories exist that describe the alleviating effect of the presence of air on cavitation damage. The first theory is based upon the cushioning or retarding of the collapsing process by the occurrence of non-condensable gases in the vapour bubble. Undissolved air causes a change in the sonic velocity of the fluid encompassing the collapsing vapour pocket is the basis of the second theory which appears to be the most valid. Studies have shown that the rate at which non-condensable gases are diffused into a vapour pocket is extremely slow in comparison to its vaporisation rate, therefore due to the fact that the growth rate of the vapour pocket is fast it is improbable that adequate gasses exist within the pocket to considerably affect the collapse rate or generated pressures thereby (Falvey, 1990). **Figure 2.23**

graphically represents the inversely proportional relationship of the second theory, as air concentration increased the sonic velocity decreases.

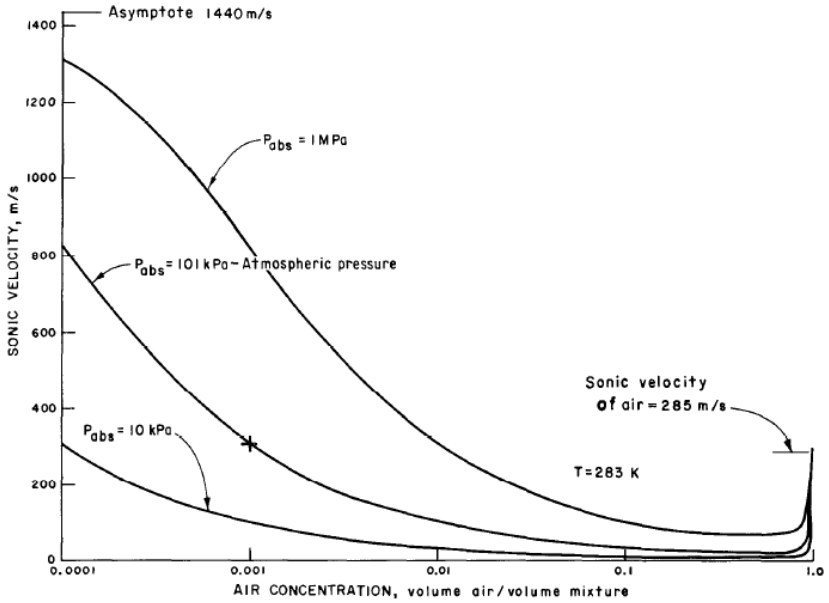


*FIGURE 2.23: SONIC VELOCITY OF AIR-WATER MIXTURE (FALVEY, 1990).*

### *2.9.1.6 Time Exposure Effect*

Though the observation of several experiments and investigations (Falvey, 1990) proved the hypothesis that on any surface the rate of erosion caused by cavitation is not constant with time. Rather there are numerous different rates taking place consecutively. For the purpose of classification these rates have been given a specific name which identifies the period in which they occur.

Initially, loss of material does not occur. This initial period can be recognised as the "incubation zone." During this period the surface will become slightly pitted. Data collection in the incubation zone is said to be the most significant for damage correlation by many investigators.

The zone following the incubation zone is known as the "accumulation zone." In this zone the rate of damage increases rapidly until reaching its peak. From this point one of two conditions may occur. The rate of damage either declines into an "attenuation zone" which is followed by a "steady-state zone" where the rate of damage remains constant or the damage rate plateaus into a steady-state zone and then decreases into an attenuation zone. **Figure 2.24** and **Figure 2.25** show the two trends of damage rate.

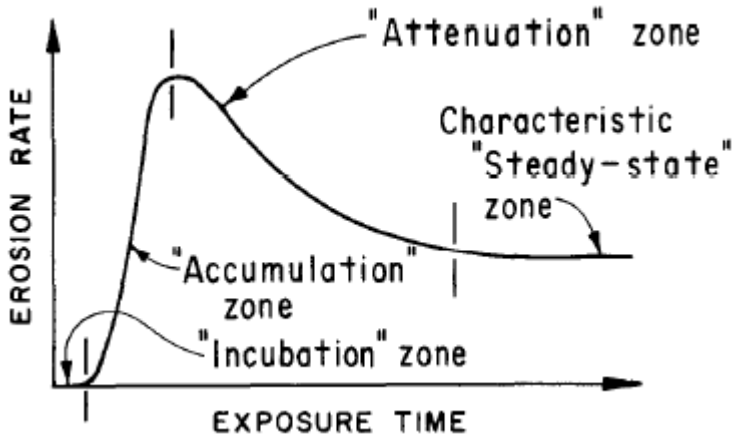


FIGURE 2.24: CHARACTERISTIC RATE-TIME CURVE ACCORDING TO THIRUVENGADAM, (FALVEY, 1990)

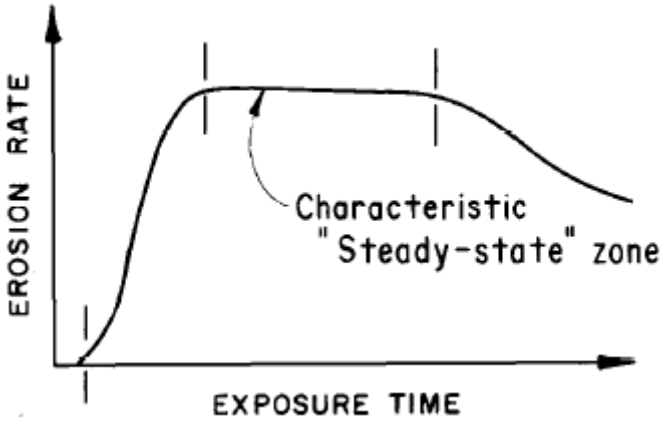


FIGURE 2.25: CHARACTERISTIC RATE-TIME CURVE ACCORDING TO PLESSET AND DEVINE (FALVEY, 1990)

Wang & Chou (1979) cited by Falvey (1990) verified, in field testing, the hypothesis that during the damage process on hydraulic structures, there is no significant variation in the location of the collapsing cavitation bubbles due to the irregularities on the boundary surface. Therefore the distance between the boundary surface and the collapsing cavitation bubble increases as the damage increases. Form this theory it was determined that an inverse relationship exists between the rate of damage and time. The field testing proved that for a constant flow rate with increasing time, the damage depth below an irregularity will appear to increase no further and remain at a constant value.

# CHAPTER 3: HYDRAULIC DESIGN CRITERIA OF SKI-JUMP/ FLIP BUCKET TYPE SPILLWAYS OR OUTLET WORKS

*There is a research gap in the design of ski-jump energy dissipators. The addition of this chapter sought to compile existing guidelines into a single document that clearly defines calculations and considerations that must be present when designing a ski-jump energy dissipator.*

## 3.1 INTRODUCTION

In the hydraulic design of a ski-jump it is essential that the designer correctly calculates and accounts for all parameters of importance including the bucket geometry, trajectory characteristics, bucket surface pressures as well as river topography. Ski-jump design is different for each and every project where very little standardisation can be implemented across various projects therefore it is required that verification of ski-jump design parameters through hydraulic model studies.

Trajectory bucket type energy dissipators are considered more suitable when (Bureau of Indian Standards, 2010):

a. the tailwater depth is considerably lower than the sequent depth of hydraulic jump and therefore the formation of the jump is prevented,
b. high tailwater depths exist where the location of the outlet must also be at a higher level, and
c. the downstream river channel bed is comprised of sound rock.

## 3.2 DESIGN CRITERIA FOR SKI-JUMP/ FLIP BUCKET

This section deals with the terminal structure and downstream channel of a typical ski-jump spillway/outlet works.

For the design of trajectory buckets the following principal hydraulic design parameters adopted from standards by the U.S. Army Corps of Engineers (1990) and the Bureau of Indian Standards (2010) should be determined:

1. bucket shape,
2. bucket invert elevation,
3. principal geometrical parameters of the bucket including radius, lip trajectory angle, lip height, bucket termination and sidewall termination,
4. alignment,
5. bucket pressures,
6. trajectory distance and impact angle,
7. discharge and other design considerations including design discharge, low flow operation and bucket drainage, and
8. estimation of scour downstream of the spillway.

By followings these design standards a general step-by-step procedure has been formulated in which most trajectory buckets may be designed. **Sections 3.2.1** *THROUGH* **3.2.8** elaborates on this design procedure.

### 3.2.1 BUCKET SHAPE

The shape of the ski-jump bucket is an aspect of the energy dissipation system that has very little effect on the geometric performance. Performance of the trajectory bucket according to the Bureau of Indian Standards (2010), is based mainly upon the trajectory distance and jet dispersion. As stated previously in **Section 2.8.2.1** there are specifically two distinct shapes; the triangular wedge-shaped bucket and the circular-shaped bucket both of which have identical trajectory performance. The preferred bucket shape is the circular-shaped bucket and is the main focus of this specific thesis.

### 3.2.2 BUCKET INVERT ELEVATION

For optimal performance, the U.S. Army Corps of Engineers (1990) states that the flip bucket must be operating in free flow conditions where submergence does not exist. According to the Bureau of Indian Standards (2010), by designing the invert elevation to remain above the maximum tailwater a clear flip action can be experienced. The fixation of the invert or lip elevation of the flip bucket is dependent on the shape of the tailwater discharge curve specific to the site and may need to be adjusted accordingly.

A recommendation by the Bureau of Indian Standards (2010) is that the bucked elevation is beneficial to be situated close to the natural bed level. One benefits of this is that less construction materials such as concrete and steel reinforcing would need to be utilised thereby reducing the costs of the project. Another benefit would be that by having a low bucket elevation, the ground roller would be close to the lip and would sweep loose ground material back up against the endsill. In doing so, less erosion immediately below the bucket is a possibility and therefore better protection against structural damage. It is essential that for cases such as these a concrete cover of no less than 1.5m over the existing bed rock is implemented. However, it is important to consider that beyond a specific level of submergence the bucket may alter its flow condition from a flip action to a roller action. The interference of the tailwater on the jet may reduce its velocity enough to prevent the flow from achieving trajectory. As a result, heavy sub-atmospheric pressures would be created at the lip. **Figure 3.1** represents the submergence, $d_4$, at with the flow condition changes from a flip action to a roller action. Research has shown that the flip bucket will convert from being constructive to destructive in nature at a submergence depth of 70 percent of that required for the formation of a hydraulic jump. The Bureau of Indian Standards (2010) states that the maximum submergence over the bucket lip elevation that is deemed 'safe' is assumed to be equal to the critical depth, $d_c$.

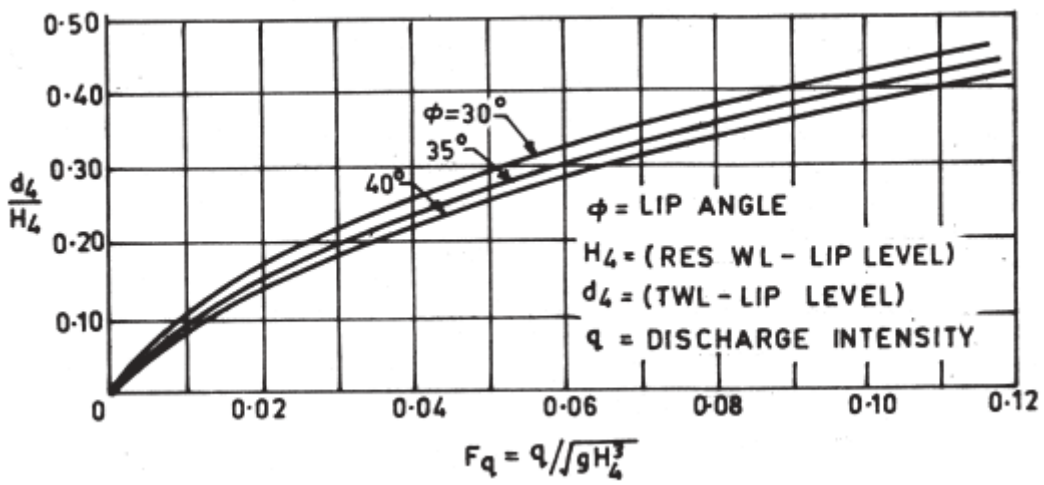


*FIGURE 3.1: SUBMERGENCE AT WHICH FLIP ACTION BECOMES ROLLER ACTION (BUREAU OF INDIAN STANDARDS, 2010)*

Tailwater conditions need to be evaluated by the designer considering the effects associated with the flip bucket trajectory jet. In some circumstances a drawdown in the tailwater elevations is said to occur as a result of ejector action of the trajectory jet as it leaves the bucket and must be considered. The operation of structures adjacent to the flip bucket may be undesirably impacted by such drawdowns. Hydraulic model studies may best represent the magnitude of drawdown occurring.

In many cases ski-jump buckets are located at a higher level on the spillway. The reason for this could be to create adequate construction space for e.g. the incorperation of a powerhouse just below the ski-jump invert at the toe of the dam. This provides further stabilization and structural support of the dam toe. Special consideration must be made in cases of high level flip buckets for the possibility of downstream scour of the abutment slopes where topographical conditions are less than ideal. Steep abutment bank slopes combined with probable downstream scour may lead to a possible landslide of unsupported earth and rock. A natural disaster such as this may cause irremediable damage to the spillway and dam. Sprays resulting from the trajectory jet may cause air satureation within structures where highly expensive electrical components vital to the operation of the dam spillway may be damaged by either short circuting or corrosion and therefore need to be protected accordingly (Bureau of Indian Standards, 2010).

### 3.2.3 PRINCIPAL GEOMETRIC PARAMETERS OF THE BUCKET

In the design of a ski-jump bucket the principal parameters required consist of the bucket radius, the minimum height of the bucket lip, the bucket trajectory angle, the bucket invert elevation as well as the directional alignment of the bucket. All these parameters are closely related and in order to achieve an acceptable design a trail-and-error adjustment may be required.

#### 3.2.3.1 Radius

The radius of a ski-jump bucket is considered to be one of the most significant parameters of a ski-jump energy dissipator along with the bucket trajectory angle. The radius governs the trajectory length as well as the pressure distribution along the bucket length. The bucket radius must be adequately large to avoid the inclination of the water to separate from the bucket surface and maintain concentric flow thereby not altering the streamline distribution by floor pressure nor allowing negative pressures to inflict cavitation to the bucket.

According to the U.S. Army Corps of Engineers (1990) the minimum radius, $R_{min}$, is a function of the theoretical unit load on the bucket invert, $P_T$, as well as the flow velocity, $V_1$, and the flow depth, $h_1$, entering the bucket. It is defined as:

$$R_{min} = \frac{\rho {V_1}^2 h_1}{P_T - \gamma h_1} \qquad \text{EQUATION 3.1}$$

However, from previous experience in model and prototype studies, as a general design guideline the Bureau of Indian Standards (2010) suggests that the minimum bucket radius should be at least 3 times the maximum flow depth over the bucket in order to prevent the tendency of flow separation from the bucket. Furthermore for preliminary design the bucket radius may be assumed as follows:

$$R = C_r H_o H_s \qquad \text{EQUATION 3.2}$$

Where $C_r$ is a radius coefficient in the range 0.6 to 0.8

$H_o$ is the design flow depth over the spillway crest (m)

$H_s$ is the total head (m) from the bucket invert elevation to the reservoir pool elevation

A recommendation by the U.S. Army Corps of Engineers (1990) is that the minimum bucket radius should not be less than 4 times the maximum design flow depth in order to assure the turning of most of the flow before exiting the bucket and therefore reducing the possibility of hurdling conditions which is also closely related to the bucket height and will be described further in **Section 3.2.3.2**.

These guidelines can only assist in the determination of a suitable radius. Model studies on the specific design will produce a better estimate for a suitable bucket radius.

#### 3.2.3.2 Lip Trajectory Angle and Lip Height

One of the most important features of any ski-jump spillway is the lip angle and lip height. Both the lip angle and lip height above the tailwater have an immediate influence on the horizontal trajectory distance. Other factors affecting the horizontal trajectory distance include the initial jet velocity, the aeration content of the initial flow as well as the bucket type. Generally accepted lip angles range from

30º to 40º for ski-jump spillways but may even be as large as 45º. The theory is that the greater the trajectory angle the greater the throw distance where the maximum throw distance will have an exit angle of 45º (Bureau of Indian Standards, 2010). According to the U.S. Army Corps of Engineers (1990) in addition to determining the jets trajectory distance, the trajectory angle is a factor used in the determination of general hydraulic characteristics in the impact area. The U.S. Army Corps of Engineers (1990) also suggests that as well as increasing the trajectory distance, steeper angles provide better energy dissipation due to the fact that the impacting jet angle becomes larger and consequently violent side eddies will be diminished. However, the more vertical the impacting jet the deeper the scour and therefore bucket lip angles should be chosen keeping in mind the minimum acceptable throw distance as well as the local rock conditions.

In the design of the height of the flip bucket lip one should be aware of the minimum height. If the lip height relative to the bucket invert elevation is insufficient the high velocity jet may completely override the lip without being turned and flipped up and out of the bucket. Guidelines by the U.S. Army Corps of Engineers (1990) suggest that in order to achieve a successful turning of the high velocity flow, the forward-projected water surface slope upstream of the invert of the bucket must intersect the flip bucket curve. **Figure 3.2** shows a graphical definition for the minimum bucket height, $h_{min}$.

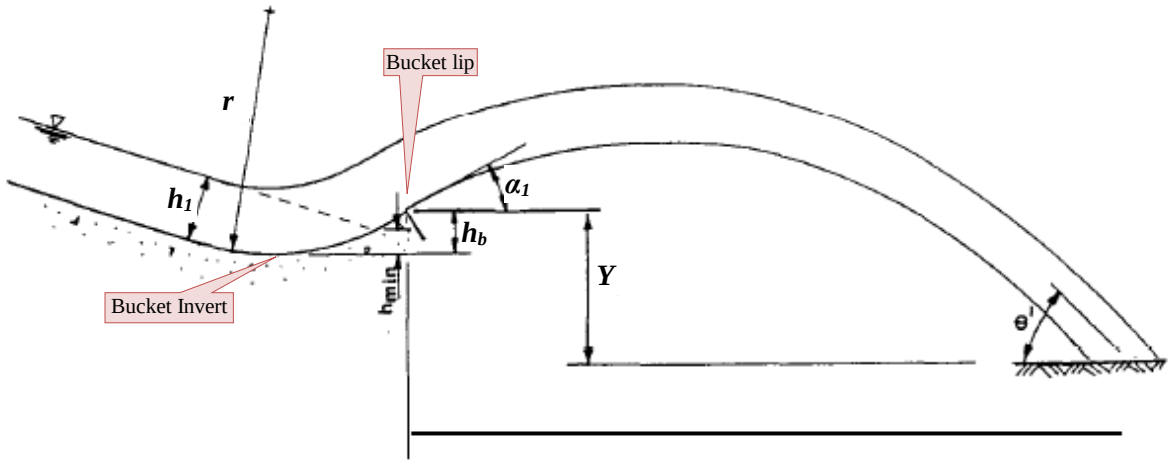


*FIGURE 3.2: DEFINITION SKETCH REPRESENTING THE MINIMUM BUCKET HEIGHT (U.S. ARMY CORPS OF ENGINEERS, 1990)*

With the desired bucket angle, $\alpha_1$, and the bucket radius, r, one can determine the required height of the bucket lip, $h_b$, above the bucket invert given the following equation (U.S. Army Corps of Engineers, 1990):

$$h_b = r(1 - cos\alpha_1) \qquad \textit{EQUATION 3.3}$$

### *3.2.3.3 Bucket and Sidewall Termination*

In the design of flip buckets it is highly imperative that the termination of the bucket should be a 90-degree cut from the bucket lip, and termination of the sidewalls should occur at the lip. This

recommended termination of the bucket and sidewalls is to permit adequate air to be drawn beneath the location of where jet separation from the bucket lip take place. In the event that inadequate air is supplied to the underside of the jet, there is a possibility that the jet will flutter causing pressure fluctuations on the bucket lip which may conceivably lead to cavitation damage (U.S. Army Corps of Engineers, 1990).

### 3.2.4 ALIGNMENT

The alignment of a flip bucket is a key aspect of a ski-jump spillway. The alignment determines the location of the trajectory impact which is generally a preselected one. This preselected location is determined with numerous factors in mind such as topographical features of the downstream channel, rock material of the river bed and alignment of the flowing river. The alignment of the flip bucket may not necessarily be the same as that of the spillway or chute, by curving or adding appurtenances the direction of the trajectory jet will be altered. In the design process it is mandatory that model studies are performed for any directional flip bucket in order to confirm the final design. According to the U.S. Army Corps of Engineers (1990) an ideal bucket alignment is one which spreads the flow at impact over as much of the river width as possible, reducing the adjustment to the river bed as well as downstream tailwater return flow.

### 3.2.5 BUCKET PRESSURES

The hydraulic forces acting on a ski-jump bucket are of high importance for the structural integrity of the bucket design. As mentioned previously the pressure distribution on a ski-jump bucket is governed by the radius of curvature and bucket deflection angle of the ski-jump bucket as well as the approach velocity and the depth of flow. Data acquired from a combination of model studies, theoretical studies and prototype investigations suggest that there is a continuous variation in the bottom pressures throughout the bucket. The Bureau of Indian Standards (2010) has identified that an indication of the effects of independent variables is given by the concept of centrifugal force and therefore the pressure on the bucket can be determined. **Equation 3.4** used the applicable variables for the calculation of the maximum bucket pressure:

$$P = \left(\frac{{v_1}^2}{gR} + 1\right)\gamma d_1 \qquad \textit{EQUATION 3.4}$$

Where:

$P$ = bucket pressure, in $kg/m^2$;

$\gamma$ = specific weight of water, in $kg/m^3$;

$v_1$= flow velocity entering bucket, in *m/s*;

$g$ = gravitational acceleration, in $m/s^2$;

$R$ = radius of bucket curvature, in m; and

$d_1$ = depth of flow entering bucket, in m.

A guideline for the determination of the maximum theoretical bucket pressures has been created by the Bureau of Indian Standards (2010) as is presented in **Figure 3.3**. Theoretical bucket pressures can be determined for velocities in the range for 10 to 40 m/s as well as radius/depth ratios in the range of 4 to 10. The hydraulic pressures retrieved from this figure should only be regarded as an estimate as actual values deviate substantially. The only way to accurately determine the actual pressure distribution over a specific ski-jump bucket as well as the deviation is with the assistance of physical hydraulic model studies. In the design of a ski-jump bucket it is important to take note that it is not only the bucket itself that must be able to withstand these pressure distributions but also the adjacent training walls. Parameters for **Figure 3.3** are defined below:

*d1* = flow depth over the flip bucket,

$p$ = pressure on the flip bucket surface,

$R$ = radius of curvature of the flip bucket, and

$v_a$ = flow velocity approaching the flip bucket.

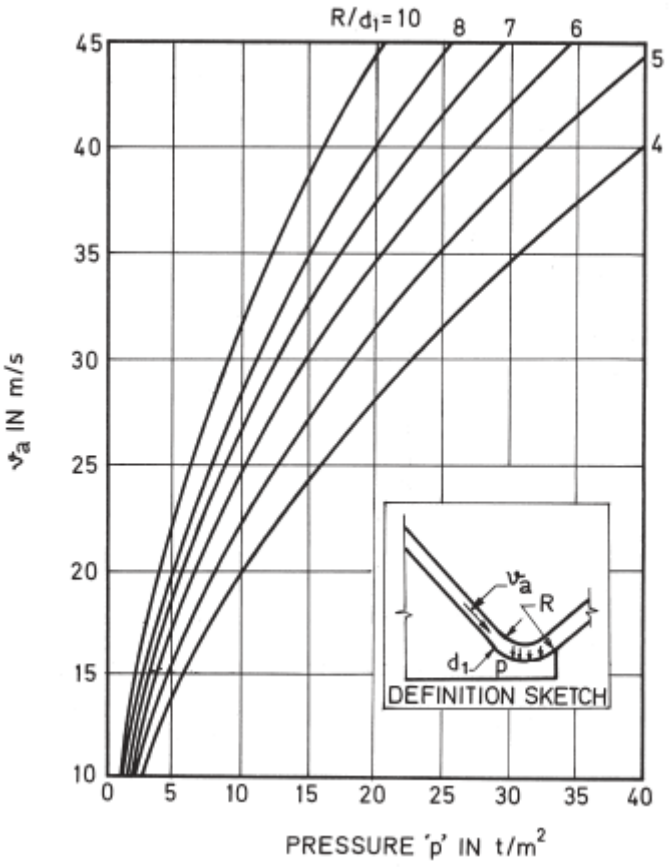


*FIGURE 3.3: THEORETICAL BUCKET PRESSURES (BUREAU OF INDIAN STANDARDS, 2010)*

For the design of relatively large dams the U.S. Army Corps of Engineers (1990) has determined through a study that bucket pressure head could also be represented by **Equation 3.5**.

$$h_P = f\left(\frac{q}{R(2gH_s)^{1/2}} \cdot \frac{\alpha}{\alpha_o}\right) \qquad \textit{EQUATION 3.5}$$

Where:

$h_P$ = pressure head, m water

$H_s$ = total initial head at bucket invert, m

$\alpha$ = rotational angle from beginning of curvature, degrees

$\alpha_o$ = bucket deflection angle from spillway to lip, degrees

The term $\alpha/\alpha_o$ represents the relative position with which the pressure head should be determined along the curvature.

### 3.2.6 TRAJECTORY DISTANCE AND IMPACT ANGLE

The trajectory distance of a ski-jump energy dissipator is dependent on various parameters including the flow velocity exiting the flip bucket at the bucket lip, the angle of trajectory and the tailwater depth relative to the flip bucket lip elevation. **Figure 3.4** and **Figure 3.5** show the relevant parameters used for the calculation of the trajectory distances. These parameters will be used for the remainder of this document. It is important to note that the datum level was set at the level of the tailwater to correspond with the experimental setup discussed in the following chapters.

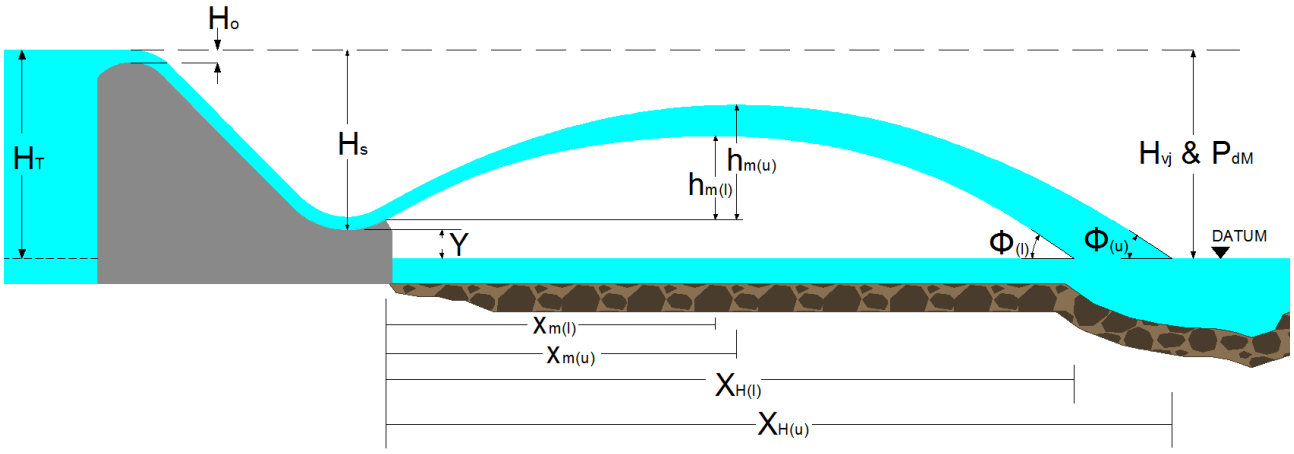


*FIGURE 3.4: SKI-JUMP ENERGY DISSIPATOR TRAJECTORY PARAMETERS (1)*

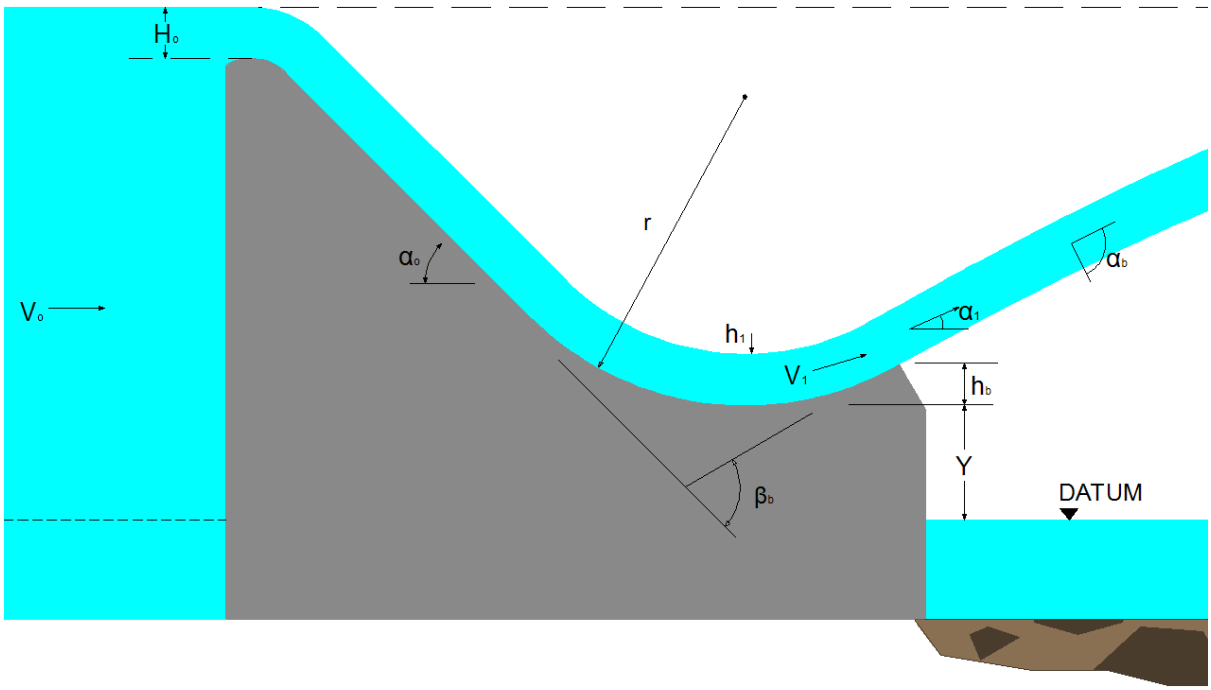


*FIGURE 3.5: SKI-JUMP ENERGY DISSIPATOR TRAJECTORY PARAMETERS (2)*

The trajectory distance, $X_H$, of a ski-jump energy dissipator may be defined as the horizontal distance the water jet covers from the flip bucket lip to the location of impact and is governed by the following equation derived in **Section 2.8.3** (U.S. Army Corps of Engineers, 1990).

$$X_H = kH_s\, Sin\, 2\alpha_1 + 2kcos\alpha_1[H_S(H_S sin^2\alpha_1 + Y)]^{1/2} \qquad \textit{EQUATION 3.6}$$

Where

$X_H$ = horizontal throw distance from bucket lip to the point of impact with tailwater, in m;

$Y$ = elevation difference between the bucket lip and tailwater, in m;

$H_s$ = velocity head of jet at the ski-jump bucket lip, in m;

$\alpha_1$ = bucket lip angle relative to the horizontal, in degrees;

k = air resistance.

A simple graph based on **Equation 3.6** may be used in the design of a ski-jump energy dissipator to determine the trajectory distance. This graph is a plot of the theoretical throw distance relative to the velocity head, $H_s$ plotted against the elevation difference between the bucket lip and tailwater relative to the velocity head, $H_s$. By factoring the theoretical throw distance and elevation difference by the velocity head the graph may be applied to discharges of any scale and magnitude. **Figure 3.6** below shows this comparison for jet trajectory angles 0°, 10°, 20° 30°, 40° and 45° used for the determination of the point of jet impingement with the tailwater. It is important to take note that actual horizontal trajectory distance may be significantly smaller than what may be read off **Figure 3.6** as this does not account for specific energy losses and air entrainment related to the spillway (Bureau of Indian

Standards, 2010). For a greater accuracy in the determination of the impact location of a ski-jump jet prototype measurements for spillway specific energy losses are required (U.S Army Corps of Engineers, 1977).

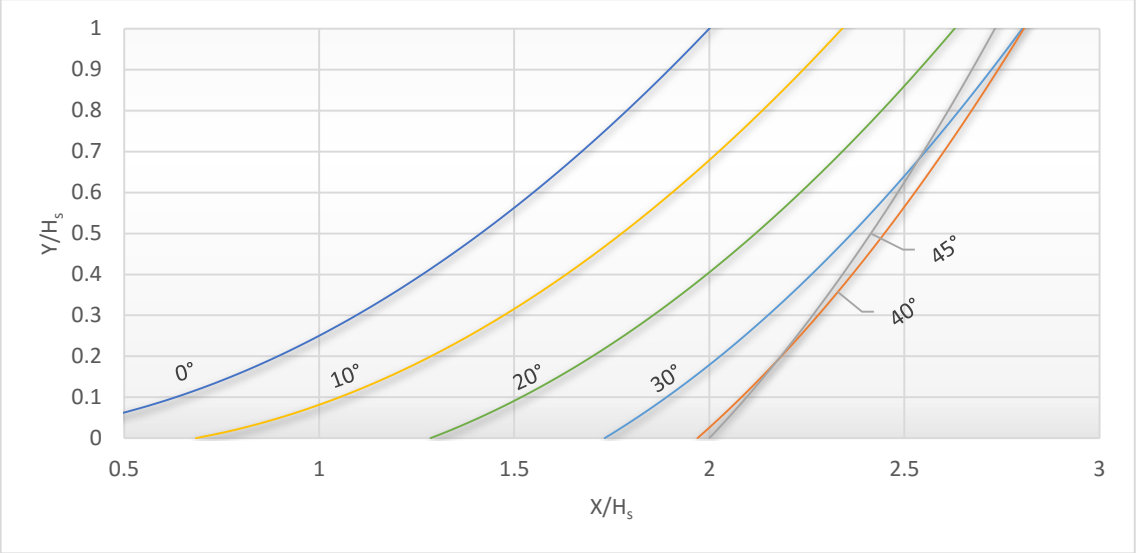


*FIGURE 3.6: THEORETICAL TRAJECTORY DISTANCE RELATIVE TO THE VELOCITY HEAD*

In certain cases where conditions cause Y to be negative (tailwater greater than bucket lip elevation), model studies must be conducted to confirm horizontal trajectory distances, $X_H$ as well as maximum vertical throw heights, $h_m$. Generally ski-jump energy dissipators are designed so that conditions such as this are eliminated unless the design is submerged bucket type energy dissipator.

### 3.2.7 DISCHARGE CONSIDERATIONS

The ideal operation of flip buckets occur when low unit discharge with high velocity flow exists at the invert. Conditions such as these consequently cause substantial fraying of the jet by air resistance. However, unit discharges of a moderately high proportion, although not the ideal condition, should not cause problems if the primary consideration does not include the adjustment of the downstream channel.

It is highly recommended that model studies be conducted for proposed ski-jump spillway flip buckets that are designed to carry unit discharges in excess of 250 $ft^3/s/ft$ (approximately 23 $m^3/s/m$). There are existing flip buckets that convey discharges in excess of 1000 $ft^3/s/f$ (93 $m^3/s/m$) but cavitation of these designs are tremendously critical due to deep flow depths at extremely high velocities causing subatomospheric pressure (U.S. Army Corps of Engineers, 1990).

#### *3.2.7.1 Low Flow Operation*

During low flows the water entering the flip bucket is likely to pool. Due to this pooling the water is unable to be flipped into the air as desired but rather spills over the lip of the bucket impacting the toe of the spillway. Although velocities are low, the continual impact of water can cause extensive damage to the toe of the spillway in the form of erosion and this must be considered in the design. Possible

solutions to prevent impairment to the spillway structure is to integrate a concrete slab, cutoff wall or a large rock at its toe (U.S. Army Corps of Engineers, 1990).

**Figure 3.7** below depicts the construction of St. Mary's dam spillway toe in Alberta, Canada and **Figure 3.8** shows the St. Mary's ski-jump operating under relatively low flow conditions.

*FIGURE 3.7: CONSTRUCTION OF ST. MARY SPILLWAY TOE, (GOMACO WORLD, 2000)*

*FIGURE 3.8: LOW FLOW AT ST. MARY SPILLWAY, ALBERTA, CANADA (GOMACO WORLD, 2000)*

### *3.2.7.2 Bucket Drainage*

The drainage within the flip bucket must be sufficient enough to prevent the impoundment of water which has the potential for flow choking during low flows. The drains must be located at the sidewalls

and drained laterally. It is highly recommended that floor drains be avoided as they are highly susceptible to cavitation damage under the extremely high velocities (U.S. Army Corps of Engineers, 1990).

### 3.2.8 ESTIMATION OF SCOUR IN THE DOWNSTREAM EXIT CHANNEL

The performance of a ski-jump energy dissipator is assessed predominantly by the dispersion of the jet trajectory at the point of impingement with the downstream tailwater and river bed. Optimum performance is said to be present when dispersion occurs over the entire width of the river channel.

A scour hole is expected to occur at the point of the jet trajectory impact with the river bed unless the underlying material is made up of highly durable rock. The scoured material will be transported by the turbulent flow to a downstream location where velocities are low enough for settling to occur. Correct operation of a ski-jump may be adversely affected by the deposition of material and therefor a performer scour hole may be utilised to reduce the quantity of deposited material (U.S. Army Corps of Engineers, 1990).

The impingement of the water jet with the river is expected to create areas of violent wave action and high velocity turbulence which is likely to extend laterally across the width of the river channel and downstream. Conditions such as these could potentially cause damage to the river embankments unless sufficient erosion protection is provided (U.S. Army Corps of Engineers, 1990).

Scour below jet trajectories of a ski-jump are governed by various factors including:

- discharge intensity,
- height of fall,
- water level,
- lip angle, mode of operation of spillway,
- degree of homogeneity of rock,
- type of rock, and
- time factor involved in the process of scour.

In order to accurately assess the extent of scour created by a ski-jump, a combined evaluation of all above factors and their effect must be conducted which in practice is an extremely difficult task. However, by focussing the analysis on the correlation between the depth of scour and the two most important factors (discharge intensity, q and the dam head $H_s$). This relationship is defined in the following equation (Bureau of Indian Standards, 2010):

$$d_s = m(q\,H_s)^{0.5} \qquad \textit{EQUATION 3.7}$$

Where $d_s$ = depth of scour in m below tailwater level;

m = constant (0.36 for minimum expected scour), (0.54 for probable scour under sustained spillway operation), (0.65 for ultimate scour);

q = discharge intensity ($m^3/s$ )/m; and

$H_s$= difference in elevation from the reservoir pool to ski-jump bucket invert, in m.

NOTES
1. Ultimate scour means the final stabilised scour.
2. Probable scour means the scour which may reasonably be expected in any individual case of sustained spillway operation.
3. Minimum scour means the minimum scour in any case.

Another formula (**Equation 3.8**) may also be used for the prediction of the scour depth of a trajectory jet which uses the total head, $H_T$ instead of $H_s$ (Bureau of Indian Standards, 2010):

$$d_s = 1.9 H_T^{0.225} q^{0.54} \qquad \textit{EQUATION 3.8}$$

Where $d_s$ = depth of scour, in m

$H_T$ = difference in elevation from the reservoir pool to tailwater, in m.

In certain scenarios plunge pools are pre-excavated below a ski-jump energy dissipator to minimise the deposition of material downstream. This provides a water cushion for the plunging jet with geometric properties such that sufficient energy is reduced creating lower velocities within the downstream channel and ultimately mitigating the uncontrolled erosion and avoiding any impairment to the stability of the dam structure. For the design of plunge pools various hydraulic parameters of the ski-jump structure are required to ensure an adequate design. These parameters include horizontal trajectory distances for the entire range of discharges as well as the magnitude and location of the deepest scour. A plunge pool design may be based on a theoretical approach, however hydraulic model studies are required where geologic and morphologic characteristics of the downstream river bed are considered, (Bureau of Indian Standards, 2010).

### 3.2.9 SUMMARY OF ASPECTS RELEVANT TO THIS THESIS

The purpose of this thesis is to design and test a ski-jump energy dissipating structure to maximise the energy dissipation and aeration. This was achieved through the design of various ski-jump flip buckets which were hydraulically tested to determine the best operating bucket in terms of energy dissipation. The evaluation of the energy dissipation efficiency was based upon various factors. The aspects of the literature that are relevant to the aims of this thesis include:

- ogee spillway design,
- geometric design and considerations of a ski-jump bucket including the bucket radius, bucket height, deflection angles and sidewalls, and

- trajectory equations and recommendations including the trajectory distance, trajectory height, longitudinal and transverse impact widths.

# CHAPTER 4: PHYSICAL HYDRAULIC MODEL AND TEST PROCEDURE

*In the physical hydraulic model chapter, a general description of the hydraulic model is introduced followed by a section on the scale effects of physical modelling. Next a detailed description of the experimental model is given including the model setup and construction of all components. Finally, a detailed description of the experiments is presented along with the testing and data retrieval procedures.*

## 4.1 INTRODUCTION (GENERAL DESCRIPTION)

A hydraulic model of a ski-jump energy dissipator was designed, constructed and tested to determine a design that would ultimately maximise energy dissipation and aeration of the free falling water jet. The design of the model was based upon the theoretical research compiled in the previous two chapters.

The ski-jump hydraulic model study was conducted inside the Stellenbosch University hydraulics laboratory in Stellenbosch, South Africa. The laboratory created a controlled environment where no external factors, such as weather, could have an influence on the specific tests or the data acquired. There are four sump pumps in the hydraulics laboratory capable of conveying flows of up to 600 l/s, well above the required 200 l/s for the model tests. These pumps are able to convey discharges accurately with an error of about ±0.5 l/s for discharges up to 100 l/s and about ±1 l/s for discharges up to 200 l/s. Therefore the accuracy of the flows for model testing is ±0.5% which is more than acceptable. Water was pumped to a reservoir at the top of the hydraulics lab where a constant water level of ±6m above the model was maintained. **Figure 4.1** below shows a schematic diagram of the experimental setup with all relevant components which are described in detail in the following Sections.

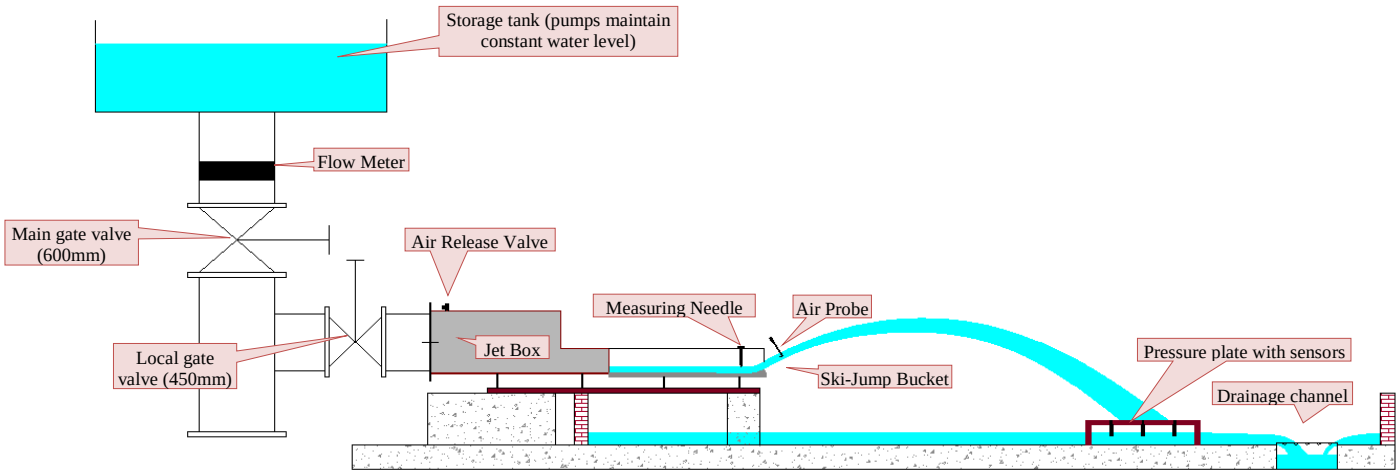


*FIGURE 4.1: SCHEMATIC DIAGRAM OF EXPERIMENTAL SETUP*

The physical model was spread over a total area of 108 m$^2$ with a total length of 18 m and with of 6 m. This area was divided into two sections, namely the ski-jump model area and the impact basin/pool area. The model area consisted of a 450mm diameter gate valve which was connected to the main pipe network running along the perimeter underneath the hydraulics laboratory ground floor with a 90$^o$ bend

section, a 6m length of 450mm diameter steel pipe connected the valve and a 1m x 0.5m jet box and 1.6m horizontal chute which encroached into the impact basin area. The impact basin was a 12m x 6m bricked up rectangular area with the sole purpose of containing the flow after impact and reintroducing it back into the system.

The main components associated with the Hydraulic model include (**Figure 4.2**):

- Water supply and control valve,
- Jet box,
- Air release valve,
- Sluice gate,
- Approach channel,
- Ski-jump flip bucket, and
- Pressure Plate.

These components are described in more detail in **Section 4.3**.

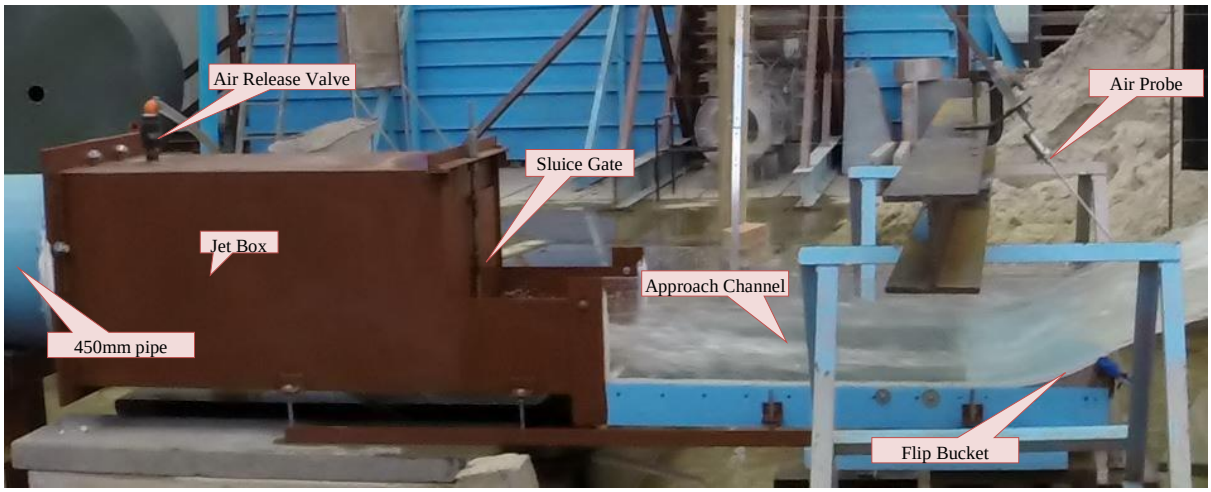


*FIGURE 4.2: MAIN COMPONENTS*

## 4.2 SCALE EFFECTS IN PHYSICAL HYDRAULIC MODELS

Scale effects arise as a result of non-identical force ratios between a model and its real-world prototype and therefore observed deviations occur between model and prototype (Heller, 2011). This section of this dissertation touches on model - prototype similarities

When considering hydraulic engineering a scale model has the function of solving a hydraulic problem by carrying out experiments on a physical simulation of the hydraulic phenomena. In order for the experiments to be valid the fulfilment of the existing scale laws is required. Therefore the scale model must be designed and operated with the existing scale laws in consideration (Novak, et al., 2007).

It is inevitable that a certain degree of flow distortion and scale effects will occur when performing a flow analysis, even for a hydraulic model that is geometrically similar. Taking a free falling jet experimental model as an example where the hydraulic model will experience significantly less air entrainment and air resistance than what would be experienced in prototype scale. this would result in higher velocities and therefore a longer horizontal trajectory distance causing a scour hole further downstream than where scour would occur in the case of the real life situation. Generally the majority of design difficulties associated with hydraulic structures nowadays are investigated on geometrically similar models regardless of the fact that flow distortion and scale effects occur (Novak, et al., 2007).

### 4.2.1 SIMILARITIES

#### *4.2.1.1 Mechanical Similarity*

A physical model is said to be completely similar to its full scale prototype where the presence of scale effects are inexistent if mechanical similarity is satisfied thereby inferring geometric, kinematic, or dynamic similarity.

*Geometric Similarity*

The requirements of geometric similarity are predominantly focused on shape, where all model dimensional lengths are shorter by a factor of $\lambda$ than its real-world prototype. Therefore in relation to the prototype, the model can be scaled by $\lambda$, $\lambda^2$ and $\lambda^3$ for the length, area and volume respectively (Heller, 2011).

*Kinematic Similarity*

Kinematic similarity suggests that the particles in motion of the model and prototype must be similar in addition to geometric similarity. At all times there should be constant relationships of time, velocity, acceleration and discharge between model and prototype (Heller, 2011).

*Dynamic Similarity*

According to Heller (2011), dynamic similarity requires that all force ratios within geometric and kinematic similarity be identical. The most important forces when dealing with fluid dynamics are (Hughes, 1993) cited by Heller (2011):

$$Inertia\ Force = Mass\ x\ Acceleration = (\rho L^3)\left(\frac{V^2}{L}\right) = \rho L^2 V^2 \quad \text{EQUATION 4.1}$$

$$Gravitational\ Force = Mass\ x\ Gravitational\ Acceleration = \rho L^3 g \quad \text{EQUATION 4.2}$$

$$Viscous\ Force = Dinamic\ Viscocity\ x\ \frac{Velocity}{Distance}\ x\ Area\ = \mu\left(\frac{V}{L}\right)L^2 = \mu VL \quad \text{EQUATION 4.3}$$

$$Surface\ Tension\ Force = Unit\ Surface\ Tension\ x\ Length = \sigma L \quad \text{EQUATION 4.4}$$

$$Elastic\ Compression\ Force = Young's\ Modulus\ x\ Area = EL^2 \quad \text{EQUATION 4.5}$$

$$Pressure\ Force = Unit\ Pressure\ x\ Area = pL^2 \quad \text{EQUATION 4.6}$$

---

ρ (kg/m$^3$) - fluid density

L (m) - characteristic length

g (m/s$^2$) - gravitational acceleration

V (m/s) - characteristic flow velocity

p (N/m$^2$) - pressure

σ (N/m) - surface tensions

μ (kg/(m.s)) - dynamic viscosity

E (N/m$^2$) - Young's modulus

And the most relevant force ratios are:

$$\textbf{Froude Number, } Fr = \left(\frac{Inertial\ Force}{Gravity\ Force}\right)^{1/2} = \frac{V}{(gL)^{1/2}} \quad \text{EQUATION 4.7}$$

$$\textbf{Reynolds Number, } Re = \frac{Inertial\ Force}{Viscous\ Force} = \frac{\rho VL}{\mu} \quad \text{EQUATION 4.8}$$

$$\textbf{Weber Number, } W = \frac{Inertial\ Force}{Surface\ Tension\ Force} = \frac{\rho V^2 L}{\sigma} \quad \text{EQUATION 4.9}$$

$$\textbf{Cauchy Number, } C = \frac{Inertial\ Force}{Elastic\ Force} = \frac{\rho V^2}{E} \quad \text{EQUATION 4.10}$$

$$\textbf{Euler Number, } E = \frac{Pressure\ Force}{Inertial\ Force} = \frac{p}{\rho V^2} \quad \text{EQUATION 4.11}$$

#### *4.2.1.2 Froude Similarity*

Froude similarity occurs when the ratio of gravitational and inertial forces acting on a fluid particle are equal in the model and prototype. The Froude number (Fr) is defined by the equation:

$$F_r = \frac{V}{\sqrt{gL}} \quad \text{EQUATION 4.12}$$

Where:

V is the flow velocity, in m/s

G is the acceleration due to gravity, taken as 9.81 m/s$^2$

L is the characteristic dimension (depth or length)

#### 4.2.1.3 *Reynolds Similarity*

The Reynolds number may be defined as a measurement of similar an experimental model is to its prototype design. This dimensionless number is used to assess the validity of hydraulic phenomena in scale models. It is far more practical and economical to construct a scale model and simulate hydraulic scenarios than to test in prototype scale. A relationship is required to exist between the experimental model and prototype for the result to be valid. This relationship is shown in **Equation 4.13** below. Upon determining the Reynolds number for the specific hydraulic model, $R_{e(m)}$ the Reynolds number of the prototype, $R_{e(p)}$ may be determined given the scale with which the model operates in, $\lambda$.

$$R_{e(p)} = \lambda^{3/2} R_{e(m)} \qquad \textit{EQUATION 4.13}$$

As previously mentioned, even perfectly geometric similar models experience scale effects, the most common scale effects are aeration and flow distortion. However these scale effects may be mitigated by assigning a sufficiently large Reynolds number. In order to reduce scale effects relating to energy dissipation including turbulence, aeration and friction, a Reynolds number of $10^5$ is required.

## 4.3 EXPERIMENTAL PHYSICAL MODEL SETUP

### 4.3.1 MODEL SCALE

Since gravitational and inertial forces are the fundamental and dominant forces that influence the motion of water within any ski-jump whether as a spillway or bottom outlet design, the Froude law was applied in this study. In order to accurately model two phase flow, (water and air) the simulation of viscosity and surface tension is required. This suggests the simultaneous fulfilment of the Froude, Reynolds and Weber laws. Considering that the Froude law is used, an adequately large scale is required to alleviate the scale effects of unfulfilled Reynolds and Weber laws.

Therefore, the ski-jump hydraulic model was designed at a scale of 1:25 which was the largest practically possible in the laboratory. This scale was determined by the trajectory throw distance of the ski-jump jet relative to the allotted area in the hydraulics laboratory. It was recommended that a large scale be used in order to mitigate the scale effects. It is suggested that for a Froude scale model of spillways the scale should be greater than 1:30 (Bureau of Indian Standards, 2010).

The hydraulic model was designed to be geometrically similar to the prototype and therefore the flows act in agreement with the Froude's Law. Which is valid when the ratio of gravitational and inertial forces acting on a fluid particle are equal in the model and prototype therefore resulting in the following relationship between the prototype and model:

$$Fr_{prototype} = Fr_{model}$$

Assuming that Froude number and geometric similarity between prototype and the model are equivalent, the following scale relationships are valid for the ski-jump energy dissipator model for a scale of 1:λ (model representation is denoted by suffix 'm' and prototype by suffix 'p).

| | |
|---|---|
| Linear ratio: | $\frac{L_P}{L_m} = \lambda = 25$ |
| Area ratio: | $\frac{{L_P}^2}{{L_m}^2} = \lambda^2 = 625$ |
| Volume ratio: | $\frac{{L_P}^3}{{L_m}^3} = \lambda^3 = 15625$ |
| Velocity ratio: | $\frac{V_p}{V_m} = \lambda^{o.5} = 5$ |
| Pressure Head ratio | $\frac{P_p}{P_m} = \lambda = 25$ |
| Discharge ratio: (Velocity ratio) x (Area ratio) | $\frac{V_p}{V_m} \; x \; \frac{{L_P}^2}{{L_m}^2} = \lambda^{2.5} = 3125$ |
| Time ratio: | $\frac{Length\ Ratio}{Velocity\ Ratio} = \lambda^{0.5}$ |
| Froude number ratio: | $\frac{Fr_p}{Fr_m} = 1$ |

## 4.4 HYDRAULIC DESIGN OF THE SKI-JUMP MODEL

The design phase of the ski-jump model was a period in which many assumptions and recommendations were made by the author and study leader with regards to testing procedures and modifications which resulted in a minimalistic approach to the design. With model modifications in mind it was believed that flip bucket interchangeability would be the most laborious and intricate part of the testing procedure. It was therefore decided that by isolating the flip bucket portion of a ski jump spillway the testing period would be reduced, as well as material and construction costs could be minimised. Due to the required model scale building a 4m high ogee spillway was an inefficient use of space in the hydraulics laboratory as well as impractical for what was to be tested.

It was decided that a similar approach to that of the research conducted by Juon, et al. (2000) where a jet box sluice gate would replace the concept of an ogee spillway. A jet box is a steel box connected to a pipe on the one end and a sluice gate on the other side. The purpose of the jet box is to transform full pipe flow to a plane horizontal jet flow at the ski-jump invert level with the ability to vary the flow depth and velocity.

### 4.4.1 CONTROL STRUCTURE

The control structure of a ski-jump energy dissipator is generally an over fall spillway, either a straight ogee type spillway or side channel spillway. The design of the ski-jump hydraulic model was based

upon the assumption that the control structure was an ogee type spillway with a head, $H_s$ of 97m above the ski-jump bucket invert and crest length, $L_s$ of 12.5m in prototype scale. The design capacity of 625m$^3$/s was assumed based on a general guideline previously mentioned in Chapter 3 where a general design capacity of a ski-jump spillway is in the region of 50m$^3$/s/m (refer to Appendix I). Using the hydraulic design equations for an ogee crest in **Section 2.8.1** the following stage-discharge relationship was determined for the fictitious ogee spillway (prototype scale). From **Figure 4.3** the design head, $H_o$, was determined to be 8.24m above the crest of the ogee spillway (refer to **Figure 3.4** and **Figure 3.5** for all ski-jump parameters).

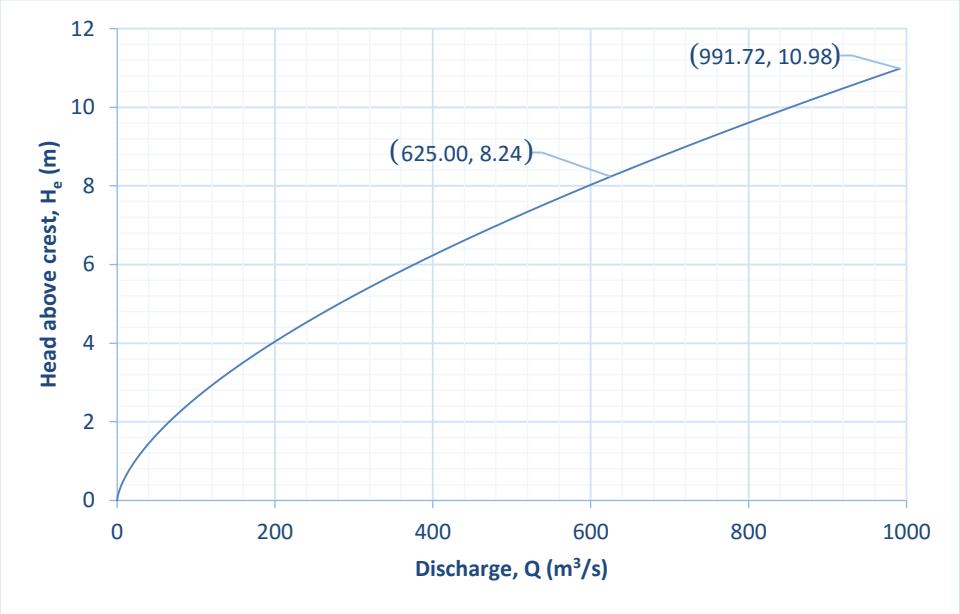


*FIGURE 4.3: STAGE-DISCHARGE RELATIONSHIP FOR $Q_o$ = 625m$^3$/S, $L_S$= 12.5m, $H_s$ = 97m and $H_o$ = 8.24m*

In order to limit construction costs of this model and to achieve the largest scale possible in the University of Stellenbosch hydraulic laboratory, a sluice gate type control structure was used for the model instead of a 4.5m high ogee spillway where a large portion of the spillway would have to be changed to accommodate the different flip bucket designs.

The sluice gate type control structure was considered because a similar flow profile could be achieved where the flow variables could also be better controlled. The Bernoulli equation was used to derive the equation for sluice gate flow along with **Figure 4.4**, **Figure 4.5** and **Figure 4.6**.

$$\frac{P_o}{\rho g} + \frac{{v_o}^2}{2g} + y_0 = \frac{P_1}{\rho g} + \frac{{v_1}^2}{2g} + y_1 + h_f + h_l \qquad \textit{EQUATION 4.14}$$

Where P is the pressure value at the respective positions (N/m$^2$),

ρ is the density of the fluid (kg/m$^3$),

g is the gravitational constant (9.81m/s),

v is the velocity at the respective positions (m/s),

z is the height from the datum to the water level (m),

$h_f$ is the frictional head losses, and

$h_l$ is the local head losses.

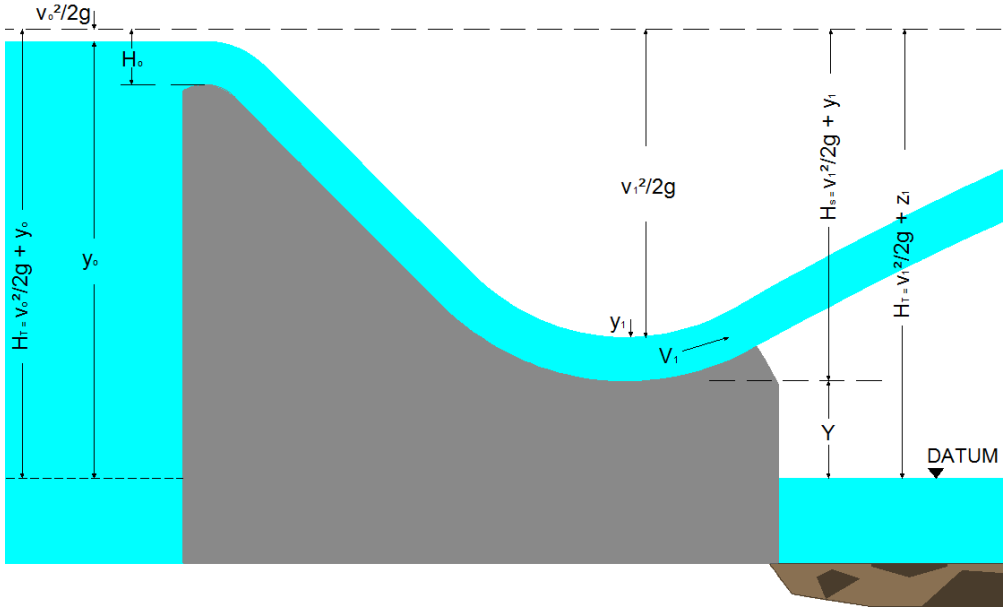


FIGURE 4.4: OGEE SPILLWAY

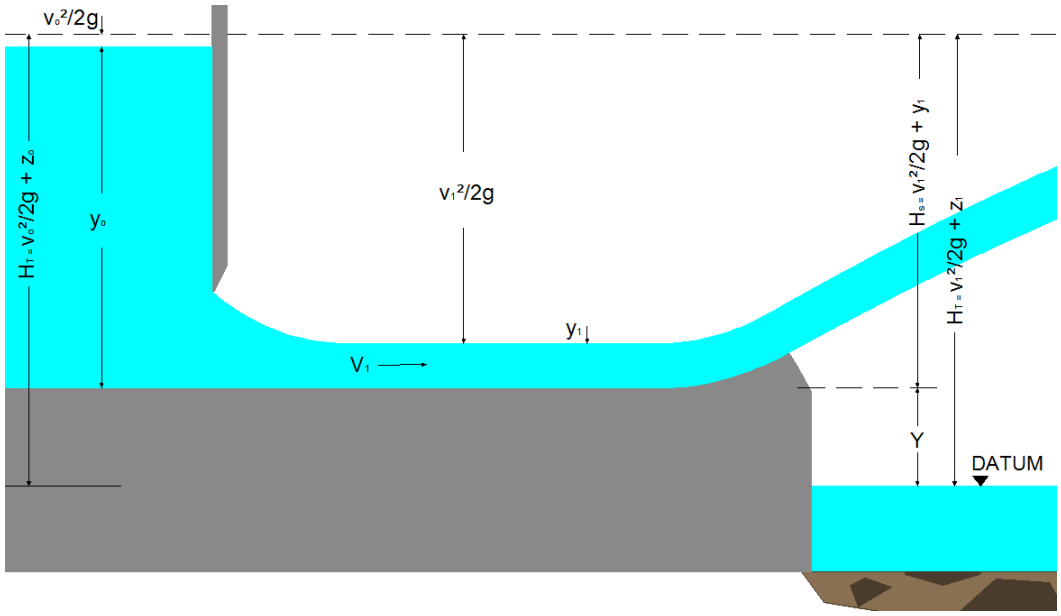


FIGURE 4.5: SLUICE GATE

From the Bernoulli equation the water depth at the flip bucket invert could be determined for various heads assuming flow over an ogee spillway with negligible frictional and local losses. These same flow parameters could then be achieved assuming sluice gate flow with specific gate openings relating to the required depths.

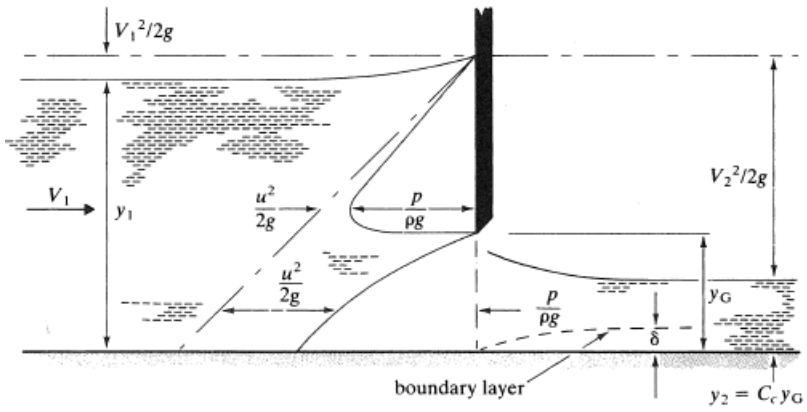


FIGURE 4.6: VERTICAL SLUICE GATE PARAMETERS (CHADWICK, ET AL., 2004)

The following equation derived from the Bernoulli equation was used in the hydraulic design of the sluice gated jet box:

$$Q = bC_c y_G \sqrt{2gy_1 \frac{y_1}{y_1 + y_2}} \qquad \text{EQUATION 4.15}$$

Where $y_G$ = *Gate opening, in m*

$C_c$ = *contraction coefficient relative to* $y_G$ *(0.61 for vertical sluice gate under free discharge)*

$y_1$ and $y_2$ as per **Figure 4.6**

### 4.4.2 APPROACH CHUTE

The approach chute of a ski-jump energy dissipator may be either a steep inclined spillway or a horizontal channel. Due to the chosen control structure a horizontal channel was used. The approach chute had the sole purpose of conveying the flow to the flip bucket. The length of the approach chute was chosen as 1.6m in the model (or 40 m in prototype).

### 4.4.3 DEFLECTION AND TAKE-OFF

When designing a ski-jump bucket the first thing that must be considered is what the trajectory requirements are in terms of performance. Due to the fact that this thesis is based on achieving a ski-jump design that would maximise energy dissipation and aeration of a variety of buckets needed to be tested.

Three types of flip bucket were designed, namely diverging flip buckets, converging flip buckets and composite flip buckets. For the remainder of this thesis these bucket types will be referred to as Type I, Type II and Type III flip buckets respectively. This will be described in detail below.

In total there were eight flip bucket designs that were tested. The design of all flip buckets were based on the theoretical approach discussed in Chapter 3 where each flip bucket was designed for the maximum flow condition.

#### 4.4.3.1 General Flip Bucket Design

As mentioned above the flip buckets were designed for a maximum head of 97m and Froude number of 13. In model scale the design head is 3.876m. Using **Equation 4.14** with $v_1^2 = (Q/(h_1B))^{2-}$, $h_1$ could be determined. Due to the fact that the spillway is open to the environment $P_o$=$P_1$=atmospheric pressure and that the $v_o$ relative to $v_1$ is so small that $v_o$ may be considered negligible. For design purposes the assumption is made that no energy losses are present upon the spillway, this is consider to be a conservative approach, therefore terms $h_f$ and $h_l$ fall away leaving the following term:

$$z_0 - z_1 = \frac{{v_1}^2}{2g} \qquad \text{EQUATION 4.16}$$

Where $z_1$-$z_2$ is the elevation difference between the initial water level in upstream section and the water level at the bottom of the spillway ($H_s$), therefore

$$Hs = \frac{{v_1}^2}{2g} \qquad \text{EQUATION 4.17}$$

Now the design flow condition suggests $H_s$ = 97m (3.876m in model scale), therefore the design velocity of the ski-jump buckets is equal to 44m/s (8.86m/s model scale).

#### 4.4.3.2 Type I - Diverging Flip Buckets

The Type I flip buckets are made up of the general circular-shaped flip bucket with diverging sidewalls. Type I flip buckets were designed with three deflection angles i.e. 30º, 40º and a 45º with $H_s$ of a prototype ogee spillway equal to 97m (3.876m model scale). The design guideline presented in Chapter 3 were followed for the geometric design. **Table 4.1** below shows the geometric design parameters of the Type I flip buckets and **Figure 4.7** shows a graphical representation of these parameters.

TABLE 4.1: TYPE I FLIP BUCKET DESIGN PARAMETERS (MODEL DIMENSIONS)

| Type I Flip Bucket Design | | | | |
|---|---|---|---|---|
| **Scale from prototype** | **1/λ** | 1/25 | | |
| **Deflection Angle (º)** | **$\alpha_1$** | 30 | 40 | 45 |
| **Radius (m)** | **r** | 0.597 | 0.342 | 0.273 |
| **Length (m)** | **$L_b$** | 0.299 | 0.220 | 0.193 |
| **Height (m)** | **$h_b$** | 0.08 | 0.08 | 0.08 |
| **Divergence Angle (º)** | **$\beta_s$** | 1.435 | 1.435 | 1.435 |
| **Elevation Difference (m)** | **Y** | 0.433 | 0.433 | 0.433 |

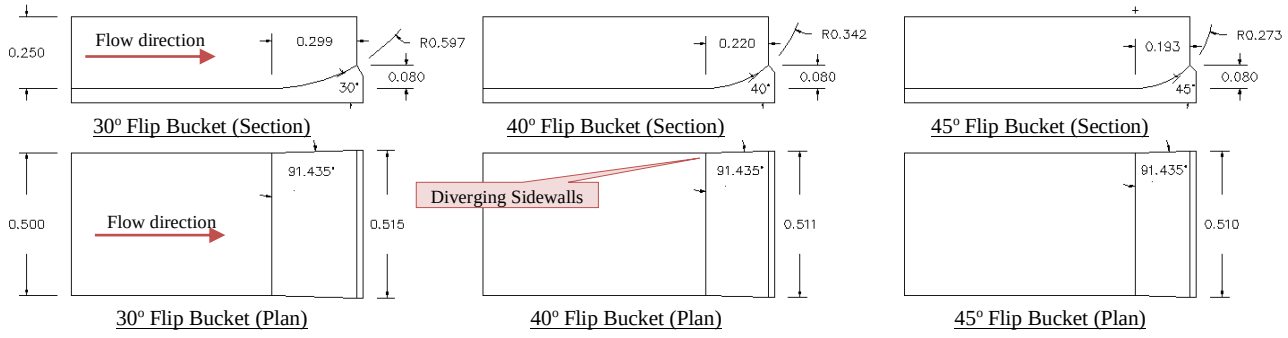


*FIGURE 4.7: TYPE I FLIP BUCKET MODEL DIMENSIONS*

### 4.4.3.3 *Type II - Converging Flip Buckets*

The converging Type II flip buckets were designed based on the research conducted on the slit type flip buckets as described in **Section 2.8.2.1**. Type II flip buckets were designed with three deflection angles i.e. 30°, 40° and a 45° with $H_s$ of a prototype ogee spillway equal to 97m (3.876m model scale). The design guidelines presented in Chapter 3 were followed for the geometric design. With the maximum Froude number of 13 the contraction ratio was chosen as $\beta_s = 0.25$. **Table 4.2** below shows the geometric design parameters of the Type II flip buckets and **Figure 4.8** shows a graphical representation of these parameters.

*TABLE 4.2: TYPE II FLIP BUCKET DESIGN PARAMETERS (MODEL DIMENSIONS)*

| **Type II Flip Bucket Design** | | | | |
|---|---|---|---|---|
| **Scale from prototype** | **1/λ** | 1/25 | | |
| **Deflection Angle (°)** | **$\alpha_1$** | 30 | 40 | 45 |
| **Radius (m)** | **r** | 0.597 | 0.342 | 0.273 |
| **Length (m)** | **$L_b$** | 0.299 | 0.220 | 0.193 |
| **Height (m)** | **$h_b$** | 0.08 | 0.08 | 0.08 |
| **Convergence Angle (°)** | **$\beta_s$** | 14 | 14 | 14 |
| **Elevation Difference** | **Y** | 0.433 | 0.433 | 0.433 |

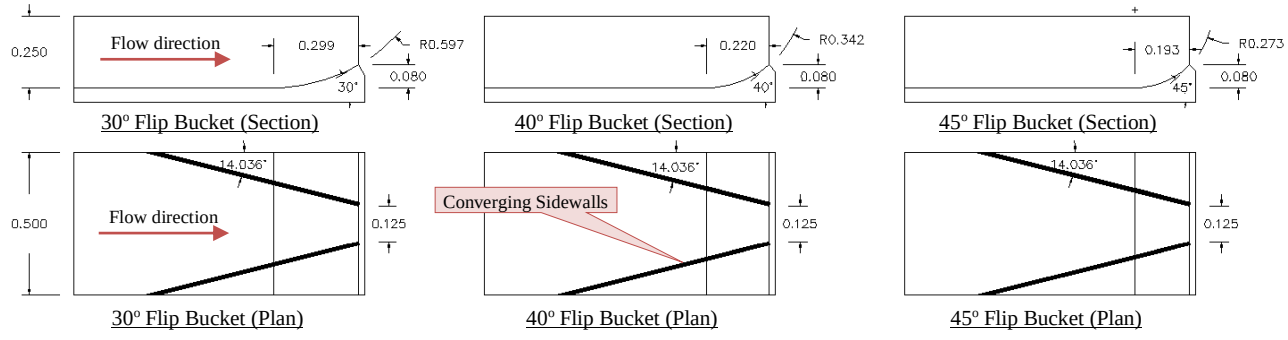


*FIGURE 4.8: TYPE II FLIP BUCKET MODEL DIMENSIONS*

### 4.4.3.4 *Type III Composite*

The final set of flip buckets to be designed were the experimental composite flip buckets. These flip buckets are the author's design and different from previous research conducted. Two versions of this type of bucket were tested as part of this study, i.e. a Scoop type and a Butterfly type. These two flip

buckets have the fundamentals of a typical ski-jump flip bucket, but incorporate features that are different from any other that could be found by the author in the literature. As stated in **Section 2.8.2.1**, the composite flip bucket generally includes a non-uniform bucket radius over the circumference of the bucket or side-by-side flip buckets of different trajectory angles, however it is assumed that very little research has been conducted on a non-uniform bucket radius over the width of the bucket with varies trajectory angles as the author did not come across any associated literature. The intention of these designs is to improve the spread of the water jet over a larger area at the point of impingement in order to reduce the peak forces, as well as the mean force per square meter. These flip buckets were designed by utilising a combination of plain circular bucket general designs and incorporating features that promote the dispersion of the water jet into a single flip bucket such as the diverging sidewalls, non-uniform cross sections across the width of the flip bucket and varied trajectory angles. The two Type III flip bucket model dimensions are shown in **Figure 4.9** below.

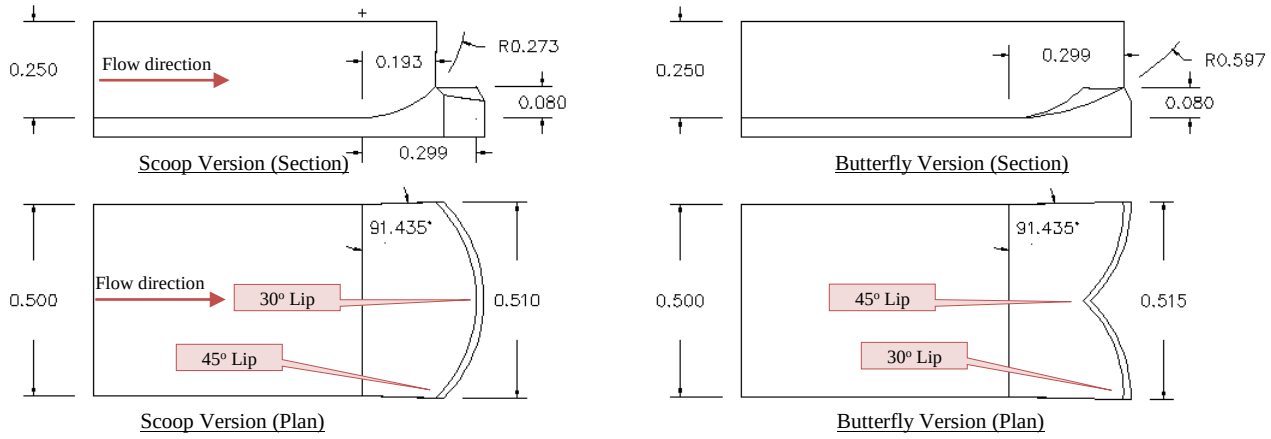


*FIGURE 4.9: TYPE III FLIP BUCKET MODEL DIMENSIONS*

### *45°-30°-45° Bucket – Scoop version*

The design of the first composite flip bucket was achieved by using the three previously designed Type I buckets; 30°, 40° and 45°, and combining them into one where the trajectory angle starts at 30° at the centre and ends at 45° at the sidewalls. All angles between the centreline and sidewalls were interpolated accordingly. Henceforth this multi trajectory bucket will be referred to as the Scoop flip bucket due to its spoon type shape.

The intended function of the Scoop type flip bucket was to increase the longitudinal spread of the water jet with the varied trajectory angles. The shape of the Scoop flip bucket with its concave curvature promotes angular streamlines slightly directing the flow towards the centreline, however the varied bucket lip angles encourages increased dispersion of the jet in the longitudinal direction.

### *30°-45°-30° Bucket – Butterfly version*

The design of the second multi trajectory arch flip bucket was achieved by using the three previously designed Type I buckets; 30°, 40° and 45°, and combining them into one where the trajectory angle

starts at 45° at the centre and ends at 30° at the sidewalls. All angles between the centreline and sidewalls were interpolated accordingly. Henceforth this multi trajectory bucket will be referred to as the Butterfly flip bucket due to its butterfly wing type shape.

The intended function of the Butterfly type flip bucket was to increase the transverse deflection of the water jet. The shape of the Butterfly flip bucket with its raised centre promotes angular streamlines slightly directing the flow towards the sidewalls thereby increasing the potential lateral dispersion of the jet. Additionally the varied bucket lip angles encourages increased dispersion of the jet in the longitudinal direction.

## 4.5 CONSTRUCTION OF THE SKI-JUMP MODEL

### 4.5.1 CONTROL VALVE AND PIPE INSTALLATION

The initial stages of the construction of the ski-jump hydraulic model was installing and connecting a 6m, 450 mm diameter pipe to the existing pipe network within the water laboratory at Stellenbosch University. The pipe was aligned and levelled according to typical design specifications. The length of pipe was required to be as long as possible so that the momentum of flow was directly parallel to the direction of the intended ski-jump trajectory. Due to space restrictions and economic considerations a 6m length pipe was recommended. The pipe diameter was chosen to restrict the maximum velocity to 1.3 m/s with in the pipe thereby alleviating turbulence and sustaining uniform flow. A gate valve was procured and installed at the far end of the 6m pipe length (relative to the model) with the sole purpose of isolating flow to the model during periods between tests. This would allow better repeatability of tests as well as test efficiency as the pipe network would not be depressurised in between tests. The pipe setup is depicted in **Figure 4.10**.

*FIGURE 4.10: CONTROL VALVE AND 450MM DIAMETER PIPE*

### 4.5.2 JET BOX DESIGN AND CONSTRUCTION

Initially the jet box was designed to be constructed of Perspex, but upon review it was decided that Perspex would not be able to contain the pressure forces created within the jet box. Although more expensive and labour intensive the material chosen for the construction of the jet box was steel. A detailed plan layout of the individual mild steel plates that were used in the construction are shown in Appendix II. **Figure 4.11** below shows the completed jet box after all steel plates had been welded together and attached to the system. As stated above a sluice gate was used as the control structure for the hydraulic model. A groove was routed into the sidewalls of the jet box sidewalls where the sluice gate (**Figure 4.12**) could slide into place. A rubber strip was glued to the back face of the sluice gate to create a watertight seal which prevented any water escaping at the top. It was predicted that the watertight rubber seal would create too much frictional resistance to be operated by hand, therefore a threaded rod was used with nuts welded to the sluice gate to mechanically raise and lower it to obtain the desired opening.

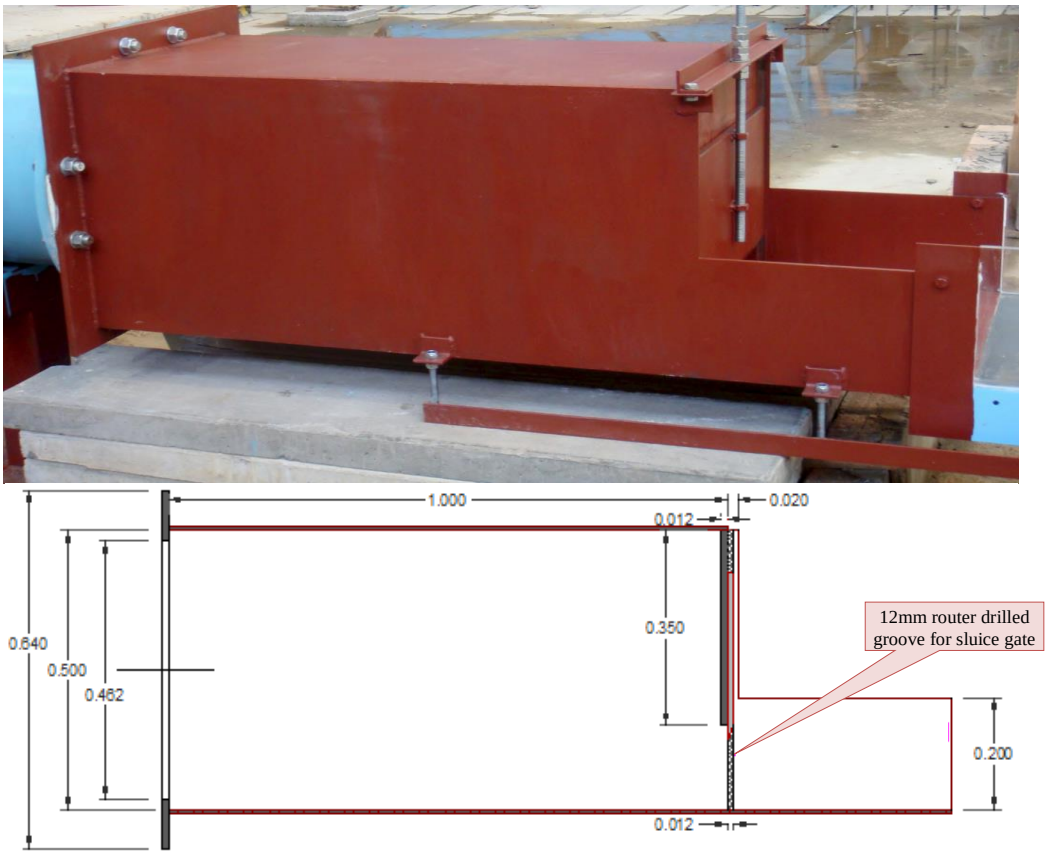


*FIGURE 4.11: STEEL JET BOX DESIGN (MODEL DIMENSIONS IN m)*

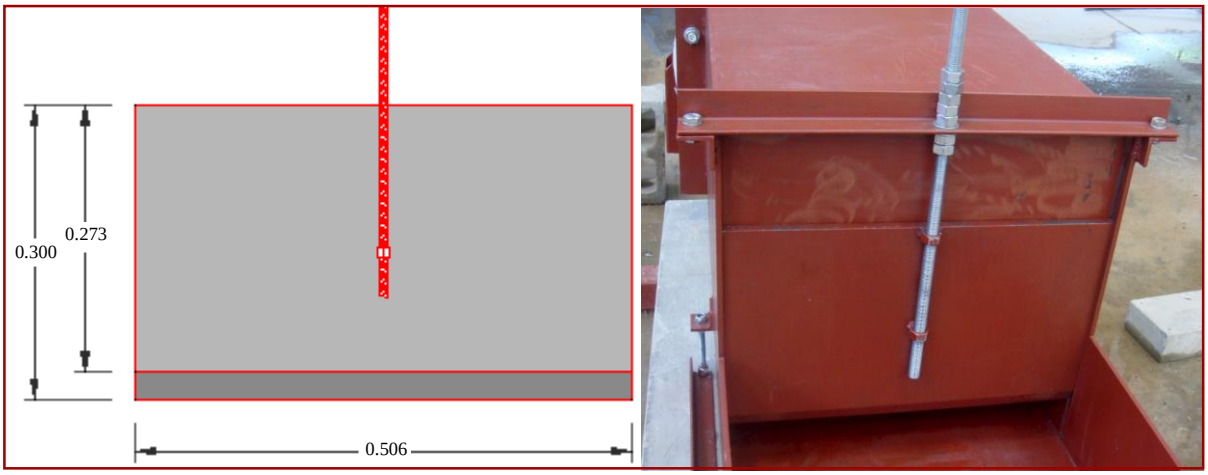


FIGURE 4.12: STEEL SLUICE GATE DESIGN (MODEL DIMENSIONS IN m)

### 4.5.3 APPROACH CHANNEL

The approach channel was constructed of a wooden frame with Perspex sidewalls to ensure visibility and a PVC channel floor which folded over the ski-jump flip buckets to ensure that a smooth transition of flow could take place without introducing any flow disturbance due to surface irregularities. The approach channel had a total length of 1.6m (model dimensions) from the sluice gate opening to the ski-jump bucket lip. Concrete slabs were used to support the entire model. Small sections of angle iron were welded and bolted to the sides of the model where threaded rods and nuts were used to manually adjust the slope of the approach channel and make sure it was completely level. **Figure 4.13** shows the approach channel and levelling system.

FIGURE 4.13: SKI-JUMP HORIZONTAL CHANNEL

### 4.5.4 FLIP BUCKETS

For all flip buckets the material of choice was sheet plywood with a PVC sheet surface. The reason for this material choice was that these materials are the cheapest and preferred materials used in the hydraulics laboratory given the available machinery. The plywood was cut into the respective side profile bucket shapes and glued together with a rod running through the middle for added support. The bucket was then sanded and painted with a water proofing paint to ensure no swelling of the plywood and to obtain a smooth finish.

#### *4.5.4.1 Type I Diverging Flip Buckets*

The Type I bucket was a simple design and relatively easy to construct as the same sectional profile was present throughout. One of the completed Type I flip buckets is shown in **Figure 4.14**.


*FIGURE 4.14: 30° TYPE I FLIP BUCKET MODEL DESIGN*

#### *4.5.4.2 Type II Converging Flip Buckets*

To save construction costs and time the Type I buckets were used for the Type II buckets. Once all testing of a Type I bucket was completed, converging perspex sidewalls were constructed and inserted into the channel and sealing with a heavy duty silicone sealant. **Figure 4.15** below shows one of the completed Type II flip buckets.

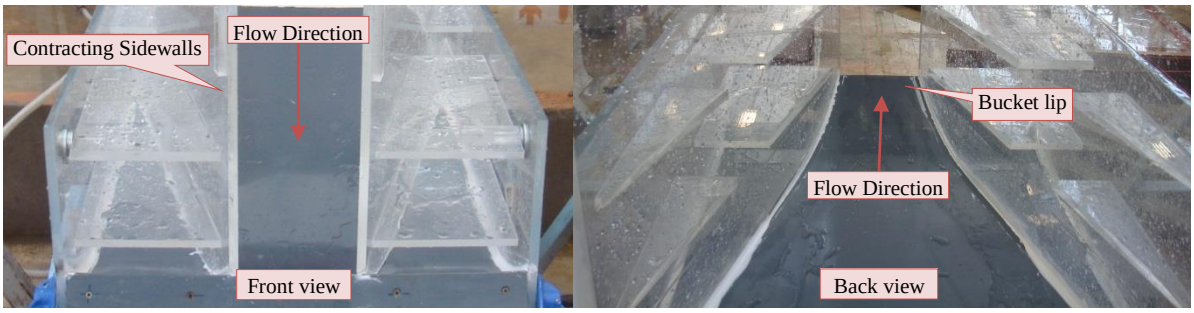


*FIGURE 4.15: 40° TYPE II FLIP BUCKET MODEL DESIGN*

#### *4.5.4.3 Type III Composite Flip Buckets*

The Type III flip buckets were the most difficult and labour intensive to construct due to the fact that the bucket radius, length and lip angle varied throughout the width. Each piece of plywood that was cut was unique. **Figure 4.16** shows the different plywood sections in the initial stages of its construction.

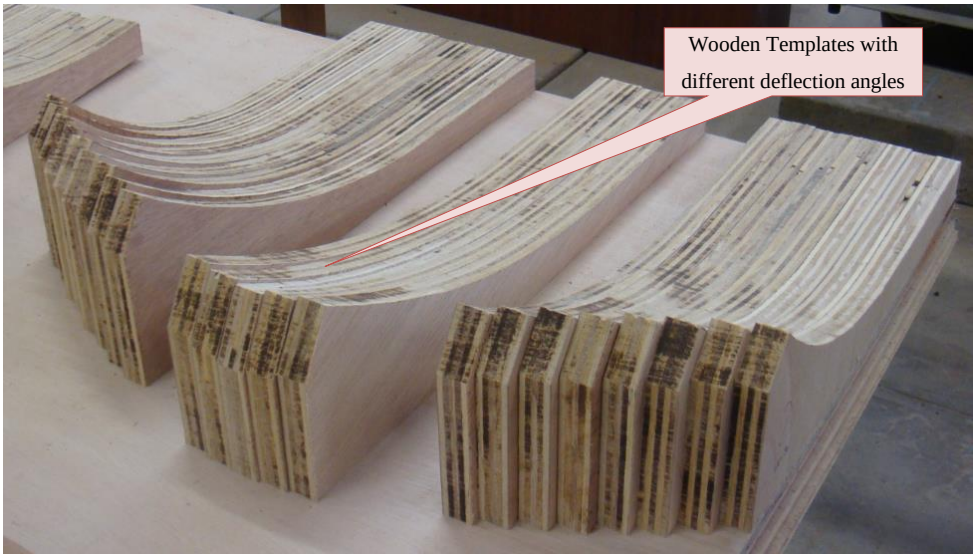


FIGURE 4.16: TYPE III FLIP BUCKET CONSTRUCTION (WOODEN TEMPLATES)

Once all the pieces had been cut, glued and supported poly filler was used to backfill all the irregularities. The pieces were sanded and painted for a smooth finish and water proofing. **Figure 4.17** and **Figure 4.18** show the completed Scoop and Butterfly Type III flip buckets respectively.

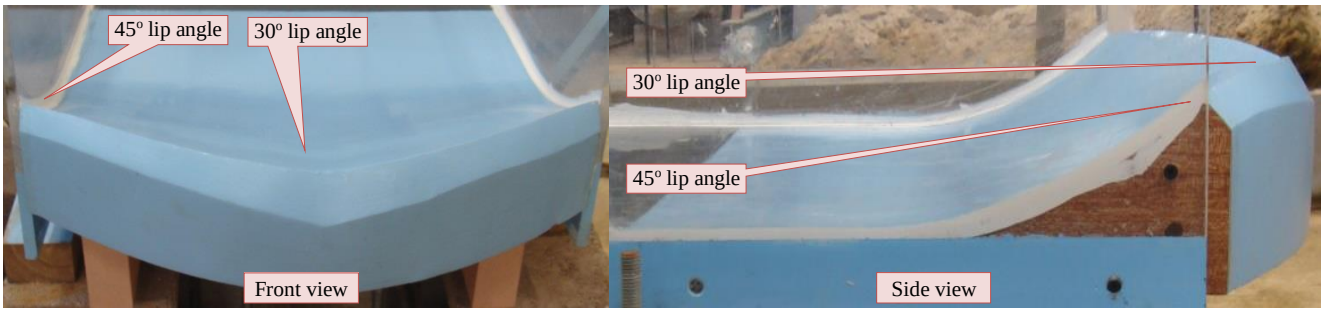


FIGURE 4.17: SCOOP TYPE III FLIP BUCKET MODEL DESIGN

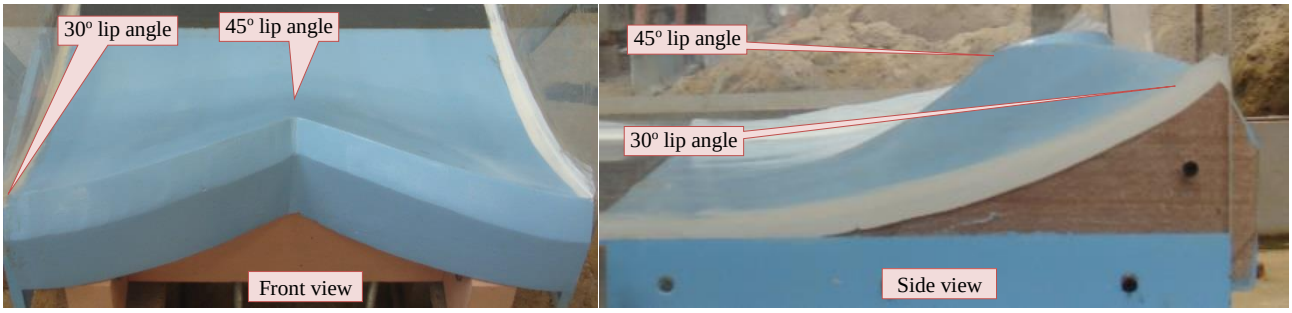


FIGURE 4.18: BUTTERFLY TYPE III FLIP BUCKET MODEL DESIGN

## 4.6 TESTS CONDUCTED

All testing experiments conducted were carried out in specific order to accomplish the thesis goal of determining a ski-jump design that would maximise energy dissipation and aeration. The tests were initiated in a sequence that allow smooth progression when interchanging flip buckets.

To encapsulate most flow scenarios present on a ski-jump, both varied flow conditions and varied flow depth conditions were studied. Four Froude numbers were tested; namely 6, 8, 10 and 13. Each Froude number had two conditions associated. **Table 4.3** shows the different flow conditions that were conducted on each flip bucket. Flow conditions 1 to 3 represent varied discharge while the flow depth remains constant and flow conditions 5-7 simulates varied flow depth while the discharge remains constant at the maximum. Flow condition 4 is the design flow condition which all flip bucket designs were based upon. This flow condition was used in the simulation of both varied discharge and varied flow depth.

*TABLE 4.3: FLOW CONDITIONS TO BE TESTED FOR EACH BUCKET*

| Flow Condition | Head above invert, $H_s$ (Prototype Scale) (m) | Head above invert, $H_s$ (Model Scale) (m) | Discharge, Q (prototype Scale) ($m^3/s$) | Discharge, Q (model Scale) (l/s) | Flow Depth, $h_1$ (prototype Scale) (m) | Flow Depth, $h_1$ (model Scale) (m) |
|---|---|---|---|---|---|---|
| **1** | 21 | 0.826 | 288.42 | 92.3 | 1.15 | 0.0459 |
| **2** | 37 | 1.468 | 384.69 | 123.1 | 1.15 | 0.0459 |
| **3** | 57 | 2.293 | 480.63 | 153.8 | 1.15 | 0.0459 |
| **4** | 97 | 3.876 | 625.00 | 200.0 | 1.15 | 0.0459 |
| **5** | 35 | 1.382 | 625.00 | 200.0 | 1.92 | 0.0768 |
| **6** | 51 | 2.029 | 625.00 | 200.0 | 1.59 | 0.0634 |
| **7** | 68 | 2.732 | 625.00 | 200.0 | 1.37 | 0.0546 |

**Table 4.4** shows all tests conducted on the ski-jump hydraulic model excluding calibration tests which will be highlighted in the proceeding sections. For each Froude number two conditions were tested. One condition was tested using the minimum flow depth and the other was tested using the maximum discharge.

TABLE 4.4: SUMMARY OF ALL TEST CONDITIONS CONDUCTED

| Bucket Type | Deflection angle $\alpha_o$ (°) | Two flow depths for each Froude Number $F_o$ | | | | n |
|---|---|---|---|---|---|---|
| | | 6 | 8 | 10 | 13 | |
| I | 30 | 0.0459; 0.0768 | 0.0459; 0.0634 | 0.0459; 0.0546 | 0.0459 | 7 |
| II | 30 | 0.0459; 0.0768 | 0.0459; 0.0634 | 0.0459; 0.0546 | 0.0459 | 7 |
| I | 40 | 0.0459; 0.0768 | 0.0459; 0.0634 | 0.0459; 0.0546 | 0.0459 | 7 |
| II | 40 | 0.0459; 0.0768 | 0.0459; 0.0634 | 0.0459; 0.0546 | 0.0459 | 7 |
| I | 45 | 0.0459; 0.0768 | 0.0459; 0.0634 | 0.0459; 0.0546 | 0.0459 | 7 |
| II | 45 | 0.0459; 0.0768 | 0.0459; 0.0634 | 0.0459; 0.0546 | 0.0459 | 7 |
| III | 45-30-45 | 0.0459; 0.0768 | 0.0459; 0.0634 | 0.0459; 0.0546 | 0.0459 | 7 |
| III | 30-45-30 | 0.0459; 0.0768 | 0.0459; 0.0634 | 0.0459; 0.0546 | 0.0459 | 7 |
| | | | | **Total Number** | | **56** |

## 4.7 DATA ACQUISITION EQUIPMENT AND ACCURACY

This section highlights the apparatus used for all testing conducted as well how the data was captured and the accuracy thereof.

### 4.7.1 WATER DISCHARGE MEASUREMENTS

The model jet discharge rate, $Q_m$, was measured with the use of a SAFMAG electromagnetic flowmeter, which has a good accuracy and repeatability and is able to measure the flows and velocities of any conductive liquid with no head loss across the meter. According to Flow Metrix (2013) this flowmeter has an accuracy of +/- 0.5% of flow rate and a repeatability of +/- 0.1% of flow rate. **Figure 4.19** shows the SAFMAG flowmeter and a diagram of how it works.

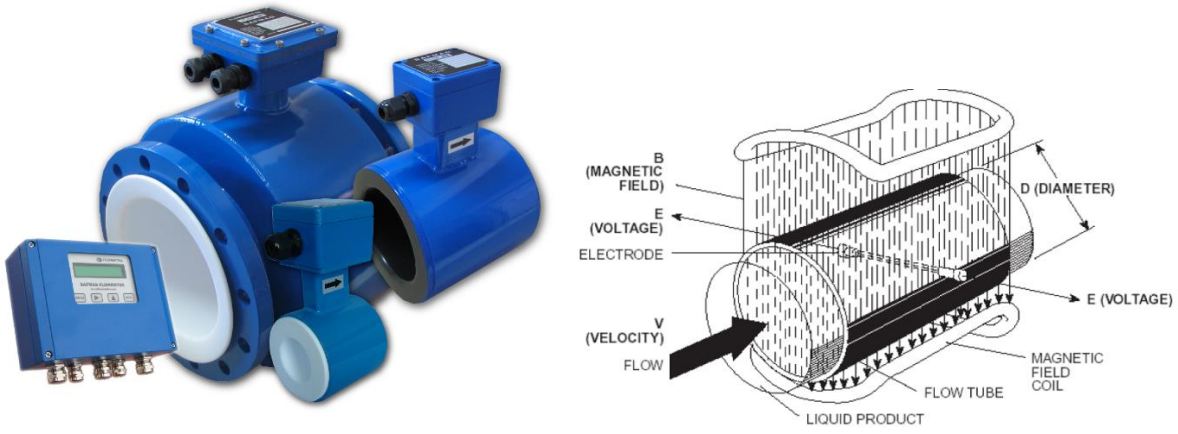


FIGURE 4.19: SAFMAG ELECTROMAGNETIC FLOW METER (FLOW METRIX, 2013)

According to Flow Metrix (2013), "the operation of an electromagnetic flow meter can be explained by Faraday's law of electromagnetic induction. A voltage moving at a right angle to an electromagnetic

field through an electrical conductor, is directly proportional to the velocity of that conductor through the field".

### 4.7.2 ACQUISITION OF GEOMETRIC MEASUREMENTS

For the retrieval of geometric results of the ski-jump trajectory jet two techniques were used, namely the dumpy level technique and photographic dimensioning. These techniques both involved manual operation and therefore human error is a factor that had to be considered. Multiple tests were conducted with these two techniques for each flow condition of each bucket type and the results were averaged in order to retrieve the final dimensions.

#### *4.7.2.1 Dumpy Level Method, Associated Errors and Correction Thereof*

The use of a dumpy level was the initial proposed method for acquiring the geometric data of the trajectory jet, specifically the heights and lengths of the trajectory upper and lower apexes. The initial procedure for this method of measurement for a specific test required setting out the dumpy level at a distance and level similar to that of the corresponding theoretical values. The dumpy level staff was positioned directly opposite against the vertical grid. The specific flow would then be initiated and measurements taken. However, this method resulted in a parallax error where in order to obtain the most accurate reading the dumpy level must be set to a position and elevation exactly that of the unknown reading which is required. The dumpy level was set numerous times before a sufficient reading could be taken. Due to the fact that measurements were taken on a geometric grid 2.67 m behind the side profile of the jet trajectory from an instrument 3 m before the side profile of the jet trajectory, a small inaccuracy in the level and distance of the measuring instrument would yield even greater inaccuracies in the results.

A parallax is defined as, "*The effect whereby the position or direction of an object appears to differ when viewed from different positions*". A parallax error is basically a line of sight error where unless the readings are not taken at a position directly perpendicular to the point of measurement then an inaccurate reading will be the result. This parallax error has a significant contribution to the validity of the raw results.

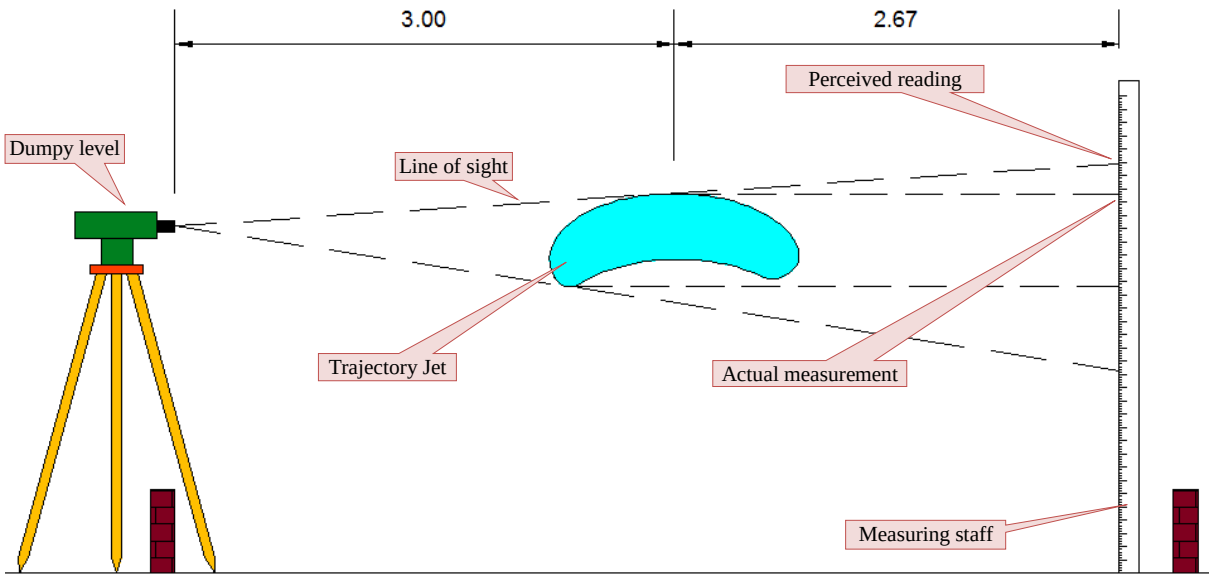


FIGURE 4.20: ILLUSTRATION OF DUMPY LEVEL METHOD

In order to correct or limit the effects of parallax errors a new procedure for the acquisition of geometric measurements was developed. Firstly the dumpy level was set out at a distance and level similar to that of the lower jet trajectory. This exact position was recorded. The measuring staff was positioned directly opposite as before. Readings were taken for both the lower and upper trajectories of the jet at this position using the swivel function of the dumpy level to rotate the line of sight in the x and z direction. The dumpy level was then positioned at a distance and level similar to that of the upper trajectory and readings were recorded. Due to the fact that these readings contain a degree of parallax error, post-processing of the data was required whereby using simple trigonometry the true values which represent the geometry of the trajectory jet could be determined. **Figure 4.20** above shows a simple sketch of this method.

#### *4.7.2.2 Photographic Scaling Dimensioning, Associated Errors and Correction Thereof*

The second and most preferred method for retrieving the geometric data for the trajectory jet was by means of photographic images. This method included capturing a photograph of the trajectory characteristics of the ski-jump water jet with certain markers for scaling and dimensioning in the AutoCAD Civil 3D software. One of the major errors associated with image capturing is that there is a degree of distortion that is perceived in the final image. When a photograph is captured distortion is either caused by a characteristic of the lens or the relative position of the camera to the object. This type of distortion may be corrected and reduced by capturing the photo as parallel to the object as possible. The focal point of a photo is considered to have very little to no distortion but increases substantially towards the outside of the image. These effects were limited by making sure that the point of measurement and scaling were both at the focal point. For accurate measurement a 1m ruler was positioned underneath the trajectory at the centreline and measured distance from the flip bucket lip.

This would allow for accurate scaling and dimensioning. **Figure 4.21** and **Figure 4.22** show examples of how the geometry of the trajectories were dimensioned.

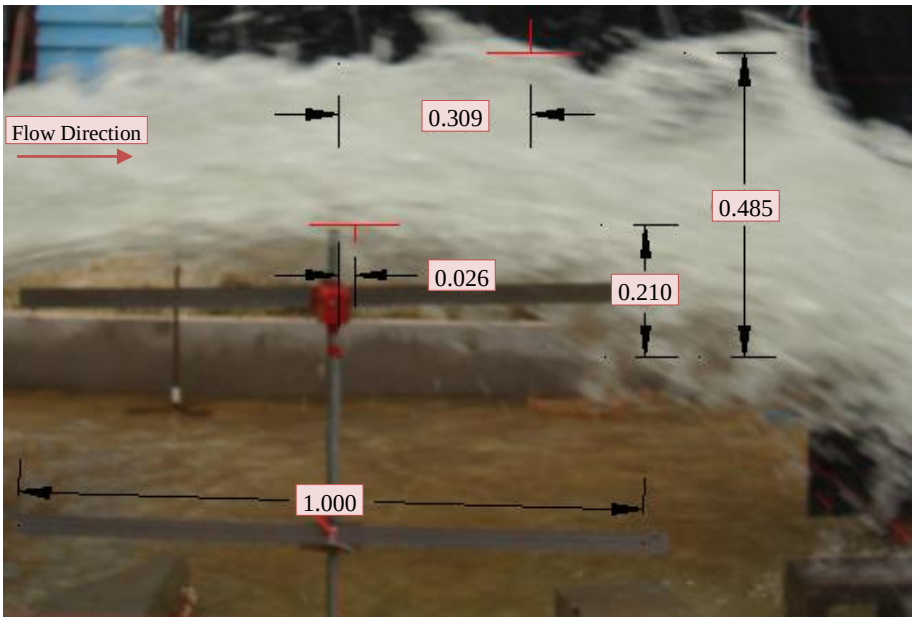


*FIGURE 4.21: PHOTOGRAPHIC DIMENSIONING EXAMPLE OF TRAJECTORY HEIGHT AND ASSOCIATED POSITION*

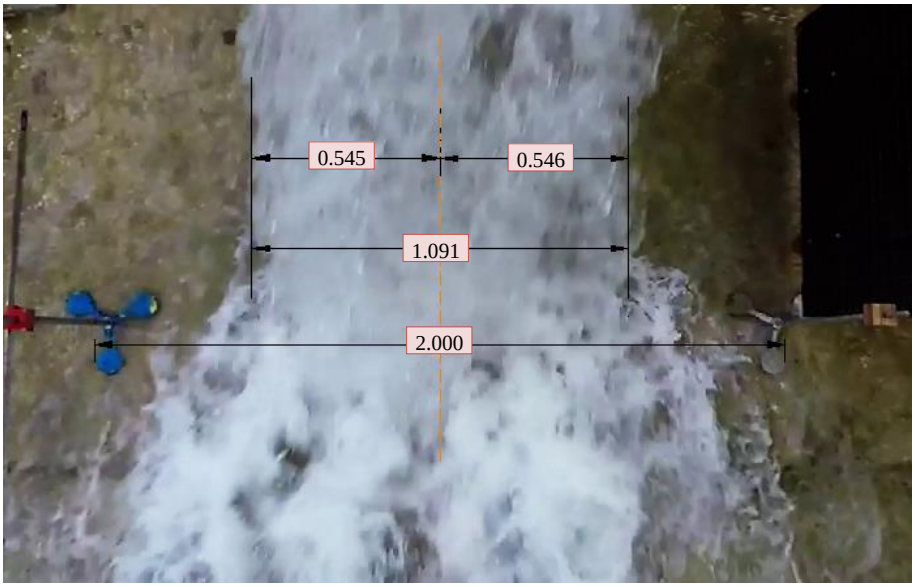


*FIGURE 4.22 PHOTOGRAPHIC DIMENSIONING EXAMPLE OF TRANSVERSE IMPACT WIDTH*

### 4.7.3 ACQUISITION OF WATER IMPACT PRESSURES

Nine S-10 type pressure transducers, manufactured by WIKA, were used for the measurement of the dynamic pressure of the water jet impacting the plate. A 3X3 grid with spacing of 250mm was used for the placement of the pressure transducers on a 900mm X 900mm plate as show in **Figure 4.23**.

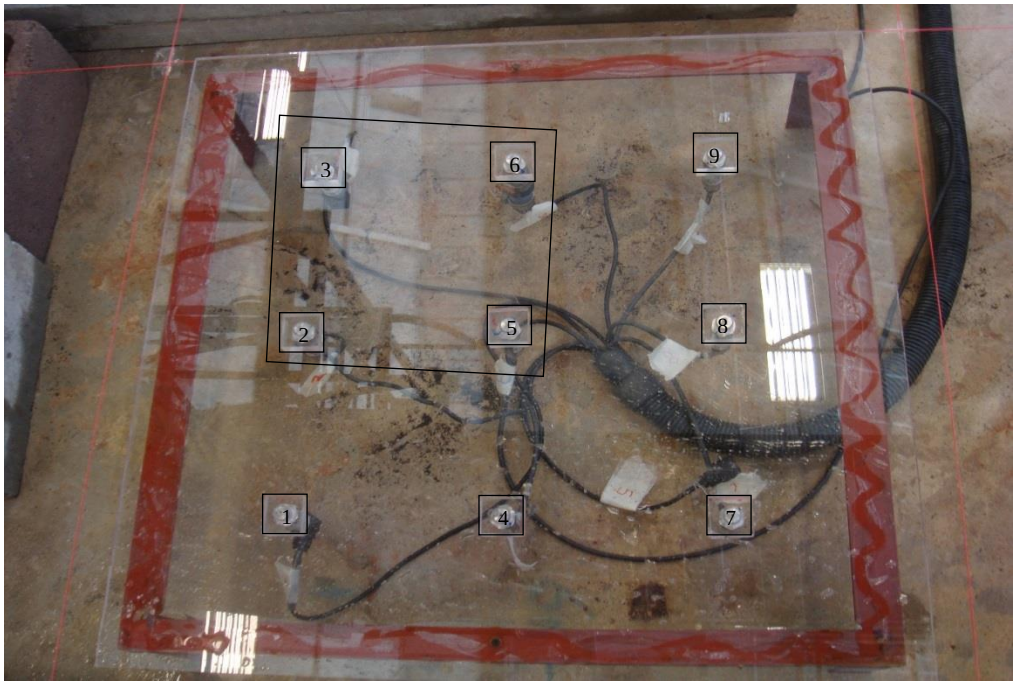


FIGURE 4.23: PRESSURE PLATE AND PRESSURE TRANSMITTER LOCATIONS

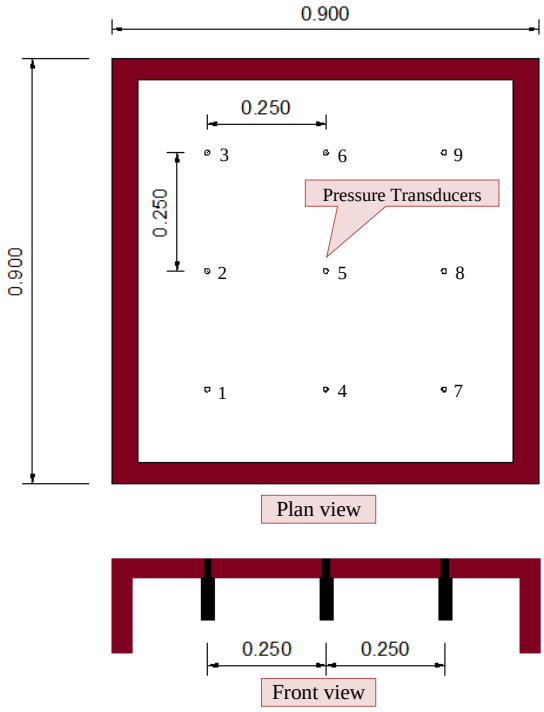


FIGURE 4.24: PRESSURE PLATE DIMENSIONS

Two different types of S-10 pressure transducers were used, namely a 600 mbar range and a 200 mbar range. **Figure 4.25** shows the two different pressure transducer types.

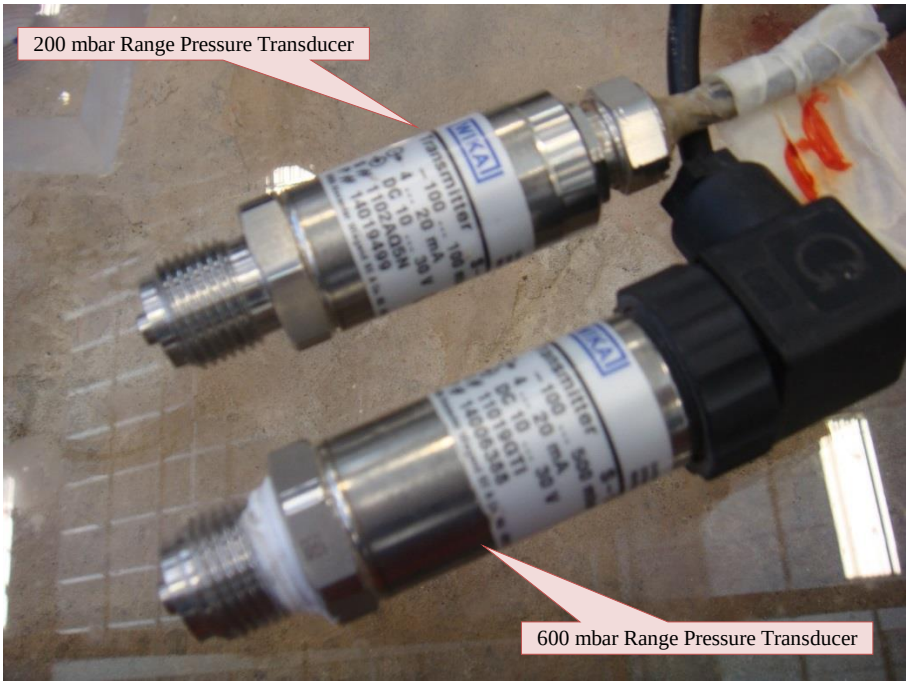


*FIGURE 4.25: 200 AND 600 mbar PRESSURE TRANSMITTERS*

A summary of the of the two types of pressure transducers including their output signals, maximum and minimum pressure ranges as well as their installed locations on the plate is shown in **Table 4.5**.

*TABLE 4.5: S-10 PRESSURE TRANSDUCERS*

| **Pressure Transmitters Range** | **Minimum Measure Range** | **Maximum Measure Range** | **Location on Pressure Plate (**Figure 4.24**)** |
|---|---|---|---|
| **600 mbar** | -1 m water | +5 m water | 2,3,5 and 6 |
| **200 mbar** | -1 m water | +1 m water | 1,4,7,8 and 9 |

The pressure transducers take readings of the current in milli-Ampere (mA) which is directly converted, using a data logging box, to a voltage (V) over a 120 Ω resistor using Ohm's Law (V = I x R). With the use of this relationship one is able to use the pressure head range (m water) and relate it to the voltage readings of the pressure transducers to return a pressure head (m water). This relationship is shown in **Equation 4.18** and **Equation 4.19** for the 600 mbar and 200 mbar pressure transducers respectively (as obtained from the manufacturer).

$$Y_{(m)} = \frac{(+5_{(m)}) - (-1_{(m)})}{20_{(mA)} - 4_{(mA)}} \, x \, \frac{x_{(V)}}{120_{(\Omega)}} \, x \, 1000 - 2.5 \qquad \textit{EQUATION 4.18}$$

$$Y_{(m)} = \frac{(+1_{(m)}) - (-1_{(m)})}{20_{(mA)} - 4_{(mA)}} x \frac{x_{(V)}}{120_{(\Omega)}} x\, 1000 - 1.5 \qquad \text{EQUATION 4.19}$$

#### 4.7.3.1 Calibration

The values of 2.5 and 1.5 in **Equation 4.18** and **Equation 4.19** account for the atmospheric hydrostatic pressure reading of the pressure transducers, but because atmospheric pressure is dependent on various factors such as temperature and altitude it cannot be treated as a constant if highly accurate result are to be captured. By assuming a constant value for the pressure transducers, a maximum deviation of 5.34% from the actual initial zero reading occurred in the results. Therefore, it was decided to take an average initial reading for each pressure transducer and deduct it from the corresponding test reading resulting in the following equations for the 600 mbar and 200mbar pressure transducers respectively:

$$Y_{(m)} = \frac{(+5_{(m)}) - (-1_{(m)})}{20_{(mA)} - 4_{(mA)}} x \frac{\left(x_{(Volt)} - x_{initial\,(Volt)}\right)}{120_{(\Omega)}} x\, 1000 \qquad \text{EQUATION 4.20}$$

$$Y_{(m)} = \frac{(+1_{(m)}) - (-1_{(m)})}{20_{(mA)} - 4_{(mA)}} x \frac{\left(x_{(V)} - x_{initial\,(Volt)}\right)}{120_{(\Omega)}} x\, 1000 \qquad \text{EQUATION 4.21}$$

A frequency of 100 Hz was used over the 5 minutes to yield a data set of 30000 pressure readings for each pressure transducer with an accuracy of ±0.5% over the total pressure range. Therefore the accuracies of the 600 mbar and 200 mbar pressure transducers are 30mm and 10mm respectively. A 0.1% exceedance probability was used in order to obtain the peak pressures for each transducer

### 4.7.4 ACQUISITION OF AIR CONCENTRATION PERCENTAGE

The acquisition of the air content within the ski-jump jet at the point of trajectory was retrieved with a Thermo Needle Probe System (TNP) which includes an air probe needle (**Figure 4.26**), TNP device also referred to a data logger and data acquisition software (TNP Control 2.0).

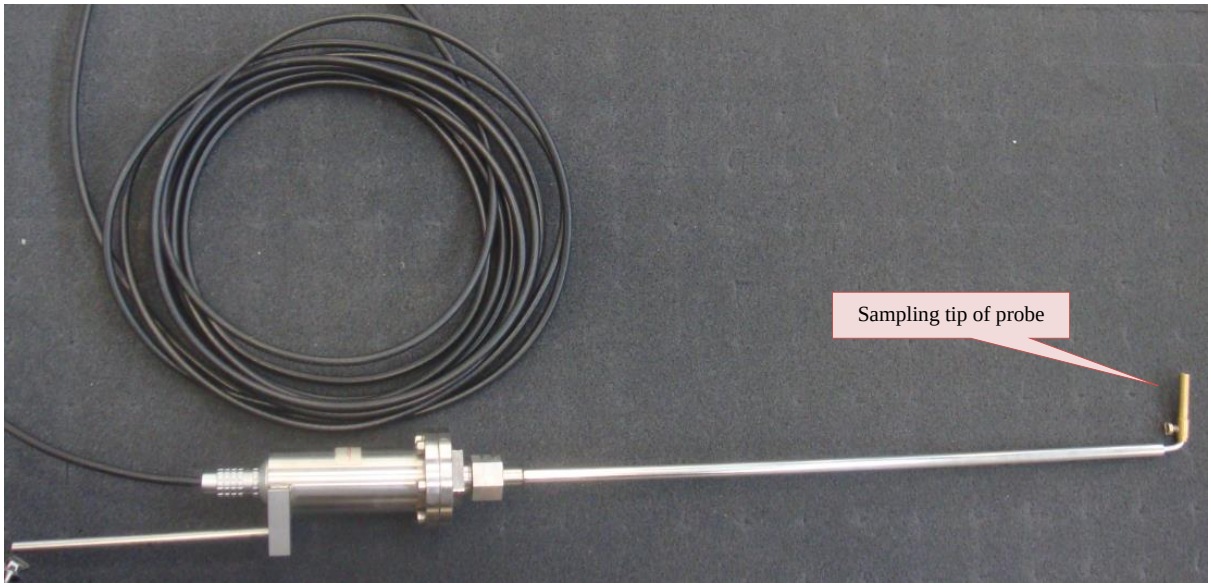


FIGURE 4.26: AIR PROBE

The air probe was inserted into the water jet directly after the point of separation from the flip bucket. The idea behind this was to calculate the immediate air entrainment of flip bucket at different locations within the jet core. This would show which flip bucket entrains air the best which theoretically displays signs of better dispersion, spray and ultimately a contributing factor to better energy dissipation.

Three different positions were measured within the horizontal trajectory jet including the centreline, 125mm from the centreline (quarter of bucket width) and 20mm from the sidewall as shown in **Figure 4.27**. All these measurements were taken perpendicular to the direction of flow at a horizontal distance of 150mm from the flip bucket lips. **Figure 4.28** shows the air probe inserted into the jet flow while a test was being conducted.

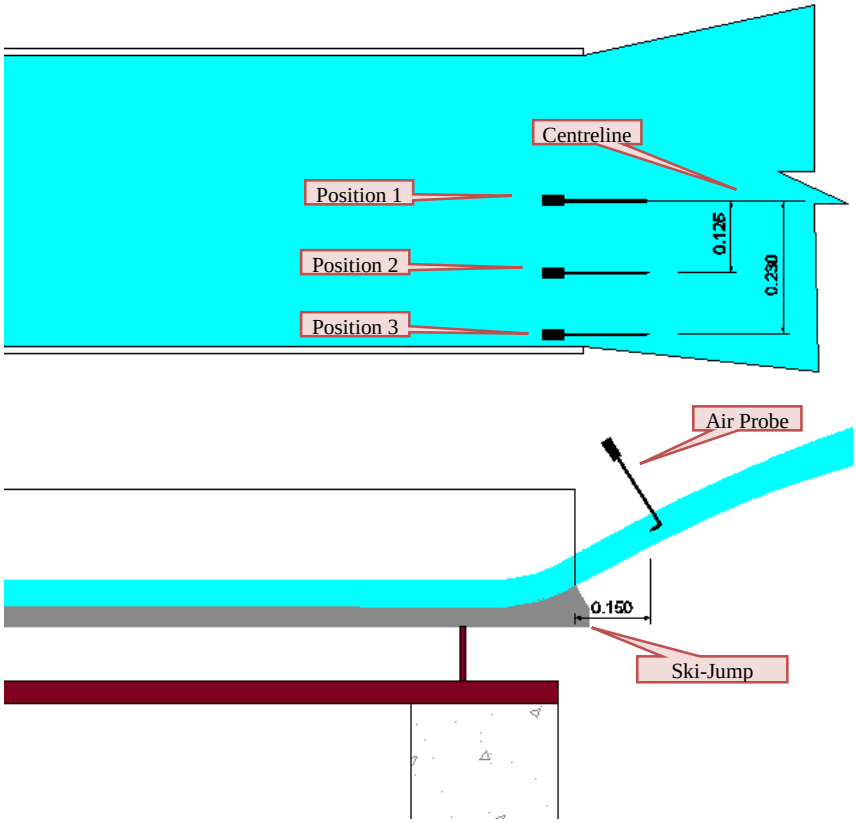


FIGURE 4.27: AIR PROBE POSITIONS


FIGURE 4.28: AIR PROBE TESTING

### 4.7.4.1 Calibration

Calibration of the TNP was required to achieve the most accurate results. Due to the fact that the TNP system is highly sensitive in the measurements it takes, the composition of the mediums in which are being tested play a significant role in the results. In order to account for the medium properties of the two fluids (air and water) which were to be tested on the ski-jump hydraulic model a baseline test

needed to be conducted. This test measures the conductivity of the two different mediums and automatically calibrates the system accordingly.

### 4.7.5 ACQUISITION OF VELOCITY AND IMPACT ANGLE MEASUREMENTS

The velocities and impact angles of the trajectory jets requires the greatest processing of all data. The instrumentation used for the acquisition included a GoPro waterproof video recorder, black screen with measuring lines spaced 50mm apart in both vertical and horizontal directions positioned 1m to 1.5m behind the centreline of the jet and a reference ruler placed 1m to 1.5m in the foreground of the impacting water jet. **Figure 4.29** shows the setup of the measuring apparatus.

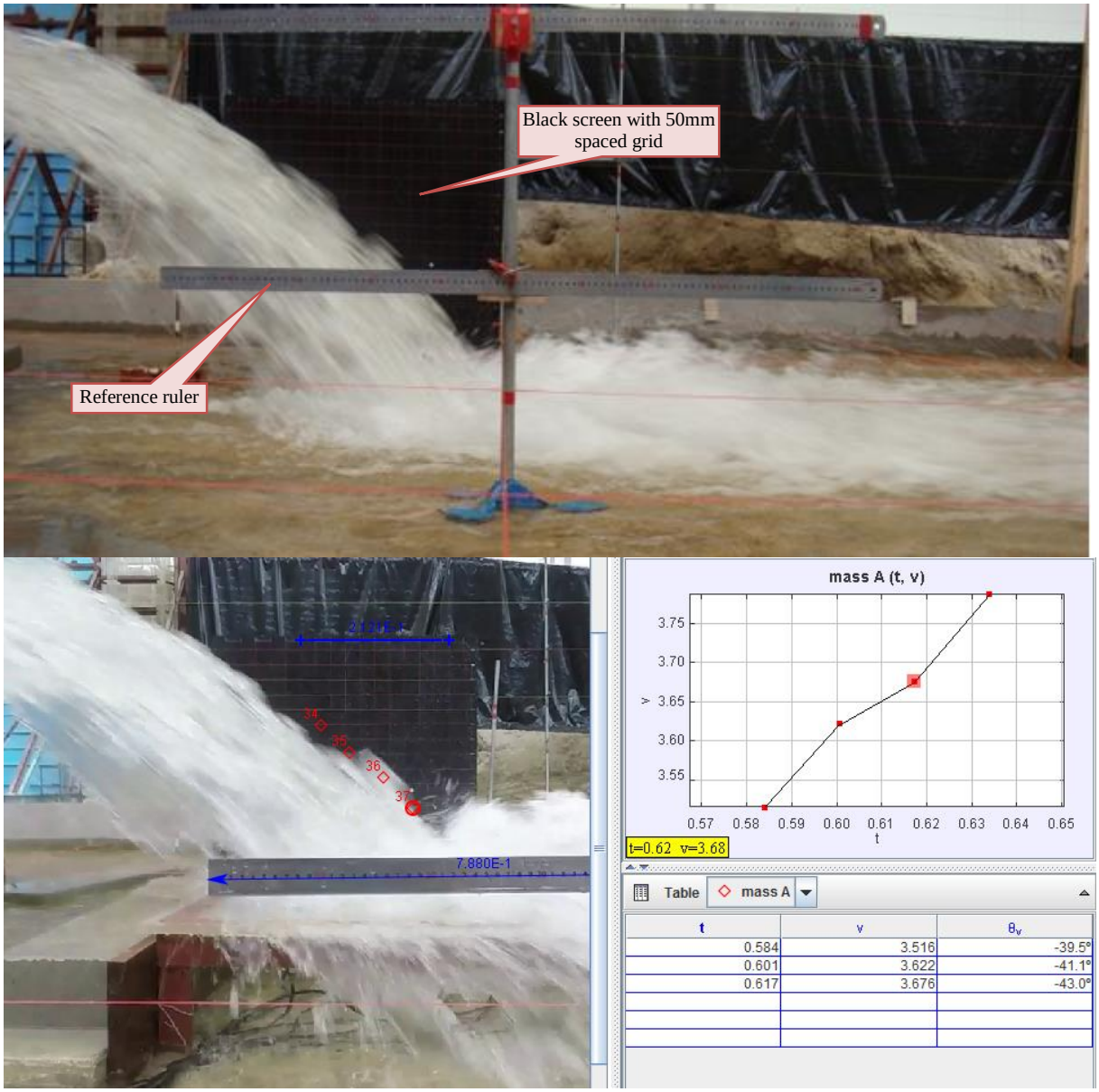


*FIGURE 4.29: VELOCITY AND IMPACT ANGLE MEASURING APPARATUS*

A short video clip was recorded for each test conducted and uploaded to a video analysis software which has the ability of calculating the velocity and angle at the point of impact. The software used the frame

rate of the captured video together with the measured distance a water particle moves per frame for the calculation.

## 4.8 EXPERIMENTAL PROCEDURES

A standard procedure was followed in the execution of the experimental work.

There were two valves controlling the flow from the pumps, the main gate valve on the pipe network as well as a local gate valve which isolates the ski-jump hydraulic model from the pipe network. In order for successful operation of the model both valves needed to be operated at the same time.

By operating only the local valve while the main valve remained fully open smooth uniform flow was unable to be achieved due to the valve obstructing full pipe flow. For best operation the flow had to be controlled from the main valve with the local valve completely open but due to the fact that the pumps could not control the flow below 50 l/s, initial priming of the jet box could potentially damage the model where the flow would instantly increase from 0 l/s to 50 l/s creating a large pressure force on the sluice gate which could potentially eject the sluice gate from the jet box.

The method for priming the jet box included keeping the local gate valve closed while the pumps were started. Once the pumps were up and running and the reservoir was at the correct water level, the local gate valve was opened slowly introducing flow into the jetbox at a controlled rate while releasing the trapped air through the air release valve until the jetbox was completely full. At this stage the testing could be initialised.

### 4.8.1 FLOW PHENOMENA

#### *4.8.1.1 Jet Box and Sluice gate*

The jet box and sluice gate created some irregularities in the flow profile. During the initial priming of the jet box there is an abundance of air that gets trapped in a pocket at the top of the jet box which created a vortex effect as air is released through the sluice gate creating a short period of turbulence and inconsistent flow. This vortex and flow irregularity was alleviated with the assistance of the air release valve.

### 4.8.2 ROLE OF STUDENT

The author conducted all tests on the ski-jump energy dissipator model himself with the assistance of the water laboratory staff to control the pumps when required, as well as to move the pressure plate and heavy concrete supporting slabs. The author directed all tests performed, and measured, retrieved and processed data from the ski-jump hydraulic model with the guidance and consultation of study leader, Professor G.R. Basson.

## 4.9 TESTING REPEATABILITY

Repeatability is the variability of the measurements obtained by one person while measuring the same item repeatedly. In the case of any model study the repeatability of testing is a highly important factor for the accuracy of results. During the course of the initial testing phase of this thesis separate experiments were conducted to test the repeatability of certain flow properties and trajectory parameters including discharge repeatability, flow depth repeatability, trajectory repeatability and dynamic impact repeatability. Without the ability to reproduce the same conditions to a certain accuracy for each flow condition the testing result would be regarded as invalid.

### 4.9.1 DISCHARGE REPEATABILITY

As mentioned previously, the flow was measured with the assistance of a SAFMAG electromagnetic flowmeter which has undergone vigorous quality control and calibration during its production by the manufacturer and therefore can be accepted as a highly accurate device in the measurement of pipe flow. Manufacturer's specifications of this product state that it has an accuracy of +/- 0.5% of the flow rate and a repeatability of +/- 0.1% of flow rate. To prove the flow repeatability was indeed as highly accurate as stipulated by the manufacturing company of the flowmeter two quick tests were conducted.

The first test was done by opening the valve so that a specific flow was achieved and allowing the jetbox to fill up leaving the air release valve open until there was a constant flow of water coming through it. Now for a certain flow the pressure within the jetbox should be constant and therefore the flow from the air release valve should be constant too. A 20 litre container was filled up while being timed. All valves were shut and the test was repeated two more times. The findings of this short experiment showed that the 20 litre container was filled up at identical rates for all three tests.

The second test that was conducted was on the flowmeter itself. For all flow the reading fluctuates a little depending on the magnitude of flow. For discharges up to 100 l/s the flowmeter reading fluctuates in the region of +/- 0.5 l/s and flows up to 200 l/s the reading fluctuates in the region of +/- 1 l/s. From this quick test we can identify that the accuracy of the flowmeter is indeed +/- 0.5%.

Therefore it can be concluded that the repeatability of discharge is highly accurate and that any error in the results obtained for this thesis if any cannot be attributed to the discharge readings.

### 4.9.2 FLOW DEPTH REPEATABILITY

The depth of flow just before the flip bucket was measured with a measuring needle (**Figure 4.30**). The measurements were recorded to the nearest millimetre. Although there were slight fluctuations in the flow depth during testing the average flow depth was easily identified when assessed over a 10 second period. This method was used in the calibration of the jet box sluice gate.

The sluice gate was mechanically operated with a threaded bar and bolt assembly welded to the sluice gate and therefore could be adjusted when necessary. The flow depth created by the jet box is a function

of the flow and gate opening. The repeatability of the sluice gate itself can be considered to be accurate to 1mm as it was designed to be lifted or lowered to any height between 0 and 150mm above the chute invert. Therefore once the jet box had been calibrated to produce a specific flow depth for a specified flow it could be reproduced with the same repeatability as that of the discharge.

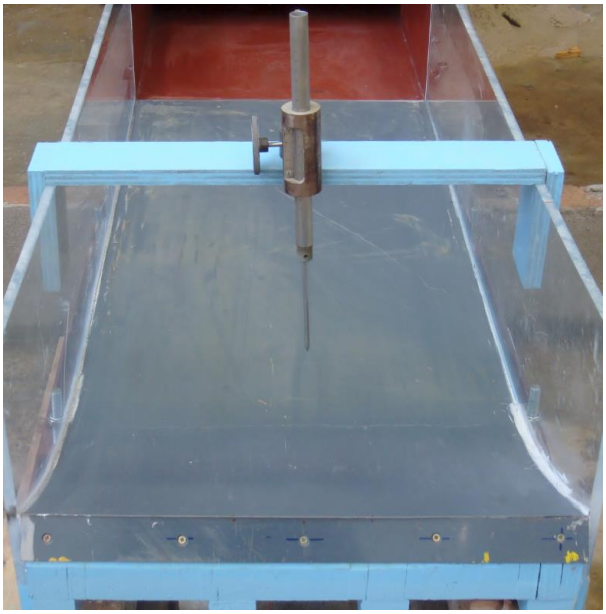

*FIGURE 4.30: FLOW DEPTH MEASURING NEEDLE*

### 4.9.3 TRAJECTORY REPEATABILITY

The trajectory of the ski-jump model was measured with the use of photograph scaling in the AutoCAD Civil 3D software as well as the dumpy level method. The repeatability of the trajectory for a specific flow was considered to be very high after conducting the following tests:

- Immediate Trajectory Repeatability – this included taking a few photos for a specific flow and sluice gate height, waiting a few minutes and then retaking the photos. These photos were then scaled, dimensioned in AutoCAD and compared. The results of this test indicated a maximum deviation in the results of 5%.
- Delayed Trajectory Repeatability - this included using the scaled and dimensioned photos from the immediate trajectory repeatability test and comparing them to scaled and dimensioned photos taken a day or two later after flow and sluice gate manipulations have been conducted, therefore this tests may be considered as the trajectory repeatability after a complete system reset. The results captured displayed almost identical figures to that of the immediate trajectory repeatability.

From the above two tests it may be concluded that the trajectory repeatability is about 95% provided the flow and sluice gate opening are controlled with high accuracy.

### 4.9.4 PRESSURE REPEATABILITY AND SYMMETRY

As previously mentioned the pressure measurements were recorded with nine pressure transducers equally spaced on a pressure plate. Specifications of these pressure transducers state that they have 0.5% accuracy over the total pressure range. In order to validate this accuracy a simple test was conducted for each transducer where pressure measurements were taken in a vertical 1m pipe filled with water. In theory the static water head is 1m. The results of this quick test yielded a 2% pressure difference between the recorded pressures and the actual static head of the pipe. Due to the fact that a proper seal could not be established between the pressure transducer and the 1m pipe water leaked out, which meant the pipe was continuously filled with water which could possibly account for the reduced accuracy of the results.

#### *4.9.4.1 Pressure Symmetry*

To limit testing time an assumption was made that if the hydraulic model was correctly levelled and aligned the trajectory profile would be symmetrical about the centreline parallel to the flow direction and therefore the pressure distribution would theoretically be symmetrical too. Without this assumption the testing period would have been doubled. To validate whether the pressure distribution was in fact symmetrical some tests were conducted where the centreline of the trajectory jet at impact was determined and pressure measurements were recorded on both sides of the centreline. These measurements were compared and as expected the pressure distribution was relatively symmetrical.

# CHAPTER 5: EXPERIMENTAL RESULTS AND ANALYSIS

*In this chapter of the dissertation the results of the ski-jump hydraulic model are presented and briefly discussed. The results include the geometric data obtained from photograph scaling, the dynamic impact pressure data obtained from the pressure transducers, the aeration data captured with the air probe and the impact velocity data acquired from the GoPro action camera and tracker software.*

A comprehensive testing period was conducted for the ski-jump hydraulic model that lasted 3 months. The testing period was lengthy due to the methods chosen for the acquisition of data as well as the construction and installation of the eight different flip bucket designs. Generally the data for each flip bucket design was accumulated over one week as well as a day or two for the removal and installation of a new flip bucket design. Due to the material choice of the flip buckets it was not possible to accurately repeat tests for a certain flip bucket once it had been removed from the model, therefore it was critical that a complete set of data was obtained before interchanging the designs. It is important to note that all results obtained from the experimental model are presented in the following chapters in prototype scale.

## 5.1 DATA PROCESSING, REPRESENTATION AND ANALYSIS

After the testing period was completed the data required processing. The data processing period lasted three months due to the large quantity of data, type of data and the methods chosen to accurately process and display the data.

### 5.1.1 DATA PRE-PROCESSING

#### *5.1.1.1 Geometric Data Pre-Processing*

The acquisition of the geometric data was done predominantly with photo dimensioning and scaling as mentioned in the previous chapter. This required hours of preparation and editing of the photographs before the dimensions could be extracted. The first part of the pre-processing was sieving out the best quality photos for each test. Ten to twelve photos were taken for each test where six were chosen for further processing; two photos for the measurement of the distance and maximum elevation of the turning point of the trajectory profile, two photos for the total horizontal trajectory distance and two photos for the impact width. These photos were chosen according to clarity and the general smoothness of the profile. AutoCAD Civil 3D was then used to scale each photo with the dimensioning ruler included in the shot, as well as to align it with the horizontal axis. The next step included choosing the points of highest elevation, impact and width so that dimensions could be associated relative to the scale. In total 336 photos were scaled and dimensioned for the seven flow conditions of the eight flip buckets. All these dimensions were manually exported to excel format where they could be compared and analysed.

#### 5.1.1.2 *Pressure Sensor Data Pre-Processing*

The data for each pressure sensor was numbered and arranged according to the reference position of the sensor on the pressure plate (**Figure 4.23** and **Figure 4.24**). The data set for each pressure transducer contained the time interval and the corresponding voltage reading (total of atmospheric pressure and dynamic pressure). With **Equation 4.20** and **Equation 4.21** the raw data was able to be converted into a pressure head. Taking the static atmospheric pressure and deducting it from the total pressure head, the dynamic pressure head was determined. Due to the method of capturing the pressure data there were huge spikes in the pressure which were theoretically far too high and therefore these spikes were considered to be outliers.

#### 5.1.1.3 *Air Probe Data Pre-Processing*

The raw data retrieved from the air probe sensor initially was un-calibrated in terms of the fluid properties and required pre-processing. The air probe measures the conductivity of the liquid that it is inserted into, however the base conductivity of air and water needs to be saved into the system as the initial conditions to ensure that as air passes through the water the software can compare the conductivity of the air-water mixture and to the initial conditions. Pre-processing the data with a software where the conductivity of the base fluids are entered, calibrates the data.

### 5.1.2 STATISTICAL ANALYSIS OF DYNAMIC PRESSURE DISTRIBUTIONS

A statistical analysis was conducted on the processed raw data where the $99.8^{th}$ percentile of the data was used for the maximum pressures. The remaining 0.2 percent was assumed to be complete outliers as it included high pressure spikes that were inconsistent with any theoretical trend and in a few instances exceeding the range of the pressure transducers. In the data set of a single pressure transducer, 30 000 data points were recorded and for the worst case experienced 20 pressure spikes. The pressure value that is exceeded by 0.1% of the values was used as the maximum dynamic pressure head.

## 5.2 DATA PRESENTATION

The sheer quantity of data captured with the tests conducted was so extensive that not all of it could be presented and discussed within the text. Due to the fact that flow condition 4 was the design flow condition it was the main focus for presenting and comparing results of the different ski-jump bucket designs.

### 5.2.1 LINE GRAPHS

Line graphs were the predominant method for displaying the data. The data for the respective test parameters were displayed in scatter graph format with a trend line as the best fit of the data. The trajectory profiles, impact widths, maximum dynamic impact pressure heads, impact velocity heads and relative energy are all displayed in line graph format.

### 5.2.2 2D-CONTOUR GRAPH REPRESENTATION

The best possible way of displaying the pressure distributions was on 2D contour maps (colour shaded and contoured). This method made the analysis of the pressure distribution relatively simple and comparisons were able to be achieved easily.

## 5.3 TRAJECTORY AND GEOMETRIC RESULTS

As mentioned in the previous chapter the trajectory profiles and geometric properties for all tests conducted were measured with the method of photo scaling and dimensioning. This section of this dissertation shows the different upper and lower trajectory profiles for the eight different flip buckets for the seven flow conditions as well as the impact width of the water jet in both the transverse and horizontal directions. All jet trajectory dimensions were recorded for the centreline (i.e. the maximum distance for that parameter). A constant elevation difference between the bucket invert and tailwater level (pressure plate level), Y, was used for all cases. It is important to take note that only the upper trajectory profiles were displayed in graphical format, the lower trajectory profiles are only displayed in tabular format.

### 5.3.1 TYPE I GEOMETRIC RESULTS

The Type I flip bucket design was based upon a general circular-shaped ski-jump flip bucket. The geometric results for these flip buckets were used as a baseline for the Type II and III flip buckets which include features that would possibly change the jet trajectory.

#### *5.3.1.1 30º Flip Bucket Trajectory Profile*

The first flip bucket tested was the Type I 30º bucket. **Table 5.1** shows the results of the Type I 30º flip bucket trajectory profiles recorded for the upper and lower surfaces at the centreline. **Figure 5.1** show a graphical representation of these results. For the bucket design flow condition (flow condition 4) the results reveal a trajectory throw distance ($X_H$) of 162.50m when impacting the pressure plate with a maximum upper trajectory height ($h_m$) of 21.65m which acts at 68.95m from the bucket lip.

TABLE 5.1: TYPE I 30°FLIP BUCKET TRAJECTORY RESULTS (PROTOTYPE VALUES)

| Flow Condition | Discharge (m3/s) | Max Height of Upper Trajectory, $h_{m(u)}$ | Max Height of Lower Trajectory, $h_{m(l)}$ | Distance to $h_{m(u)}$, $X_{m(u)}$ | Distance to $h_{m(l)}$, $X_{m(l)}$ | Upper Trajectory Distance, $X_{H(u)}$ | Lower Trajectory Distance, $X_{H(l)}$ |
|---|---|---|---|---|---|---|---|
| **1** | 288.42 | 4.55 | 1.65 | 13.43 | 10.80 | 43.40 | 37.03 |
| **2** | 384.69 | 8.45 | 3.13 | 26.45 | 20.33 | 70.05 | 57.35 |
| **3** | 480.63 | 13.78 | 6.00 | 42.40 | 35.13 | 103.35 | 85.10 |
| **4** | 625.00 | 21.65 | 9.50 | 68.95 | 56.10 | 162.50 | 137.50 |
| **5** | 625.00 | 9.98 | 3.68 | 27.80 | 24.10 | 73.90 | 65.65 |
| **6** | 625.00 | 12.38 | 5.00 | 37.58 | 30.63 | 94.00 | 80.00 |
| **7** | 625.00 | 16.28 | 7.78 | 48.93 | 43.33 | 119.73 | 98.45 |

Note: Refer to **Figure 3.4** in **Section 3.2.6** for a visual representation of the parameters in **Table 5.1**.

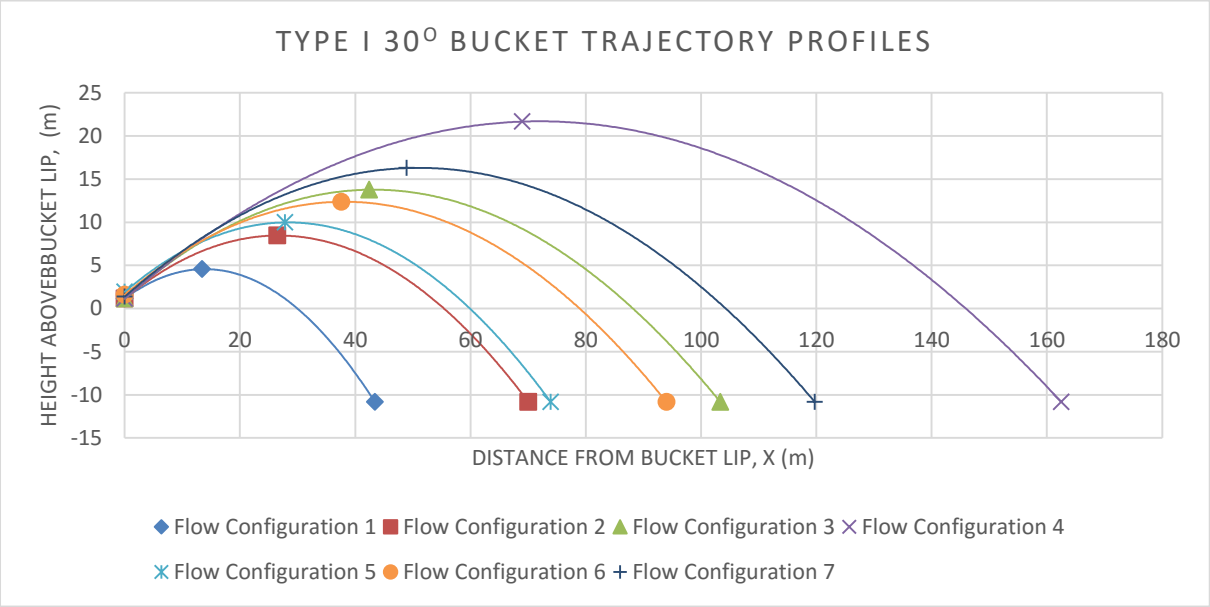


FIGURE 5.1: GRAPHICAL REPRESENTATION OF THE TYPE I 30° UPPER TRAJECTORY RESULTS PRESENTED IN TABLE 5.1 WITH BEST FIT TREND LINES

### 5.3.1.2 40° Flip Bucket Trajectory Profile

The second Type I flip bucket to be tested was the 40° bucket. The trajectory profile results for this flip bucket are displayed in **Table 5.2** along with a graphical representation in **Figure 5.2**. For The design flow condition the results for the upper trajectory show $X_H$ = 174.35m and $h_m$ = 28.65m which acts at $X_m$ = 72.80m from the bucket lip. These results when compared to the 30° flip bucket are all larger, which was expected from a theoretical perspective.

TABLE 5.2: TYPE I 40°FLIP BUCKET TRAJECTORY RESULTS (PROTOTYPE VALUES)

| Flow Condition | Discharge (m3/s) | Max Height of Upper Trajectory, $h_{m(u)}$ | Max Height of Lower Trajectory, $h_{m(l)}$ | Distance to $h_{m(u)}$, $X_{m(u)}$ | Distance to $h_{m(l)}$, $X_{m(l)}$ | Upper Trajectory Distance, $X_{H(u)}$ | Lower Trajectory Distance, $X_{H(l)}$ |
|---|---|---|---|---|---|---|---|
| **1** | 288.42 | 7.30 | 3.48 | 16.00 | 13.40 | 45.08 | 34.65 |
| **2** | 384.69 | 11.95 | 5.95 | 28.90 | 25.78 | 72.70 | 62.48 |
| **3** | 480.63 | 17.83 | 10.58 | 48.13 | 41.50 | 109.73 | 87.50 |
| **4** | 625.00 | 28.65 | 16.05 | 72.80 | 67.20 | 174.35 | 145.00 |
| **5** | 625.00 | 11.80 | 5.40 | 31.80 | 25.75 | 72.95 | 60.00 |
| **6** | 625.00 | 17.08 | 8.75 | 42.40 | 24.65 | 100.23 | 84.83 |
| **7** | 625.00 | 23.03 | 12.30 | 58.18 | 51.93 | 132.63 | 118.00 |

Note: Refer to **Figure 3.4** in **Section 3.2.6** for a visual representation of the parameters in **Table 5.2**.

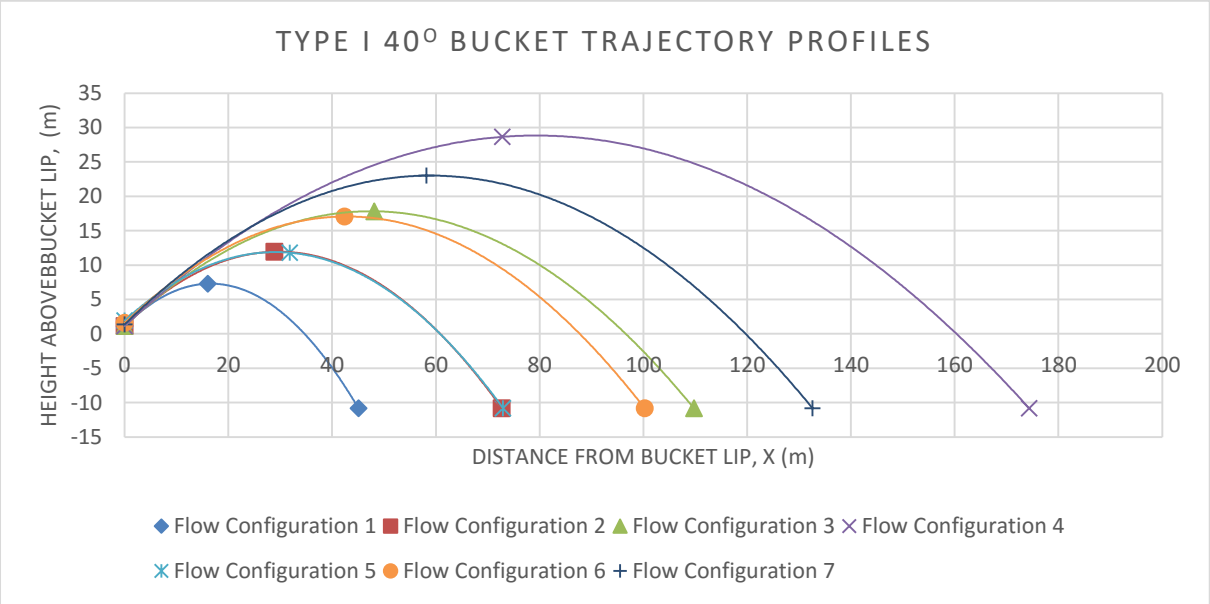


FIGURE 5.2: GRAPHICAL REPRESENTATION OF THE TYPE I 40° UPPER TRAJECTORY RESULTS PRESENTED IN TABLE 5.2 WITH BEST FIT TREND LINES

### 5.3.1.3 45° Flip Bucket Trajectory Profile

The final Type I flip bucket to be tested was the 45° bucket. The trajectory profile results for this flip bucket are displayed in **Table 5.3** along with a graphical representation in **Figure 5.3** For the design flow condition the results for the upper trajectory show $X_H$ = 175.23m and $h_m$ = 34.10m which acts at $X_m$ = 82.40m from the bucket lip. These results when compared to the 40° flip bucket are all larger which was expected from a theoretical perspective.

TABLE 5.3: TYPE I 45°FLIP BUCKET TRAJECTORY RESULTS (PROTOTYPE VALUES)

| Flow Condition | Discharge (m3/s) | Max Height of Upper Trajectory, $h_{m(u)}$ | Max Height of Lower Trajectory, $h_{m(l)}$ | Distance to $h_{m(u)}$, $X_{m(u)}$ | Distance to $h_{m(l)}$, $X_{m(l)}$ | Upper Trajectory Distance, $X_{H(u)}$ | Lower Trajectory Distance, $X_{H(l)}$ |
|---|---|---|---|---|---|---|---|
| **1** | 288.42 | 8.28 | 4.38 | 16.95 | 12.70 | 47.50 | 38.93 |
| **2** | 384.69 | 14.45 | 7.35 | 32.30 | 30.35 | 72.63 | 60.43 |
| **3** | 480.63 | 20.75 | 12.23 | 49.98 | 43.43 | 109.25 | 89.98 |
| **4** | 625.00 | 34.10 | 19.00 | 82.40 | 72.90 | 175.23 | 138.75 |
| **5** | 625.00 | 13.45 | 5.80 | 30.30 | 27.88 | 71.93 | 63.63 |
| **6** | 625.00 | 19.88 | 10.15 | 45.78 | 41.58 | 99.58 | 87.33 |
| **7** | 625.00 | 25.00 | 16.00 | 62.50 | 35.75 | 133.20 | 117.05 |

Note: Refer to **Figure 3.4** in **Section 3.2.6** for a visual representation of the parameters in **Table 5.3**.

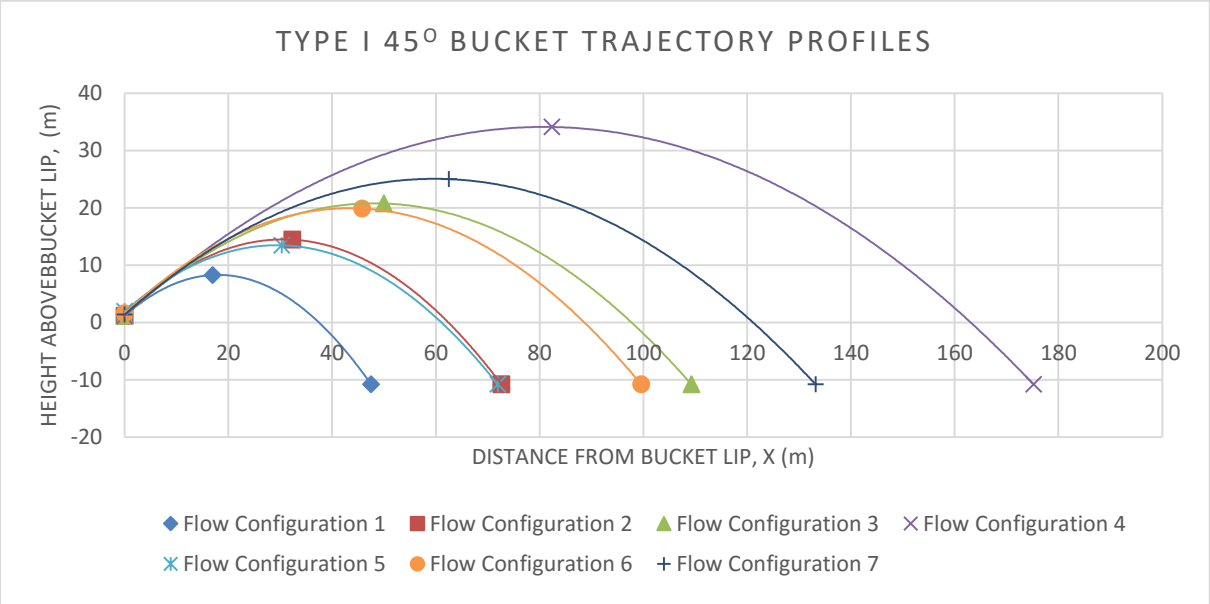


FIGURE 5.3: GRAPHICAL REPRESENTATION OF THE TYPE I 45° UPPER TRAJECTORY RESULTS PRESENTED IN TABLE 5.3 WITH BEST FIT TREND LINES

### 5.3.1.4 Type I Transverse and Horizontal Impact Widths

The impact widths of a ski jump energy dissipator are an important factor in the evaluation of energy dissipation, the more spread the water jet is at the point of impingement the greater the interaction with air, thus leading to increased air entrainment and energy dissipation. A simple sketch showing the parameters of the impact widths is shown in **Figure 5.4**.

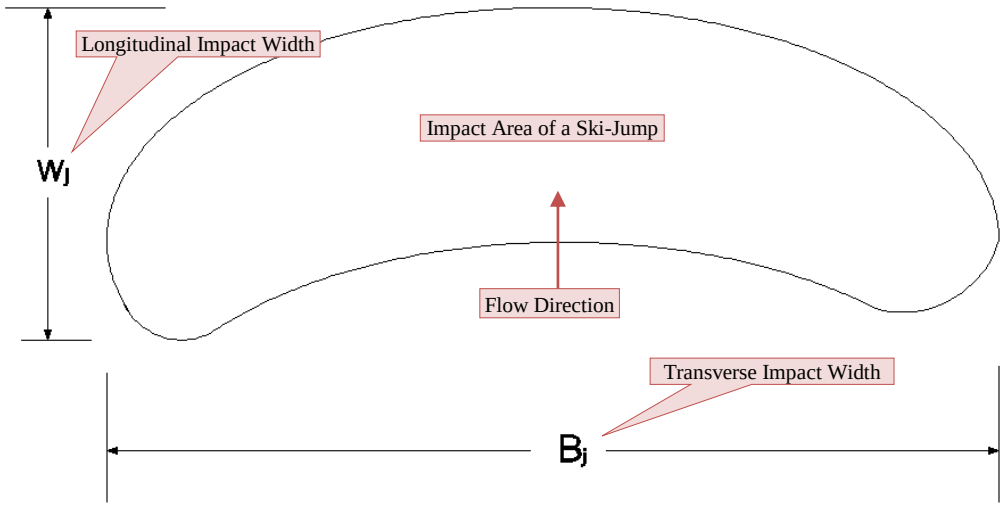


*FIGURE 5.4: LONGITUDINAL AND TRANSVERSE IMPACT WIDTHS*

**Table 5.4** and **Figure 5.5** shows the results of the Type I 30º, 40º and 45º transverse and longitudinal impact widths.

*TABLE 5.4: TYPE I FLIP BUCKET TRANSVERSE AND HORIZONTAL IMPACT WIDTH RESULTS (PROTOTYPE VALUES)*

| Flow Condition | Discharge (m3/s) | 30º Transverse Impact Width $B_j$ | 40º Transverse Impact Width $B_j$ | 45º Transverse Impact Width $B_j$ | 30º Longitudinal Impact Width, $W_j$ | 40º Longitudinal Impact Width, $W_j$ | 45º Longitudinal Impact Width, $W_j$ |
|---|---|---|---|---|---|---|---|
| **1** | 288.42 | 20.83 | 21.25 | 26.10 | 6.38 | 10.45 | 8.60 |
| **2** | 384.69 | 26.83 | 31.78 | 33.28 | 12.70 | 10.23 | 12.20 |
| **3** | 480.63 | 29.90 | 35.18 | 39.48 | 18.25 | 22.23 | 19.28 |
| **4** | 625.00 | 37.90 | 47.70 | 50.50 | 25.00 | 29.35 | 36.48 |
| **5** | 625.00 | 28.78 | 33.25 | 32.98 | 8.28 | 12.95 | 8.30 |
| **6** | 625.00 | 37.20 | 36.35 | 44.25 | 14.00 | 15.40 | 12.25 |
| **7** | 625.00 | 37.53 | 43.38 | 53.08 | 21.28 | 14.60 | 16.15 |

Note: Refer to **Figure 5.4** for a visual representation of the parameters in **Table 5.4**.

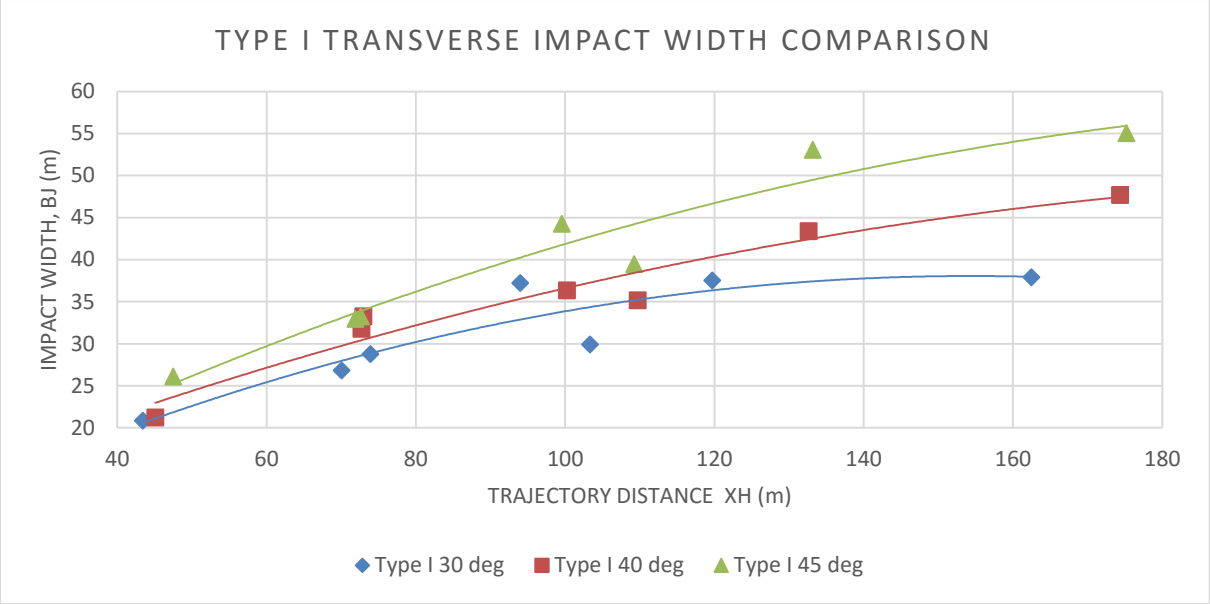


*FIGURE 5.5: TYPE I TRANSVERSE IMPACT WIDTHS RELATIVE TO THE TRAJECTORY DISTANCE*

A clear trend is depicted from the results presented in **Table 5.4** and **Figure 5.5**. It can be seen that as the trajectory distance increases so does the transverse impact width. The same applies for the horizontal impact widths of the Type I flip buckets. The results also show that the trajectory width increases with the increased bucket deflection angle. For the design flow condition transverse impact widths were 37.90m, 47.70m and 50.50m for the 30º, 40º and 45º Type I buckets. The longitudinal impact widths were 25.00m, 29.35m and 36.48m for the design flow condition.

### 5.3.2 TYPE II FLIP BUCKETS

The trajectory profiles of the Type II flip buckets were slightly different to that of the plain Type I buckets. Due to the constriction of the sidewalls there was a more concentrated jet of water, which did not disperse laterally but rather longitudinally. The contraction created substantial turbulence and a considerably thicker jet of water. The flow profiles generally reached a higher maximum elevation, but due to the interaction of the side walls the velocity of the jet was expected to decrease as well as the horizontal throw distance. For the first flow condition (low flow), chocking of the flow occurred due to the constriction. This resulted in an incomplete data set for the Type II buckets (refer to **Figure 5.6**). The horizontal trajectory widths for all tests were also unable to be recorded due to the spray created on the lower jet trajectory, which deemed it impossible to determine an accurate impact location for the lower jet profile (refer to **Figure 5.7)**.

FIGURE 5.6: FLOW CHOCKING OF TYPE II FLIP BUCKETS FOR FIRST FLOW CONDITION

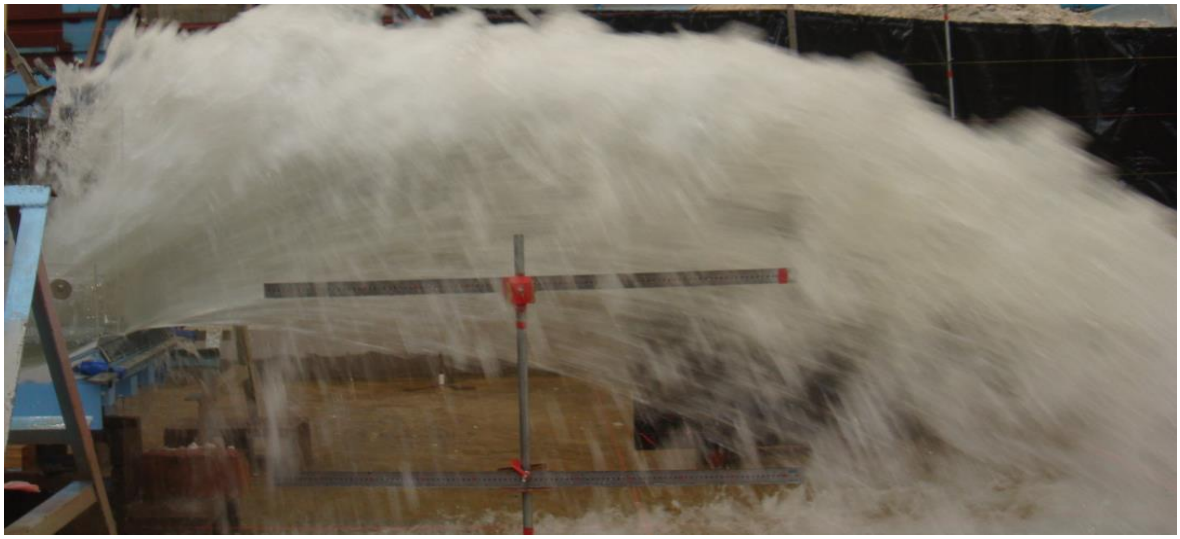

FIGURE 5.7: UNABLE TO OBTAIN LOWER IMPACT LOCATION DUE TO EXCESSIVE SPRAY

#### 5.3.2.1 $30^o$ Flip Bucket

The first Type II flip bucket to be tested was the $30^o$ flip bucket. The trajectory profile results for this flip bucket are displayed in **Table 5.5** along with a graphical representation in **Figure 5.8**. For the design flow condition the results for the upper trajectory shows $X_H$ = 149.93m and $h_m$ = 30.48m which acts at $X_m$ = 72.78m from the bucket lip. When comparing these results to the $30^o$ Type I flip bucket a shorter throw distance is seen, but the trajectory height is much greater.

*TABLE 5.5: TYPE II 30°FLIP BUCKET TRAJECTORY RESULTS (PROTOTYPE VALUES)*

| Flow Condition | Discharge (m3/s) | Max Height of Upper Trajectory, $h_{m(u)}$ | Max Height of Lower Trajectory, $h_{m(l)}$ | Distance to $h_{m(u)}$, $X_{m(u)}$ | Distance to $h_{m(l)}$, $X_{m(l)}$ | Upper Trajectory Distance, $X_{H(u)}$ | Lower Trajectory Distance, $X_{H(l)}$ |
|---|---|---|---|---|---|---|---|
| **1** | 288.42 | Flow Choking | Flow Choking | Flow Choking | Flow Choking | Flow Choking | Flow Choking |
| **2** | 384.69 | 14.93 | n/a | 28.38 | n/a | 70.43 | n/a |
| **3** | 480.63 | 17.35 | n/a | 38.65 | n/a | 98.03 | n/a |
| **4** | 625.00 | 30.48 | n/a | 72.78 | n/a | 149.93 | n/a |
| **5** | 625.00 | 17.15 | n/a | 27.63 | n/a | 66.98 | n/a |
| **6** | 625.00 | 24.48 | n/a | 32.58 | n/a | 97.38 | n/a |
| **7** | 625.00 | 28.83 | n/a | 57.78 | n/a | 126.23 | n/a |

Note: Refer to **Figure 3.4** in **Section 3.2.6** for a visual representation of the parameters in **Table 5.5**.

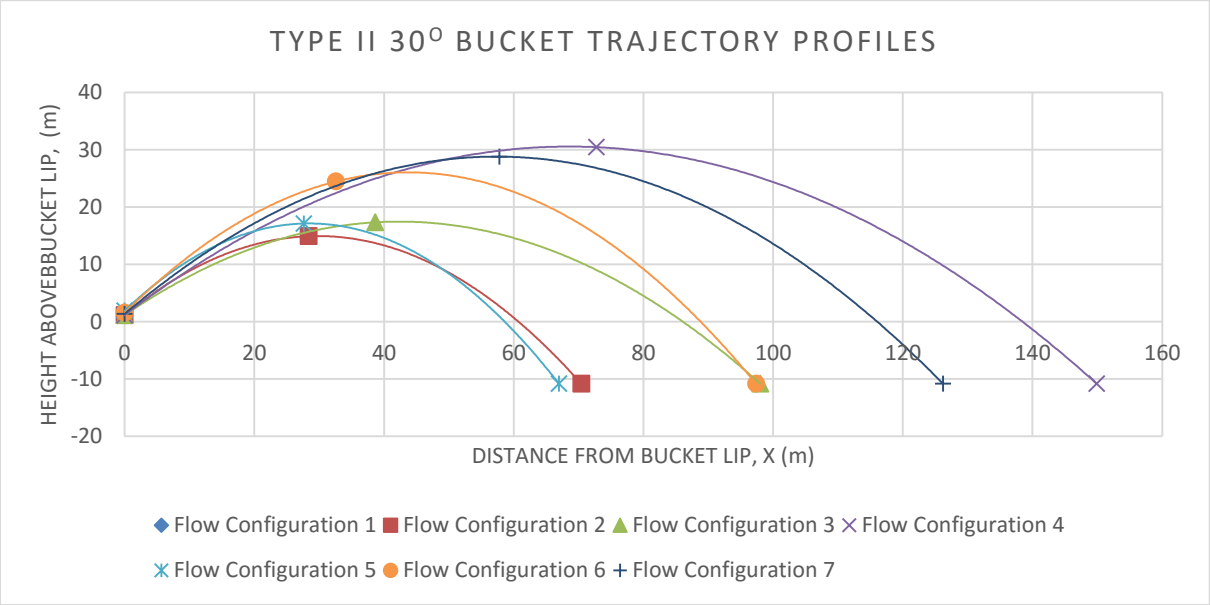


*FIGURE 5.8: GRAPHICAL REPRESENTATION OF THE TYPE II 30° UPPER TRAJECTORY RESULTS PRESENTED IN TABLE 5.5 WITH BEST FIT TREND LINES*

### *5.3.2.2 40° Flip Bucket*

The Second Type II flip bucket to be tested was the 40° flip bucket. The trajectory profile results for this flip bucket are displayed in **Table 5.6** along with a graphical representation in **Figure 5.9**. For The design flow condition the results for the upper trajectory shows $X_H$ = 163.60m and $h_m$ = 31.18m which acts at $X_m$ = 61.48m from the bucket lip. When comparing these results to the 40° Type I flip bucket a shorter throw distance is seen, but the trajectory height is much greater. When compared to the 30° Type II flip bucket it can be seen that the trajectory distance and height are both greater for the 40° Type II flip bucket which was expected due to the trajectory angle.

TABLE 5.6: TYPE II 40°FLIP BUCKET TRAJECTORY RESULTS (PROTOTYPE VALUES)

| Flow Condition | Discharge (m3/s) | Max Height of Upper Trajectory , $h_{m(u)}$ | Max Height of Lower Trajectory , $h_{m(l)}$ | Distance to $h_{m(u)}$, $X_{m(u)}$ | Distance to $h_{m(l)}$, $X_{m(l)}$ | Upper Trajectory Distance, $X_{H(u)}$ | Lower Trajectory Distance, $X_{H(l)}$ |
|---|---|---|---|---|---|---|---|
| **1** | 288.42 | Flow Choking | Flow Choking | Flow Choking | Flow Choking | Flow Choking | Flow Choking |
| **2** | 384.69 | 14.63 | n/a | 30.05 | n/a | 70.38 | n/a |
| **3** | 480.63 | 22.20 | n/a | 49.50 | n/a | 103.45 | n/a |
| **4** | 625.00 | 31.18 | n/a | 61.48 | n/a | 163.60 | n/a |
| **5** | 625.00 | 15.40 | n/a | 29.10 | n/a | 68.88 | n/a |
| **6** | 625.00 | 23.00 | n/a | 38.88 | n/a | 98.78 | n/a |
| **7** | 625.00 | 28.03 | n/a | 63.53 | n/a | 130.70 | n/a |

Note: Refer to **Figure 3.4** in **Section 3.2.6** for a visual representation of the parameters in **Table 5.6**.

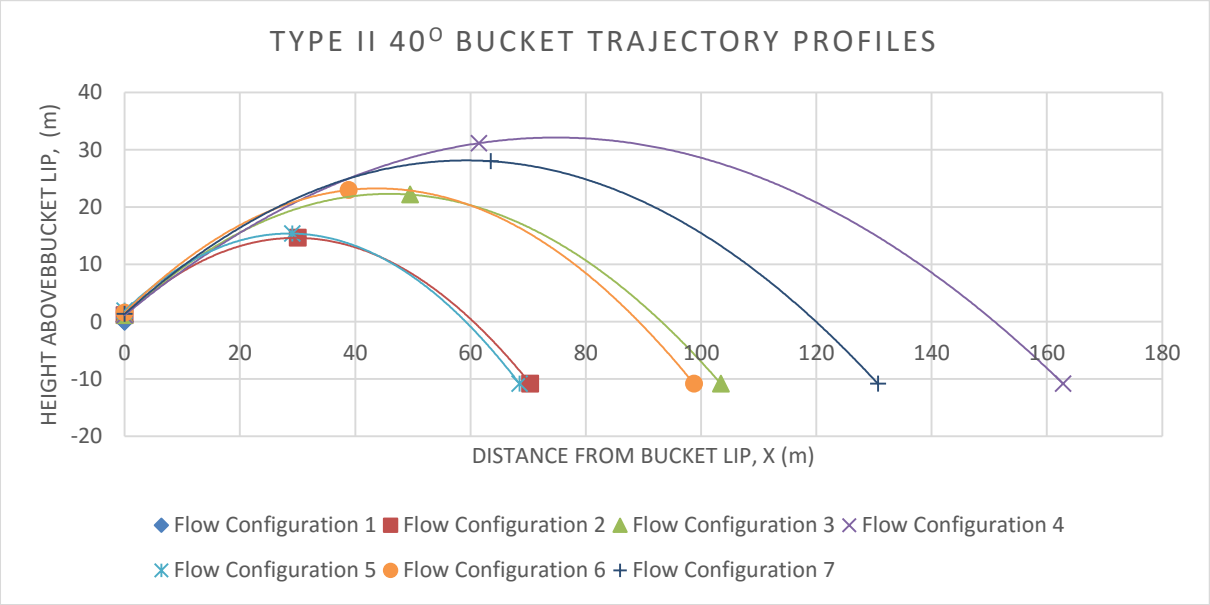


FIGURE 5.9: GRAPHICAL REPRESENTATION OF THE TYPE II 40° UPPER TRAJECTORY RESULTS PRESENTED IN TABLE 5.6 WITH BEST FIT TREND LINES

### 5.3.2.3 45° Flip Bucket

The final Type II flip bucket to be tested was the 45° flip bucket. The trajectory profile results for this flip bucket are displayed in **Table 5.7** along with a graphical representation in **Figure 5.10**. For The design flow condition the results for the upper trajectory shows $X_H$ = 171.80m and $h_m$ = 30.48m which acts at $X_m$ = 83.95m from the bucket lip. When comparing these results to the 45° Type I flip bucket a shorter throw distance is seen but the trajectory height is much greater. When compared with the 40° Type II flip bucket it can be seen that the height of the trajectory is lower and the trajectory distance is greater for the 45° flip bucket. The reason for this could be due to the combination of the short radius of the 45° flip bucket and contraction which makes it difficult to flip all of the flow, therefore reducing the trajectory height.

TABLE 5.7: TYPE II 45°FLIP BUCKET TRAJECTORY RESULTS (PROTOTYPE VALUES)

| Flow Condition | Discharge (m3/s) | Max Height of Upper Trajectory , $h_{m(u)}$ | Max Height of Lower Trajectory , $h_{m(l)}$ | Distance to $h_{m(u)}$, $X_{m(u)}$ | Distance to $h_{m(l)}$, $X_{m(l)}$ | Upper Trajectory Distance, $X_{H(u)}$ | Lower Trajectory Distance, $X_{H(l)}$ |
|---|---|---|---|---|---|---|---|
| **1** | 288.42 | Flow Choking | Flow Choking | Flow Choking | Flow Choking | Flow Choking | Flow Choking |
| **2** | 384.69 | 15.78 | n/a | 26.85 | n/a | 70.28 | n/a |
| **3** | 480.63 | 23.05 | n/a | 36.80 | n/a | 104.58 | n/a |
| **4** | 625.00 | 30.48 | n/a | 83.95 | n/a | 171.80 | n/a |
| **5** | 625.00 | 12.10 | n/a | 28.23 | n/a | 67.38 | n/a |
| **6** | 625.00 | 23.08 | n/a | 37.63 | n/a | 99.70 | n/a |
| **7** | 625.00 | 29.78 | n/a | 60.55 | n/a | 129.58 | n/a |

Note: Refer to **Figure 3.4** in **Section 3.2.6** for a visual representation of the parameters in **Table 5.7**.

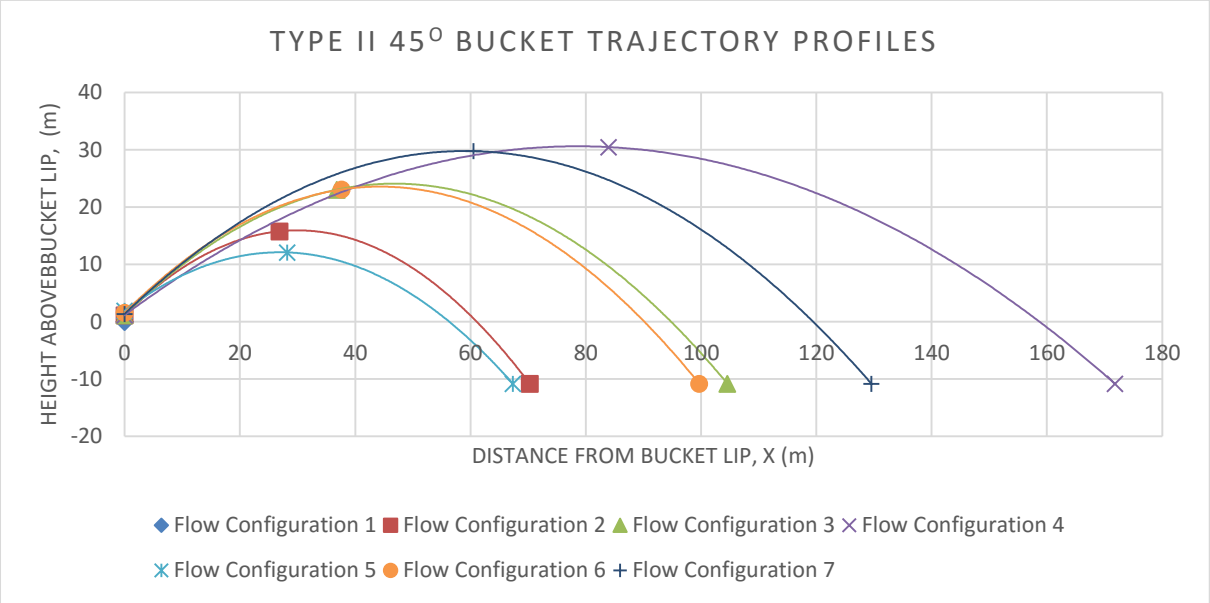


FIGURE 5.10: GRAPHICAL REPRESENTATION OF THE TYPE II 45° UPPER TRAJECTORY RESULTS PRESENTED IN TABLE 5.7 WITH BEST FIT TREND LINES

### 5.3.2.4 *Type II Transverse and Longitudinal Impact Widths*

The constriction in the width of the Type III flip buckets created spray on the lower profile of the waster jet. This spray helps introduce air entrainment on the lower profile. Due to the substantial spray on the lower trajectory profile the longitudinal impact widths were unable to be determined from a visual perspective. **Table 5.8** and **Figure 5.11** shows the results of the Type II 30°, 40° and 45° transverse impact widths.

TABLE 5.8: TYPE II FLIP BUCKET TRANSVERSE AND LONGITUDINAL IMPACT WIDTH RESULTS (PROTOTYPE VALUES)

| Flow Condition | Discharge (m3/s) | 30° Transverse Impact Width $B_j$ | 40° Transverse Impact Width $B_j$ | 45° Transverse Impact Width $B_j$ | 30° Longitudinal Impact Width, $W_j$ | 40° Longitudinal Impact Width, $W_j$ | 45° Longitudinal Impact Width, $W_j$ |
|---|---|---|---|---|---|---|---|
| **1** | 288.42 | Flow Choking | Flow Choking | Flow Choking | Flow Choking | Flow Choking | Flow Choking |
| **2** | 384.69 | 18.33 | 17.65 | 19.08 | n/a | n/a | n/a |
| **3** | 480.63 | 16.95 | 23.80 | 21.33 | n/a | n/a | n/a |
| **4** | 625.00 | 24.48 | 34.75 | 41.35 | n/a | n/a | n/a |
| **5** | 625.00 | 20.30 | 28.73 | 22.90 | n/a | n/a | n/a |
| **6** | 625.00 | 25.58 | 29.88 | 26.90 | n/a | n/a | n/a |
| **7** | 625.00 | 28.23 | 34.63 | 37.48 | n/a | n/a | n/a |

Note: Refer to **Figure 5.4** for a visual representation of the parameters in **Table 5.8**.

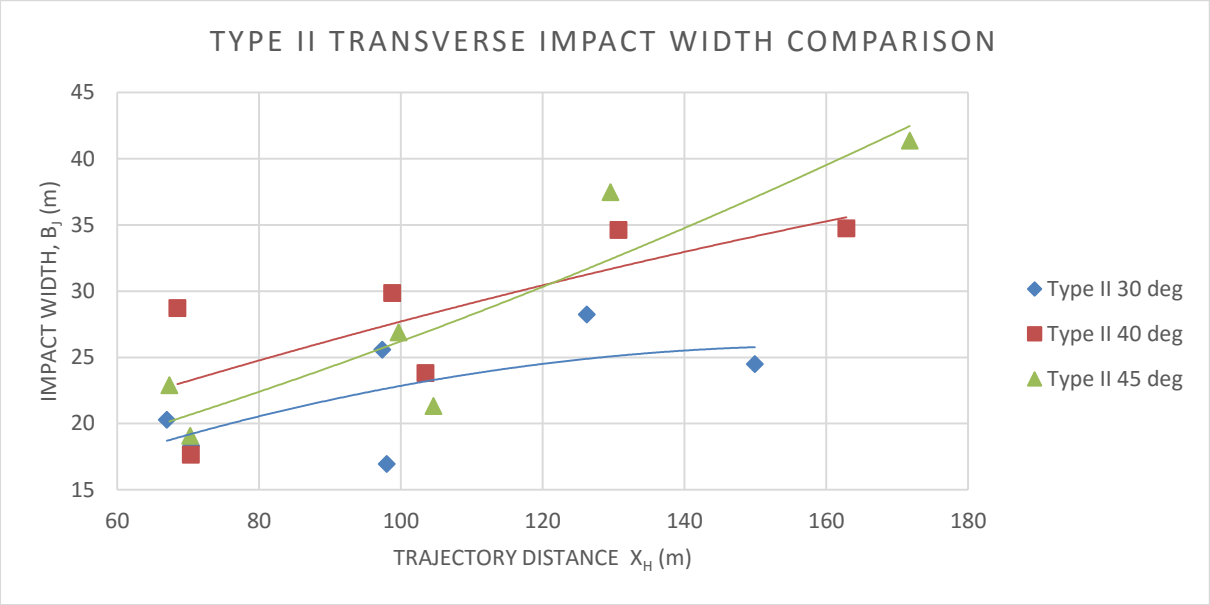


FIGURE 5.11: TYPE II TRANSVERSE IMPACT WIDTHS RELATIVE TO THE TRAJECTORY DISTANCE

It seems as though there is a trend occurring between the 30° and the 45° flip buckets when looking at the results presented in **Table 5.8** and **Figure 5.11**. The results of the 40° bucket display values that diverge too much between flow conditions. This divergence of data could possibly be due to an error in the capturing and processing stages. However for the design condition there seems to be relevant transverse impact width results which are 24.48m, 34.75m and 41.35m for the 30°, 40° and 45° Type II buckets.

### 5.3.3 TYPE III FLIP BUCKETS

The final set of flip buckets that were tested were the experimental composite flip buckets. As previously mentioned these flip buckets are a completely new design which was intended to improve the dispersion of the jet trajectory either horizontally or laterally.

### 5.3.3.1 Scoop Flip Bucket Trajectory Profiles

The first Type III flip bucket to be tested was the Scoop flip bucket. The trajectory profile results for this flip bucket are displayed in **Table 5.9** along with a graphical representation in **Figure 5.12**. All seven flow conditions were able to be tested with a complete set of data. For The design flow condition the results for the upper trajectory shows $X_H$ = 161.78m and $h_m$ = 25.18m which acts at $X_m$ = 74.15m from the bucket lip. When comparing to the other flip buckets already tested the trajectory profile seems to fall somewhere between the 30º and 40º Type I flip buckets.

*TABLE 5.9: TYPE III SCOOP FLIP BUCKET TRAJECTORY RESULTS (PROTOTYPE VALUES)*

| Flow Condition | Discharge (m3/s) | Max Height of Upper Trajectory, $h_{m(u)}$ | Max Height of Lower Trajectory, $h_{m(l)}$ | Distance to $h_{m(u)}$, $X_{m(u)}$ | Distance to $h_{m(l)}$, $X_{m(l)}$ | Upper Trajectory Distance, $X_{H(u)}$ | Lower Trajectory Distance, $X_{H(l)}$ |
|---|---|---|---|---|---|---|---|
| **1** | 288.42 | 5.95 | 2.08 | 17.08 | 15.20 | 44.83 | 35.03 |
| **2** | 384.69 | 9.98 | 4.18 | 29.78 | 27.05 | 71.58 | 57.43 |
| **3** | 480.63 | 14.75 | 6.80 | 47.13 | 42.48 | 102.98 | 87.38 |
| **4** | 625.00 | 25.18 | 11.00 | 74.15 | 67.63 | 161.78 | 138.35 |
| **5** | 625.00 | 11.13 | 3.88 | 30.70 | 27.95 | 69.98 | 58.15 |
| **6** | 625.00 | 14.63 | 5.35 | 41.95 | 39.48 | 99.48 | 85.70 |
| **7** | 625.00 | 19.43 | 6.43 | 57.28 | 54.93 | 129.83 | 110.95 |

Note: Refer to **Figure 3.4** in **Section 3.2.6** for a visual representation of the parameters in **Table 5.9**.

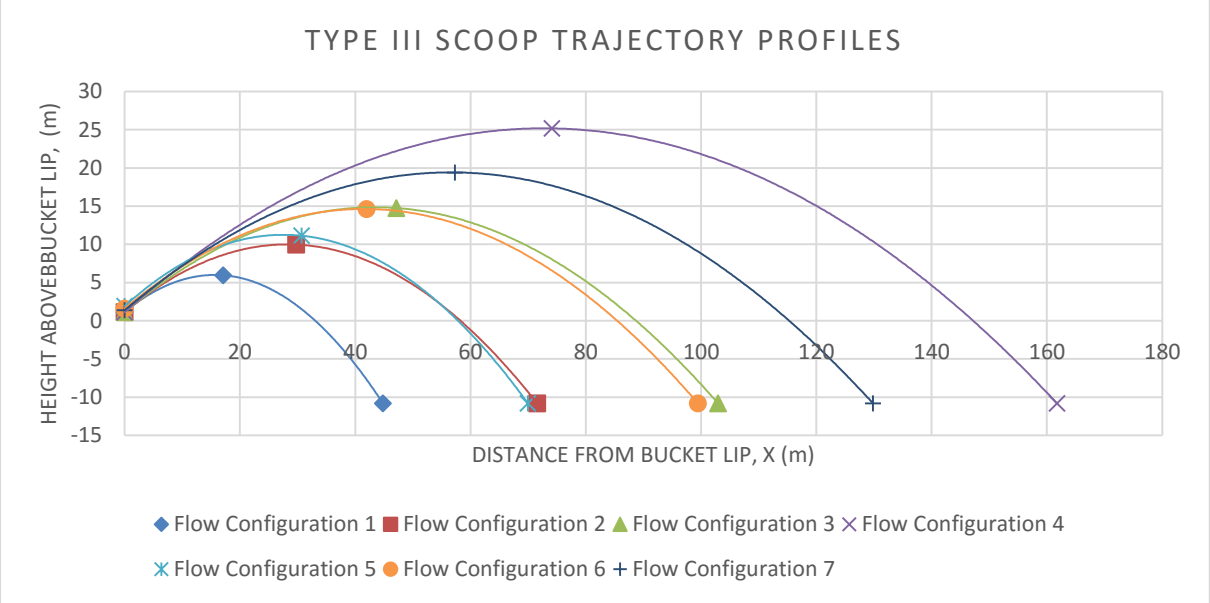


*FIGURE 5.12: GRAPHICAL REPRESENTATION OF THE TYPE III SCOOP UPPER TRAJECTORY RESULTS PRESENTED IN TABLE 5.9 WITH BEST FIT TREND LINES*

### 5.3.3.2 Butterfly Flip Bucket Trajectory Profiles

The second Type III flip bucket to be tested was the Butterfly flip bucket. The trajectory profile results for this flip bucket are displayed in **Table 5.10** along with a graphical representation in **Figure 5.13**. All seven flow conditions were able to be tested with a complete set of data. For The design flow condition the results for the upper trajectory shows $X_H$ = 176.63m and $h_m$ = 28.08m, which acts at $X_m$

= 77.53m from the bucket lip. When comparing to the other flip buckets already tested the Butterfly bucket seems to outperform all other flip buckets achieving the greatest trajectory length, $X_H$.

*TABLE 5.10: TYPE III BUTTERFLY FLIP BUCKET TRAJECTORY RESULTS (PROTOTYPE VALUES)*

| Flow Condition | Discharge (m3/s) | Max Height of Upper Trajectory, $h_{m(u)}$ | Max Height of Lower Trajectory, $h_{m(l)}$ | Distance to $h_{m(u)}$, $X_{m(u)}$ | Distance to $h_{m(l)}$, $X_{m(l)}$ | Upper Trajectory Distance, $X_{H(u)}$ | Lower Trajectory Distance, $X_{H(l)}$ |
|---|---|---|---|---|---|---|---|
| **1** | 288.42 | 6.70 | 2.65 | 16.25 | 14.10 | 45.23 | 37.90 |
| **2** | 384.69 | 10.83 | 5.08 | 29.45 | 25.98 | 74.10 | 63.35 |
| **3** | 480.63 | 16.88 | 6.68 | 47.98 | 41.03 | 107.90 | 83.75 |
| **4** | 625.00 | 28.08 | 11.68 | 77.53 | 66.33 | 176.63 | 151.25 |
| **5** | 625.00 | 11.00 | 4.85 | 29.88 | 26.20 | 70.80 | 59.63 |
| **6** | 625.00 | 16.90 | 6.03 | 42.20 | 38.80 | 99.63 | 84.50 |
| **7** | 625.00 | 20.50 | 8.80 | 60.45 | 54.90 | 132.55 | 110.73 |

Note: Refer to **Figure 3.4** in **Section 3.2.6** for a visual representation of the parameters in **Table 5.10**.

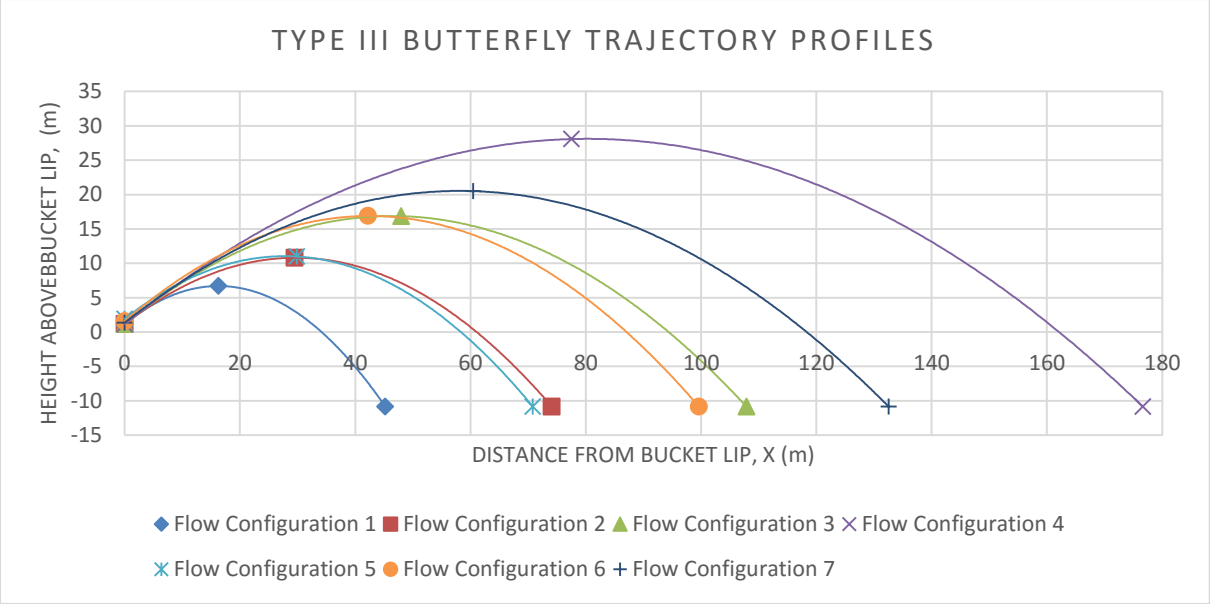


*FIGURE 5.13: GRAPHICAL REPRESENTATION OF THE TYPE III BUTTERFLY UPPER TRAJECTORY RESULTS PRESENTED IN TABLE 5.10 WITH BEST FIT TREND LINES*

### *5.3.3.3 Type III Transverse and Longitudinal Impact Widths*

**Table 5.11** and **Figure 5.14** shows the results of the Type III Scoop and Butterfly transverse and longitudinal impact widths. Due to the fact that these flip buckets are completely new designs it was unknown how the water jet would react and what shape of impact profile would be created. The designs were created with the intention of creating better dispersion of the jet at the point of impingement with the downstream river bed. The increased dispersion was assumed to be longitudinally for the Scoop flip bucket and laterally for the Butterfly flip bucket.

TABLE 5.11: TYPE III FLIP BUCKET TRANSVERSE AND LONGITUDINAL IMPACT WIDTH RESULTS (PROTOTYPE VALUES)

| Flow Condition | Discharge (m3/s) | Scoop Transverse Impact Width, $B_j$ | Butterfly Transverse Impact Width, $B_j$ | Scoop Longitudinal Impact Width, $W_j$ | Butterfly Longitudinal Impact Width, $W_j$ |
|---|---|---|---|---|---|
| **1** | 288.42 | 21.05 | 22.10 | 9.80 | 7.33 |
| **2** | 384.69 | 26.60 | 28.23 | 14.15 | 10.75 |
| **3** | 480.63 | 30.35 | 35.35 | 15.58 | 24.15 |
| **4** | 625.00 | 40.05 | 52.55 | 23.43 | 25.38 |
| **5** | 625.00 | 32.85 | 32.08 | 11.80 | 11.20 |
| **6** | 625.00 | 38.80 | 40.80 | 13.75 | 15.15 |
| **7** | 625.00 | 42.35 | 50.93 | 18.90 | 21.83 |

Note: Refer to **Figure 5.4** for a visual representation of the parameters in **Table 5.11**.

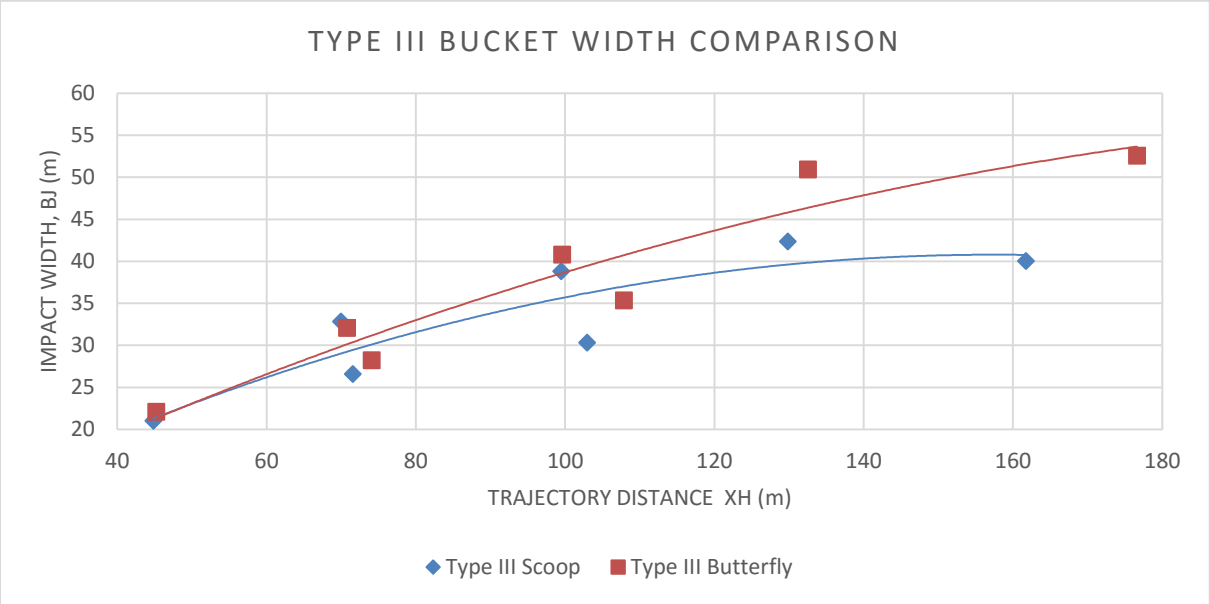


FIGURE 5.14: TYPE III TRANSVERSE IMPACT WIDTHS RELATIVE TO THE TRAJECTORY DISTANCE

A clear trend is depicted from the results presented in **Table 5.11** and **Figure 5.14**. It can be seen that as the trajectory distance increases so does the transverse impact width. The same applies for the longitudinal impact widths of the Type III flip buckets. As expected, the Butterfly flip bucket has better dispersion in the lateral direction while the longitudinal dispersion for the two buckets is relatively similar unexpectedly. For the design flow condition transverse impact widths were 40.05m and 52.55m for the Scoop and Butterfly Type III buckets. The horizontal impact widths were 23.43m and 25.38m for the design flow condition. The results show that the impact area for the Butterfly flip bucket is larger than that of the Scoop flip bucket based on the longitudinal and transverse impact widths.

## 5.4 AERATION RESULTS

The aeration results presented in this section display the air concentration percentage within the jet core at three positions; at the centreline, at a distance of 3.125m from the centreline and at a distance of 6.25m from the centreline (sidewall). The expectation was to show a distribution of the air content

within the jet core across the width of the flip buckets at a point directly after the jet leaves the bucket lip with the intention of determining which flip bucket best entrains air.

### 5.4.1 TYPE I AERATION RESULTS

The aeration results for the Type I flip buckets are presented in **Figure 5.15**, **Figure 5.16** and **Figure 5.17**.

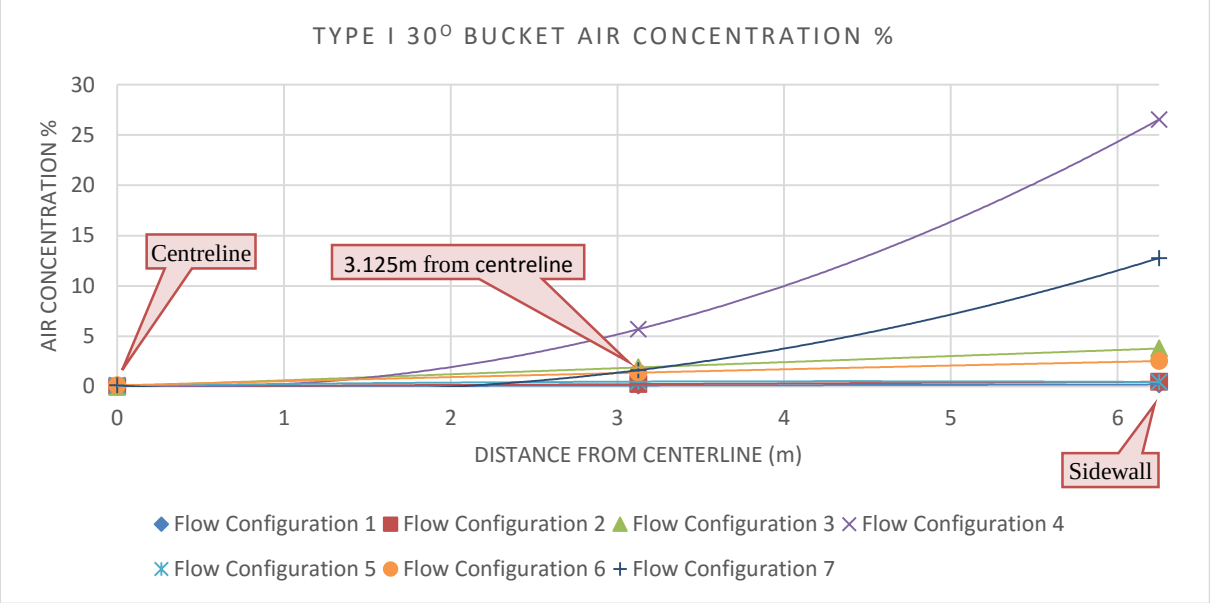


*FIGURE 5.15: AIR CONCENTRATION PERCENTAGE OF TYPE I 30O FLIP BUCKET AT THE JET CORE*

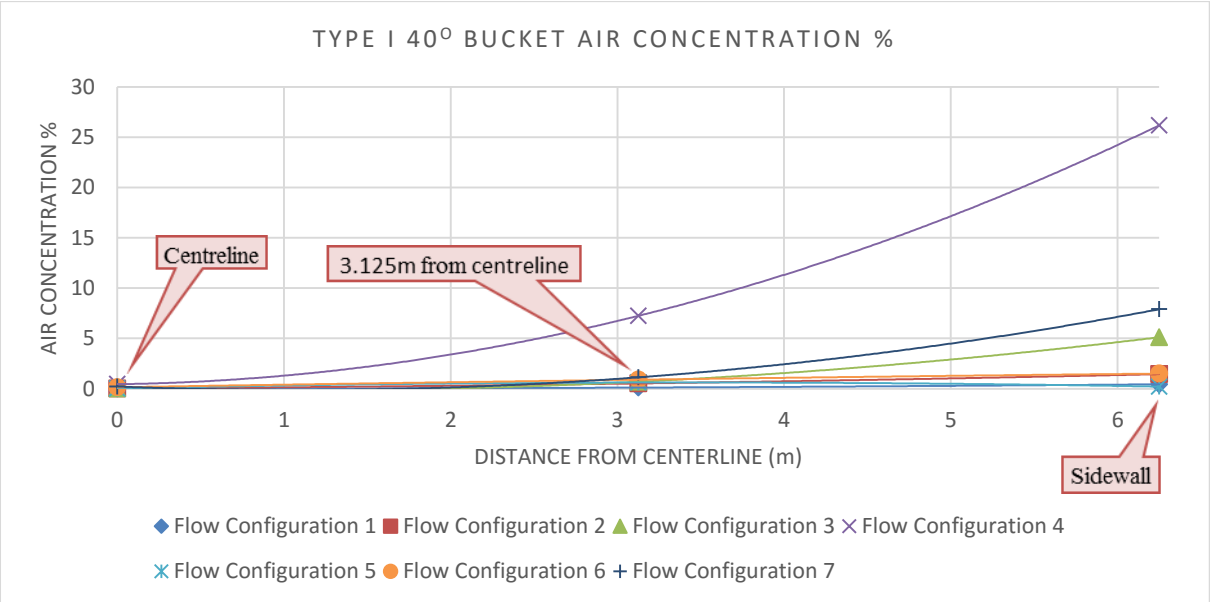


*FIGURE 5.16: AIR CONCENTRATION PERCENTAGE OF TYPE I 40O FLIP BUCKET AT THE JET CORE*

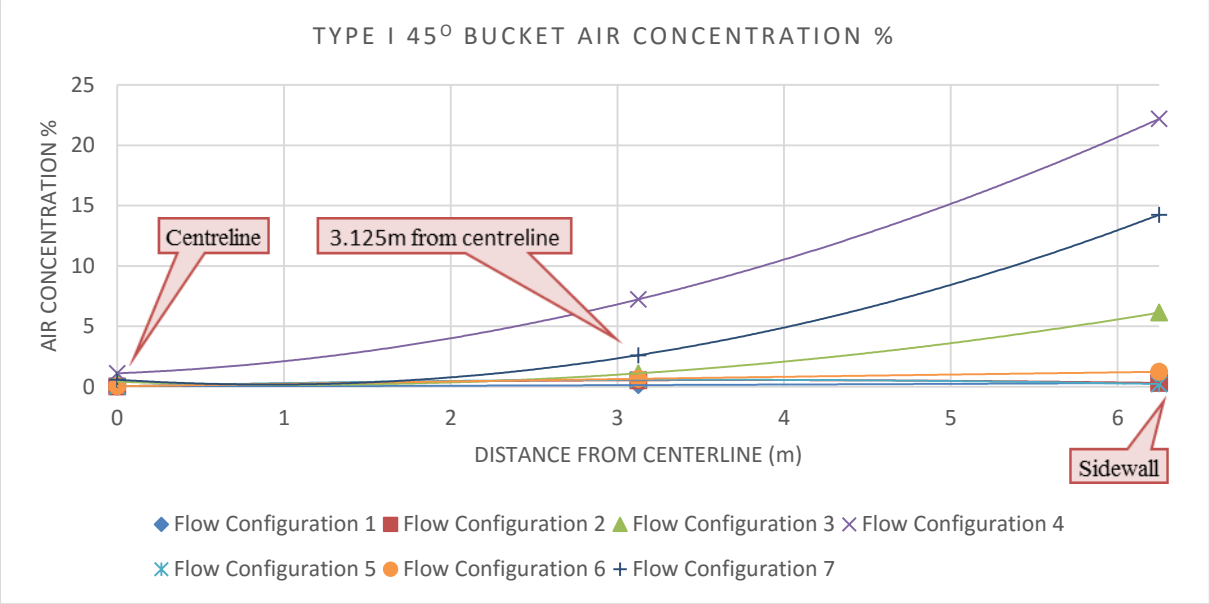


*FIGURE 5.17: AIR CONCENTRATION PERCENTAGE OF TYPE I 45O FLIP BUCKET AT THE JET CORE*

When comparing the aeration results of the Type I buckets presented in **Figure 5.15**, **Figure 5.16** and **Figure 5.17,** it can be seen that for the design flow condition all air concentrations are relatively similar with the 30º bucket having the maximum concentration at the sidewalls of 26.6% and the 45º bucket having the maximum at the centreline of 1.1%. There is a trend that suggests with the increased deflection angle the centreline air concentration percentage increases.

### 5.4.2 TYPE II AERATION RESULTS

The aeration results for the Type II flip buckets are presented in **Figure 5.18**, **Figure 5.19** and **Figure 5.20**.

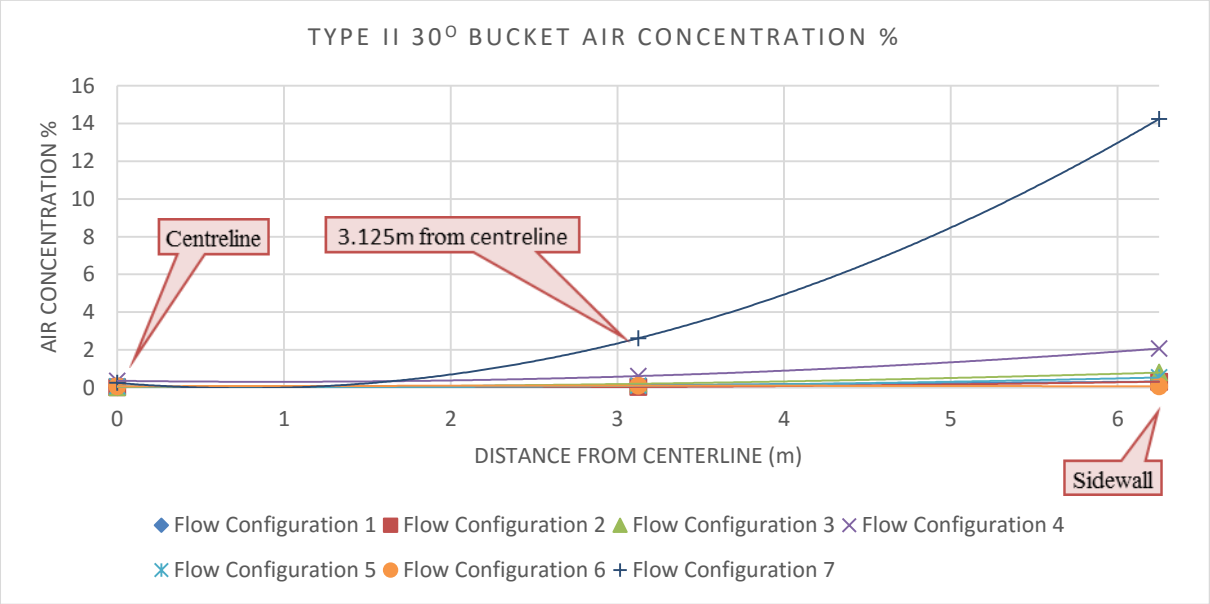


*FIGURE 5.18: AIR CONCENTRATION PERCENTAGE OF TYPE II 30O FLIP BUCKET AT THE JET CORE*

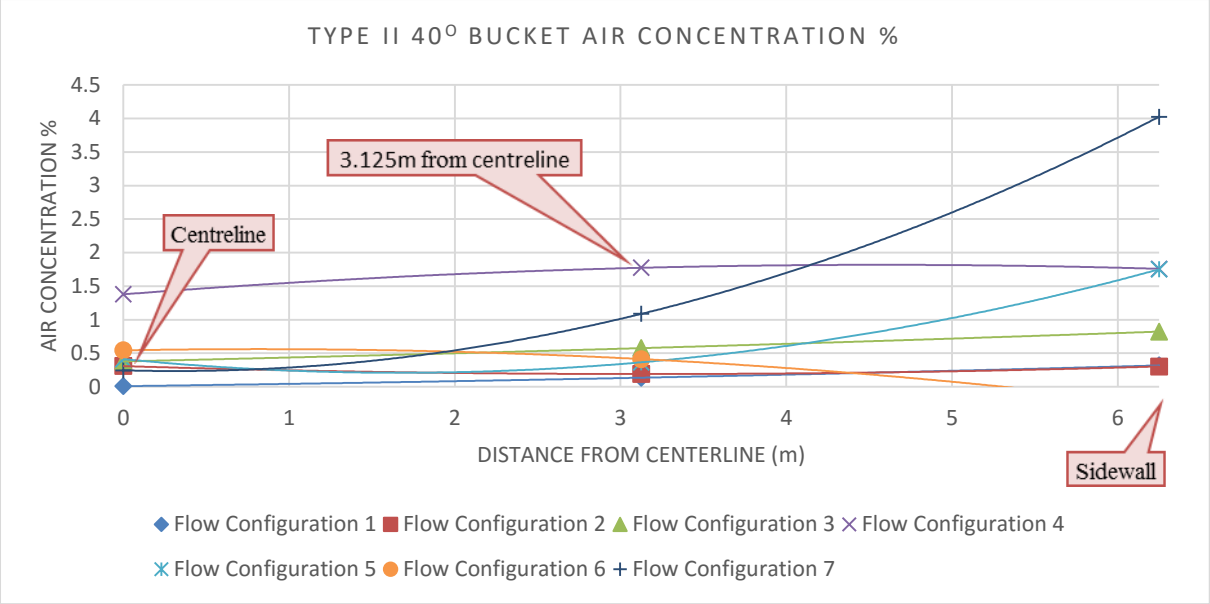


*FIGURE 5.19: AIR CONCENTRATION PERCENTAGE OF TYPE II 40° FLIP BUCKET AT THE JET CORE*

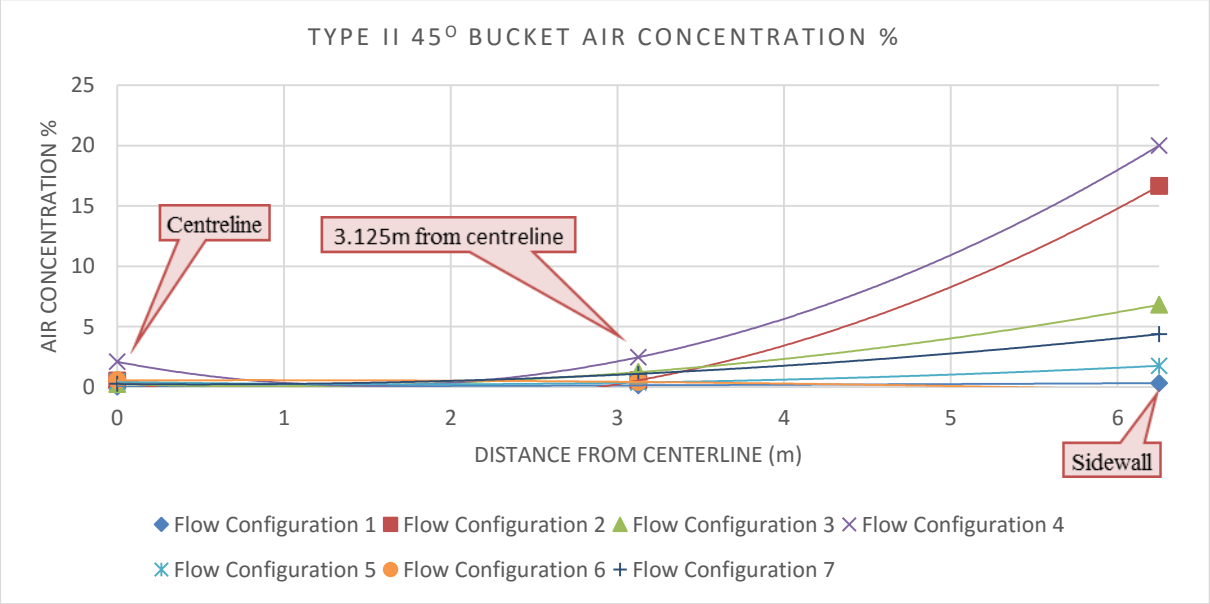


*FIGURE 5.20: AIR CONCENTRATION PERCENTAGE OF TYPE II 45° FLIP BUCKET AT THE JET CORE*

When comparing the aeration results of the Type II buckets presented in **Figure 5.18**, **Figure 5.19** and **Figure 5.20,** it can be seen that the 45° bucket yields the best results for the design flow condition with the air concentration at the centreline being 2.1% and at the sidewall is 20%.

### 5.4.3 TYPE III AERATION RESULTS

The aeration results for the Type I flip buckets are presented in **Figure 5.21** and **Figure 5.22**.

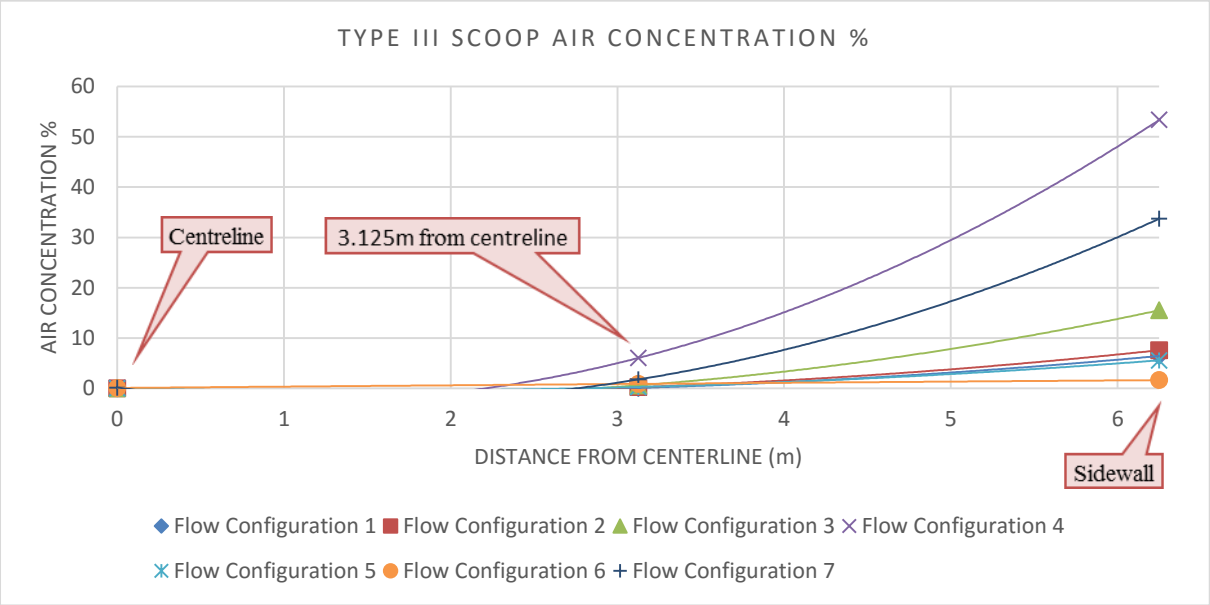


*FIGURE 5.21: AIR CONCENTRATION PERCENTAGE OF TYPE III SCOOP FLIP BUCKET AT THE JET CORE*

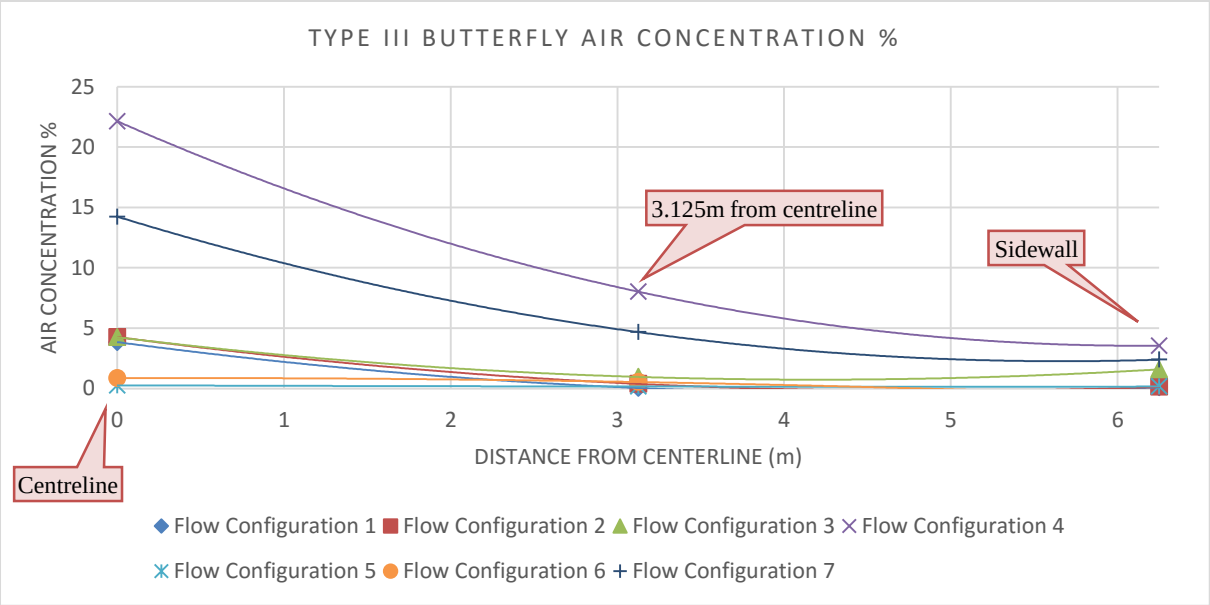


*FIGURE 5.22: AIR CONCENTRATION PERCENTAGE OF TYPE III BUTTERFLY FLIP BUCKET AT THE JET CORE*

When comparing the aeration results of the Type III buckets presented in **Figure 5.21** and **Figure 5.22**, it can be seen that the air concentration distributions are very different. The Butterfly bucket air concentration percentage distribution is different to all the other buckets with the maximum concentration percentage at the centreline. For the design flow condition, air concentration percentages at the centreline for the Scoop and Butterfly flip buckets are 0.08% and 22.14%. At a distance of 3.125m from the centreline the air concentrations are 6.02% and 8.02%, and at the sidewalls the air

concentrations are 53.37% and 3.55%. The air entrainment at the sidewalls of the Scoop flip bucket is much greater than that of all the other buckets. This is a result of the bucket shape where the bulk of the flow is present at the centreline, therefore there is a smaller flow depth at the sidewalls allowing greater air entrainment into the core of the jet. The same principle applies to the Butterfly flip bucket, where the flow depth is the smallest at the centreline allowing greater air entrainment into the jet core.

## 5.5 SPATIAL PRESSURE DISTRIBUTION MAPS

The spatial pressure distribution maps presented in this section display the 0.1% exceedance dynamic impact pressure heads for the design flow condition with a discharge equal to 625$m^3$/s at a flow depth of 1.15m. From these maps the impact areas can be identified as well as the positions of the highest impact pressures. The results obtained from the pressure transducers were recorded with their locations within the impact basin where the 0.1% exceedance for each transducer was determined. These results were then imported into a software package called Surfer 11 as an x,y,z file, where x and y represented the coordinate of the transducer within the basin and the z value represented the dynamic impact pressure head. The Surfer 11 software then displayed these points on a contour may and associated a colour scale to the range of pressures.

### 5.5.1 TYPE I FLIP BUCKET SPATIAL PRESSURE DISTRIBUTION MAPS

The Type I flip buckets incorporated the diverging sidewalls with the purpose of increasing the jet dispersion so the expectation was to have a pressure distribution that was spread transversely. **Figure 5.23**, **Figure 5.24** and **Figure 5.25** show the results of the impact pressure distributions presented on a contour map.

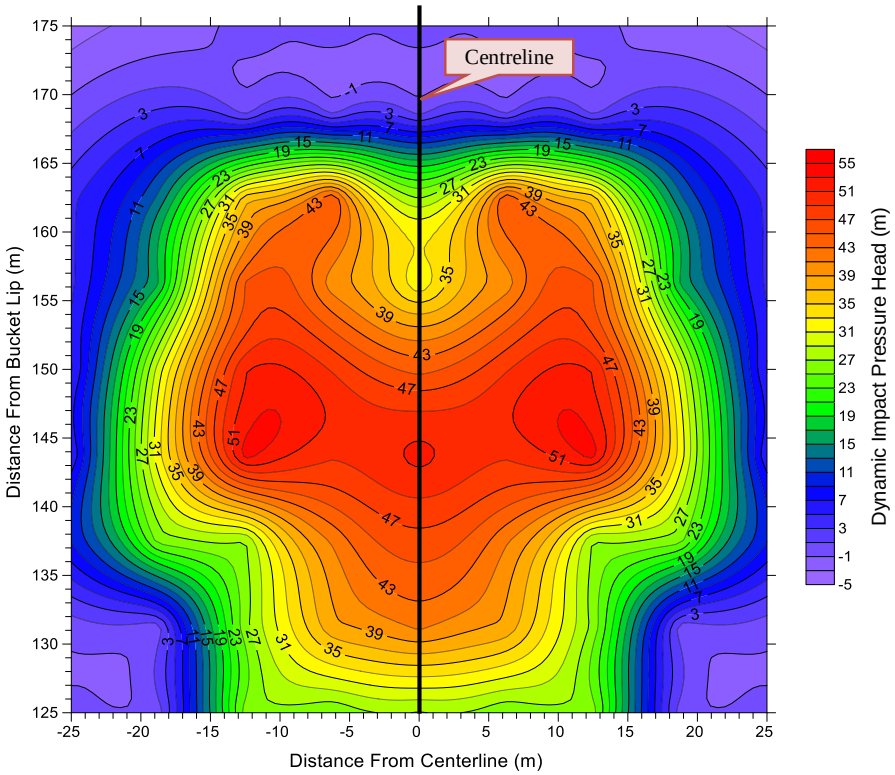


*FIGURE 5.23: TYPE I 30$^{O}$ FLIP BUCKET SPATIAL PRESSURE DISTRIBUTION MAP (0.1% EXCEEDANCE DYNAMIC HEAD IN M WATER)*

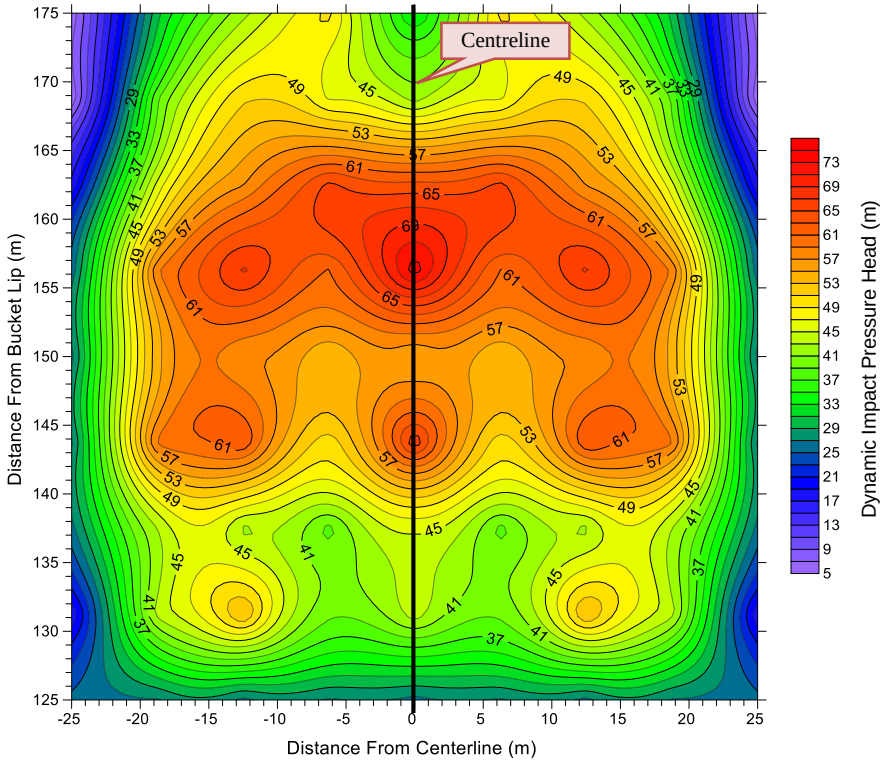


*FIGURE 5.24: TYPE I 40$^{O}$ FLIP BUCKET SPATIAL PRESSURE DISTRIBUTION MAP (0.1% EXCEEDANCE DYNAMIC HEAD IN M WATER)*

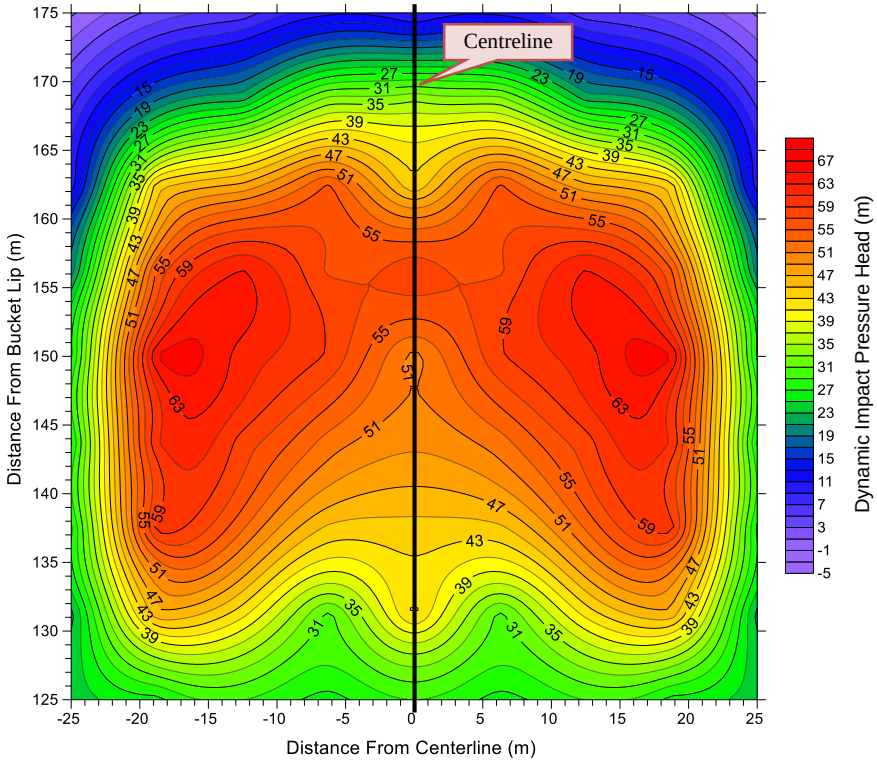


*FIGURE 5.25: TYPE I 45º FLIP BUCKET SPATIAL PRESSURE DISTRIBUTION MAP (0.1% EXCEEDANCE DYNAMIC HEAD IN M WATER)*

From **Figure 5.23**, **Figure 5.24** and **Figure 5.25,** it can be seen that the 40º yielded the highest dynamic pressure for the Type I buckets and the 30º yielded the lowest, however the distribution of the 30º bucket is not the best as the maximum pressures seem to be fairly concentrated in the centre, whereas a better distribution can be seen with the 45º bucket. The 40º bucket has the best distribution of the three buckets where the pressures are distributed over a much larger surface area.

### 5.5.2 TYPE II FLIP BUCKET SPATIAL PRESSURE DISTRIBUTION MAPS

The Type II flip buckets incorporated the converging sidewalls with the purpose of decreasing the jet dispersion transversely but increasing the dispersion longitudinally, therefore the expectation was to have a pressure distribution that was spread longitudinally. **Figure 5.26**, **Figure 5.27** and **Figure 5.28** show the results of the impact pressure distributions presented on a contour map.

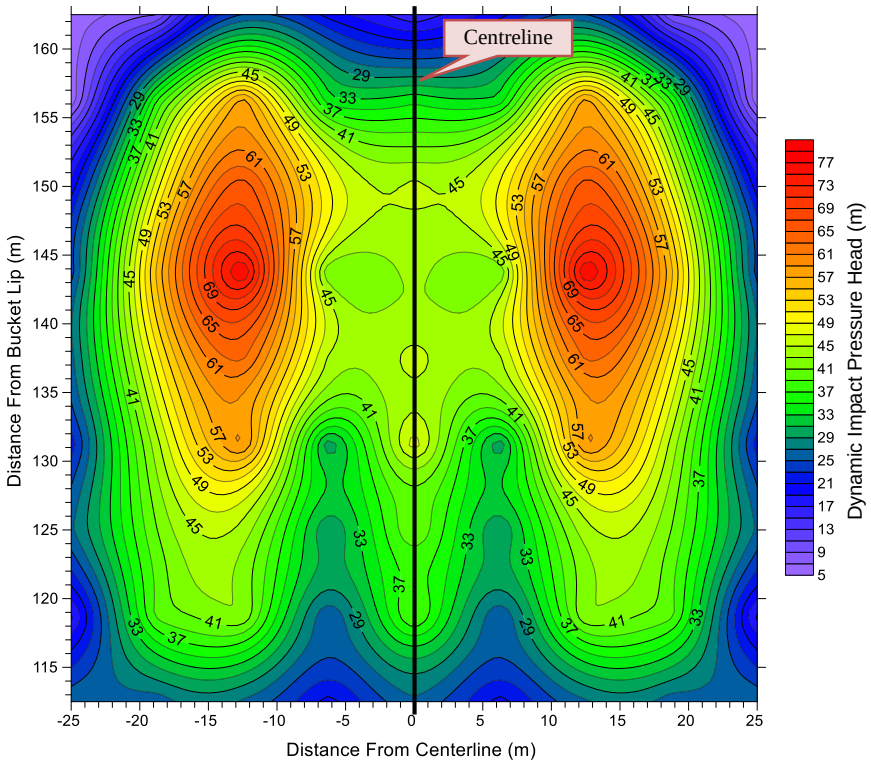


*FIGURE 5.26: TYPE II 30$^{O}$ FLIP BUCKET SPATIAL PRESSURE DISTRIBUTION MAP (0.1% EXCEEDANCE DYNAMIC HEAD IN M WATER)*

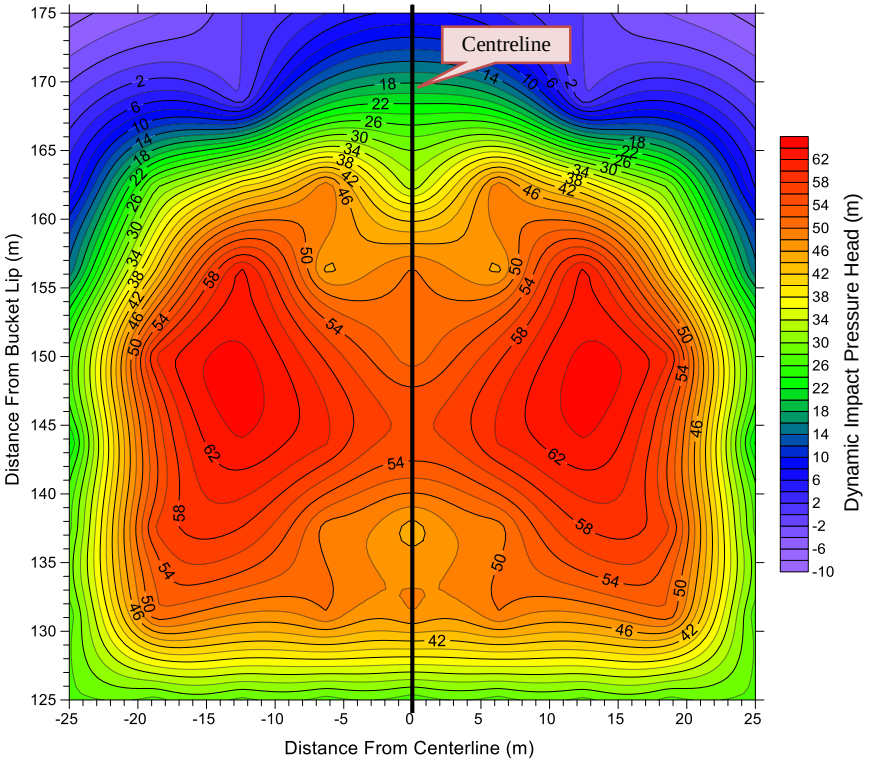


*FIGURE 5.27: TYPE II 40$^{O}$ FLIP BUCKET SPATIAL PRESSURE DISTRIBUTION MAP (0.1% EXCEEDANCE DYNAMIC HEAD IN M WATER)*

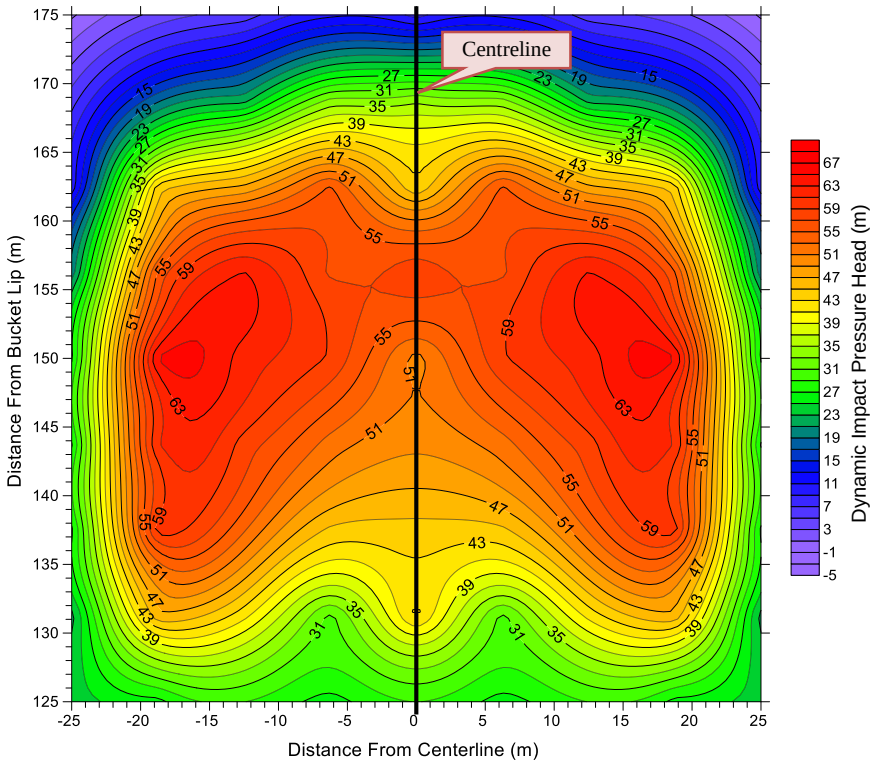


*FIGURE 5.28: TYPE II 45° FLIP BUCKET SPATIAL PRESSURE DISTRIBUTION MAP (0.1% EXCEEDANCE DYNAMIC HEAD IN M WATER)*

From **Figure 5.26**, **Figure 5.27** and **Figure 5.28,** it can be seen that the 30° bucket yielded the greatest dynamic pressure for the Type II buckets and the 40° bucket yielded the lowest, however the maximum pressures of the 30° bucket seems to be fairly concentrated on either side of the centreline. This shows that the dispersion of the 30° bucket is not great. The pressure distributions of the 40° and 45° buckets are relatively similar where the 40° bucket distribution has a slightly better distribution with the maximum pressures spread over a larger surface area. Therefore the 40° bucket has the lowest maximum dynamic pressure head, as well as the best distribution out of the three Type II buckets.

### 5.5.3 TYPE III FLIP BUCKET SPATIAL PRESSURE DISTRIBUTION MAPS

The Type III flip buckets incorporated the diverging sidewalls as well as varied deflection angles of the bucket lip. These buckets were designed with the intention to increase the jet dispersion both transversely and longitudinally, but increasing the dispersion longitudinally therefore the expectation was to have a pressure distribution that was spread over a much larger area than the other buckets. **Figure 5.29** and **Figure 5.30** show the results of the impact pressure distributions presented on a contour map for the Scoop and Butterfly buckets respectively.

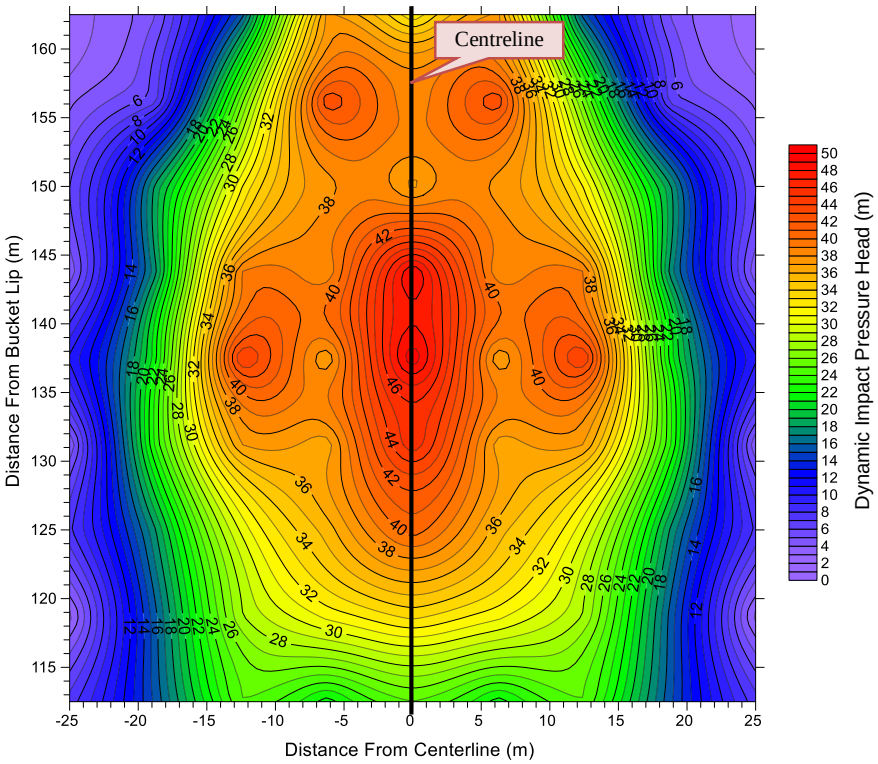


FIGURE 5.29: TYPE III SCOOP SPATIAL PRESSURE DISTRIBUTION MAP (0.1% EXCEEDANCE DYNAMIC HEAD IN M WATER)

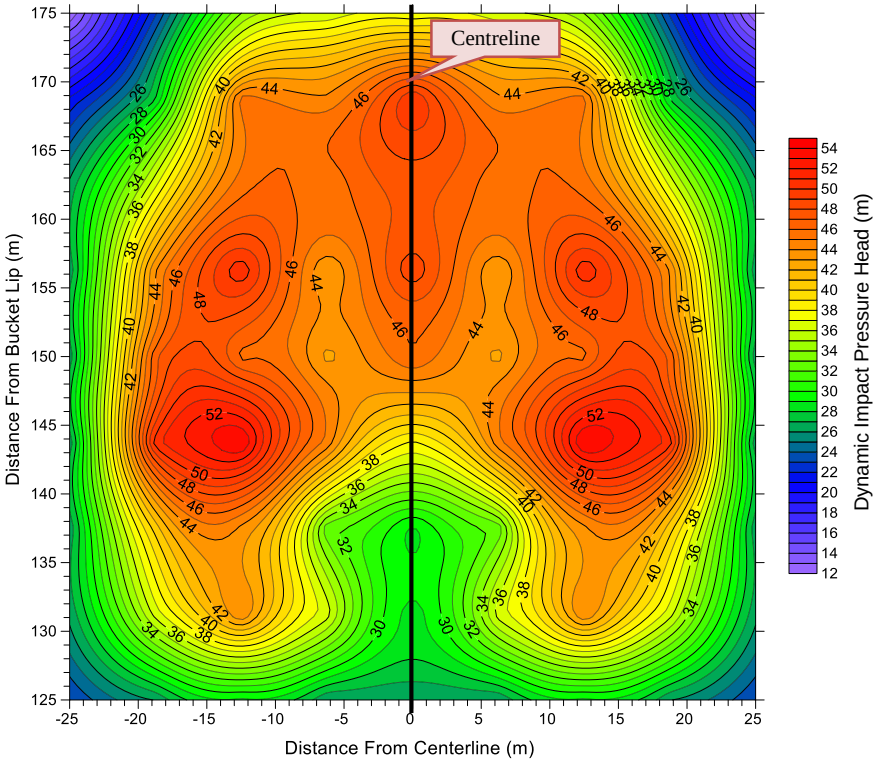


FIGURE 5.30: TYPE III BUTTERFLY SPATIAL PRESSURE DISTRIBUTION MAP (0.1% EXCEEDANCE DYNAMIC HEAD IN M WATER)

From **Figure 5.29** and **Figure 5.30,** it can be seen that the Butterfly bucket yielded the greatest dynamic pressure for the Type III buckets and the Scoop bucket yielded the lowest. As expected, the Scoop bucket appears to increase the longitudinal dispersion at the impact area, however the lateral spread

appears to decrease as can be seen from **Figure 5.29**, where the maximum dynamic pressures are located along the centreline. The Butterfly bucket increased the longitudinal and transverse dispersion at the impact area which was the intended function. The high pressures are distributes over a much larger area and so can be considered the best option out of the two Type III buckets in terms of the spatial pressure distribution.

## 5.6 MAXIMUM DYNAMIC IMPACT PRESSURE HEAD RESULTS

In the previous chapter it was identified that the maximum dynamic pressure head is defined as the 99.8$^{th}$ percentile of maximum pressure value within the impact location over a time period of five minutes. As previously stated there were some very high spikes in the pressure distribution that exceeded the range of the pressure transducers. These peaks were all located within the top 0.1% of the pressure data and were excluded due to the fact that the energy that they represented was greater than the initial energy of the system which should be theoretically impossible.

### 5.6.1 TYPE I DYNAMIC PRESSURE HEAD

The Type I flip buckets portrayed a jet trajectory of a general ski-jump design with no constrictions or non-uniform shape present. The dynamic pressure head was tested for the three Type I flip buckets at all flow conditions. The results for these test are displayed in **Table 5.12** and **Figure 5.31**.

*TABLE 5.12: TYPE I DYNAMIC IMPACT PRESSURE RESULTS (0.1% EXCEEDANCE DYNAMIC HEAD IN M WATER)*

| Flow Condition | Discharge (m3/s) | 30º Flip Bucket $P_{dM}$ (m) | 40º Flip Bucket $P_{dM}$ (m) | 45º Flip Bucket $P_{dM}$ (m) |
|---|---|---|---|---|
| **1** | 288.42 | 32.43 | 27.90 | 32.98 |
| **2** | 384.69 | 49.00 | 45.73 | 47.90 |
| **3** | 480.63 | 50.00 | 67.55 | 55.30 |
| **4** | 625.00 | 53.85 | 74.13 | 66.70 |
| **5** | 625.00 | 37.23 | 51.05 | 53.38 |
| **6** | 625.00 | 43.50 | 51.85 | 54.15 |
| **7** | 625.00 | 48.73 | 60.23 | 59.85 |

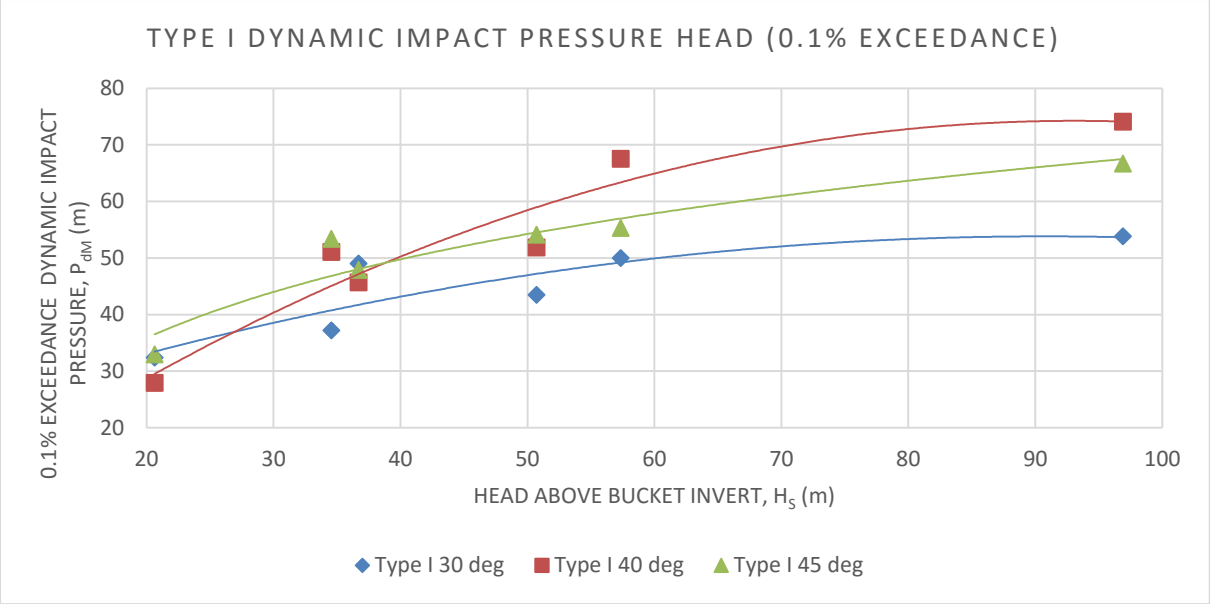


*FIGURE 5.31: GRAPHICAL REPRESENTATION OF THE TYPE I DYNAMIC IMPACT PRESSURES (0.1% EXCEEDANCE DYNAMIC HEAD IN M WATER)*

When looking at the data presented in **Table 5.12** and **Figure 5.31,** it can be seen that the 30° flip bucket generally has the lowest impact pressures with a design flow condition $P_{dM}$ of 53.85m. It was expected that this would have the lowest impact pressure due to the jet trajectory having a lower angle. Surprisingly the 40° flip bucket had the largest impact pressures with 74.13m at the design flow condition. The 45° bucket impact pressures were slightly lower than that of the 40° bucket with 66.70m at the design flow condition. Due to higher trajectory elevations reached, the 45° bucket should in theory have a higher impact pressure, but as a result of a longer throw distance and wider impact width, the interaction with air was to some extent longer, which could have possibly reduced the dynamic impact pressures.

### 5.6.2 TYPE II DYNAMIC PRESSURE HEAD

The Type II flip buckets portrayed a jet trajectory of a slit type ski-jump design with a general flip bucket shape and contraction of the sidewalls to 25% of the original spillway width. The dynamic pressure head was tested for the three Type II flip buckets for six of the seven flow conditions. Chocking flow was present in the first flow condition and the dynamic impact pressures were excluded. The results for these test are displayed in **Table 5.13** and **Figure 5.32** below.

TABLE 5.13: TYPE II DYNAMIC IMPACT PRESSURE RESULTS (0.1% EXCEEDANCE DYNAMIC HEAD IN M WATER)

| Flow Condition | Discharge (m3/s) | 30º Flip Bucket $P_{dM}$ (m) | 40º Flip Bucket $P_{dM}$ (m) | 45º Flip Bucket $P_{dM}$ (m) |
|---|---|---|---|---|
| **1** | 288.42 | Flow Choking | Flow Choking | Flow Choking |
| **2** | 384.69 | 34.95 | 36.60 | 41.28 |
| **3** | 480.63 | 57.63 | 52.15 | 50.10 |
| **4** | 625.00 | 77.38 | 64.53 | 65.20 |
| **5** | 625.00 | 49.05 | 38.20 | 41.78 |
| **6** | 625.00 | 55.73 | 55.15 | 49.10 |
| **7** | 625.00 | 65.43 | 63.28 | 57.10 |

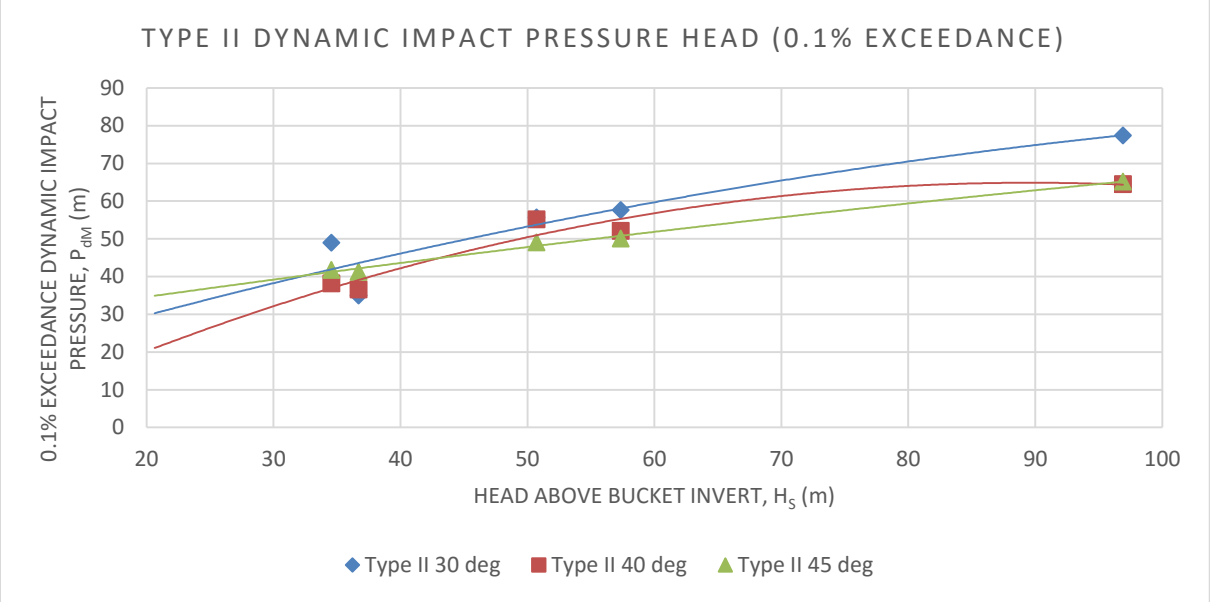


FIGURE 5.32: GRAPHICAL REPRESENTATION OF THE TYPE II IMPACT PRESSURES (0.1% EXCEEDANCE DYNAMIC HEAD IN M WATER)

From the data presented in **Table 5.13** and **Figure 5.32,** it can be seen that the 30º flip bucket generally has the highest impact pressures with a design flow condition $P_{dM}$ of 77.38m. The 40º bucket had a $P_{dM}$ of 64.53m for the design flow condition while the 45º bucket had a $P_{dM}$ of 65.20m. These results were completely unexpected as they are somewhat reversed relative to the trajectory elevations perceived in **Table 5.5**, **Table 5.6** and **Table 5.7**. It is possible that due to the constriction substantially greater dispersion was perceived with the 40º and 45º buckets in the horizontal direction, however this cannot be validated due to the inability to collect this data (refer to **Table 5.8**).

### 5.6.3 TYPE III DYNAMIC PRESSURE HEAD

The Type III flip buckets portrayed a jet trajectory of a compound type ski-jump design with two completely new designs based on a theoretical approach. These buckets included a non-uniform radius over the width of the bucket as well as a varied deflection angle. The dynamic pressure head was tested for the two Type III flip buckets for all seven flow conditions. The results for these test are displayed in **Table 5.14** and **Figure 5.33**.

TABLE 5.14: TYPE III DYNAMIC IMPACT PRESSURE RESULTS (0.1% EXCEEDANCE DYNAMIC HEAD IN M WATER)

| Flow Condition | Discharge (m3/s) | Scoop Flip Bucket $P_{dM}$ (m) | Butterfly Flip Bucket $P_{dM}$ (m) |
|---|---|---|---|
| **1** | 288.42 | 26.30 | 32.85 |
| **2** | 384.69 | 33.83 | 41.53 |
| **3** | 480.63 | 45.38 | 52.38 |
| **4** | 625.00 | 49.83 | 54.25 |
| **5** | 625.00 | 40.38 | 44.20 |
| **6** | 625.00 | 44.20 | 55.68 |
| **7** | 625.00 | 43.28 | 51.75 |

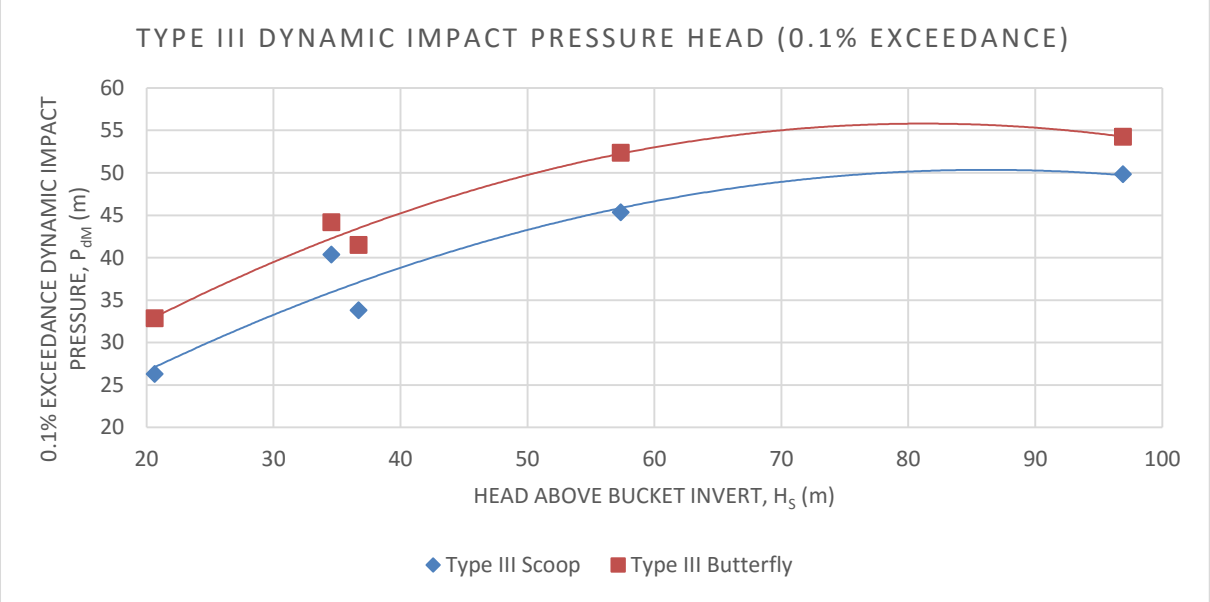


FIGURE 5.33: GRAPHICAL REPRESENTATION OF THE TYPE III IMPACT PRESSURES (0.1% EXCEEDANCE DYNAMIC HEAD IN M WATER)

When viewing the data presented in **Table 5.14** and **Figure 5.33,** it can be seen that the Scoop flip bucket generally has the lowest impact pressures with a design flow condition $P_{dM}$ of 49.83m. It was expected that this would have the lowest impact pressure due to the jet trajectory having a lower angle at the centreline. The Butterfly flip bucket impact pressures were generally slightly larger than that of the Scoop bucket with 54.25m at the design flow condition. Due to higher trajectory elevations reached the Butterfly bucket should in theory have a higher impact pressure which it does.

## 5.7 IMPACT VELOCITY HEAD RESULTS

The measurement of the impact velocity head, $H_{vj}$, was another way of determining the hydraulic energy present at the point of impact and like the dynamic impact pressure head, $P_{dM}$ can be compared to the initial theoretical energy level, $H_T$, with the intention of calculating the energy loss as a percentage of the initial energy.

The acquisition of $H_{vj}$ required a meticulous approach where accuracy was a concern. As stated in the previous chapter the velocity data was captured with a GoPro action camera that recorded a video with

a dimensioned backing board. This video was then processed by motion tracking software which analysed the video frame by frame to determine the velocity of the jet trajectory at impact. A vast quantity of time was spent on the acquisition and processing of this data to make sure the results were as accurate as possible where multiple measurements were taken for each flow condition of every flip bucket design at different sections of the captured videos.

With the used of the equation $H_{vj} = v^2/2g$, the velocities were converted to a velocity head.

### 5.7.1 TYPE I IMPACT VELOCITY

The Type I impact velocity head results are presented in **Table 5.15** and a graphical representation of these results are depicted **Figure 5.34**.

*TABLE 5.15: TYPE I IMPACT VELOCITY HEAD RESULTS (PROTOTYPE VALUES)*

| Flow Condition | Discharge (m3/s) | 30º Flip Bucket $H_{vj}$ (m) | 40º Flip Bucket $H_{vj}$ (m) | 45º Flip Bucket $H_{vj}$ (m) |
|---|---|---|---|---|
| **1** | 288.42 | 25.65 | 21.43 | 19.05 |
| **2** | 384.69 | 33.43 | 36.35 | 29.68 |
| **3** | 480.63 | 42.33 | 52.75 | 42.30 |
| **4** | 625.00 | 56.00 | 69.38 | 58.50 |
| **5** | 625.00 | 33.75 | 35.85 | 26.40 |
| **6** | 625.00 | 36.85 | 39.90 | 40.40 |
| **7** | 625.00 | 43.45 | 62.40 | 50.95 |

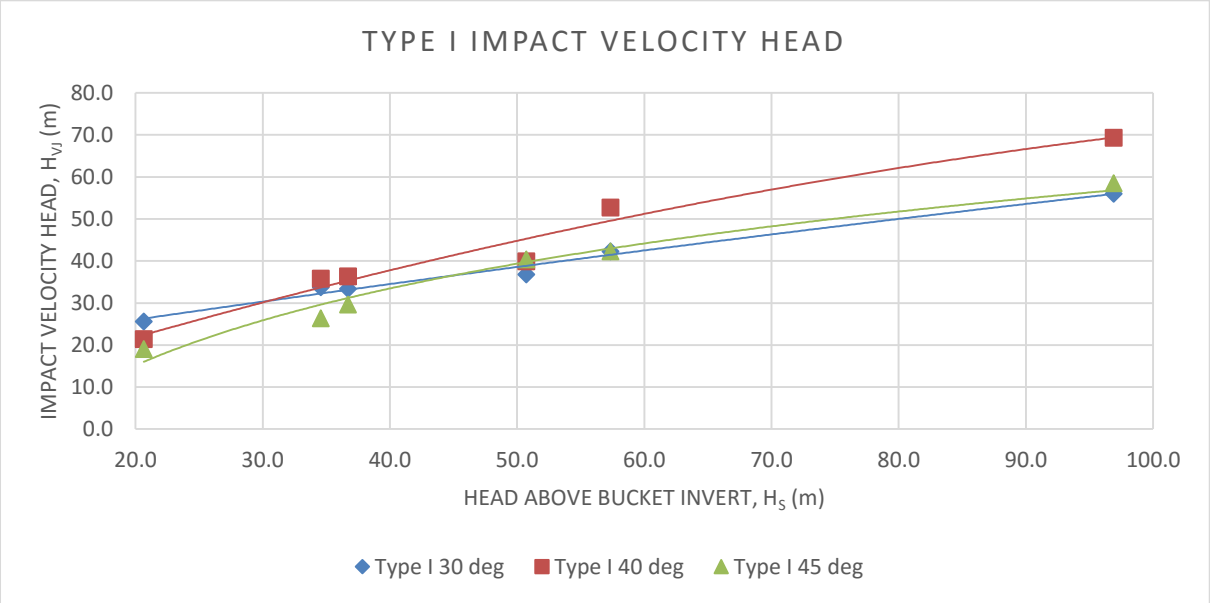


*FIGURE 5.34: GRAPHICAL REPRESENTATION OF THE TYPE I IMPACT VELOCITY HEAD RESULTS*

The results of the Type I impact velocity heads displayed above clearly show a trend for each flip bucket. It can be seen that in general the 40º flip bucket yielded the greatest impact velocity heads with $H_{vj}$ = 69.38m for the design flow condition. The 30º and 45 º flip buckets surprisingly had very similar

velocity heads for each flow condition. For the design flow condition the 45° flip bucket had $H_{vj}$ = 58.50m and the 30° flip bucket had $H_{vj}$ = 56.00m differing by only 4%.

### 5.7.2 TYPE II IMPACT VELOCITY

The Type II impact velocity head results are presented in **Table 5.16** and a graphical representation of these results are depicted in **Figure 5.35**.

*TABLE 5.16: TYPE II IMPACT VELOCITY HEAD RESULTS (PROTOTYPE VALUES)*

| Flow Condition | Discharge (m3/s) | 30° Flip Bucket $H_{vj}$ (m) | 40° Flip Bucket $H_{vj}$ (m) | 45° Flip Bucket $H_{vj}$ (m) |
|---|---|---|---|---|
| **1** | 288.42 | Flow Choking | Flow Choking | Flow Choking |
| **2** | 384.69 | 24.98 | 28.85 | 25.78 |
| **3** | 480.63 | 42.23 | 42.50 | 31.43 |
| **4** | 625.00 | 63.20 | 48.60 | 53.88 |
| **5** | 625.00 | 24.53 | 25.23 | 21.28 |
| **6** | 625.00 | 32.85 | 34.38 | 27.35 |
| **7** | 625.00 | 56.25 | 43.45 | 37.50 |

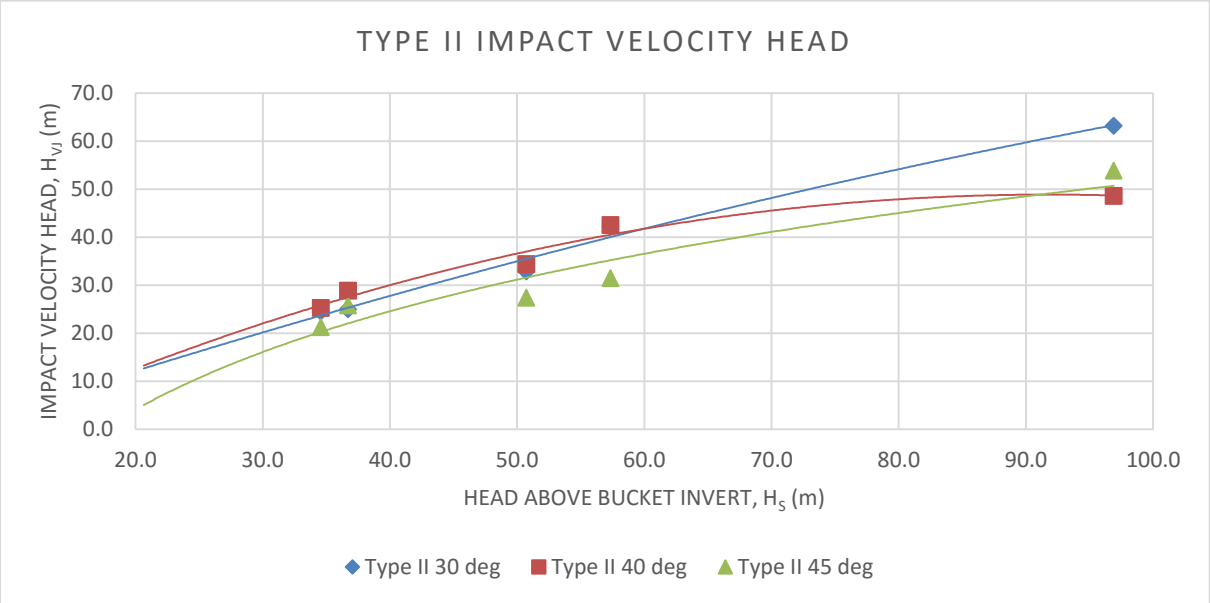


*FIGURE 5.35: GRAPHICAL REPRESENTATION OF THE TYPE II IMPACT VELOCITY HEAD RESULTS*

The results of the Type II velocity heads displayed above clearly show a trend for each flip bucket. It can be seen that in general the 30° flip bucket yielded the greatest impact velocity heads with an $H_{vj}$ = 63.20m for the design flow condition while the 40° flip bucket yielded the lowest with $H_{vj}$ = 48.60m. For the design flow condition the 45° flip bucket had $H_{vj}$ = 53.88m.

### 5.7.3 TYPE III IMPACT VELOCITY

The Type III impact velocity head results are presented in **Table 5.17** and a graphical representation of these results are depicted in **Figure 5.36**.

*TABLE 5.17: TYPE III IMPACT VELOCITY HEAD RESULTS (PROTOTYPE VALUES)*

| Flow Condition | Discharge (m3/s) | Scoop Flip Bucket $H_{vj}$ (m) | Butterfly Flip Bucket $H_{vj}$ (m) |
|---|---|---|---|
| **1** | 288.42 | 13.55 | 15.58 |
| **2** | 384.69 | 19.58 | 23.15 |
| **3** | 480.63 | 21.58 | 24.50 |
| **4** | 625.00 | 22.68 | 29.30 |
| **5** | 625.00 | 35.25 | 36.65 |
| **6** | 625.00 | 34.83 | 38.88 |
| **7** | 625.00 | 44.08 | 51.98 |

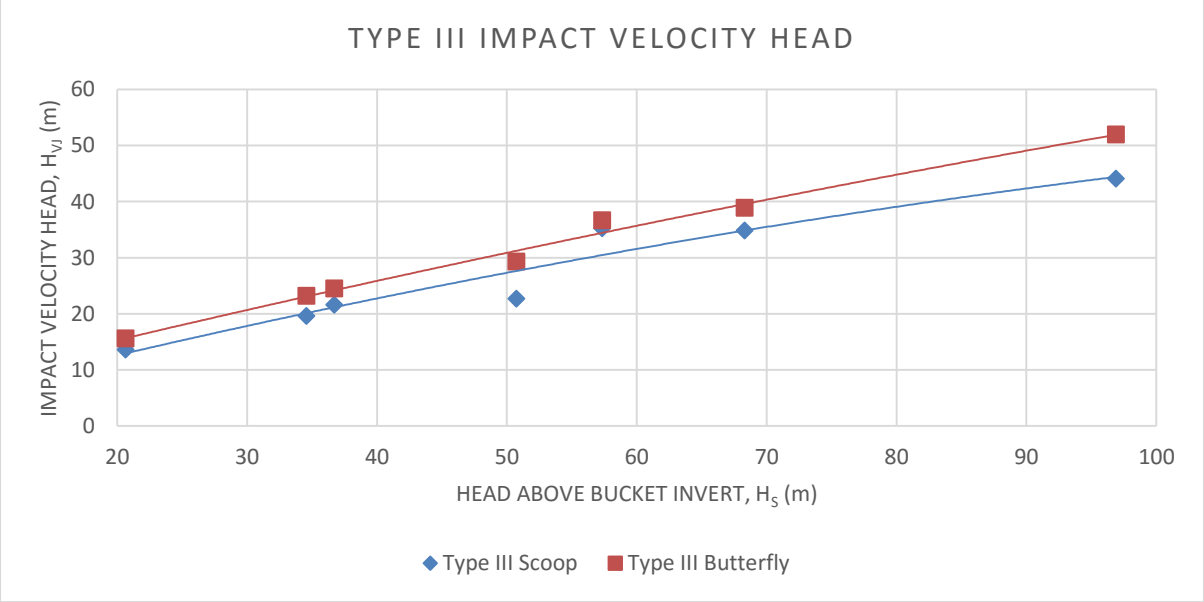


*FIGURE 5.36: GRAPHICAL REPRESENTATION OF THE TYPE III IMPACT VELOCITY HEAD RESULTS*

The results of the Type III velocity heads displayed above clearly show a trend for each flip bucket. It can be seen that in general the Butterfly flip bucket yielded the greatest impact velocity heads with an $H_{vj}$ = 29.30m for the design flow condition while the Scoop flip bucket yielded the lowest with $H_{vj}$ = 22.68m. The reason for the Scoop flip bucket having a slightly lower impact velocity head than that of the Butterfly flip bucket is due to the fact that at the trajectory angle is 30° at the middle of the Scoop flip bucket where the majority of the flow is, thus a lower trajectory profile is seen.

# CHAPTER 6: ANALYSIS OF EXPERIMENTAL RESULTS

*In this chapter, the results retrieved from the hydraulic model are analysed which includes comparing the results with their theoretical equivalents. The analysis is divided into 3 main parts; trajectory analysis, aeration analysis and pressure distribution analysis.*

## 6.1 GEOMETRIC ANALYSIS

### 6.1.1 VALIDATION OF THE AIR RESISTANCE FACTOR

Theoretically the trajectory of a free-falling jet of water follows a parabolic path. One can predict the trajectory profile of any free-falling water jet with **Equation 2.10** where the factor for air resistance, *k*, is 0.9. This factor is accounts for the energy losses experienced by the interaction of the two mediums; air and water. Although there are certain other energy losses that may affect the trajectory profile of the water jet, such as wind turbulence, altitude and temperature, they are significantly more difficult to quantify, especially in prototype scale. Given a controlled environment such as the water laboratory at Stellenbosch University where wind turbulence is negligible and altitude and temperature remains constant, the trajectory profiles for the different flip buckets and flows of the ski-jump hydraulic model were determined as presented in **Section 5.3**.

These profiles were then compared to their theoretical profiles given the specific flow conditions, as well as an air resistance factor of 1 (assuming no air resistance). The results of this analysis are presented in **Table 6.1**.

*TABLE 6.1: RATIOS OF MEASURED TRAJECTORY HORIZONTAL DISTANCE TO THEORETICAL UN-FACTORED DISTANCES*

| **Bucket type** / **Flow Condition** | **Type I** | | | **Type II** | | | **Type III** | | **Average Per Flow Condition** |
|---|---|---|---|---|---|---|---|---|---|
| | 30 | 40 | 45 | 30 | 40 | 45 | Scoop | Butterfly | |
| **1** | 0.880 | 0.885 | 0.946 | N/A | N/A | N/A | 0.908 | 0.901 | 0.904 |
| **2** | 0.890 | 0.871 | 0.875 | 0.895 | 0.843 | 0.847 | 0.909 | 0.893 | 0.878 |
| **3** | 0.895 | 0.881 | 0.877 | 0.849 | 0.830 | 0.839 | 0.892 | 0.866 | 0.866 |
| **4** | 0.879 | 0.859 | 0.859 | 0.811 | 0.802 | 0.842 | 0.875 | 0.865 | 0.849 |
| **5** | 0.987 | 0.921 | 0.915 | 0.895 | 0.865 | 0.857 | 0.935 | 0.900 | 0.909 |
| **6** | 0.906 | 0.899 | 0.895 | 0.939 | 0.886 | 0.896 | 0.959 | 0.895 | 0.909 |
| **7** | 0.888 | 0.906 | 0.908 | 0.937 | 0.893 | 0.883 | 0.963 | 0.904 | 0.910 |
| **Average per Bucket** | 0.904 | 0.889 | 0.896 | 0.888 | 0.853 | 0.861 | 0.920 | 0.889 | |
| **Average per Type** | 0.895 | | | 0.867 | | | 0.905 | | |

When analysing the data presented in **Table 6.1,** it can be seen that the measured trajectory lengths in comparison to their theoretical counterparts are relatively constant. These values represented in the table can be considered to be the air resistance factors for each test. As previously mentioned in **Section 2.8.3,** the theoretical factor of air resistance for a water jet is 0.9. For the flip buckets tested Type II buckets seem to diverge the most from the theoretical value with a maximum of 5.2% for the 40° bucket. Type I flip buckets experiences a maximum divergence of 1.2%, while Type III buckets experienced a maximum divergence of 2.2%. When averaging the air resistance factors experience by type, it was

calculated that Type I and Type III flip buckets diverge by 0.5% from the theoretical, while Type II flip buckets diverge by 3.3%. From this trend it may be concluded that the trajectory profiles follow the theoretical.

### 6.1.2 COMPARISON OF THE TRAJECTORY PROFILES

When analysing the jet trajectory profiles of the ski-jump flip buckets it is important to choose the best performing flip bucket not only based on the horizontal throw distance, but also on the dispersion of the jet trajectory.

Generally the trajectory profile of the Type I flip buckets performed as one would have expected relative to the theoretical. The 30° Type I flip bucket had the shortest throw distance and dispersion characteristics for the design condition with $X_H$ = 162.50m, $h_m$ = 21.65m and the transverse impact width of 37.90m. The 40° flip bucket general jet trajectory characteristics were slightly greater than that of the 30° flip bucket with $X_H$ = 174.35m, $h_m$ = 28.65m and a transverse impact width of 47.70m. The 45° flip bucket general jet trajectory characteristics were slightly greater than that of the 40° flip bucket with $X_H$ = 175.23m, $h_m$ = 34.10m and a transverse impact width of 50.50m. The theory states that as the trajectory angle increases up to the angle of 45°, the horizontal throw distance and maximum jet elevation should also increase. When analysing the measured data we can clearly see that this statement is valid for the Type I flip buckets as with each bucket angle increase the trajectory characteristics increased accordingly. From **Table 6.1** it can be seen that the Type I flip buckets, when compared to the theoretical values, have an air resistance factor of 0.895. These results are more accurate than what was initially expected.

The trajectory profiles of the Type II flip buckets were also relatively close to the theoretical, however the contraction of the sidewall decreased the horizontal throw distances slightly. The 30° Type II flip bucket had the shortest throw distance and dispersion characteristics for the design condition with $X_H$ = 149.93m, $h_m$ = 30.48m and a transverse impact width of 24.48m. The 40° flip bucket general jet trajectory characteristics were slightly greater than that of the 30° flip bucket with $X_H$ = 163.60m and $h_m$ = 31.18m and a transverse impact width of 34.75m.The 45° flip bucket general jet trajectory characteristics were slightly greater than that of the 40° flip bucket $X_H$ = 171.8m and $h_m$ = 30.48m and a transverse impact width of 41.35m. When comparing each Type II Trajectory characteristic against the Type I flip buckets, there is a noticeable decrease in the values. This decrease is a direct result of the contracting sidewalls, which forces the jet cross sectional area to increase thereby decreasing the take-off velocity, according to the continuity equation Q=VA. The impact widths of the Type II flip buckets are considerably narrower than all other buckets. When comparing the measures data with the theoretical data (**Table 6.1**), one can evidently see that the trajectory profiles are less than the theoretical with an air resistance coefficient of 0.867.

Like the Type I flip buckets the Type III flip buckets were expected to have trajectory profiles very similar to the theoretical. When comparing the two buckets for the design flow condition the Scoop flip bucket had the shortest horizontal throw distance and dispersion characteristics with $X_H$ = 161.78m, $h_m$ = 25.18m and the transverse impact width of 40.05m. The Butterfly flip bucket general jet trajectory characteristics were slightly greater than that of the Scoop flip bucket with $X_H$ = 176.63m, $h_m$ = 28.08m and a transverse impact width of 52.55m. According to the results displayed in **Table 6.1,** the Type III flip bucket trajectory profiles when compared with their theoretical values yield an air resistance factor of 0.905, which suggests that the trajectory profiles for the Type III flip buckets are accurate to 99.5%.

## 6.2 AERATION ANALYSIS

When analysing the air concentration results of the different buckets it is important to select the flip bucket that has the greatest air concentration distribution through the core of the water jet. The most important position where air entrainment will have the most significant effect on the dispersion and disintegration of the water jet is at the centreline.

From the eight flip buckets designed, the best performing flip bucket in terms of the air concentration for the design flow condition from each bucket type was chosen for further analysis. The best performing flip bucket out of the Type I buckets was the 30º flip bucket with an air concentration at the centreline of 1.1% and 26.6% and the sidewalls (refer to **Figure 5.15**). The 45º bucket yields the best results out of the Type II flip buckets with an air concentration of 2.1% at the centreline and 20% at the sidewalls (refer to **Figure 5.20**). When analysing the aeration results of the Type III buckets presented in **Figure 5.21** and **Figure 5.22**, the air concentration results portrayed very different distributions compared to the other buckets, with the Butterfly bucket deviating the most with the maximum air concentration percentage present at the centreline. For the design flow condition, air concentration percentages at the centreline for the Scoop and Butterfly flip buckets are 0.08% and 22.14%. At a distance of 3.125m from the centreline the air concentrations are 6.02% and 8.02%, and at the sidewalls the air concentrations are 53.37% and 3.55%.

The Butterfly flip bucket was chosen as the best performing flip bucket from all bucket types based upon the air concentration percentage at the centreline being far greater than any other flip bucket by 20%.

## 6.3 SPATIAL PRESSURE DISTRIBUTION MAPS

Initially in the previous Chapter one flip bucket from each of the three flip bucket types was chosen as the best performing bucket in terms of their pressure distribution. Out of the Type I flip buckets the 40º flip bucket had the best pressure distribution. For the Type II flip buckets it was also the 40º flip bucket that had the best pressure distribution. The Butterfly flip bucket had the best pressure distribution when compared to the other Type III flip bucket. By reviewing **Figure 5.24**, **Figure 5.27** and **Figure 5.30,** a comparison was made between these three flip buckets where the Butterfly flip bucket seems to have

the best distribution of the maximum pressures by a small margin. However the maximum pressure value for the Butterfly flip bucket is substantially smaller than the other two buckets.

## 6.4 MAXIMUM DYNAMIC IMPACT PRESSURE ANALYSIS (0.1% EXCEEDANCE)

### 6.4.1 TYPE I DYNAMIC IMPACT PRESSURE COMPARISON

When comparing the impact pressures of the Type I buckets (refer to **Figure 5.31**) it is clear that the dynamic impact pressure of the 30º flip bucket are significantly lower than that of the 40º and 45º buckets. Although all bucket pressures are relatively similar for the 1st flow condition as the dam head increases, a deviation in impact pressure by the 40º and 45º buckets from the 30º bucket is evident. For the 4$^{th}$ flow condition (design discharge of 625 m$^3$/s and flow depth of 1.148m (prototype scale)), the maximum dynamic pressure is 43.68m, 74.13m and 66.70m for the 30º, 40º and 45º flip buckets respectively. The test results show that the 40º flip bucket has the maximum impact pressure of the three Type I buckets. Theoretically this should not be the case due to the fact that when comparing the trajectory profiles, the 45º bucket reached the highest flight path (refer to **Figure 5.1**, **Figure 5.2** and **Figure 5.3**). During the testing is was witnessed that the trajectories of the different buckets displayed slightly different characteristics. As the bucket angle increased, the trajectory height increased as well as the trajectory distance induces significantly more spray as well as dispersion at the impact location. The spray and dispersion created by the 45º buckets could have possibly been enough to reduce the dynamic impact pressures to values below that of the 40º bucket.

### 6.4.2 TYPE II DYNAMIC IMPACT PRESSURE COMPARISON

When comparing the dynamic impact pressures of the Type II buckets (refer to **Figure 5.32**), it can be seen that during the lower velocity flow conditions the impact pressures are of relatively similar magnitude. As the velocity increases there is a greater separation in the maximum dynamic impact pressures of the Type II buckets. **Figure 5.32** shows us that the 30º flip bucket has the maximum dynamic impact pressure head for the design flow condition of 77.38m where the 40º flip bucket has the lowest $P_{dM}$ of 64.53m. When comparing the entire trend for the different Type II buckets, the 45º flip bucket has the lowest $P_{dM}$ while the 30º flip bucket has the greatest $P_{dM}$. Theoretically the trends should be the other way around with the 45º flip bucket having the maximum impact pressure head, however this appears not to be the case. The possible reason for this is that due to the sidewall contraction of the slit type flip bucket with the combination of a smaller bucket radius (shorter curvature) there were greater energy losses as compared with the 30º bucket which has a larger radius with a longer curvature. A smaller bucket radius turns the flow over a sort length and flow may not be as smooth as that of a larger radius therefore greater energy losses exist which would decrease the take-off velocity.

### 6.4.3 TYPE III DYNAMIC IMPACT PRESSURE COMPARISON

When comparing the dynamic impact pressures of the two Type III buckets (refer to **Figure 5.33**) we can see that that the pressures corresponding to each flow condition do no differ considerably and follow the same pattern. It was initially anticipated that the Scoop type bucket would produce a larger maximum dynamic pressure than that of the Butterfly type bucket but this is not the case as the Scoop flip bucket impact pressures are lower than that of the Butterfly flip bucket. It was thought that because the Scoop bucket concentrates the trajectory jet the pressures would be greater, but upon further analysis the higher pressures of the Butterfly flip bucket could possibly be due to the greater trajectory angle located in the centre of the bucket where the flow velocity is less affected by surface friction and therefor a higher trajectory profile may be seen (refer to **Figure 5.12** and **Figure 5.13**). When analysing the pressures between the two buckets it was identified that there is a maximum difference in impact pressure of 11.45m and an average difference of 7.08 m. For the 4$^{th}$ flow condition (design discharge of 625 m$^3$/s and flow depth of 1.148m (prototype scale)), the maximum dynamic pressure is 49.83m and 54.25m for the Scoop and Butterfly flip buckets respectively. With only a 4.43m difference for the maximum design flow condition these two buckets may be considered to be very similar in terms of their impact pressures.

## 6.5 ENERGY LOSS BY SKI-JUMP

As a means of quantifying the energy loss over the ski-jump a comparison between the initial energy level or total Head, $H_T$, and energy level at the point of impact, $E_2$ was conducted. The calculation of $H_T$ is based upon the theoretical approach where the static dam level is considered. For each flow condition of each flip bucket design the initial energy head remains constant as per **Table 4.3**. Assuming the datum level to correspond with the level of the point of impact with the pressure plate, $H_T$ is determined as per the equation below;

$$H_T = Hs + Y \qquad \textit{EQUATION 6.1}$$

Where $H_s$ is the elevation difference between the Energy head and the ski-jump invert, and
Y is the elevation difference between the ski-jump invert and tailwater.

The energy level at the point of impact was determined by two methods; ie. the dynamic pressure head at the point of impact and the impact velocity head. Therefor the following two equations apply for $E_2$ with subscript ‘P’ considering pressure and subscript ‘V’ considering velocity.

$$E_{2P} = P_{dM} \qquad \textit{EQUATION 6.2}$$

$$E_{2V} = H_{vj} \qquad \textit{EQUATION 6.3}$$

Where $P_{dM}$ is the maximum dynamic impact pressure head, and
$H_v$ is the impact velocity head.

In order to determine the energy loss the $E_{2P}$ and $E_{2V}$ were factored with $H_T$ to yield a percentage. **Figure 6.1** to **Figure 6.8** shows the relative energy at the point of impact for all Type I, II and III flip buckets.

### 6.5.1 TYPE I RELATIVE ENERGY COMPARISON

**Figure 6.1**, **Figure 6.2** and **Figure 6.3** show calculated results for the relative impact velocity and impact pressure head for the 30º, 40º and 45º Type I flip buckets respectively.

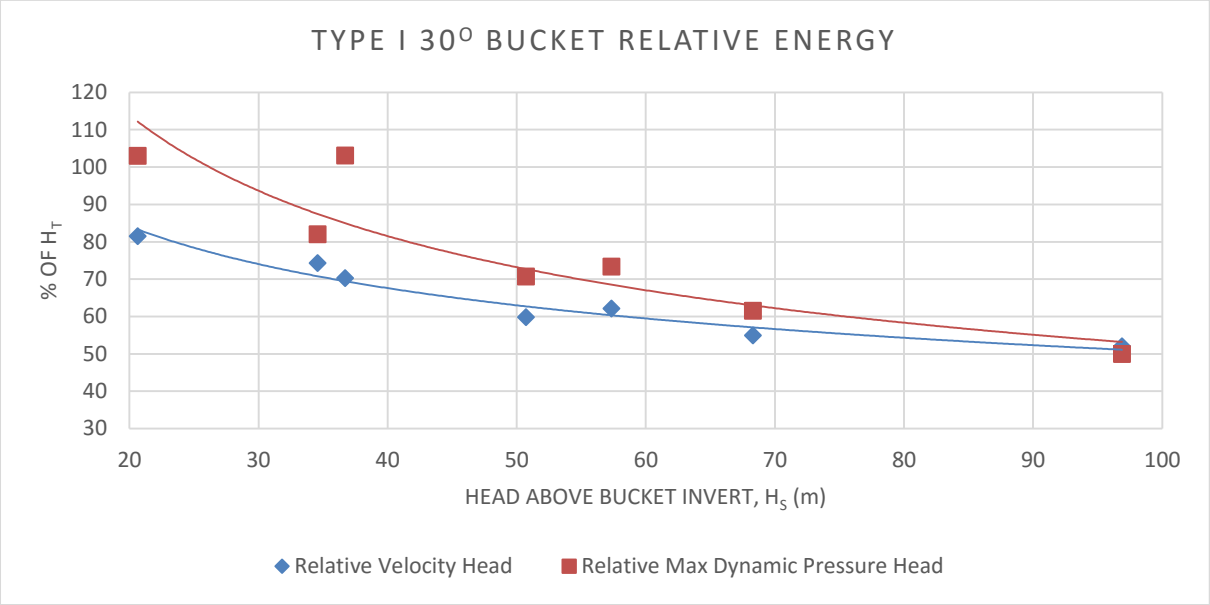


*FIGURE 6.1: ANALYSIS OF THE TYPE I 30º BUCKET IMPACT VELOCITY AND PRESSURE HEADS RELATIVE TO THE TOTAL INITIAL ENERGY LEVEL*

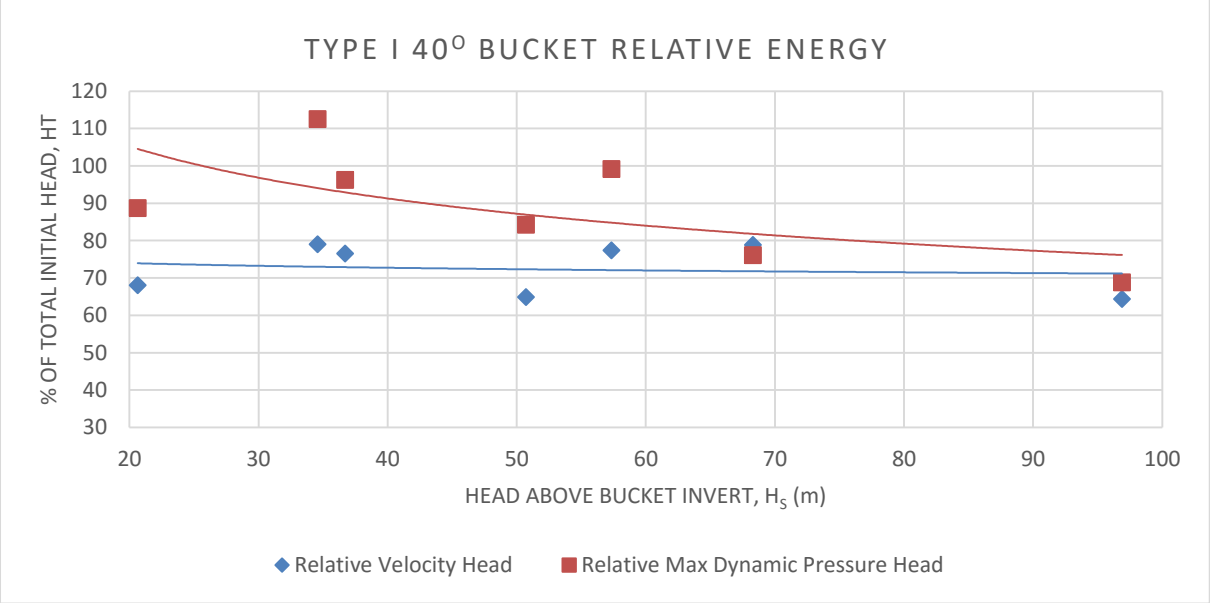


*FIGURE 6.2: ANALYSIS OF THE TYPE I 40º BUCKET IMPACT VELOCITY AND PRESSURE HEADS RELATIVE TO THE TOTAL INITIAL ENERGY LEVEL*

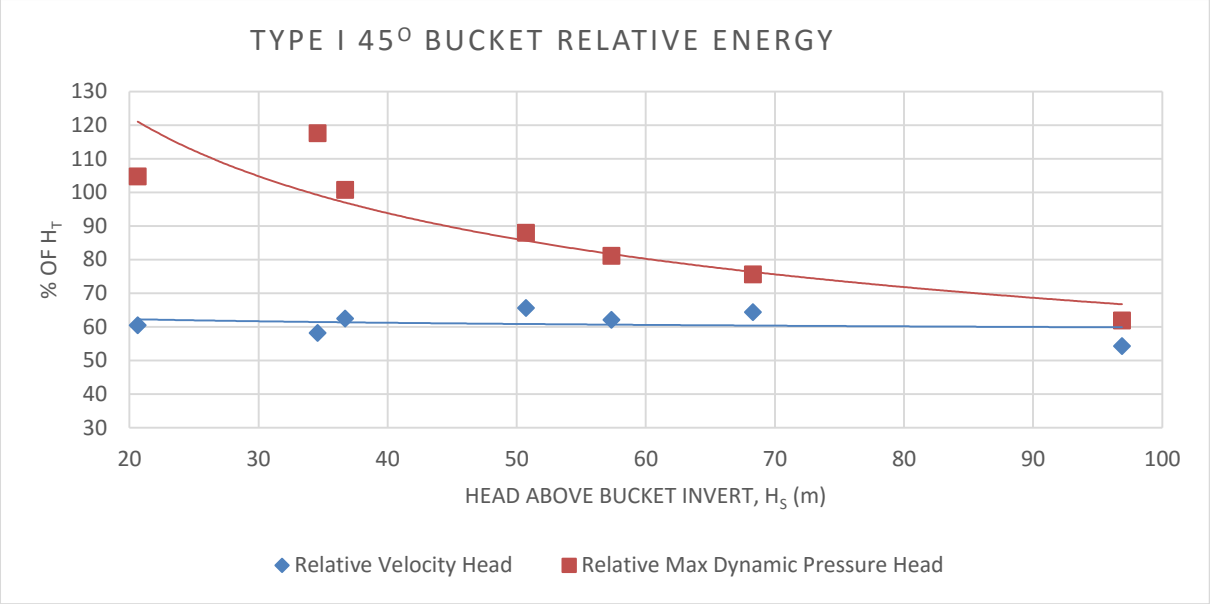


*FIGURE 6.3: ANALYSIS OF THE TYPE I 45° BUCKET IMPACT VELOCITY AND PRESSURE HEADS RELATIVE TO THE TOTAL INITIAL ENERGY LEVEL*

When analysing the data presented in **Figure 6.1**, **Figure 6.2** and **Figure 6.3** for the Type I flip buckets a general trend may be identified that suggests with the increase of $H_o$ the relative maximum dynamic pressure head decreases and therefore the energy losses increases. For the 40º and 45º Type I flip buckets the relative velocity head does not seem to change as much.

For the maximum flow condition the relative velocity head is 52%, 64.4% and 54.3% for the 30º, 40º and 45º flip buckets respectively. This means that the velocities show a total energy loss of 48%, 35.6% and 45.7% for the three flip buckets.

For the maximum flow condition the relative dynamic pressure head is 50%, 68.8% and 61.9% for the 30º, 40º and 45º flip buckets respectively. This suggests that the pressures yield a total energy loss of 50%, 31.2% and 38.1% for the three flip buckets.

When comparing all the Type I flip buckets we can see that the 30º flip bucket performs the best in terms of energy loss with 48% when analysing the velocity head and an energy loss of 50% when analysing the dynamic impact pressure.

### 6.5.2 TYPE II RELATIVE ENERGY COMPARISON

**Figure 6.4**, **Figure 6.5** and **Figure 6.6** show calculated results for the relative impact velocity and impact pressure head for the 30º, 40º and 45º Type II flip buckets respectively.

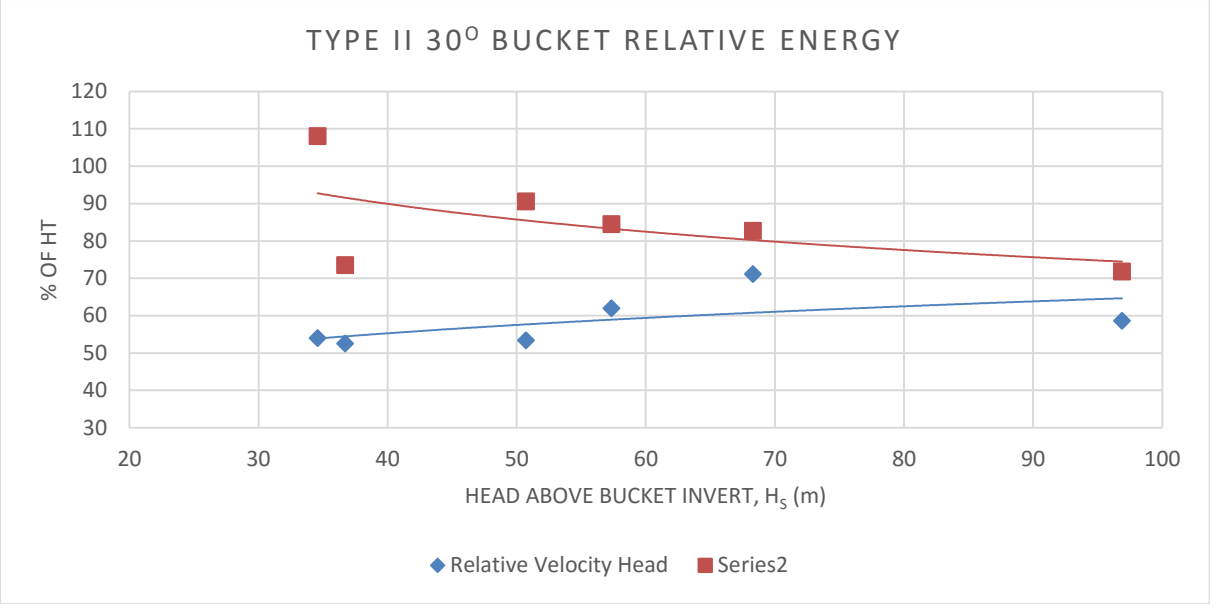


*FIGURE 6.4: ANALYSIS OF THE TYPE II 30O BUCKET IMPACT VELOCITY AND PRESSURE HEADS RELATIVE TO THE TOTAL INITIAL ENERGY LEVEL*

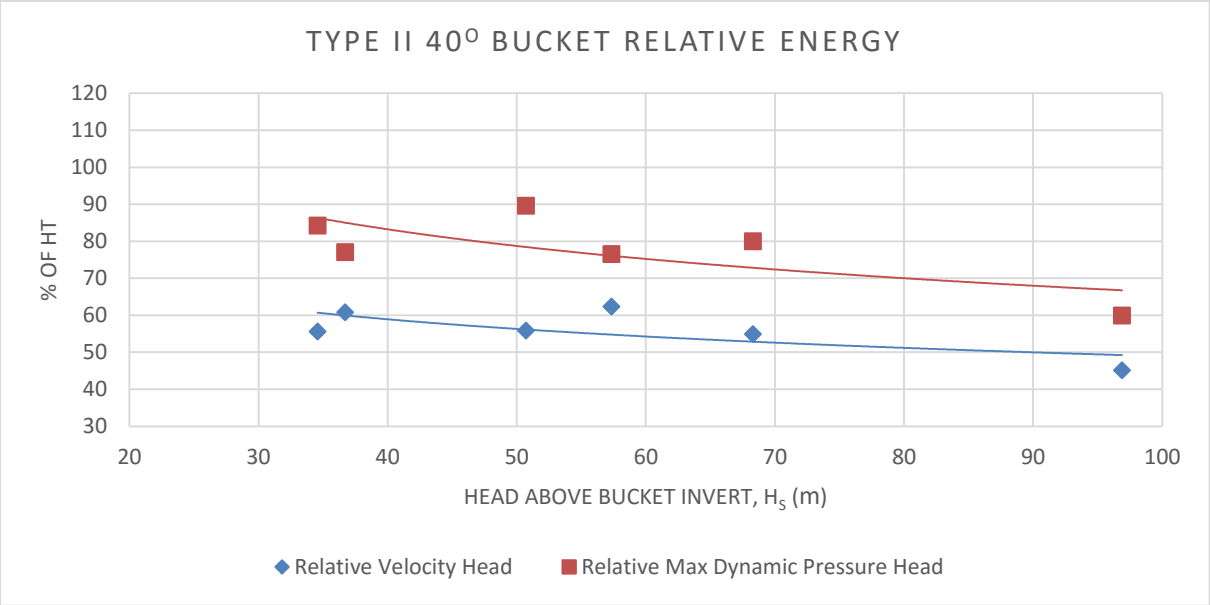


*FIGURE 6.5: ANALYSIS OF THE TYPE II 40O BUCKET IMPACT VELOCITY AND PRESSURE HEADS RELATIVE TO THE TOTAL INITIAL ENERGY LEVEL*

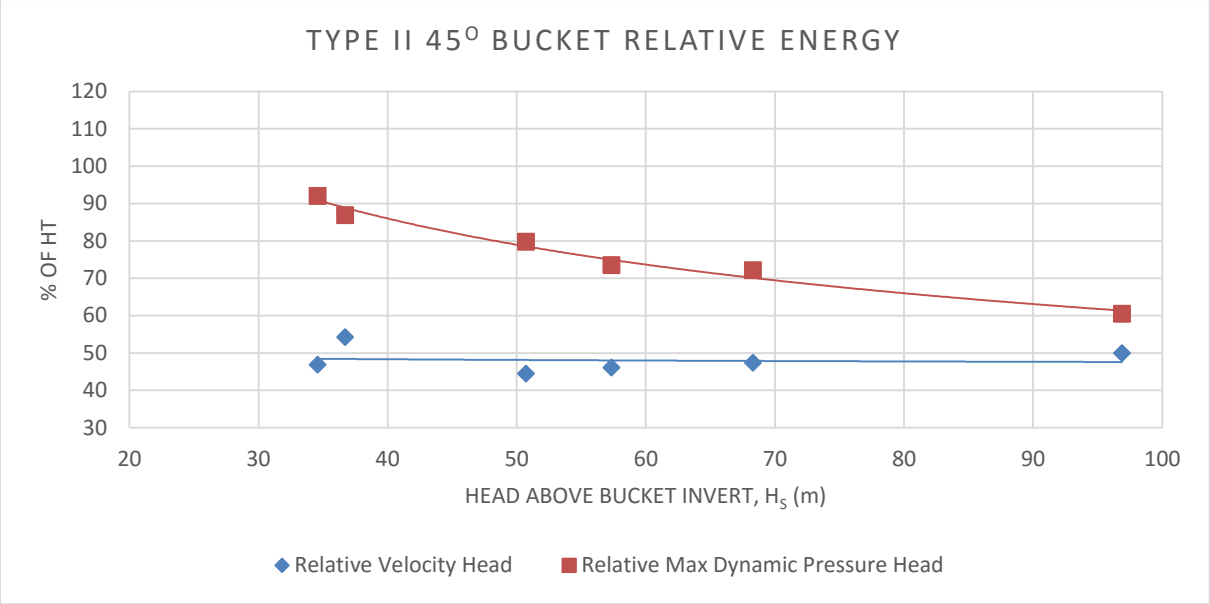


*FIGURE 6.6: ANALYSIS OF THE TYPE II 45° BUCKET IMPACT VELOCITY AND PRESSURE HEADS RELATIVE TO THE TOTAL INITIAL ENERGY LEVEL*

When analysing the data presented in **Figure 6.4**, **Figure 6.5** and **Figure 6.6** for the Type II flip buckets a general trend may be identified that suggests with the increase of $H_o$ the relative maximum dynamic pressure head decreases and therefore the energy losses increases. For the 30º, 40º and 45º Type II flip buckets the relative velocity head does not seem to change as much.

For the maximum flow condition the relative velocity head is 58.7%, 45.1% and 50% for the 30º, 40º and 45º flip buckets respectively. This means that the velocities show a total energy loss of 41.3%, 54.9% and 50% for the three flip buckets.

For the maximum flow condition the relative dynamic pressure head is 71.8%, 59.9% and 60.5% for the 30º, 40º and 45º flip buckets respectively. This suggests that the pressures yield a total energy loss of 28.2%, 40.1% and 39.5% for the three flip buckets.

When comparing all the Type II flip buckets we can see that the 40º flip bucket performs the best in terms of energy loss with 54.9% when analysing the velocity head and an energy loss of 40.1% when analysing the dynamic impact pressure.

### 6.5.3 TYPE III RELATIVE ENERGY COMPARISON

**Figure 6.7** and **Figure 6.8** show calculated results for the relative impact velocity and impact pressure head for the Scoop and Butterfly Type III flip buckets respectively.

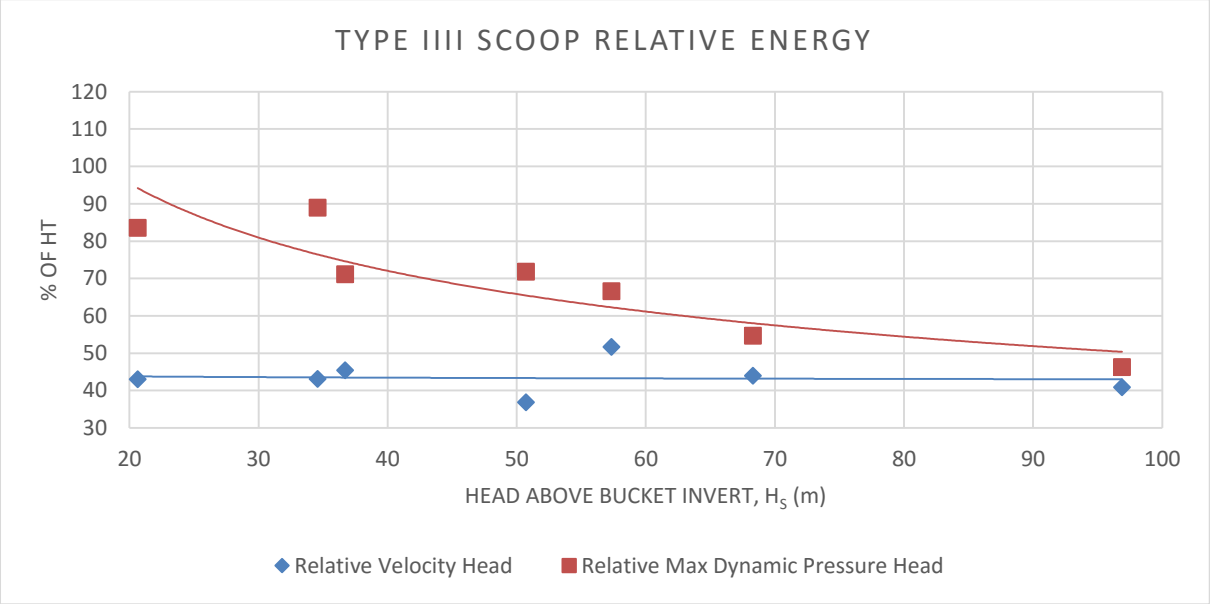


*FIGURE 6.7: ANALYSIS OF THE TYPE III SCOOP IMPACT VELOCITY AND PRESSURE HEADS RELATIVE TO THE TOTAL INITIAL ENERGY LEVEL*

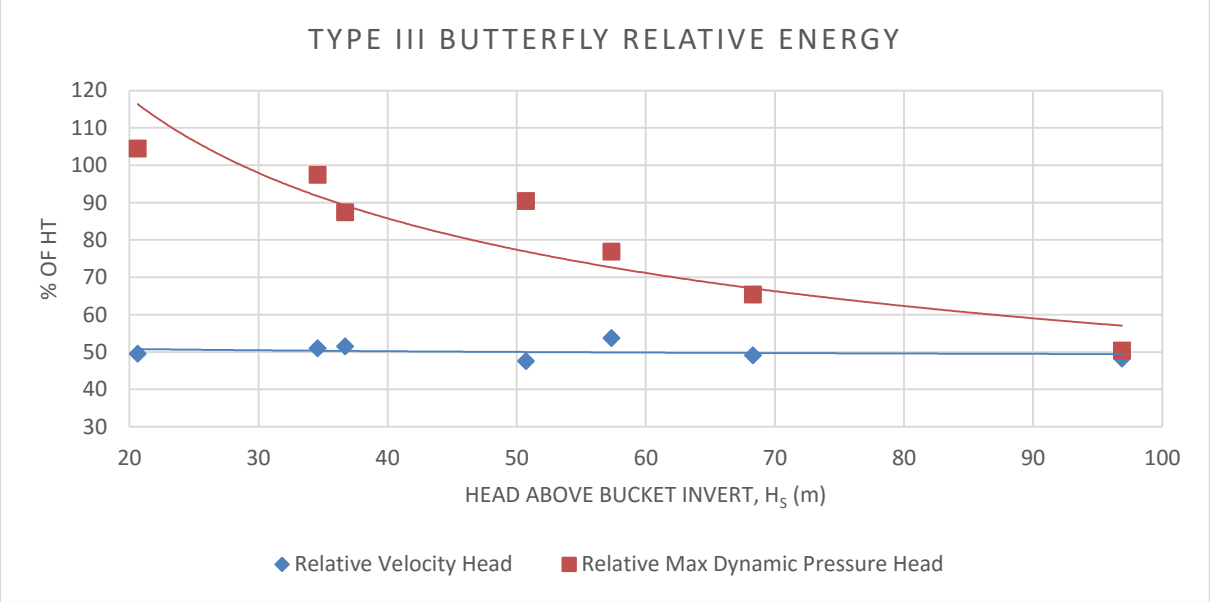


*FIGURE 6.8: ANALYSIS OF THE TYPE III BUTTERFLY IMPACT VELOCITY AND PRESSURE HEADS RELATIVE TO THE TOTAL INITIAL ENERGY LEVEL*

For the maximum flow condition the relative velocity head is 40.92% and 48.2% for the Scoop and Butterfly flip buckets respectively. This means that the velocities show a total energy loss of 59.0% and 51.8% for the two flip buckets.

For the maximum flow condition the relative dynamic pressure head is 46.2% and 50.4% for the Scoop and Butterfly flip buckets respectively. This suggests that the pressures yield a total energy loss of 53.8 % and 49.6% for the two flip buckets.

When comparing all the Type III flip buckets we can see that the Scoop flip bucket performs the best in terms of energy loss with 59.0% when analysing the velocity head and an energy loss of 53.8% when analysing the dynamic impact pressure.

# CHAPTER 7: CONCLUSIONS

*In this conclusions chapter, the purpose of this thesis, to design a ski-jump that maximises energy dissipation and aeration will be answered for the ski-jump designs discussed and the most important outcomes of the analysis will be emphasised.*

## 7.1 SUMMARY OF FINDINGS

This thesis gives a detailed account into the design and construction of ski-jump energy dissipating structures including design guidelines and considerations.

In this thesis, a 1:25 physical model of a ski-jump was hydraulically tested where eight different ski-jump bucket designs with seven flow conditions were analysed to determine a design that maximises energy dissipation and aeration and minimise peak impact pressures at tailwater pool level. In order to quantify the energy dissipation of the different flip bucket designs, a combined analysis of the trajectory profiles, maximum dynamic impact pressures, spatial pressure distribution, impact velocities and air entrainment at a point was conducted.

Energy dissipation is a function of various factors and one cannot make a decision for the most suitable ski-jump bucket by considering these factors individually. For most of the tests conducted there were buckets that performed well in some aspects but poor in others.

The trajectory profiles of the analysed flip buckets all acted in accordance with the theoretical values where the horizontal throw distances were almost identical producing an air resistance coefficient of around 0.9. When comparing all the flip buckets it is evident that the Butterfly flip bucket yielded the best results with regard to the horizontal throw distance as well as the impact widths. These results in combination surpassed all other flip bucket designs by a substantial margin. A comparison of all flip bucket trajectory distances and transverse impact widths are presented in **Figure 7.1** and **Figure 7.2** in the form of a histogram.

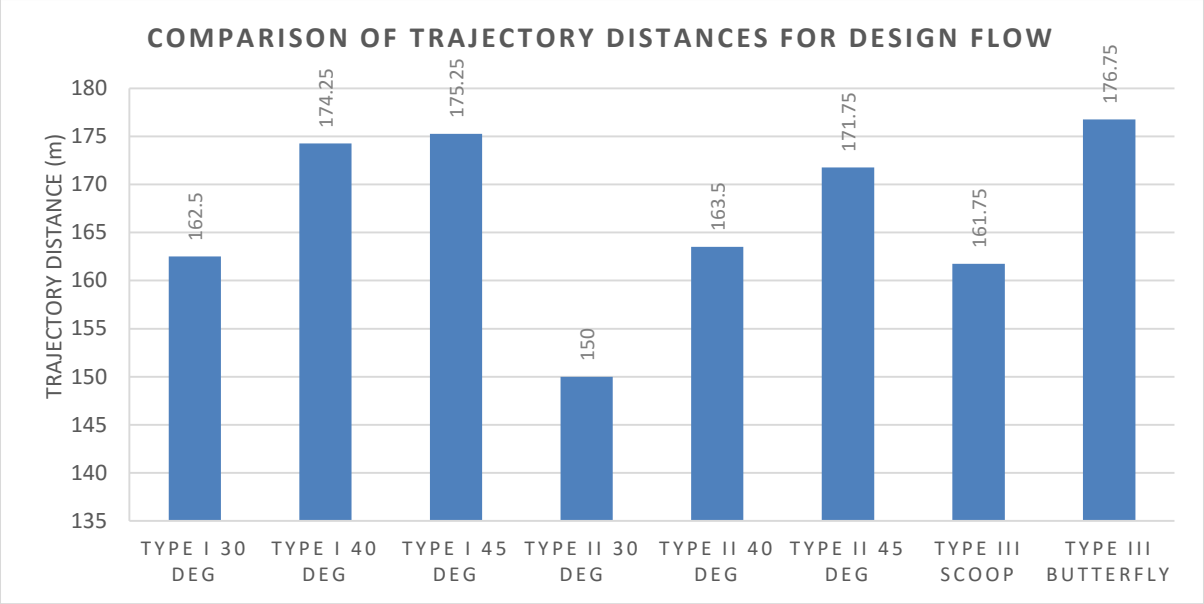


*FIGURE 7.1: COMPARISON OF ALL FLIP BUCKET TRAJECTORY DISTANCES FOR DESIGN FLOW CONDITION (PROTOTYPE VALUES)*

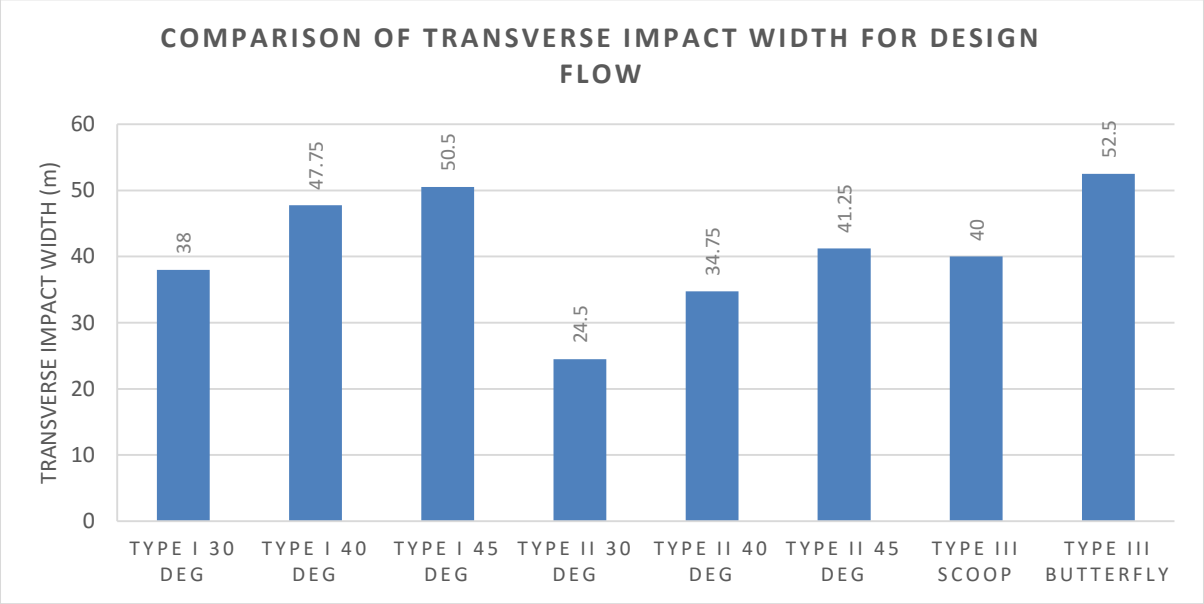


*FIGURE 7.2: COMPARISON OF ALL FLIP BUCKET TRANSVERSE IMPACT WIDTHS FOR DESIGN FLOW CONDITION (PROTOTYPE VALUES)*

In the analysis of the air concentration results (for the design flow condition) the Butterfly Type III flip bucket yielded the best results, especially at the centreline. The distribution of the air concentration percentages for the Butterfly bucket showed a 25.33% air concentration at the centreline, 8.02% air concentration at a distance of 3.125m from the centreline and 3.55% air concentration at the sidewalls. The air concentrations at the centreline and 3.125m from the centreline were the maximum of all flip buckets while the air concentration at the sidewall was exceeded by five other flip buckets, however the air entrainment into the centre of the trajectory jet is an important factor and will play a greater role in the energy dissipation efficiency. Therefore the Butterfly flip bucket was chosen as the bucket with the

best air entrainment. A comparison of all flip bucket air concentration percentages are presented in **Figure 7.3** in the form of a histogram.

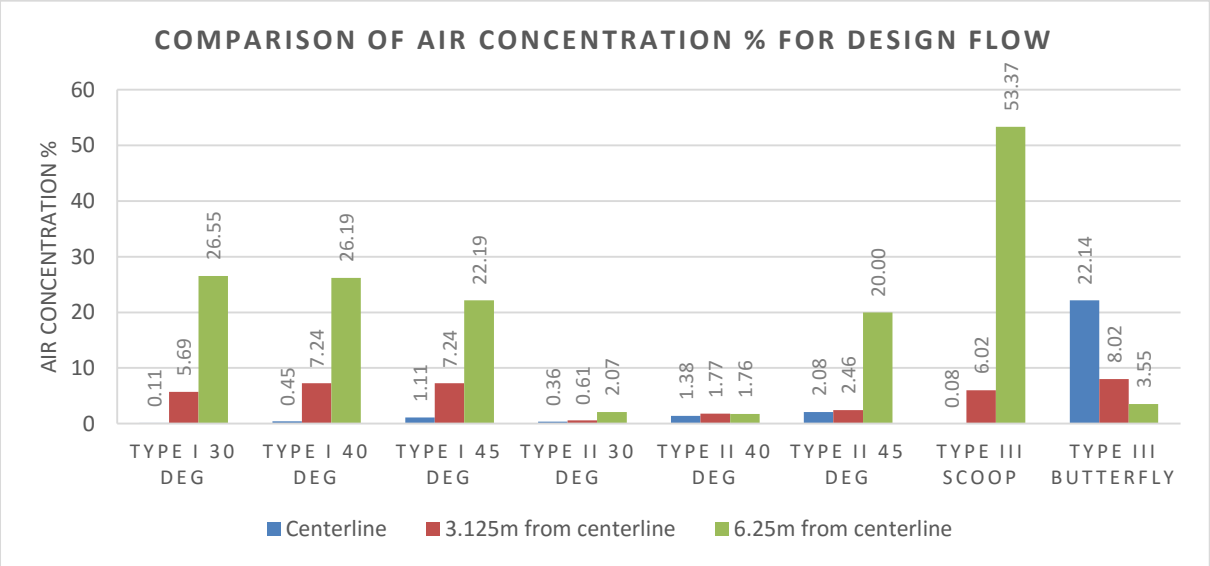


*FIGURE 7.3: COMPARISON OF ALL FLIP BUCKET AIR CONCENTRATION % FOR DESIGN FLOW CONDITION (PROTOTYPE VALUES)*

In the analysis of the maximum dynamic impact pressure head, for the design flow condition the Scoop flip bucket yielded the best results with a $P_{dM}$ of 49.83m, the Butterfly flip bucket was not far behind with a $P_{dM}$ of 54.25m. These pressures were compared to the initial total energy to determine the energy loss over the system where the Scoop flip bucket has an energy loss of 53.8%, while the Butterfly flip bucket has an energy loss of 49.6%. This shows how similar these two flip buckets are in terms of energy loss with only a 4.2% difference. A comparison of all flip bucket dynamic impact pressure heads are presented in **Figure 7.4** in the form of a histogram.

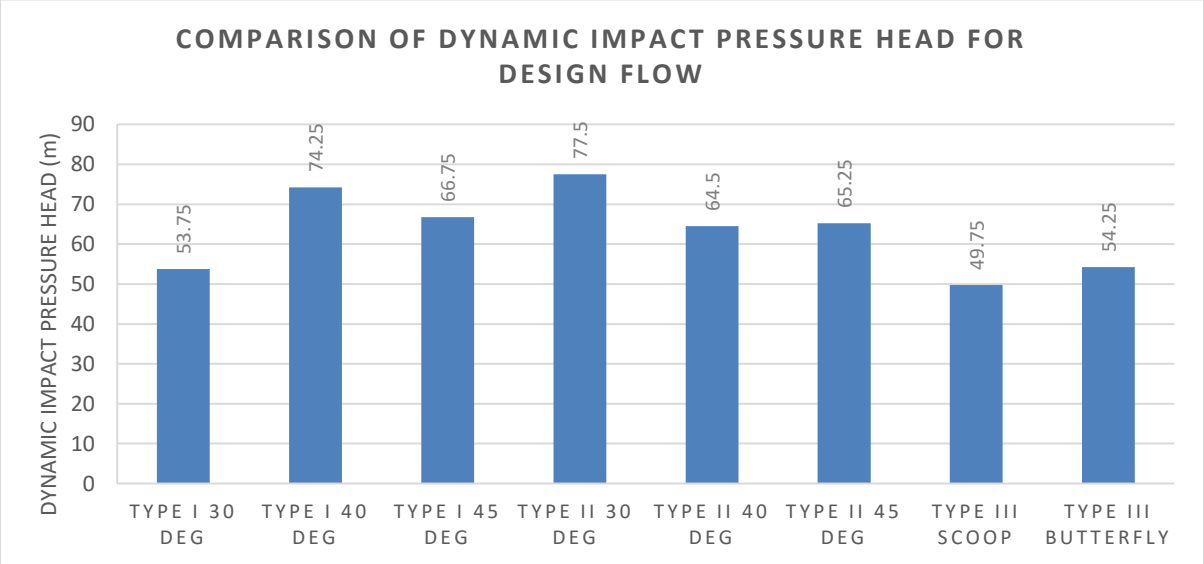


*FIGURE 7.4: COMPARISON OF ALL FLIP BUCKET DYNAMIC IMPACT PRESSURE HEADS FOR DESIGN FLOW CONDITION (PROTOTYPE VALUES)*

When analysing the impact velocity head, for the design flow condition the Scoop flip bucket yielded the best results with an $H_v$ of 22.68m, the Butterfly flip bucket was not far behind with an $H_v$ of 29.3m. These velocity heads were compared to the initial total energy to determine the energy loss over the system where the Scoop flip bucket has an energy loss of 59.0% while the Butterfly flip bucket has an energy loss of 51.8%. There is 7.2% separating the results of the two Type III flip buckets. A comparison of all flip bucket impact velocity heads are presented in **Figure 7.5** in the form of a histogram.

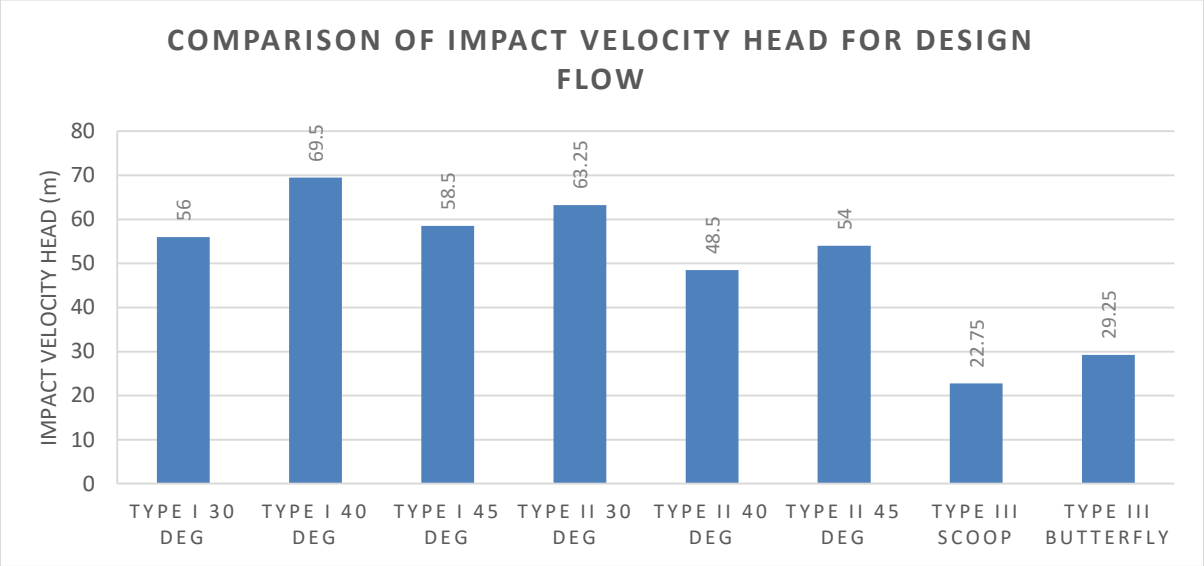


*FIGURE 7.5 COMPARISON OF ALL FLIP BUCKET IMPACT VELOCITY HEADS FOR DESIGN FLOW CONDITION (PROTOTYPE VALUES)*

After analysing all the results the two flip buckets that performed the best when considering all parameters were the Type III flip buckets. The Scoop flip bucket achieved the best results for the dynamic impact pressure head, impact velocity head and as a result the energy loss was the greatest, however in all parameters that the Scoop flip bucket excelled, so did the Butterfly flip bucket where the performance was only marginally poorer with a maximum of 7.2% difference. In addition, the Butterfly flip bucket surpassed all others in the geometric characteristics of the jet trajectories including the Scoop flip bucket by 14.95m for the design flow condition.

As previously stated, because this is a geometrically similar hydraulic model based on the Froude Law there are scale effects that are present. One of these scale effects is that air resistance in a physical model behaves somewhat different to the prototype due to the velocity of the trajectory jet. In model scale the velocity of the design flow condition does not exceed 9m/s, whereas in prototype scale the velocity is about 45m/s. Air resistance for flow only plays a significant role above 20m/s and so in prototype scale there would be significantly more air entrainment therefore the length of the trajectory is a highly important characteristic. The longer the jet trajectory is in the air the greater the dispersion. This is proven with the spatial pressure distribution maps and will have a proportional effect on the energy

dissipation. It is for this reason that the Butterfly flip bucket is the chosen bucket that maximises energy dissipation and air entrainment from the eight flip bucket designs tested.

## 7.2 FUTURE RESEARCH AND RECOMMENDATIONS

For the purpose of reducing costs and reducing testing time the design of the ski-jump model was simplified in many ways. Another contributing factor of the simplified design was that purpose of the dissertation was to identify a design that could improve the energy dissipation and aeration, therefore many designs were tested in order to choose the most suitable. It is recommended that further research be conducted on the designs of the ski-jump models used in this thesis. The author recommends that the following be considered:

- Due to the fact that eight flip buckets were tested there was insufficient time to spend on additional testing. It is recommended that a more focussed approach be taken where one or two bucket designs are chosen and additional experimentation conducted such as; flip bucket pressure distribution curves and scour profiles.
- All flows of the ski-jump hydraulic model were black water flows where a pre-aerated approach flow was not considered. It would be of great value to investigate the effect of a pre-aerated approach flow on the flip buckets, specifically the Type III flip buckets.
- It is also recommended that the flip buckets be tested on an ogee and chute spillway condition.
- The measurement of the dynamic impact pressures can also be improved. This dissertation assumed the jet trajectory impacting the ground without a static water cushion where in a real ski-jump energy dissipator there would be a tailwater depth to help cushion the impacting jet. By measuring the dynamic impact pressures on the river bed at varied tailwater depths, the cushioning effect of the water can then also be studied.

# CHAPTER 8: REFERENCES

Azmathullah, H., Deo, M. & Deolalikar, P., 2006. Estimation of Scour Below Spillways Using Neutral Networks. *Journal of Hydraulic Research*, 44(1), pp. 61-69.

Balloffet, A., 1961. Pressures on Spillway Flip buckets. *Journal of Hydraulic Engineering*, pp. 87-98.

Bollaert, E. & Schleiss, A., 2003. Scour of Rock due to the impact of plunging high velocity jets Part I. *Journal of Hydraulic Engineering*, 00(0), pp. 1-14.

Bureau of Indian Standards, 2010. *Criteria for Hydraulic Design of Bucket Type Energy Dissipators*, New Delhi: Bureau of Indian Standards.

Bureau of Indian Standards, 2012. *Guidelines for Selection of Spillways and Energy Dissipators*, New Delhi: Bureau of Indian Standards.

Chadwick, A., Morfett, J. & Borthwick, M., 2004. *Hydraulics in Civil and Environmental Engineering*. London: Spon Press.

Chanson, H., 1993. Self-Aerated Flows on Chutes and Spillways. *Journal of Hydraulic Engineering ASCE*, 119(2), pp. 220-243.

Chen, T. & Yu, Y., 1965. Pressure Distribution on Spillway Flip Buckets. *Journal of Hydraulic Engineering ASCE 91(2)*, pp. 51-63.

De Almeida Manso, P. F., 2006. *The Influence of Pool Geometry and Induced Flow Patterns on Rock Scour by High-Velocity Plunging Jets*, Lausanne: EPFL.

Falvey, H. T., 1990. *Engineering Monograph No. 42 - Cavitation in Chutes and Spillways*, Denver Colorado: USBR.

FEMA, 2010. *Technical Manual: Outlet Works Energy Dissipators*, s.l.: Federal Emergency Management Agency.

Flow Metrix, 2013. *User's Guide - Installation and Operation Instructions of Electromagnetic Flowmeter*, s.l.: SABS.

Gardo, V. & Lindholm, Y., 2013. *Safety Analysis of the Baihetan Dam By Investigating the Pressure Distribution on the Plunge Pool Floor*, Uppsala: Uppsala University.

GOMACO World, 2000. St. Mary's Spillway. *GOMACO World*, December.28(3).

Hager, W. & Boes, R., 2014. Hydraulic Structures: A Positive Outlook into the Future. *Journal of Hydraulic Research*, 52(3), pp. 299-310.

Heller, V., 2009. *Ski Jump Hydraulics.* [Online] Available at: http://www.drvalentinheller.com/Dr%20Valentin%20Heller_files/Page364.htm [Accessed 2014 June 14].

Heller, V., 2011. Scale effects in physical hydraulic engineering models. *Journal of Hydraulic Research*, 49(3), pp. 293-306.

Heng, S., Tingsanchali, T. & Suetsugi, T., 2009. *Analysis of Plunge Pool Scour Hole Formation Below a Chute Spillway with Flip Bucket using a physical model,* Thailand: Asian Institute of Technology.

Juon, R., Hager, W. H. & F.ASCE, 2000. Flip Bucket without and with Deflectors. *Journal of Hydraulic Engineering,* November, 126(11), pp. 837-845.

Lenau, C. & Cassidy, J., 1969. Flow Through Spillway Flip Bucket. *Journal of Hydraulic Engineering ASCE 95(5),* pp. 633-648.

Mason, P., 1993. Practical guidelines for the design of flip buckets and plunge pools. *Water Power and Dam Construction,* 45(9), pp. 40-45.

Minestry of Science and Technology, 2013. *Design of Hydraulic Structures.* [Online] Available at: http://www.most.gov.mm/techuni/media/CE_05016_ch1.pdf

Novak, P., Moffat, I., Nalluri, C. & Narayanan, R., 2007. *Hydraulic Structures.* 4th Edition ed. London and New York: Taylor & Francis Group.

Omidvarinia, M. & Musavi Jahromi, S., 2013. Effect of Wedge Shape Deflector on Dissipating Energy in Triangular Flip Buckets. *Journal of Civil Engineering and Urbanism,* 30 March, 3(2), pp. 56-61.

Steiner, R. et al., 2008. Deflector Ski-Jump Hydraulics. *Journal of Hydraulic Engineering,* May, 134(5), pp. 562-571.

Thandaveswara, B., n.d. *Characteristics of Self-Aerated Flow.* [Online] Available at: http://nptel.ac.in/courses/IIT-MADRAS/Hydraulics/ [Accessed 23 May 2014].

U.S Army Corps of Engineers, 1977. *Hydraulic Design Criteria (Volume 1),* Vicksburg: U.S Army Corps of Engineers.

U.S. Army Corps of Engineers, 1990. *Engineering and Design: Hydraulic Design of Spillways,* Washington D.C.: US Army Corps of Engineers.

USBR, 1987. *Design of Samll Dams.* 3rd Edition ed. Washington DC: United States Department of Interior.

Vischer, D. & Hager, W., 1995. *Energy Dissipators: IAHR Hydraulic Structures Design Manual 9.* Rotterdam: A.A. Balkema.

Vischer, D. & Hager, W., 1998. *Dam Hydraulics.* West Sussex, England: John Wiley & Sons Ltd.

Wahl, T. L., Frizell, K. H. & Cohen, E. A., 2009. Discussion of "Computing the Trajectory of Free Jets". *Journal of Hydraulic Engineering,* 134(2), pp. 256-260.

Wang, X. & Chou, L., 1979. The Method of Calculation of Controlling (or Treatment) Criteria for the Spillway Surface Irregularities. *Proceedings of the Thirteenth International Congress of Large Dams,* Q56(R56), pp. 997-1012.

Wu, J.-h., Ma, F. & Yao, L., 2012. Hydraulic Characteristics of Slit-Type Energy Dissipaters. *Journal of Hydrodynamics,* 7 November, 24(6), pp. 883-887.

Wu, W.-p., Zhang, X.-h. & Tian, J.-n., 2006. Shock Action of Jet Flow From Slit-Type Buckets on the Bottom of the Trough. *Journal of Hydrodynamics,* 18(3), pp. 511-514.

# APPENDIX I - EXISTING TRAJECTORY BUCKET PROTOTYPE DIMENSIONS

*TABLE A. 1: TRAJECTORY BUCKET PROTOTYPE DIMENSIONS (BUREAU OF INDIAN STANDARDS, 2010)*

| ***SI No.*** | ***Project*** | ***Country*** | ***Maximum Discharge*** <br> ***Q*** <br> ***$m^3/s$*** | ***Maximum Discharge per m Width*** <br> ***q*** <br> ***$m^3/s/m$*** | ***Head Above Bucket Invert*** <br> ***$H_0$*** <br> ***m*** | ***Bucket Radius*** <br> ***$R_b$*** <br> ***m*** | ***Bucket Lip Angle*** <br> ***$\theta$*** <br> ***degree*** |
|---|---|---|---|---|---|---|---|
| ***i)*** | *Banas* | *India* | *6 909* | *42.7* | *36.3* | *21.95* | *35* |
| ***ii)*** | *Gandhi Sagar* | *India* | *15 705* | *53.9* | *32.4* | *30.48* | *30* |
| ***iii)*** | *Girna* | *India* | *8 750* | *41.3* | *32.3* | *15.24* | *35* |
| ***iv)*** | *Hirakud* | *India* | *33 626* | *64.8* | *39.7* | *15.24* | *40* |
| ***v)*** | *Maithon* | *India* | *15 971* | *85.7* | *38.1* | *10.67* | *43* |
| ***vi)*** | *Mandira* | *India* | *8 496* | *42.7* | *19.8* | *7.62* | *NA* |
| ***vii)*** | *Panchet Hill* | *India* | *17 840* | *81.8* | *34.1* | *18.29* | *43* |
| ***viii)*** | *Ranapartap Sagar* | *India* | *21 238* | *61.1* | *31.4* | *16.76* | *40* |
| ***ix)*** | *Rihand* | *India* | *11 805* | *55.7* | *78.3* | *3.29* | *30* |
| ***x)*** | *Salandi* | *India* | *5 239* | *29.3* | *34.1* | *13.72* | *30* |
| ***xi)*** | *Sukhi* | *India* | *5 912* | *44* | *24.8* | *13.7* | *40* |
| ***xii)*** | *Tilaiya* | *India* | *3 851* | *24.7* | *29* | *6.1* | *30* |
| ***xiii)*** | *Ukai* | *India* | *35 963* | *97.6* | *47.9* | *27.43* | *40* |
| ***xiv)*** | *Vaitarna* | *India* | *5 663* | *27.9* | *70.7* | *24.38* | *35* |
| ***xv)*** | *Radhanagari* | *India* | *1 180* | *28.4* | *29.5* | *15* | *40* |
| ***xvi)*** | *Bhatsai* | *India* | *3 737* | *47.9* | *85.6* | *18.3* | *40* |
| ***xvii)*** | *Dimbhe* | *India* | *3 348* | *46.5* | *66.5* | *17* | *38* |
| ***xviii)*** | *Surya* | *India* | *3 180* | *44.2* | *48.2* | *13.5* | *45* |
| ***xix)*** | *Srirama Sagar* | *India* | *45 310* | *59.4* | *27.7* | *12.9* | *37* |
| ***xx)*** | *Anchor* | *USA* | *382* | *18* | *31* | *Parabolic* | *NA* |
| ***xxi)*** | *Arkport* | *USA* | *824* | *32* | *NA* | *3.11* | *45* |
| ***xxii)*** | *Chilhowee* | *USA* | *6 513* | *80.4* | *21.6* | *9.75* | *20* |
| ***xxiii)*** | *Conowingo* | *USA* | *24 919* | *36.3* | *27.9* | *12.19* | *12.5* |
| ***xxiv)*** | *Hartwell* | *USA* | *15 999* | *90.6* | *49.1* | *9.14* | *36* |
| ***xxv)*** | *Pineflat* | *USA* | *11 185* | *125.4* | *113.4* | *15.24* | *20* |
| ***xxvi)*** | *Safe Harbor* | *USA* | *27 467* | *34* | *17.8* | *12.8* | *27* |
| ***xxvii)*** | *Dnieprostroy* | *Russia* | *23 645* | *31* | *NA* | *11.55* | *NA* |
| ***xxviii)*** | *Bort* | *France* | *1 195* | *90.8* | *114.9* | *NA* | *NA* |
| ***xxix)*** | *Chastang* | *France* | *3 987* | *146.8* | *71* | *NA* | *NA* |
| ***xxx)*** | *Genissiat* | *France* | *2 690* | *179.8* | *64* | *NA* | *NA* |
| ***xxxi)*** | *L'Aigle* | *France* | *3 987* | *124.7* | *89.9* | *NA* | *NA* |
| ***xxxii)*** | *Maregos* | *France* | *1 393* | *26.9* | *77.1* | *NA* | *NA* |
| ***xxxiii)*** | *St.Etiernna Centales* | *France* | *714* | *70* | *71.1* | *NA* | *NA* |
| ***xxxiv)*** | *Castelodo Bode* | *Portugal* | *13 998* | *249.9* | *112.8* | *NA* | *NA* |
| ***xxxv)*** | *Pictoe* | *Portugal* | *NA* | *NA* | *90.8* | *NA* | *NA* |
| ***xxxvi)*** | *Clereland* | *British Columbia* | *1 226* | *50.2* | *91.4* | *NA* | *NA* |
| ***xxxvii)*** | *Kamishiiba* | *Japan* | *2 152* | *55.7* | *110* | *NA* | *NA* |

# APPENDIX II - STEEL JET BOX DIMENSIONS

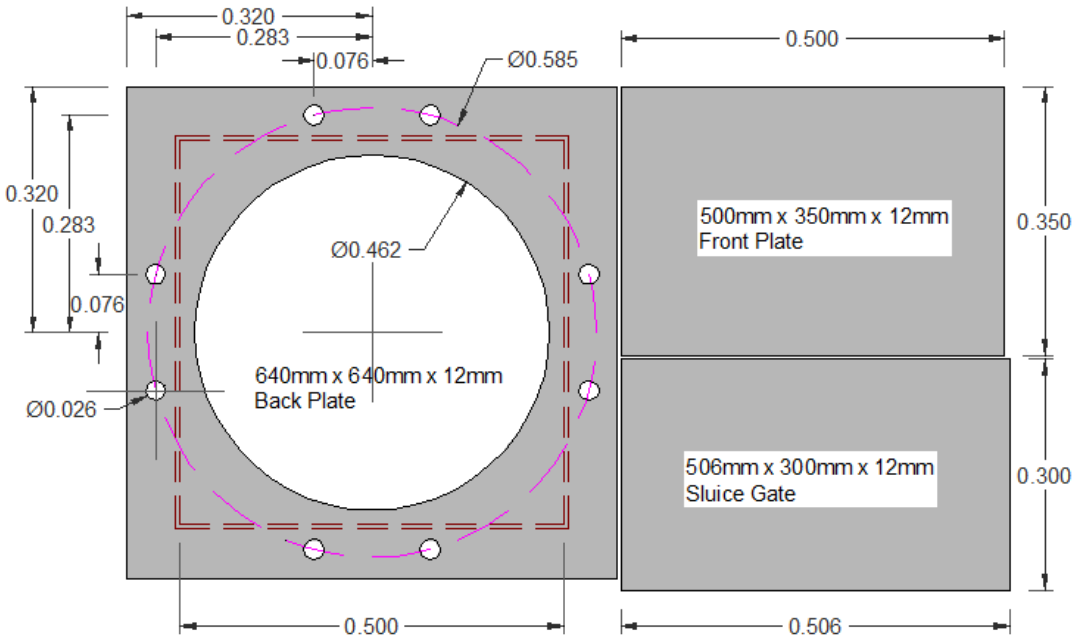


*FIGURE A- 1 FINAL STEEL JET BOX DESIGNS SENT TO MACSTEEL FOR CUTTING*

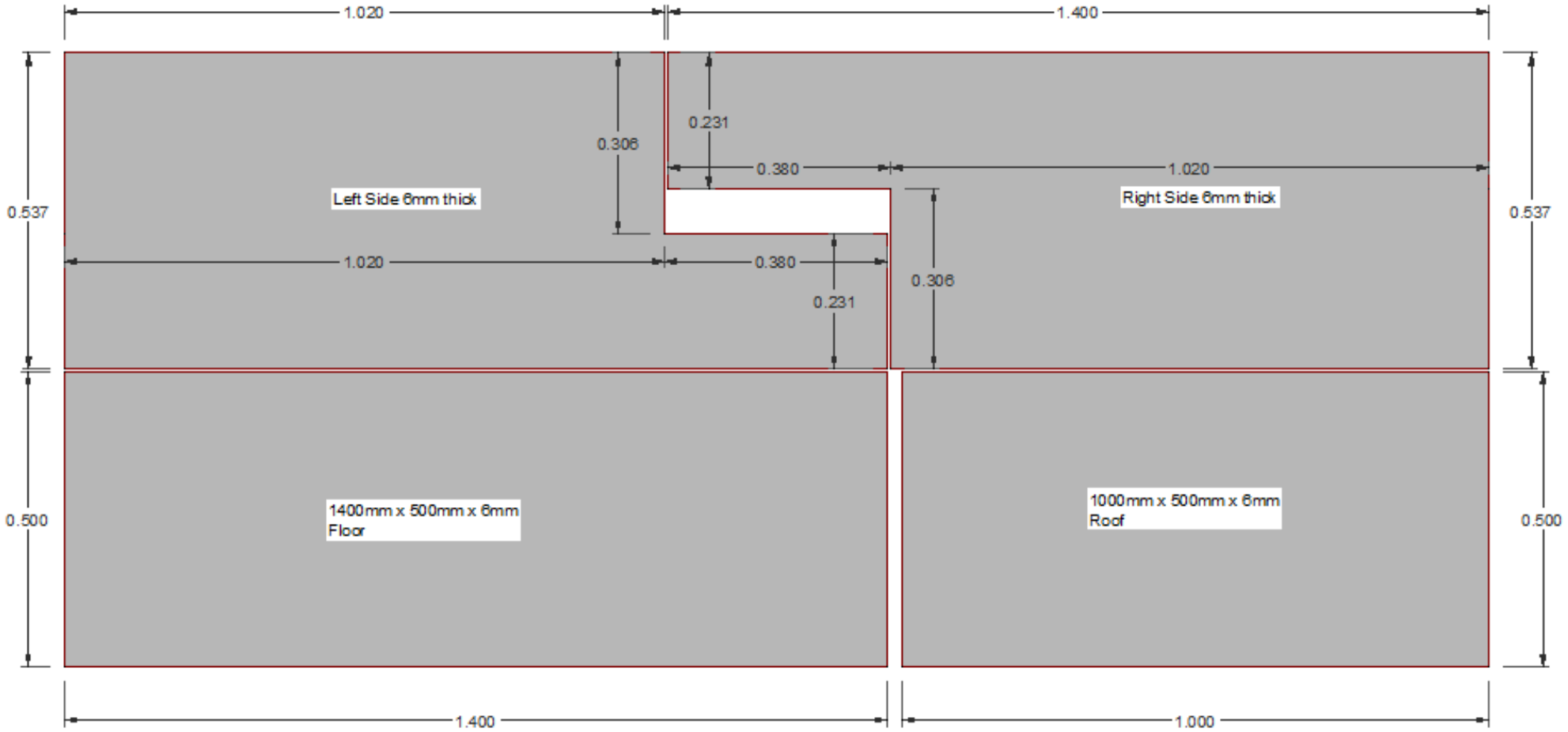


*FIGURE A- 2: FINAL STEEL JET BOX DESIGNS SENT TO MACSTEEL FOR CUTTING*

# APPENDIX III – OGEE SPILLWAY DESIGN GRAPHS

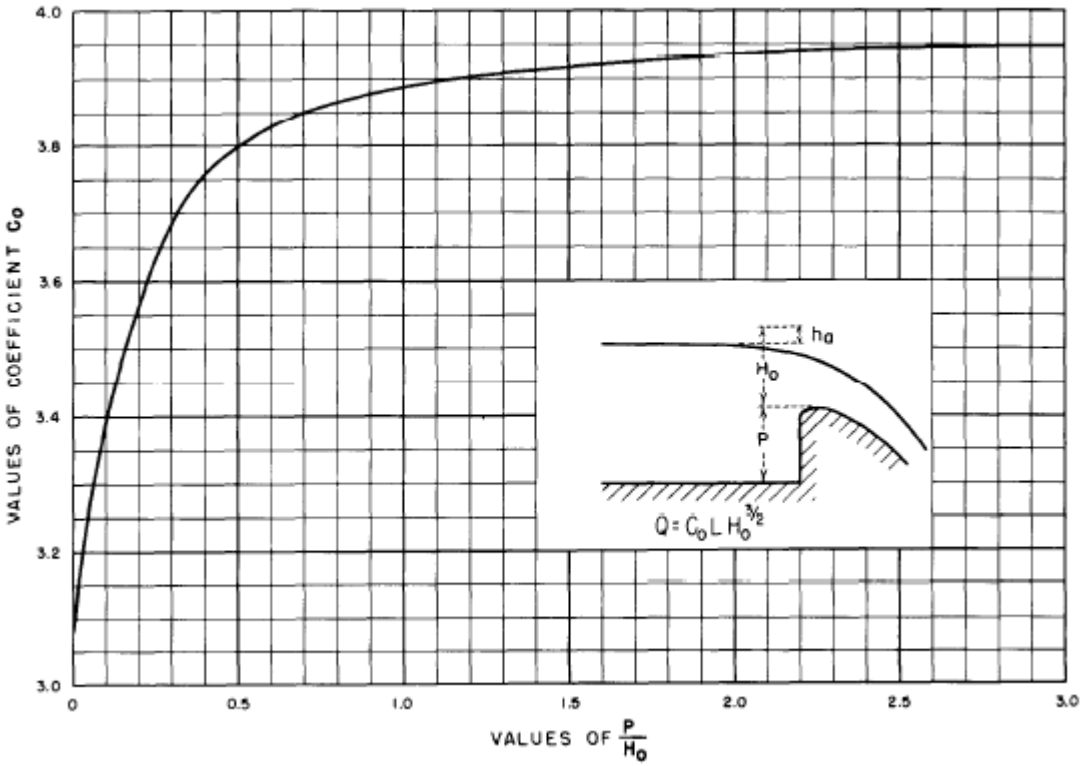


*FIGURE A- 3: DISCHARGE COEFFICIENT FOR DESIGN HEAD (USBR, 1987)*

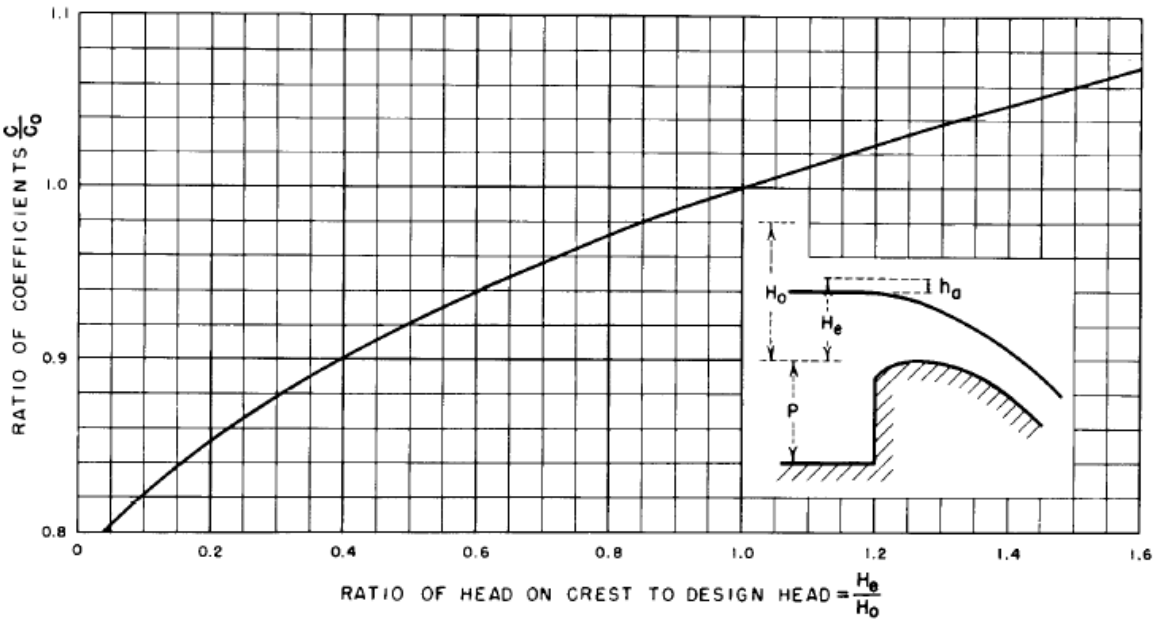


*FIGURE A- 4: DISCHARGE COEFFICIENT FOR OTHER THAN DESIGN HEAD (USBR, 1987)*

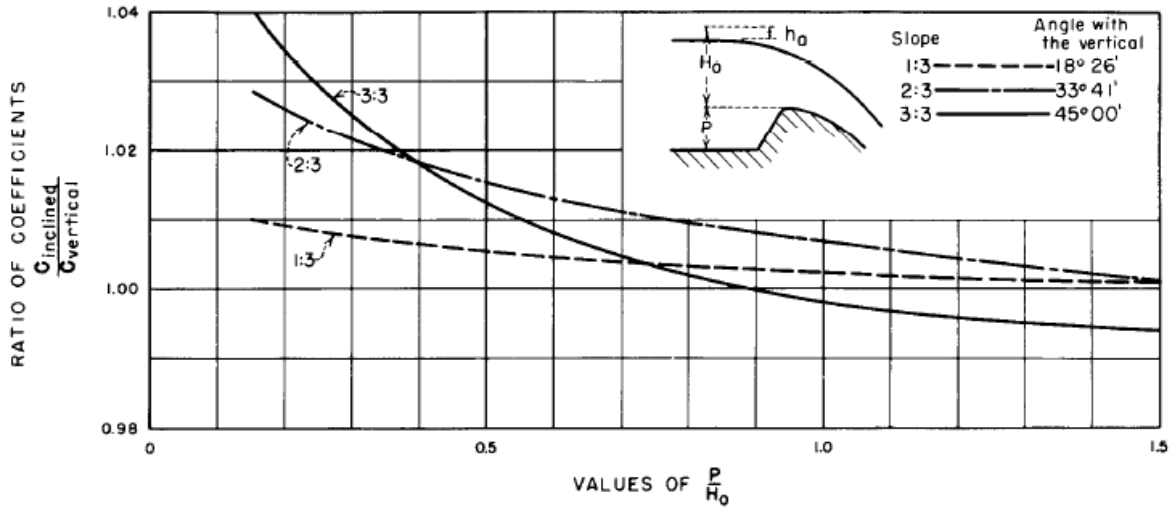


*FIGURE A- 5: UPSTREAM FACE SLOPE FACTOR (USBR, 1987)*

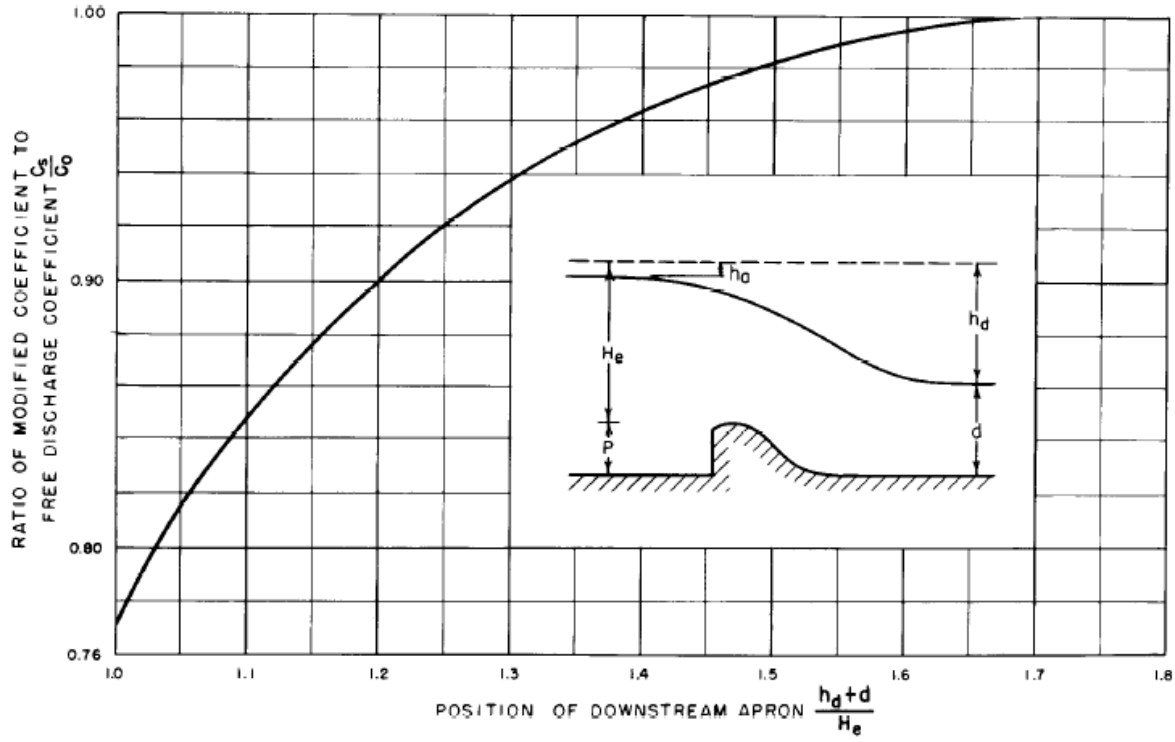


*FIGURE A- 6: DISCHARGE COEFFICIENT FOR DOWNSTREAM APRON EFFECT (USBR, 1987)*

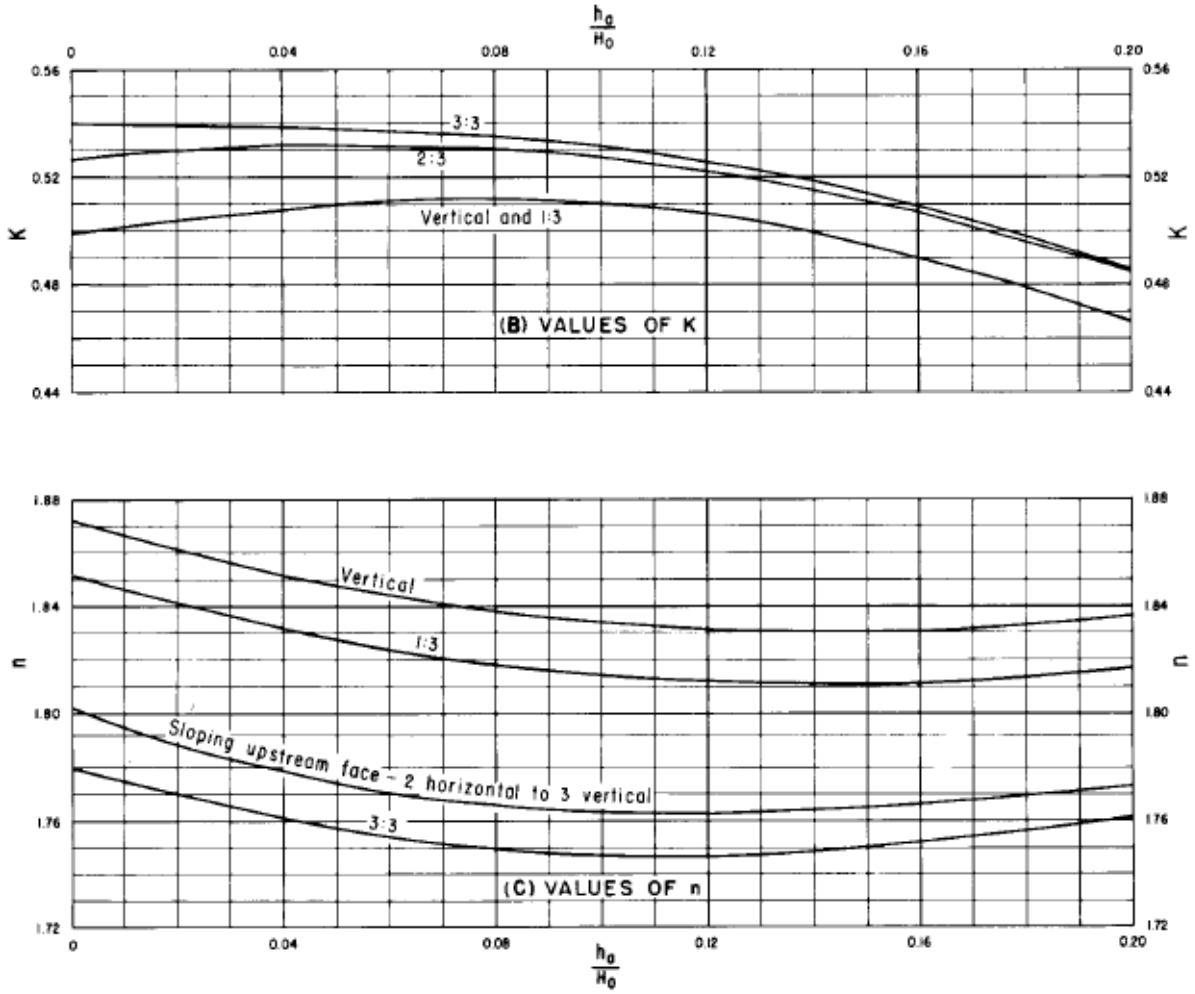


*FIGURE A- 7: K AND N VALUES FOR OGEE PROFILE (USBR, 1987)*